AN ABSTRACT OF THE DISSERTATION OF

Travis B. Peery for the degree of Doctor of Philosophy in Physics

presented on May 20, 2003.

Title: A Theoretical Description of Anisotropic Chemical Association and its Application to Hydrogen-bonded Fluids.

Redacted for Privacy

Abstract approved: Redacted for Privacy

Glenn T. Evans

The thermodynamic and structural effects of highly anisotropic, short-ranged attraction are investigated for single– and four-site interaction models using Wertheim's multi-density graph theory of chemical association. Both models consist of associating hard spheres, where the saturable attraction sites are described by conical wells centered in the hard core and evaluated in the "sticky-spot" limit. The resulting fluids then mimic many of the directional and steric-constrained properties of hydrogen-bonded fluids.

The single-site model is used to explore the effects of dimerization upon the well-known properties of a planar liquid–vapor interface. Apart from hard sphere repulsion and sticky-spot attraction, a van der Waals-like dispersion interaction is incorporated to generate the critical point. Association is treated within Wertheim's thermodynamic perturbation theory, along with classical density functional methods to determine the interfacial density profile. The direct correlation functions —which carry all bonding information— are derived by means of the *associative* Ornstein–Zernike equations with a Percus–Yevick-like closure relation. The primary effects of dimerization are manifest in system thermodynamics. Critical temperatures and densities are shifted from their non-associating values and small, non-monotonic shifts in the correlation length and surface tension are also observed. While these effects are accompanied by interface compositional changes, any influence upon the density profile seems to be subsumed by use of the proper T/T_c.

The four-site, network-forming model is investigated as a prototype for the thermodynamics and structural properties of water. Bonding interactions occur

between "hydrogen" and electron "lone pair" sites described in the sticky-spot limit. System properties are derived under the *ideal network approximation* using the same methods as for the one-site model and are found to qualitatively reproduce some thermodynamic and connectivity features characteristic of real water. Partial densities are calculated self-consistently within the theory, and most thermodynamic quantities can be written in terms of the average number of hydrogen bonds per molecule. An analytical structure factor is also derived for this model.

A Theoretical Description of Anisotropic Chemical Association and its Application to Hydrogen-bonded Fluids

by

Travis B. Peery

A DISSERTATION

submitted to

Oregon State University

in partial fulfillment of
the requirements for the
degree of

Doctor of Philosophy

Presented May 20, 2003
Commencement June 2003

Doctor of Philosophy dissertation of Travis B. Peery presented on May 20, 2003.

APPROVED:

Redacted for Privacy

Major Professor, representing Physics

Redacted for Privacy

Chair of the Department of Physics

Redacted for Privacy

Dean of the Graduate School

I understand that my dissertation will become part of the permanent collection of Oregon State University libraries. My signature below authorizes release of my dissertation to any reader upon request.

Redacted for Privacy

Travis B. Peery, Author

ACKNOWLEDGMENT

So Long and Thanks for All the "Phish"

That which I most often find obscure, inevitably becomes transparent when "polished" through discussion with others; science, at heart, is a social endeavor. As such, I would be remiss if I did not collectively thank all those from whom I have learned so much. Specifically, I wish to thank my advisor, Dr. Glenn T. Evans, for his patience and support while introducing me to the field of theoretical chemical physics. My parents also deserve special thanks, for they have given me continued support through all my years of undergraduate and graduate work. I would also like to thank all of the professors and staff members of the Physics Department, especially Dr. Henri Jansen. As department chair, he has faithfully provided financial support to all physics graduate students like myself, and, as an instrumental member of my committee, has provided me with invaluable intellectual and career advice.

Thanks to numerous friends and colleagues for their accompaniment during my graduate years: Tracy Lee, Rick Muirhead, Scott Bennett, Brian Schlatter, Jason Janesky, Emily Townsend, and Bodhi Rogers —without whose help I never would have passed the qualifying exam— all deserve special mention. Additionally, I wish to thank those friendly coffee purveyors at the *Interzone Cafe*: thank you, Bill and Iris, for always being there with fresh-brewed coffee and a smile to keep me going through all the research and teaching rigors of graduate school.

Finally, I wish to thank the National Science Foundation and the Department of Education for their partial support of this work.

"Great understanding is broad and unhurried; little understanding is cramped and busy."

— Chuang Tzu

TABLE OF CONTENTS

TABLE OF CONTENTS (Continued)

Page

TABLE OF CONTENTS (Continued)

LIST OF FIGURES

LIST OF FIGURES (Continued)

Figure | Page

LIST OF FIGURES (Continued)

Figure Page

LIST OF TABLES

Table Page

DEDICATION

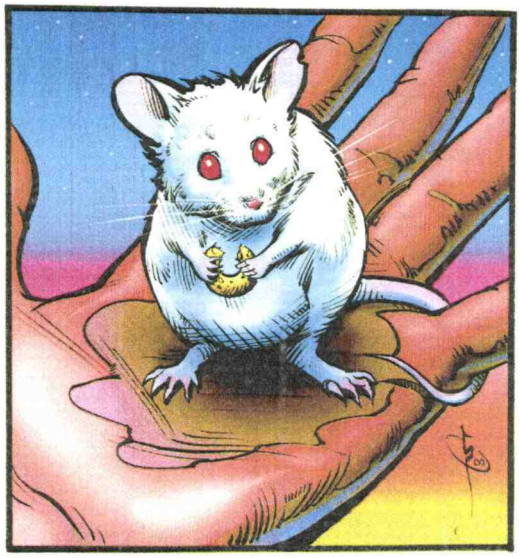

By Cutter Hayes

Of Rodents and Men

On May 13, 2002, President George W. Bush signed into law farm bill H.R. 2646. Attached to that bill —at the eleventh hour— was an amendment introduced by Senator Jesse Helms (R–North Carolina) that exempts rats, mice, and birds used in medical research from the *Animal Welfare Act*, which is administered by the U.S. Department of Agriculture (USDA). By effectively repealing that act, the Congress and President Bush left these animals —who constitute 95% of all animals used for medical research— unprotected against cruel or negligent treatment at the hands of research institutions.

This dissertation is dedicated to all those *involuntary* test subjects, for they have given, and will continue to give, more in the name of "Science"... than I could ever imagine. If we do not respect these animals enough to alleviate or even eliminate their suffering, the least we can do is acknowledge their *ultimate* sacrifice for our health and safety.

PREFACE

I.

We knowers are unknown to ourselves, and for good reason: how can we ever hope to find what we have never look for? There is a sound adage which runs: "Where a man's treasure lies, there lies his heart." Our treasure lies in the beehives of our knowledge. We are perpetually on our way thither, being by nature winged insects and honey gatherers of the mind. The only thing that lies close to our heart is the desire to bring something home to the hive. As for the rest of life —so-called "experience"— who among us is serious enough for that? Or has time enough? When it comes to such matters, our heart is simply not in it —we don't even lend our ear. Rather, as a man divinely abstracted and self-absorbed into whose ears the bell has just drummed the twelve strokes of noon will suddenly awake with a start and ask himself what hour has actually struck, we sometimes rub our ears after the event and ask ourselves, astonished and at a loss, "What have we really experienced?" —or rather, "Who are we, really?" And we recount the twelve tremulous strokes of our experience, our life, our being, but unfortunately count wrong. The sad truth is that we remain necessarily strangers to ourselves, we don't understand our own substance, we *must* mistake ourselves; the axiom, "Each man is the farthest from himself," will hold for us to all eternity. Of ourselves we are not "knowers". . . .

—Friedrich Nietzsche
preface to *The Genealogy of Morals*

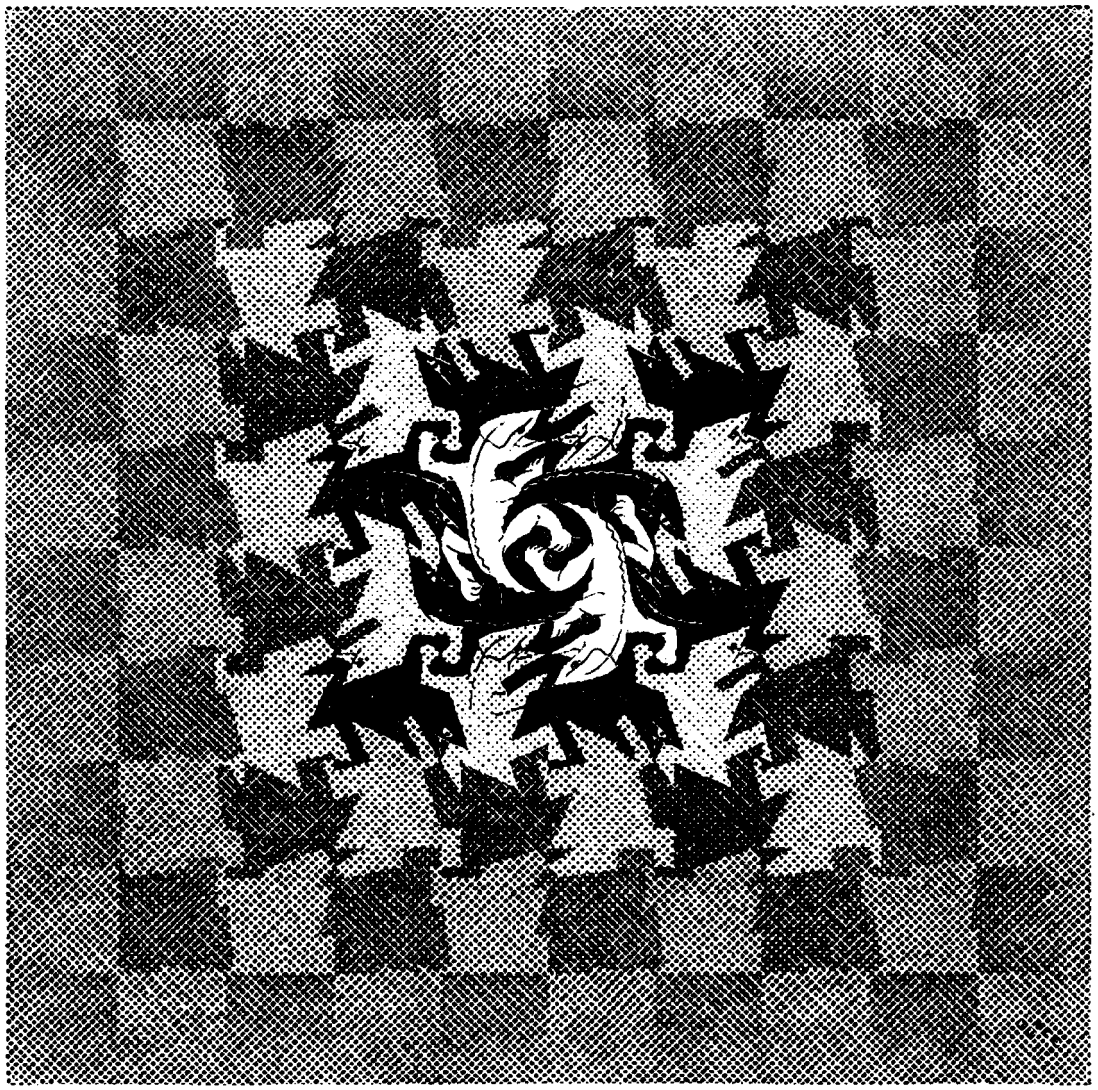

M. C. Escher's image "Development II"

A THEORETICAL DESCRIPTION OF ANISOTROPIC CHEMICALASSOCIATION AND ITS APPLICATION TO HYDROGEN-BONDED FLUIDS

1. GENERAL INTRODUCTION

'The time has come,' the Walrus said,
'To talk of many things:
Of shoes — and ships — and sealing wax —
Of cabbages and kings. . .'

— L. Carroll

1.1. A SMALL AMERICAN DREAM

Explosive progress is being made on many fronts in the biosciences, the complete mapping of the mouse and human genome, for example. In her opening statement concerning the FY 2003 presidential budget request [1], Dr. Ruth Kirschstein, acting director of the National Institutes of Health, stated "Although scientific accomplishments often take years to produce new treatments or diagnostic tools, the confluence of generous budgets and extraordinary scientific opportunity has already begun to yield amazing results." This renaissance, in large part, has been made possible by fundamental improvements in areas like miniturization, robotics, synthesis methods, and computing power. Such advances have allowed an increasingly savy, molecular-level characterization of biophysical processes that span many disciplines. Emerging fields such as *proteomics*[1], as well as existing ones like *combinatorial chemistry,*[2] for example, which involve the structural calculation of complex molecular and macromolecular assemblies —most of which

---

[1]The computer-aided analysis of patterns present in large sets of proteins used to understand their function.

[2]A new way to generate large libraries of molecules and macromolecules which can be tested for possible drug use.

occur in liquid (aqueous) environments— are fertile arenas of current research. Although the link between microscopic, statistical, and macroscopic descriptions of aqueous solutions is extremely subtle, sophisticated laboratory techniques coupled with powerful computers have sped up the analysis via complicated numerical and simulation techniques.

The relatively new field of proteomics[3], for example, exemplifies in a general sense the current microscopic scale of research that stands to revolutionize development of innovative clinical diagnostics and pharmaceutical theraputics. While the human genome itself has been mapped, linking the roughly one-half million human proteins to the 30,000 genes that encoded them is not a trivial matter. Proteomics, or the identification, characterization, and quantification of all forms of proteins, their function, and all pathways by which they participate in biological processes, seeks to unravel the biological and physiological mechanisms of complex multivariate diseases at the functional molecular level. If the genome represents the words of a "dictionary", then the proteome provides the definitions of those words. The patterns of how these proteins interact with each other, their environment, as well as other molecules then represents the grammar and syntax required to form meaningful language. Fluency in that language, however, requires a subtle level of "micro-engineering", and that means understanding the liquid environments in which these proteins exist, *i.e.* water.

This is a tall order by any standard, given the complexity of aqueous solutions. What molecular interactions or pertinent building blocks hold the keys to understanding a particular biochemical process? What is a useful paradigm in their description? —to use Thomas S. Kuhn's vocabulary. Pure water is such a prominent element in biological solutions that deciphering its fundamental properties such that comprehensive predictions can be made stands as an important challenge in liquid state theory. Yet no simple theory of associating or hydrogen-bonded fluids like water currently exist. Despite its importance, simple structure, and ubiquity [2–4], water is a very difficult fluid to treat using current liquid state theories because it can form *hydrogen bonds,* or short-ranged and highly directional

---

[3] *Proteome*, coined by an Australian graduate student, is an acronym for PROTEin complement to a genOME.

bonds between a proton on one water molecule and a lone pair of electrons on the oxygen atom of another.

The hydrogen bond (the prototypical example of chemical association), in addition to its traditional role as a liquid structural element, carries other important processes. Series of hydrogen bonds (H-bonds) appear to be vital in the functioning of a number of enzymes, and play a crucial role in biological electron transport across distances longer than the much stronger covalent bonds [5]. Principles of H-bonding furthermore are used as a means to design new materials capable of self-assembly into well-ordered crystal structures, for molecular recognition of organic molecules [6], and for the self-assemlby of spherical, helical, cylindrical structures [7, 8]. As another example, new dynamic combinatorial chemistry methods are being used in the search for reduced toxicity of drugs, increased absorbtion, and improved release profiles requires an understanding of very subtle association effects. Bioadhesive polymers are being used to improve the absorption of drugs by epithelial cells [9]. Theses adhesive molecules bring the delivery system closer to the mucosa, but success depends upon "light", instead of strong covalent, bonding. Hence these polymer delivery systems are being designed with a high amount of carboxylic acid, which hydrogen bonds with the carboxylic acids in epithelial cells. Moreover, as drugs become larger, water solubility is often a major concern. Molecular imprinting involves monomers which polymerize around a template molecule. The template is then removed, leaving a "vacancy" that will interact selectively with the template; hydrophilic or hydrophobic interactions are vitally important in these processes. Hybrid delivery systems consisting of linear polymers attached to dendrimers also show promise as drug delivery systems. Dendrimers provides multiple drug attachment sites, while the linear polymer provides water solubility.

Statistical mechanics provides a link between the intermolecular interactions, like hydrogen bonding, and the thermodynamic and structural properties of fluids, the success of which is largely measured by its ability to formulate an accurate and useful equation of state. While the theory of fluids and fluid mixtures[4] has made great progress recently, those advances have been mainly phenomeno-

---

[4]Fluid mixtures that can be considered as ideal are mixtures whose components have either identical molecular sizes and interaction energies or such similar residual Helmholtz

logical and produce quite sophisticated equations of state. However, the accuracy of either smoothing or predicting phase equilibria in (biological) mixtures depends heavily upon the accuracy of the known equations of state, the extent of our knowledge of intermolecular forces, and their temperature and density dependence [10]. Differences between the the repulsive and attractive terms in quantities like the compressibility factor $Z(\rho, T)$ or residual Helmholtz free energy $A^r(\rho, T)$ are essential in the calculation of the phase equilibria of fluids and fluid mixtures. In order to apply the phase equilibria and stability conditions (derived by Gibbs) it is necessary to distinguish a perfect gas from a real fluid, expressed by the residual functions. Such functions can be evaluated once the molecular properties of the fluid and an equation of state are known. Equations of state for hard bodies have been developed, with perturbation theories and simulation techniques used to treat the attractive forces, but numerical solutions of the Gibbs equilibrium conditions are usually required. It is therefore often the case that radial distribution functions, which are coupled to interaction potentials through scattering data, are replaced with functions of reduced density and reduced temperature based upon simulations or PVT properties of a reference fluid. A fundamental understanding of complex interactions is therefore a vital component in the judicious pursuit of further advances in the design and control of complex chemical processes in technology and biology like the ones discussed above.

1.2. CHEMICAL ASSOCIATION

Atomic or molecular "clusters" generally consist of finite aggregates of atoms or molecules bound together by metallic, covalent, ionic, hydrogen-bonded, or van der Waals forces, and provide a bridge between the limits of isolated atoms or molecules and bulk matter. The nucleation process itself, along with the fundamental behavior of isolated, small clusters is typically the focus of cluster science, a rapidly expanding interdisciplinary field [11]. The evolution of system properties with cluster size and structure, however, is the major goal of statistical mechanics-

---

energies that the molecular arrangements and the concentrations of the components can be freely changed without affecting the system free energy [10].

based theories of chemical association. Furthermore, chemical association usually refers to reversible aggregation processes, characterized by ease of dissociation and relatively low energy of formation; examples include dimerization, polymerization, gelation, hydrogen bonding, coordinate covalent bonding, *etc.* —although occasionally chemical reactions are loosely grouped under the same rubric. Physical (as opposed to chemical) bonding forces are strong enough to hold all but the lightest atoms and molecules together in solids and liquids at room temperature, as well as in colloidal and biological assemblies. While *physical* bonds between discrete atoms or molecules in liquids often lack the specificity, stoichiometry, and strong directionality of *chemical* or *covalent* bonds, some types of physical bonds, such as hydrogen bonding, are difficult to model.

Reversible association, specifically hydrogen bonding, will be our focus in Chapters 4 and 5, and can be viewed from two different standpoints [12]: (i) either aggregates are thought to form and breakup continuously, or (ii) aggregates are thought to be concentration fluctuations of individual particles. Whichever approach is most useful depends entirely upon the fluid of interest. For short-ranged attraction, we generally speak of reversible aggregation, while for long-ranged attraction concentration fluctuations may be more appropriate. Typically concentration fluctuations are invoked to explain phase transitions, but no real physical difference exists between the two viewpoints, and thus reversible association can be equally thought to drive phase or structural transitions.

The definition of a "cluster" is, in fact, arbitrary, and we may think of two molecules as either belonging to the same cluster or as two separate particles whose position is correlated to the other by the influence of an attractive potential. Distinguishing inter– from intra-molecular forces can therefore be a vague one, as aggregated structures are somewhat "fluid-like", with molecules constantly moving around under thermal action, giving aggregate structures no definite size or shape, only a distribution about some mean value. This occurs because such structures are not held together by strong covalent or ionic bonds, but instead by the relatively weak van der Waals, hydrophobic, hydrogen bonding, or screened electrostatic bond interactions. Changes in external conditions, like pressure, temperature, concentration, *etc.* , will then not only affect the inermolecular interactions but also the intramolecular interactions.

Hence the choice of a monomer in associating fluids is not a trivial matter. Moreover, both theoretical and experimental evidence [13] indicate that the equilibrium distribution of aggregates may peak at more than one size. Hence small aggregates, *e.g.* dimers, trimers, or micelles, can be in thermodynamic equilibrium with much larger aggregates, like vesicles, in a single phase, or a single phase can be a cluster of infinite size. Variations in structure size or shape do not necessarily determine what constitutes a single phase; the Gibbs phase rule merely requires that the appropriate system properties be uniform throughout the phase. Aggregates may be large or even macroscopic and yet constitute a single phase so long as their number density in solution or space remains uniform throughout the whole system. At high enough concentrations, however, complicated structures can occur, and transitions to an ordered *mesophase*[5] are possible. Both attractive and repulsive forces between aggregates can lead to such *structural* transitions. When structural transitions are caused by attractive forces, the larger structures may separate out from, or coexist with, the smaller aggregates in solution. Understanding the phase behavior of such complex fluids means discerning how the intermolecular forces in and between aggregates influence phase boundaries.

Chemical association has a profound influence upon the general properties of complex fluids, and are generally characterized [14, 15] by several basic, unique features:

(1) Distribution functions which differ markedly from those of simple fluids. Generally, their distribution functions do not exhibit the typical damped oscillatory behavior beyond the first peak, instead often decaying rapidly to the asymptotic value of unity.

(2) Low coordination numbers. In simple fluids, approximately 12 molecules can be in the nearest neighbor coordination shell of any given central molecule, whereas that number for associating fluids is closer to 4 or 5. This is reflected in the unique shape of the distribution functions described above. Moreover, the temperature dependence of the coordination number in associating fluids

---

[5]A *mesophase* is a normal phase in the thermodynamic sense, but one that is more structurally complex than a simple liquid or solid. A mesophase may contain many small molecular aggregates that can be monodisperse or polydisperse. It can also have convoluted lamellar or tubular structures that link up into a (periodic) 3-dimensional network, *e.g.* a bicontinuous phase.

contrasts sharply with that of simple liquids. Water is a prime example: its coordination number *increases* slightly with temperature, while that for argon *decreases* rapidly [4, 14].

(3) The existence of relatively long-lived polymeric complexes. Spectroscopic studies [16–18] have provided experimental evidence for such complexes.[6] These complexes include everything from chains, to rings, to networks, from 2 molecules and upward in size. Understanding the influence of these structures on thermodynamic dependence of these

(4) Unusual thermodynamic properties. Many associating liquids display thermodynamic anomalies, which are thought to be characteristic of the relatively long-lived complexes found in such fluids. Water is the prototypical example, showing numerous thermodynamic anomalies such as its unusually high heat capacity and density maximum at 4°C.

Any fundamental yet comprehensive theory of association should be able to account for many or all of the above characteristic features. Yet judiciously defining meaningful "elements" or chemical monomers which elucidate the inherent structural properties of complex liquids is a difficult task using the standard methods of liquid state theory, in part because of the energy range of hydrogen bonds. Hydrogen bonds have energies of roughly $5\,k_BT$ to $15\,k_BT$, lying intermediate between the weaker van der Waals-like forces, which roughly correspond to the k_BT range, and the much stronger ionic and covalent forces, with energies of several hundred k_BT. Treating this large energy spectrum consistently and comprehensively is a difficult matter.

1.3. LE TOUT ENSEMBLE

Based upon the successes of the hard sphere model for treating simple fluids, there is a reasonable expectation that a simple model under the Wertheim

---

[6]During the late 1960s a new, polymeric form of water was believed to exist with unusual thermodynamic properties: it boiled at higher temperatures and froze at lower temperatures than regular water. It was named "polywater", and was even considered by some as a threat to life. The frenzy continued for years, until it was discovered that polywater was nothing more than water contaminated with impurities from the tubes in which it was made.

multi-density graph formalism is capable of predicting some of the unique structural and thermodynamic properties of hydrogen-bonded fluids (especially water!). Wertheim theory appears to uniquely capture the salient steric or connectivity properties prevalent in associating fluids like water, and so aptly suited to capture much of the thermodynamic and structural properties involved. Furthermore, a primitive model which allows for an analytic assessment could then act as a reference system (*e.g.* in perturbative expansions) for more complex fluids or fluid mixtures in much the same way as the hard sphere and Lennard Jones models have acted for simple liquids. Yet an analytical description of an associating fluid is a two-fold problem. It involves finding a model that (i) microscopically describes the salient features of association, and (ii) is also amenable to an analytical treatment by existing theories such that the system properties can be adequately determined.

Wertheim's multi-density theory of association [19–22] is one of the few approaches that incorporates short-ranged, highly anisotropic forces at the start of the analysis, and does so within a rigorous graph-based statistical mechanical formalism. In addition, his graphical formalism is easily generalized to the standard methods used to treat simple liquids, *i.e.* perturbation and integral equation theories. Using the statistical mechanics results of Andersen [23] and Lockett [24] concerning the graphical definition of molecular aggregates and their summation in the grand partition function, Wertheim found that through the introduction of *partial densities* which describe the state of molecular bonding, more meaningful aggregates could be defined. These aggregates, or in chemistry terms "s-mers", then allow for a more efficient evaluation of steric incompatibility effects (the exclusion of improper bonding configurations), thereby greatly simplifying the graphical summation of the logarithm of the grand partition function, and hence, all thermodynamic properties.

The aim of this work is the wholesale evaluation of Wertheim theory as pertains to a primitive model of association or hydrogen bonding. We do so by deriving all possible thermodynamic and structural quantities in order to test the predictive power of the theory, in hopes that it might illuminate some basic but elusive associating fluid properties, especially those of water —arguably the most important associating fluid. Although some previous work on the same model proposed here has been done using Wertheim theory, no one to our knowledge has set out to fully test the theory as we have. Previous work has focused largely upon

the calculation of the radial distribution function and structure factors, not taking advantage of the general applicability of Wertheim theory, such as the possibility to test its thermodynamic consistency.

What is new about our application of Wertheim theory to the sticky-spot model of hydrogen bonding? Apart from the comprehensive determination of system properties for this model, we investigate issues that include:

(1) The general thermodynamic and structural effects of dimerization upon a planar, liquid–vapor interface;

(2) The fundamental influence of connectivity constraints or saturable bonding in one– and four-site associating fluids;

(3) The calculation of all possible thermodynamic and structural properties of a network-forming fluid using both first-order thermodynamic perturbation theory (TPT) and integral equation theory (IET) methods;

(4) The calculation of an analytical direct correlation function and static structure factor for the four-site model;

(5) A full analysis of the thermodynamic self-consistency of the equation of state for the four-site, network-forming model, illuminating the inherent instability in the compressibility-derived results in the low density, high aggregation limit;

(6) The overall pathology of the model radial distribution function $g(r)$ for the four-site model.

We address these topics in two separate sections of this dissertation, Chapters 4 and 6. These chapters each represent an expansion of a paper published in the *Journal of Chemical Physics* [25, 26]. As such both chapters are essentially "self-contained" in that they have their own specific introductions and conclusions. In both cases we chose the simplest of all possible models for association such that we can obtain analytical results: a hard sphere with "sticky spots" on its surface representing hydrogen bonding sites.

Specifically, in Chapter 4, we set out to illuminate the effects of highly directional, short-ranged association (in this case dimerization) upon a planar liquid–vapor interface. For this chapter our associating monomer contains only one attraction site through which dimerization can occur. We use a planar interface topology precisely because its theory is well-known and amenable to analytic calculations. Next, in Chapter 5, we extend our association model to include

four sticky-spot attraction sites in order to explore the thermodynamic and structural properties of network-forming fluids like water. Our goal is to fully test the four-site model under the Wertheim formalism to see how well the connectivity constraints inherently built into the theory capture the subtle properties of liquid water. Treating inhomogeneous systems is straightforward within the Wertheim formalism, and so some critical point data and coexistence information is discussed as well as basic thermodynamics. The overall intent is to move one step closer to finding a representative model of hydrogen bonding which can act as a paradigm for future work.

Before discussing these issues, however, a brief overview of liquid forces, the nature of the hydrogen bond, and the standard methods of classical statistical mechanics that Wertheim theory commandeers in order to treat associating fluids is given in Chapter 2. Since Wertheim theory is manifestly a graphical formalism concerned with the optimization of topological reduction processes and our analysis centers around the influence of connectivity constraints, a detailed description of graphs in statistical mechanics and the process of topological reduction is provided in Chapter 3. Some lengthy derivations are given in these chapters, as well as in Chapters 4 and 5, and so the final results are marked in the text for convenience by black vertical lines set just inside the left margin of the text. The main equations or results of the theory are also marked by these black lines in order to separate them from intermediate steps or stages in the analysis. Final thoughts concerning the successes and failures of the theory in treating both models of hydrogen-bonding fluids are presented in Chapter 6.

2. LIQUID STATE THEORY

Madness takes its toll. Please have exact change.

—Unknown

2.1. INTRODUCTION

The modern theory of liquids began well over one hundred years ago when Thomas Andrews [27] discovered the critical point of carbon dioxide, establishing the gas–liquid phase transition. Several years later, in 1873, van der Waals introduced his phenomenological equation of state

$$P = \frac{Nk_BT}{(V - Nb)} - \frac{N^2}{V^2}\,a\,, \tag{2.1}$$

$$= P_b + P_a\,, \tag{2.2}$$

which assumes that molecules interact via strong short-range repulsion and weaker, long range attraction; the fluid pressure P then consists of a repulsive reference P_b contribution and a negative "perturbation" component P_a arising from intermolecular attraction. The constant b was approximated by the pressure of a one-dimensional hard sphere fluid while a was derived assuming that the fluid was homogeneous. Nonetheless, van der Waals equation predicted a gas–liquid coexistence regime (*i.e.* a critical point) in two- and three-dimensions, and became the cornerstone of our understanding of liquid structure and phase behavior. Since that time the gas–liquid transition has been shown to be an amazingly generic feature of all simple fluids,[1] each displaying the same "universal" and familiar phase diagram, Fig. (2.1) on the following page. For temperatures above the critical value T_c, the fluid can be continuously compressed all the way down to the freezing point (fluid–solid transition); if $T < T_c$, however, compression leads to a first-order phase transition, wherein the fluid suddenly separates into a low-density gas and a high-density liquid phase. The rapid appearance of a new phase is of considerable theoretical interest, for it signals a *cooperative* aspect of the intermolecular attractive forces. For simple fluids at least, the cooperative nature of

---

[1]Liquid helium is a notable exception.

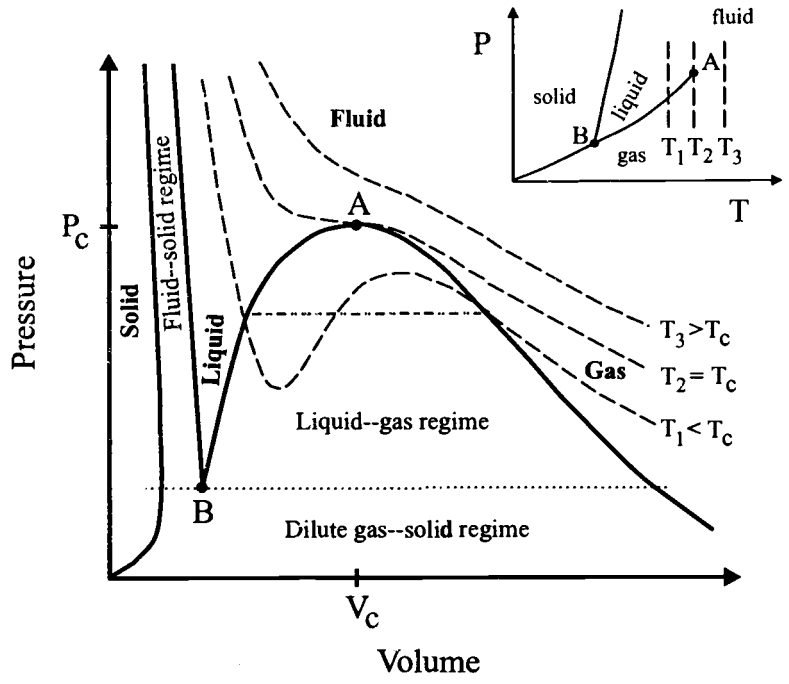

FIGURE 2.1. Typical phase diagram for simple substances. The thick solid lines indicate the boundaries between the given phases. Three Andrews isotherms, T_1, T_2, and T_3 above, at, and below the critical temperature are indicated by long-dashed lines. Point A corresponds to the critical point, below which is the two-phase region and above which only a dense fluid exists; point B corresponds to the triple point. The inset is the same diagram in P–T space, with the same 3 isotherms shown.

---

this transition can be understood as a consequence of the temperature-dependent interplay between the entropy loss due to molecular repulsion and an (isotropic) molecular attraction, as supported by the van der Waals theory [28, 29, 13]. If interactions are purely repulsive, the constant a in Eq. (2.2) becomes zero or negative and the resulting equation of state predicts a monotonic decrease of V with P: no gas–liquid transition is seen to exist. Clearly the influence of attractive forces is vital in the thermodynamic and structural description of even simple fluids.

Yet the van der Waals theory contains no information about the nature of intermolecular forces, being instead only a statement about the existence of repulsive and attractive forces. Furthermore, it is only exact in the limit of infinitely weak, long-ranged intermolecular interactions [30], and thus suggests no fundamental reason why the liquid–vapor transition should occur for every simple fluid;

nor does it expressly exclude any number of other structural or thermodynamic transitions. Any comprehensive theory, therefore, that aims to describe the more complicated phase behavior of complex fluids, must explicitly take into account the functional form of the complex molecular interactions. A rigorous statistical mechanics link between the underlying mean-field approximation and the range of the molecular interactions has long been known [31, 32], suggesting that a liquid–vapor transition should occur for any interaction potential which involves strong repulsion at short ranges and slowly varying attraction at longer ranges. The Lennard–Jones potential is perhaps the most well-known and studied potential fitting this description, and, indeed, it is often parameterized in order to fit equation of state data to model complex fluids. Yet it is evident that such a pairwise potential cannot comprehensively account for complex molecular interactions.[2] Apart from interaction range effects, modern theories must be able to incorporate orientational dependence (anisotropy) into the interaction models, and even with the availability of sophisticated computer simulation techniques, the situation is far from satisfactory.

The aim of liquid state theory is to understand the stability of particular phases in various temperature and density ranges, and to relate the stability, structure, and dynamical properties of the phases to the shapes of the molecules and the interactions between them. The problem is two-fold. Unlike the situation with simple fluids, wherein statistical mechanical-based theories are capable of predicting fluid behavior using simple interaction models, such as the hard sphere or Lennard–Jones fluid, no such general paradigms exist for complex fluids. Theories of complex or associating fluids are therefore tailored to the specific interactions thought to dominate the thermodynamic or structural behavior of the particular fluid of interest, thereby creating a myriad of approaches based upon the fluid type. As such, it is useful to loosely classify fluids according to the types of molecular interactions involved in their description.

---

[2]Often potential parameters are fit using scattering data, but there is no unique route from a given structure factor $S(k)$ to an interaction potential $u(r)$.

2.2. LIQUIDS & FORCES

The level of complexity necessary to describe various liquids of interest depends upon the complexity of the molecules themselves as well as their mutual interactions. Therefore it is useful to (loosely) classify liquids according to the types of interatomic or intermolecular forces present. Following Egelstaff [33], we can identify roughly eight fluid types:

(1) **Simple:** roughly spherical atoms or molecules interacting with van der Waals forces with steep overlap effects (*e.g.* Ar, Kr).

(2) **Homonuclear Diatomic:** similar to (1) but electric quadrupole moments and molecular shape are important (*e.g.* H_2, N_2).

(3) **Metals:** long range Coulomb forces with 'soft' overlap effects; electrical screening effects are important (*e.g.* Na, Hg).

(4) **Molten Salts:** ionic systems with long range Coulomb forces; screening effects create electric neutrality on a local scale (*e.g.* NaCl).

(5) **Polar:** simple molecules with large, permanent multipole moments (*e.g.* HBr).

(6) **Associated:** molecules which reversibly aggregate or 'self-assemble' through highly anisotropic attractive forces; lead to strong angular correlations or steric effects; hydrogen or coordinate covalent bonds (*e.g.* HF, H_2O, alkanols, amines).

(7) **Macromolecules:** large molecules or compounds which have important internal or *intra*-molecular modes of motion (*e.g.* polymers, proteins).

(8) **Quantum:** liquids in which quantum effects are important (*e.g.* He).

This categorization is by no means definitive, and classifying a general liquid might follow the flow chart shown in Fig. 2.2. We are concerned here with associating fluids, specifically hydrogen bonding, or category (6) in the list. The import of the hydrogen bond can be seen from Table 2.1, which compares boiling points of groups of compounds. Molecules of similar weights and size are arranged into groups of three: the first of each is non-polar and interacts via dispersion forces only, the second and third are polar, but the third also interacts via hydrogen bonds. Note (i) the dominance of H-bonding forces, even in very polar molecules like acetone, and (ii) the increasing importance of dispersion forces for larger

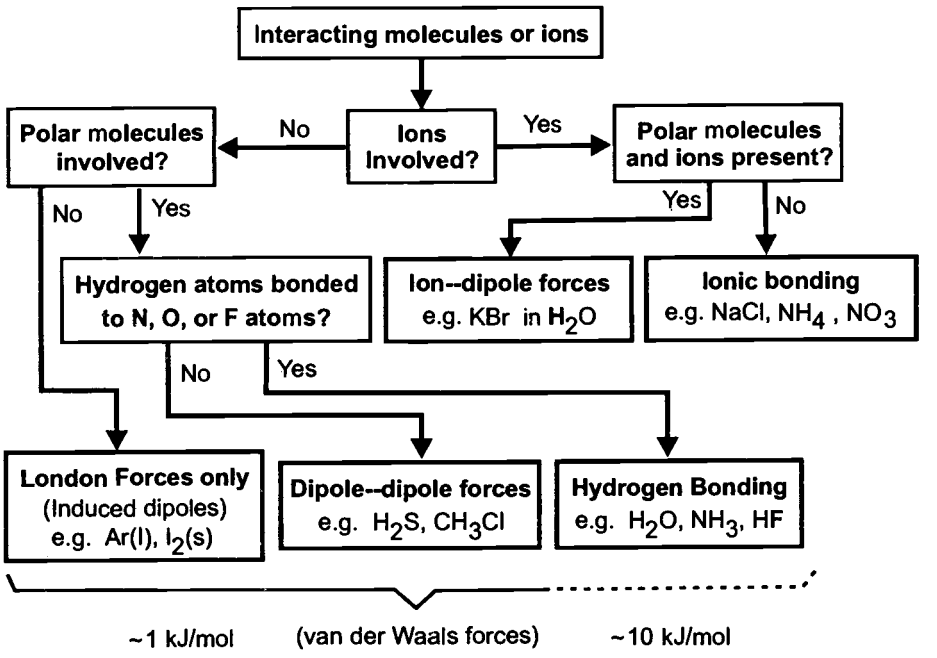

FIGURE 2.2. Flow chart of liquid classification scheme according to the intermolecular forces present.

TABLE 2.1. Relative interaction strengths of various compounds as reflected in boiling points [13]. Water has a dipole moment of 1.85 D in vacuum.

Impact of Hydrogen Bonding				
Molecule		**Molecular weight**	**Dipole moment (D)**	**Boiling point (°C)**
Ethane	CH_3CH_3	30	0	- 89
Formaldehyde	HCHO	30	2.3	-21
Methanol	CH_3OH	32	1.7	64
n-Butane	$CH_3(CH_2)_2CH_3$	58	0	-0.5
Acetone	CH_3COCH_3	58	3.0	56.5
Acetic acid	CH_3COOH	60	1.5	118
n-Hexane	$CH_3(CH_2)_4CH_3$	86	0	69
Ethyl propyl ether	$C_5H_{12}O$	88	1.2	64
1-Pentanol	$C_5H_{11}OH$	88	1.7	137

molecules. Dispersion forces generally bring molecules together, but they lack the directionality of dipolar or hydrogen bonds, and it is this characteristic that determines many of the subtle details of molecular and macromolecular structure. For relatively large molecules (excluding water), with dipoles of order $\sim$1D, for example, the dipole–dipole interaction is already weaker than k_BT at a separation of roughly 0.35 nm in vacuum, and becomes even smaller in a solvent medium. The hydrogen bond (H-bond), on the other hand, is approximately 5 k_BT–10 k_BT in the liquid state. A fundamental knowledge of the hydrogen bond is therefore important for many larger H-bonding molecules such as those in Table 2.1 because it can correspond to energies stronger than either dispersion or dipolar interactions. Dipolar forces in some (smaller) molecules like water are, of course, important, but the major influence of the H-bond in such liquids is still clearly evident.

Nevertheless, while hydrogen bonding is an important aspect in the study of many fluids and fluid mixtures, the fundamental nature of the bond itself is only partially understood. The H-bond was originally believed to be a quasi-covalent bond, sharing the proton between two electronegative ions [13], although now it is often described as a special type of dipole–dipole interaction. Even so, the underlying nature of the physical forces that hold the molecules together is not really understood. The forces that determine the bulk properties of liquids are, for the most part, electromagnetic, and, apart from small relativistic and retardation effects,[3] are electrostatic in character [34]: they originate from coulomb interactions between the electrons and nuclei.

Given the current level of computing power and modeling sophistication, we might be tempted to numerically solve the many-body Schrödinger equation (subject to the proper antisymmetry constraints) describing the motion of the electrons and nuclei,

$$\left[-\sum_i \frac{\hbar^2}{2m_i}\nabla_i^2 + \sum_{i<j}\frac{q_iq_j}{4\pi\varepsilon_0 r_{ij}}\right]\Psi = \frac{\hbar}{i}\frac{\partial\Psi}{\partial t},$$

where sums are taken over all electron and nuclei with appropriate masses m_i and charges q_i. Of course, for dealing with bulk fluids this many-body problem is far too complicated to even ponder, but even for relatively small, isolated molecules the

---

[3]These effects can be important when considering dispersion forces.

electronic interactions are nontrivial when H-bonds are involved (see next section). While several *ab initio* schemes exist [35], many more empirical or "force field" models can be found in the literature, relying upon the Hellman–Feynman theorem, which states that once the spatial distribution of the electron clouds has been determined by solving the Scrhödinger equation, the intermolecular forces may be calculated on the basis of straightforward classical electrostatics.

The condition used to qualify a classical treatment of molecular liquids involves comparing the molecular motions with the energy scale k_BT. A fluid is classical if we assume that all the molecular rotations can be treated classically (high temperature approximation) and that all the molecules are in their vibrational ground states (low temperature approximation), such that

$$\frac{\hbar^2}{2I} \ll k_BT \ll \hbar\omega_V\,, \tag{2.3}$$

where I is a molecular moment of inertia and ω_V is one of its pertinent vibrational frequencies. For nitrogen, N_2 for example, $\hbar^2/2Ik_B \approx 3$K and $\hbar\omega_V/k_B \approx 3000$K, showing a classical treatment to be reasonably valid at room temperatures. Two basic errors, nonetheless, are introduced by the use of classical statistical mechanics and statistics. First, we may be incorrect in computing the possible energy states of the many-body system when we add the classical kinetic and potential energies of the particles. The second error concerns the effect of quantum statistics in dictating the possible configurations allowed for the system. The basic condition for these quantum errors to be small is that the particles have sufficient thermal momentum such that they can be considered localized, namely

$$\rho\Lambda^3 \ll 1\,,$$

where ρ is the uniform liquid density and $\Lambda = [h^2/(2\pi mk_BT)]^{12}$ is the de Broglie thermal wavelength.

2.2.1. Hydrogen Bonding & Water

The "hydrogen bond" was first suggested over eighty years ago [36–39]. It occurs in fluids with hydrogen atoms, along with electronegative atoms like oxygen, nitrogen, or fluorine. The prototypical hydrogen-bonding fluid is water,

in large part because each H_2O molecule has two protons and two electron lone pairs, or four H-bond interaction sites, allowing for highly connected 3-dimensional networks of H-bonds to form. Other strongly H-bonded liquids include formamide, ammonia, or HF. Unlike the formation of covalent bonds, which involve massive shifts in electron density, the shifts associated with the formation of an H-bond are much more subtle [40]. There is an overall shift of the electron density from proton acceptor to donor, as in a coordinate covalent bond. This density is not only drawn from the lone pair taking part in bond however, but from the entire molecule. Rather than residing on bridging hydrogen, the density bypasses this charge center and becomes distributed throughout the donor molecule. The total electron density associated with central, bridging proton actually undergoes a decrease as the bond forms. The electron-depleted proton, because of its small size, gets pulled quite close to the electronegative donor atom (*e.g.* O, N, or F), such that the distance separating the non-hydrogen atoms involved in the H-bond, AH- - - B, is typically shorter than the sum of the vdW radii of A and B, for example; this creates an interaction energy larger than that predicted by a typical dipole–dipole. The bridging proton often tends to align with the connecting line between A and B, although the particular geometry becomes more complicated when more than one electron lone pair exists.

Describing this unique bond is made more difficult by this close approach between the proton and the electronegative atom. At large separations, electrostatic interactions can often be modeled as a multipole series: the dipole varies as r^{-3} while the ion–dipole goes as r^{-2}. The situation is much less clear cut when the molecules approach within H-bond distance. The multipole approach loses applicability in this case since, as the separation r decreases, the higher-order multipoles become important, and series does not easily converge. Full electrostatic interaction becomes more difficult to define unambiguously. Division of electrons or charge density becomes arbitrary at these distances. Lumped under the rubric of "penetration" terms in electrostatic interaction energy, these terms refer to the difference between the full electrostatic energy and the infinite summation of the multipole expansion. At an $r \simeq 3$Å separation, even summing the multipole series up through the sixth order significantly underestimates the full interaction term. Problems with the clear division of electron charge distribution as well as a relatively flat energy profile as compared to covalent bonds also leads to basis set

problems (Basis Set Superposition Error). It is important to note that quantum density functional theory methods bypass the conventional concept of individual molecular orbitals used in quantum chemistry, optimizing instead the total electron density. While these methods scale to a lower order with respect to the number of electrons, the results for modeling hydrogen bonds are, as yet, mixed [40]. Nevertheless, quantum methods are useful for refining interaction energies and electron redistributions that accompany (isolated) H-bond formation, as well as couplings to intramolecular motions.

To describe the thermodynamic and structural properties of hydrogen-bonded fluids like water on a macroscopic scale, on the other hand, a classical statistical mechanics approach is desirable, and follows from a number of simplifications. Since the nuclei are so much more heavy than the electrons, the Born–Oppenheimer approximation states that we can solve the electronic problem for stationary nuclei, thereby deriving a potential energy function U in terms of nuclear coordinates only. A second simplification arises from the fact that most intermolecular forces, including hydrogen bonds, are much weaker than the intramolecular forces (ionic and covalent) bonding atoms together into molecules. Hence, for relatively rigid molecules we can make the approximation that any coupling between intramolecular vibrations or motions of a molecule and all of its intermolecular interactions. The potential energy U then depends only upon the centers of mass (say) of the rigid molecules and their orientations, $U_N = U_N(\boldsymbol{r}_1, \boldsymbol{\Omega}_1, \ldots, \boldsymbol{r}_N, \boldsymbol{\Omega}_N)$.

In Chapters 4 and 5 we shall, in fact, treat our H-bonding molecules as rigid structures (hard spheres with anisotropic attraction sites), but it should be noted that even in this case, since these "molecules" act as our chemical monomers, the molecular aggregates they form are not necessarily rigid; their rigidity depends upon the bond angle constraints between the attraction or H-bonding sites. This issue will be discussed further in Chapters 4 and 5. Moreover, not all classical statistical mechanical models necessarily treat the molecules themselves as being rigid. Flexibility within such approaches inherently depends upon the definition of the basic building block of aggregation, or chemical monomer.

A sketch of the classical water molecules analyzed in Chapter 5 is shown in Fig. 2.3. The two protons (H) and two electron lone pairs (gray lobes) are tetrahedrally coordinated about the oxygen atom O. As these molecules or "monomers" approach, a proton pulls a lone pair L towards itself to form a linear H-bond, as

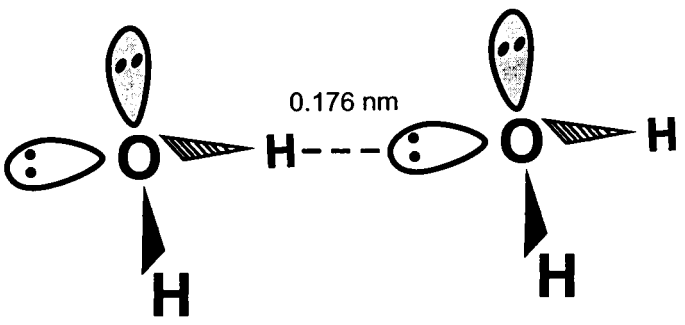

FIGURE 2.3. Classical sketch of the two water molecules forming a hydrogen bond. Covalent bonds (black triangles) between H and O atoms denote the water molecules, with the electron lone pairs indicated by the two black dots in shaded lobes. The hydrogen bond is indicated by the dashed line, with a bond length shown above; the equivalent vdW bond length would be 0.26 nm.

---

indicated in the sketch. For our single-site model in Chapter 4, each monomer will carry only one interaction site and like-site bonding will be allowed, but the general ideas of highly anisotropic and short-ranged attraction are the same. Such models are often called *structural models*. As compared to continuum models, structural models depend upon the assumption that a bond is so strongly orientational that it can be considered as either "made" or "broken", as in a chemical bond.

2.2.2. A Question of Structure

For any classical, macroscopic description of a liquid, a basic question naturally arises: What do we mean when we speak of "the structure of the liquid?" Shown in Fig. 2.4 is a logarithmic time scale of molecular motions for both ice and liquid water [4]. In this diagram of three basic structures of the liquid —we are not concerned here with ice— state, denoted by "D", "V", and "I", refer to the molecular diffusion, osciallation, and O—H stretching vibration time scales respectively. Our rigid, room-temperature, hydrogen-bonding systems in Chapters 4 and 5 both correspond to time scales that fall within the D-structure regime. Since hydrogen bonds form and break on time scales on the order of 10^{-11}s, when we speak of molecular aggregates, we shall essentially be referring to D-structure averages, like the average number of H-bonds per monomer N_{hb}.

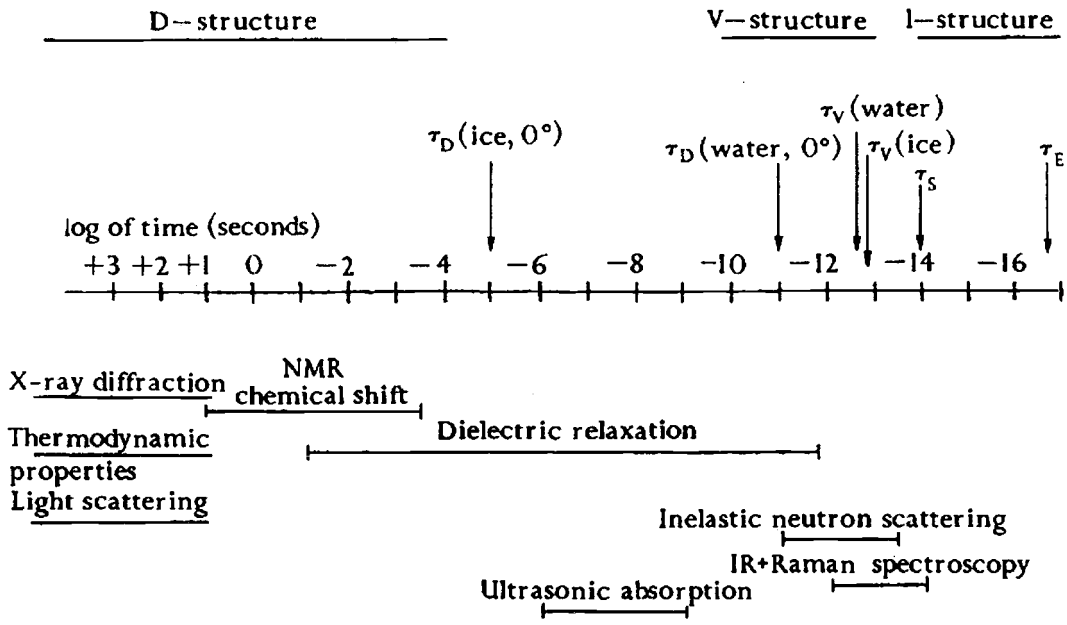

FIGURE 2.4. Time scales of molecular processes in ice and liquid water [4]. Vertical arrows mark periods associated with particular processes: τ_D , τ_V , and τ_S are representative periods for molecular displacement, oscillation, and an O–H stretching vibration respectively; τ_E is an (innermost) Bohr orbit period for an electron. The horizontal lines indicate experimental time scales.

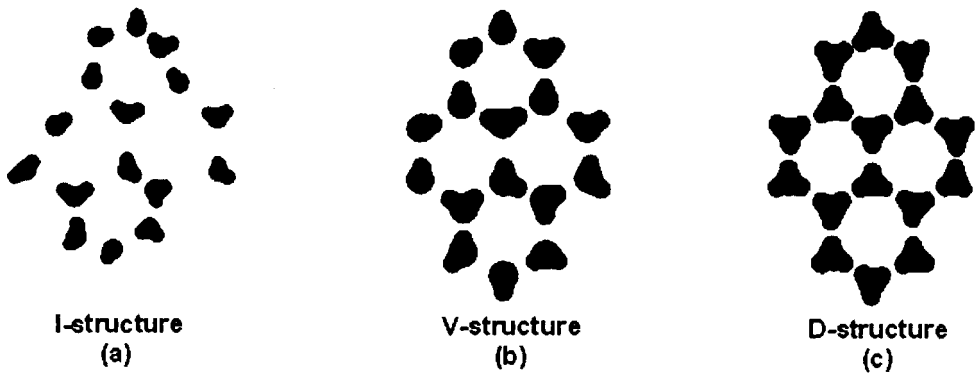

FIGURE 2.5. Different time scale structures of water. The "I-structure" (a), "V-structure" (b), and the diffusion averaged or "D-structure" (c) are defined by the time scales shown above in Fig. 2.4 [4]. The D-structures correspond to the relevant time scales for our discussion.

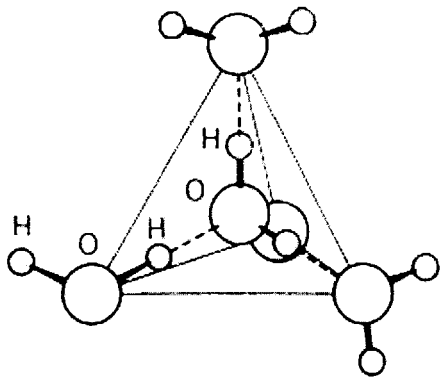

FIGURE 2.6. Sketch of tetrahedral bonding of water molecules [13]. Dashed lines indicate hydrogen bonds.

Looking at Fig. 2.5(c) we can already see traces of the tetrahedral coordination prevalent in water. Indeed, ice is known to retain much of its tetrahedral network structure upon melting, although that structure is now more disordered and labile. The average number of nearest neighbors rises to about 5 upon melting, but the mean number of H-bonds N_{hb} falls to roughly 3.5, with lifetimes estimated around 10^{-11}s. Moreover, H-bonds appear to be cooperative: the presence of H-bonds enhances their formation in nearby molecules, thereby propagating the tetrahedral structure. In this case, the H-bond interaction will not be pairwise additive.

Tetrahedral coordination, displayed in Fig. 2.6 lies at the heart of the unusual properties of water, perhaps more so, in fact, than the mere presence of H-bonds themselves [13]. Molecules that can participate in only one H-bond do not even show a liquid–vapor transition, and are limited to dimer formation. As we shall see in Chapter 4, dimer formation has little effect upon the structure of a fluid. Molecules that can form two H-bonds may combine into 1-dimensional chain or ring structures (*e.g.* HF, alcohols). For molecules that can participate in 3 H-bonds the situation is analogous to valence three atoms (*e.g.* arsenic, antimony, carbon in graphite): they can form two-dimensional sheets or layered structures held together by weaker vdW forces. Tetrahedral and higher coordination on the other hand, characteristic of carbon or silicon for example, can result in an almost infinite variety of aggregate structures, *e.g.* chains, polymers, surfactants, polypeptides, or two and 3-dimensional structures as diamond or silica.

The relationship between molecular aggregation processes and phase transitions in fluids is a subtle matter. The competition between structural energy and entropy is all the more complicated in associating fluids, where highly anisotropic attraction like hydrogen bonds are prevalent. Accurately describing the rich variety of aggregate and interface geometries is an outstanding challenge in classical liquid state theory. It is to these theories that we now turn.

2.3. THEORIES OF ASSOCIATION

The theory of associating fluids has a long and convoluted history, in part because of the variety and complexities of the relatively long-lived "clusters" of molecules that characterize such fluids. Loosely, all the various attempts to describe the behavior of associating fluids can be placed into three categories: (1) the chemical theory of solutions, (2) lattice theories, and (3) theories based upon statistical mechanics.

Methods in category 1, originating with that developed by Dolezalek [41], treat the strong, anisotropic attractive interactions in the fluid as chemical reactions which produce distinct species of aggregated molecules in the solution. If, for example, monomers A and B react to form the dimer C, we then have

$$A + B \rightleftharpoons C$$

with the corresponding equilibrium constant; the density of the "aggregate" species C, whatever it may be, is governed by the well-known *law of mass action.* Of course, for general associating fluid, species A and B may correspond to larger aggregate structures. Hence we are faced with some extremely large number of distinct, yet transient species which we are forced to arbitrarily specify as being present or not in the fluid. Furthermore, we must have some method of calculating all the attendant equilibrium constants together with their temperature dependence for each reaction. External relations are thus required in order to approximate the activity coefficients of all the transient complexes in the fluid, adding more adjustable parameters to the theory. While such a thermodynamic approach is rigorous, it is not very efficient or well suited for dealing with associating fluids on a microscopic level.

Lattice theories, on the other hand, assume that the fluid structure can be approximated by a solid-like lattice, with an initial structure that neglects the role of molecular properties in determining that structure. After making *a priori* assumptions about the arrangement of the molecules, it is possible to introduce simplifying approximations into the determination of the partition function that are analogous to those employed in the description of crystals. Various lattice models have been applied to mixtures of strongly interacting species (see Ref. [42] and references therein). Equations of state based upon lattice theories have been widely used in chemical engineering [43, 44]. Currently, lattice theories are mostly used to describe high-molecular-weight systems like polymers. For smaller systems the underlying lattice spatial constraints are too harsh, producing results that do not agree well with simulations [45]. However, there is renewed interest in lattice models. Of particular interest here is Zilman and Safran's look at the thermodynamics and structure of self-assembling chains that can branch to form networks [46]. The partition function of their generic model is mapped to onto that of a Heisenberg magnet in the mathematical limit of zero spin components. They predict the thermodynamic phase equilibria and the spatial correlations for their model the system. Nonetheless, lattice models seem to be limited in their predictive capabilities and do not offer a very clear picture of the relevant physics.

Perhaps the most promising route to a theory of associating fluids is through classical statistical mechanics, category (3) in our list. A statistical mechanics-based approach has several advantages over the previous two methods. No arbitrary structure constraints are imposed upon the molecules like there are in lattice theories. The theory determines what molecular clusters form in the solution and need not be arbitrarily defined beforehand. No external relations are required to calculate acitivity coefficients because the properties of the transient species are determined self-consistently within the theory through an *associative* law of mass action [19, 21]. There have been numerous approaches within statistical mechanics to model associating fluids; we shall only touch upon a few here, but a more thorough review is given in Refs. [47, 42, 48] Some of the main contributors to the effort include Cummings and Stell [49], Cummings and Blum [50], Andersen [23, 51], Zhou and Stell [52], Dahl and Andersen [53], Lockett [24], and finally Wertheim [19–22]. Several groups have made developments that underpin the unique approach of Wertheim, and so we shall review a few of them now.

Andersen presents one of the earliest theories of association and introduces steric incompatibility effects to renormalize the strength of the hydrogen bond. Since the hydrogen bond is short-ranged and highly anisotropic, the repulsive cores of other molecules will prevent any one attraction site from bonding with two or more sites on other molecules simultaneously (see Section 3.4.1 for more details). This effectively reduces the volume available for bonding, and Andersen uses this result to prevent non-physical results through graph cancellation.

Later Høye and Olaussen [54] extended Andersen's approach by using a fugacity instead of a density expansion in their analysis, where graph cancellations due to steric effects are more easily applied and satisfies the low density, low temperature limits more easily as well. From their study, Høye and Olaussen suggest that a renormalized perturbation expansion in terms of a monomer density would create a more rapidly convergent expansion than one written in terms of the overall density.

At about the same time, Lockett redefined the Mayer f-bond in the fugacity expansion in order to eliminate the non-physical traits of Mayer clusters (like non-interacting clusters and monomers) and put his modified Mayer clusters on an equal footing with the physical cluster methods.

Wertheim extended many of these ideas into a new theory with the added element of partial densities in the expansion that reflect the state of bonding and help impose the connectivity constraints due to steric incompatibility effects. Being based upon Lockett's split of the Mayer f-bond, the definition of a molecular cluster is still defined in terms of the potential energy only, and so satisfies the low density, low temperature limit as required. Also, Wertheim theory is a first-order theory in density, and so amenable to the standard methods employed for simple fluids. Wertheim theory has been extensively applied to mixtures of associating spheres as well as non-spherical and chain molecules, and it is in good agreement with simulations for such models. The theory has also been used to develop an equation of state formally known as the statistical associating fluid theory (SAFT) to treat many complex molecules like aromatics, alkanols, amines, esters, ketones, and polymers with large molecular masses.

The generality of Wertheim theory means that we can directly transfer its graphical formalism based upon statistical mechanics to the standard perturbation and integral equation methods used for simple liquids. Below we briefly review

those methods to build a foundation for the basic quantities that we shall rewrite in our graph analysis.

2.3.1. Classical Statistical Mechanics

For an ideal gas, where particles do not interact, that summation can be reduced to a sum over single particle states (independent of their occupation numbers), which, in turn can be reduced to an integral over the density of states $\rho(\varepsilon)d\varepsilon$ so long as the relation between the single particle energy ε and momentum p is known:

$$Z = \int d\varepsilon \, \rho(\varepsilon) e^{-\varepsilon/k_B T}$$

When particles interact, the summation is not so trivial. In some cases it is possible to take a system of interacting particles and describe its quantum states as being comprised of (possibly imaginary) *quasi-particles*, each having some energy and momentum but not interacting with each other. These new "particles" are actually collective states of the system, photons in an electromagnetic field, phonons in a crystalline solid, electrons in a metal, or cooper pairs in a superconductor for example. Once the appropriate relation between ε and p has been found, the partition sum for the resulting perfect gas of quasi-particles reduces to the same simplified integration over the density of states $\rho(\varepsilon)d\varepsilon$ above.

Unfortunately, not all the thermal behavior of interacting matter can be "reduced" to one kind or another of noninteracting quasi-particles. In fact, no such method has been found to describe classical liquids, or fluids in general. Hence we are left with trying to evaluate the infinite sum of the appropriate partition function in some other fashion. It is to this task that we now turn.

For a classical fluid, where no two particles can have the same positions and momenta, the distinguishable volume of phase space is simply the total volume divided by all possible ways, $N!$, in which the classical particles can be distributed in that volume

$$\rho(\mathcal{E})d\mathcal{E} = \frac{1}{N!} \frac{d\{\mathbf{p}_i\}d\{\mathbf{r}_i\}}{(2\pi\hbar)^{3N}},$$

where $\mathcal{E}$ is the system or many-body energy and $\{\mathbf{p}_i\}$ is shorthand notation for the product $\mathbf{p}_1 \cdots \mathbf{p}_i$, *etc.* , wherein i runs from 1 to N.[4] Under the classical approximation discussed in Chapter 2, the contributions to thermodynamic properties that arise from the thermal motion of particles can be separated from those due to the interactions between particles, *i.e.* $\rho\Lambda^3 \ll 1$, which, in terms of the total kinetic K_N and potential energy U_N of the liquid [55], means $K_N/|U_N| \sim 1$. Hence K_N depends only upon the momenta and U_N only upon the coordinates,

$$\mathcal{E}(\{\mathbf{p}_i\},\{\mathbf{r}_i\}) \;=\; \sum_{i=1}^{N} \frac{\mathbf{p}_i^2}{2m} \;+\; U(\{\mathbf{r}_i\}) \;,$$

which, after integration over the momenta, gives a canonical partition function of the form

$$Z \;=\; \frac{Z_{id}}{V^N}\, Q_N(V,T) \;=\; \frac{Q_N(V,T)}{N!\,\Lambda^{3N}} \;,$$

$$Z_{id} \;=\; \frac{1}{N!}\left(\frac{V}{\Lambda^3}\right)^N, \quad \Lambda \;=\; \frac{2\pi\hbar}{\sqrt{2\pi m k_B T}} \;,$$

where Z_{id} is the ideal gas contribution, Λ is the de Broglie wavelength, and $Q_N(V,T)$ is defined as the N-particle *configurational* integral

$$Q_N(V,T) \;=\; \int\cdots\int d\{\mathbf{r}_i\}\; \exp\Big[-U(\{\mathbf{r}_i\})/k_BT\Big] \;, \tag{2.4}$$

and represents the cohesive energy of the fluid. It is precisely this many-body *configurational* integral that is the crux of liquid state theory, that compels the use of pictures in the description of classical fluids. The inherent split into *ideal* and *excess* components here is also an important aspect in our approach and will touched upon later.

Any theoretical progress concerning Eq. (2.4), pictures or not, requires some approximation of the many-body potential $U(\{\mathbf{r}_i\})$. The standard approach at this point is to assume

$$U(\{\mathbf{r}_i\}) \;=\; \sum_{1\leqslant i<j\leqslant N} u(\mathbf{r}_i,\mathbf{r}_j) \;+\; \sum_{1\leqslant i<j<k\leqslant N} u(\mathbf{r}_i,\mathbf{r}_j,\mathbf{r}_k) \;+\; \cdots \;. \tag{2.5}$$

The two-body potential $u(\mathbf{r}_i,\mathbf{r}_j)$ is defined as that between two isolated molecules, with any modifications therein by the presence of other molecules included in

---

[4]More generally these spatial coordinates $\mathbf{r}$ also include orientational information for each molecule: $\mathbf{r}_i \to \mathbf{r}_i, \boldsymbol{\Omega}_i$ for those cases.

TABLE 2.2. Properties of various perturbation contributions to intermolecular energies [56].

INTERMOLECULAR INTERACTIONS			
Type	**Range**	**Attractive or Repulsive**	**Pairwise Additive**
Electrostatic	Long	Either	Yes
Dispersion	Long	Attractive	No
Induction	Long	Attractive	No
Exchange	Short	Repulsive	Yes
Exchange Polarization or charge transfer	Short	Attractive	No

higher-order terms, such as $u(\mathbf{r}_i, \mathbf{r}_j, \mathbf{r}_k)$. Each potential is also often assumed to be independent of P, V, and T. The intent here is that the two-body terms will dominate the sum (2.5) so that it can be truncated at the two-body terms, resulting in what's called *pair theory*. This approximation, born out of necessity more than anything, but it not too drastic[5] for simple and some (rigid) molecular liquids (*e.g.* types (1) and (7) in Section 2.1). In Table 2.2 is list displaying which forces are pairwise additive and which not. Since the hydrogen bond seems to be cooperative in nature, it too should not be a pairwise additive interaction, but for as a first step towards a basic model we shall assume that it is. Many-body effects are also important, for example, in polarization interactions and can significantly affect dispersion interactions. Axilrod and Teller [57] have determined the three-body contribution to the dispersion interaction (also known as the triple-dipole correction).

With our interactions now limited to be pairwise additive, we proceed to review the basic statistical mechanics involved in the theory. The grand canonical ensemble is appropriate for the description of an open (associating) system in which there is an interchange of molecules and energy with the surroundings, *i.e.* a

[5]Such assumptions are not valid, say, for liquid metals.

system characterized by the state variables T, V, and μ. Moreover, the fundamental relation $\beta PV = -\ln \Xi$ is central to the Wertheim analysis, as will be shown later. For a unary fluid of N particles interacting via pairwise-additive forces and in an some external potential $\phi(i)$, the grand canonical partition function is

$$\Xi(\mu, V, T) \;=\; \sum_{N=0}^{\infty} e^{\beta\mu N} \frac{Q_N(V,T)}{N!\,\Lambda^{3N}}\,, \tag{2.6}$$

where the configuration integral is

$$Q_N(V,T) \;=\; \int\cdots\int d\{\boldsymbol{i}\}\, \exp\Big[-\beta \sum_{1\leqslant i<j\leqslant N} \{u(\boldsymbol{i},\boldsymbol{j}) - \phi(\boldsymbol{i})\}\Big]\,. \tag{2.7}$$

For convenience we let $d\{\boldsymbol{i}\} \equiv d\mathbf{1}\cdots d\mathbf{N}$, where the 3-dimensional spatial coordinates like $d\mathbf{1}$ are defined as $d\mathbf{1} \equiv d\mathbf{r}_1$, and so on. We shall use this abbreviated notation for spatial coordinates hereafter. Now introduce the *local fugacity*

$$z(\boldsymbol{i}) \;\equiv\; \Lambda^{-3} e^{\beta[\mu N - \phi(\boldsymbol{i})]} \;=\; z\, e^{-\beta\phi(\boldsymbol{i})}$$

into the grand partition function can be written as

$$\Xi(\mu, V, T) \;=\; \sum_{N=0}^{\infty} \frac{1}{N!} \int\cdots\int d\{\boldsymbol{i}\}\; z(\mathbf{1})\cdots z(\mathbf{N}) \prod_{i<j}^{N} e^{-\beta u(\boldsymbol{i},\boldsymbol{j})}\,. \tag{2.8}$$

All thermodynamics now follow from this infinite sum. This is where we turn to graph theory to do so in a meaningful and efficient fashion. However, it should be noted that by doing so we effectively lose all structural information implicit within the Hamiltonian, *i.e.* is "lost" by integrating over all the coordinates. If we integrate over all but one or two coordinates, then we can obtain structural information from $\ln \Xi$.

The process of functional differentiation defines the distribution functions which provide structural information about the system. The general s-particle distribution can be found by repeated functional differentiation of Ξ,

$$\rho(\mathbf{1},\ldots,\mathbf{s}) = \frac{1}{\Xi}\, z(\mathbf{1})\cdots z(\mathbf{s})\, \frac{\delta^s \Xi}{\delta z(\mathbf{1})\cdots \delta z(\mathbf{s})} \tag{2.9}$$

$$= \frac{1}{\Xi} \sum_{N=s}^{\infty} \frac{1}{(N-s)!} \int\cdots\int z(\mathbf{1})\cdots z(\mathbf{N}) \prod_{i<j}^{N} \left[1 + f(\boldsymbol{i},\boldsymbol{j})\right] d(\mathbf{s}+\mathbf{1})\cdots d\mathbf{N}\,,$$

where the Boltzmann factor $\exp[-\beta u(i,j)]$, abbreviated as $e(i,j)$, has been replaced by the Mayer f-bond, $e(i,j) = 1 + f(i,j)$. In statistical mechanics it is usually the logarithm of Ξ that defines thermodynamic quantities, and as such we shall be interested in functional derivatives of $\ln \Xi$ as well. This distinction serves to define "truncated" s-particle distribution functions, also known as Ursell functions,

$$\hat{\rho}(\mathbf{1},\ldots,\mathbf{s}) \;=\; z(\mathbf{1})\cdots z(\mathbf{s})\,\frac{\delta^s \ln \Xi}{\delta z(\mathbf{1})\cdots\delta z(\mathbf{s})}\,, \tag{2.10}$$

which will also play a central role in our graphical analysis. Specifically, all bonding information within Wertheim theory (*i.e.* the partial densities) will be contained in the singlet density $\rho(\mathbf{1})$. Structural properties within pair theory, however, will also entail one- and two-body correlations, so it is important to note that

$$\rho(\mathbf{1}) \;=\; \hat{\rho}(\mathbf{1})\,, \quad \rho(\mathbf{1},\mathbf{2}) \;=\; \hat{\rho}(\mathbf{1},\mathbf{2}) \,+\, \rho(\mathbf{1})\rho(\mathbf{2})\,. \tag{2.11}$$

2.3.2. Integral Equation Theories

Many basic thermodynamic quantities relevant to phase coexistence are expressible in terms of structural functions which measure the degree of correlation between pairs of monomers. For homogeneous isotropic fluids the most well-known of these correlation functions is the radial distribution function $g(r)$ or RDF. The RDF measures the probability that given a particle at the origin, another particle in the fluid can be found a distance r away, and can be related to the intermolecular potential by exact (although not unique!) relations. These "exact" relations involve either three-body correlations, giving rise to an infinite hierarchy of equations, or the so-called "bridge function" which, though in principle known as a summation of infinite terms, is not expressible in terms of the RDF itself in closed form [58, 55].

Some approximation or closure condition is therefore required in order to determine the RDF or any another correlation function, and these approximations typically involve integral or integro-differential equations; hence the rubric *integral equation theory* (IET). Approximations to the pair correlations, through either their relation to the interaction potential or higher-order correlations, are essentially approximations to the full many-body structural problem. Frequently

the complexity of the closure scheme (*e.g.* interaction potential) requires numerical procedures for solution, but analytically solvable IETs should allow for a full description of the critical region and critical exponents [59].

The general s-particle distribution function from which the RDF originates is defined as

$$g(\mathbf{1},\ldots,\mathbf{s}) \equiv \frac{\rho(\mathbf{1},\ldots,\mathbf{s})}{\rho(\mathbf{1})\cdots\rho(\mathbf{s})},$$

whereas the *total* s-particle correlation function is defined in terms of the truncated densities:

$$h(\mathbf{1},\ldots,\mathbf{s}) \equiv \frac{\hat{\rho}(\mathbf{1},\ldots,\mathbf{s})}{\rho(\mathbf{1})\cdots\rho(\mathbf{s})}.$$

Within pair theory we are ultimately concerned only with calculating the two-body correlations

$$g(\mathbf{1},\mathbf{2}) = \frac{\rho(\mathbf{1},\mathbf{2})}{\rho(\mathbf{1})\rho(\mathbf{2})}, \tag{2.12}$$

$$h(\mathbf{1},\mathbf{2}) = \frac{\hat{\rho}(\mathbf{1},\mathbf{2})}{\rho(\mathbf{1})\rho(\mathbf{2})}. \tag{2.13}$$

From Eq. (2.10) the general relation between these two correlations can be seen to be

$$g(\mathbf{1},\mathbf{2}) = h(\mathbf{1},\mathbf{2}) + 1, \tag{2.14}$$

and they are thus both related to scattering data through the static structure factor, which can be written as $S(\boldsymbol{k}) = 1 + \rho\tilde{h}(\boldsymbol{k})$ for a homogeneous fluid, where $\tilde{h}(\boldsymbol{k})$ is the Fourier transform of $h(\mathbf{1},\mathbf{2})$ [33, 55]. This link is useful, but since there is not usually a unique potential curve that reproduces a particular experimental observation, it is by no means comprehensive. There is also typically no analytical connection between observations and interaction potentials, making theoretical descriptions more important.

For molecular fluids these functions are, of course, angle-dependent, such that complete pair distribution function can be generally written as $g(\boldsymbol{R}_{12},\boldsymbol{\Omega}_1,\boldsymbol{\Omega}_2)$, where the coordinates $\boldsymbol{R}_i$ are usually taken to be the molecular center of mass or some other point of high symmetry in the molecule and the $\boldsymbol{\Omega}_i$ are the molecular orientations, often described in terms of the Euler angles. Treating the angular

dependence in these correlation functions is a non-trivial matter. A simple unweighted average over the molecular orientations produces the RDF of molecular "centers",

$$\begin{aligned} g(R_c) &= \Omega^{-2} \iint d\Omega_1 d\Omega_2 \; g(\boldsymbol{R}_{12}, \Omega_1, \Omega_2) \,, \\ &\equiv \langle g(\mathbf{1},\mathbf{2}) \rangle_{\Omega_1 \Omega_2} \,, \end{aligned} \tag{2.15}$$

where Ω is the normalization constant $\Omega = \int d\Omega_i$ and equals 4π for linear and $8\pi^2$ for non-linear molecules. This is essentially the approach we shall take in this work since we will be treating our aggregating particles (dimers and water molecules) as rigid spheres with no internal degrees of freedom; that is, we factorize the kinetic and configurational phase-space densities of our monomers when we use the modified Mayer formalism of Lockett [24] in order to define our physical clusters in terms of potential energy alone —this will be discussed in detail in Chapter 3. Such a simplification does not work in general for molecular distributions because of the many-dimensional nature of the molecular pair distribution function.

Finding practical routes to thermodynamic system properties is extremely subtle and complicated in this case: the full shape of $g(\mathbf{1},\mathbf{2})$ is difficult even to visualize. Two different approaches are worth mention here: one is to expand $g(\mathbf{1},\mathbf{2})$ or $h(\mathbf{1},\mathbf{2})$ in a series of suitably-chosen, angle-dependent basis functions, while the other is to describe the correlations in terms of site–site distribution functions instead. The first method entails expanding $g(\mathbf{1},\mathbf{2})$ or $h(\mathbf{1},\mathbf{2})$ in terms of functions like the Wigner rotation matrices or generalized spherical harmonics [55]. Such methods are, in fact, currently used to describe four-site models like water [60], and can nominally reproduce the tetrahedral structure of the molecule, but do not allow analytical results and further present convergence issues when molecules approach within hydrogen bonding distance (discussed in Chapter 5). The second approach involves treating the intermolecular interaction sites of the model as the primary constituents of the theory; that is, sites are not "linked" to the molecule on which they reside, with some sites corresponding to atomic centers and others to off-center, directional attraction sites. While the site–site distribution functions can be directly related to the structure factors measure in scattering experiments, they too cannot be solved analytically and often cannot be easily related to thermodynamic functions. The *Reference Interaction Site Method* (RISM) is one example of such a site–site approach.

While the full molecular distribution functions $g(\mathbf{1},\mathbf{2})$ or $h(\mathbf{1},\mathbf{2})$ can (numerically) describe accurate short-range fluid correlations (see Ref. [55] for a detailed review), and the angle-averaged "atomic" versions can be used to obtain system thermodynamics, we need limit ourselves to these distributions, especially concerning inhomogeneous fluids. Shorter-ranged correlations are more easily approximated in inhomogeneous as well as homogeneous systems, and the direct correlation function $c(\mathbf{1},\mathbf{2})$ is just such a function.

The direct correlation function is not only shorter-ranged than either $g(\mathbf{1},\mathbf{2})$ or $h(\mathbf{1},\mathbf{2})$, but is also simpler in structure. This function is usually defined by the Ornstein–Zernike (OZ) equation,

$$h(\mathbf{1},\mathbf{2}) \;=\; c(\mathbf{1},\mathbf{2}) \;+\; \int d\mathbf{3}\; c(\mathbf{1},\mathbf{3})\rho(\mathbf{3})h(\mathbf{3},\mathbf{2})\,. \tag{2.16}$$

Ornstein and Zernike originally derived this relation to describe the phenomena of critical point opacity. The OZ equation can be generalized to mixtures as well as the multi-density graphical formalism of Wertheim. In fact, in Wertheim theory the OZ relation becomes an *associated,* matrix equation whose dimensions depend directly upon the number of attraction sites on each monomer and is generally referred to as the AOZ. We shall further discuss this topic in Chapter 5 for our four-site model of water.

As a convolution, its solution for $c(\mathbf{1},\mathbf{2})$ requires a closure condition, just as mentioned before. Approximations for $c(\mathbf{1},\mathbf{2})$, however, are more easily accomplished than those for $g(\mathbf{1},\mathbf{2})$ or $h(\mathbf{1},\mathbf{2})$. Two common closure conditions are the *hypernetted chain approximation* (HNC) and the *Percus–Yevick approximation* (PY), given as

$$c(\mathbf{1},\mathbf{2}) \;\simeq\; h(\mathbf{1},\mathbf{2}) - \ln[g(\mathbf{1},\mathbf{2})] - \beta u(\mathbf{1},\mathbf{2}) \qquad \boxed{\text{HNC}}, \tag{2.17}$$

$$c(\mathbf{1},\mathbf{2}) \;\simeq\; g(\mathbf{1},\mathbf{2})\{\,1 - \exp[\beta u(\mathbf{1},\mathbf{2})]\} \qquad \boxed{\text{PY}}, \tag{2.18}$$

The PY equation can be solved analytically for hard spheres, which will act as our reference system in our primitive model of association, and so it is the PY approximation that we shall use to solve for our direct correlation function.

For treating the long range attractive contributions in our calculation of these correlations, like the mean-field dispersion interaction we employ in Chapter 4, we use the *Mean Spherical Approximation* (MSA), which originated from the

fact that the approximation was first proposed as a generalization of the mean-spherical model of Ising spin systems [61]. The MSA is commonly used for fluids with hard sphere repulsion coupled with an attractive tail, such as "square-well" and dipolar hard sphere fluids. In fact, the MSA describes the square-well fluid better than either the PY or HNC approximations [62]. Moreover, the MSA can be solved analytically for a number of potentials, including the one here. The PY equation for hard spheres is simply the special case of the MSA when the tail of the potential is absent. The MSA takes the form

$$g(\mathbf{1},\mathbf{2}) = 0, \qquad r_{12} < R, \tag{2.19a}$$

$$c(\mathbf{1},\mathbf{2}) = -\beta u(\mathbf{1},\mathbf{2}), \qquad r_{12} > R; \tag{2.19b}$$

The first equation is exact, but the second stretches the asymptotic behavior of $c(\mathbf{1},\mathbf{2})$ to all distances $r_{12} > R$.

These closure conditions are described in terms of graph theory briefly in Appendix C. The full, analytical solution of the AOZ equation, however, still requires a complicated, intricate factorization procedure to solve. For brevity we shall omit a discussion of the details of that factorization until Chapter 5. Once these two correlations are solved for, the radial distribution function follows from an associated version of Eq. (2.14).

2.3.3. Thermodynamic Perturbation Theories

Solving the integral or integro-differential equations in IET methods must often be carried out numerically for typical interaction potentials, and are computationally intensive. Thermodynamic perturbation theories (TPTs), on the other hand, allow for relatively complicated interaction potentials to be treated on a level equal to thermodynamic or distribution functions of a simpler system chosen as the reference. Such methods are analogous to classical thermodynamic treatments with appropriately selected standard states and expansions of the excess functions (see Ref. [63] for a review of TPT methods).

The general assumption in perturbation theories is that the system free energy can be expanded in powers of inverse temperature β or some coupling parameter λ about $\beta = 0$ or $\lambda = 0$ respectively. The system potential energy U is then split into a reference or standard state U_0 and a small perturbation U_p, which may vary continuously from zero ($\lambda = 0$) up to U_p ($\lambda = 1$) in the general coupling

parameter expansion, namely

$$U = U_0 + \lambda U_p, \quad 0 \leq \lambda \leq 1,$$

such that the expansion can be written

$$A = A_0 + (\partial A/\partial\lambda)_0 \lambda + \tfrac{1}{2}(\partial^2 A/\partial\lambda^2)_0 \lambda^2 + \cdots$$

where

$$\begin{aligned}(\partial A/\partial\lambda)_{\lambda=0} &= \left[Q^{-1}\int\cdots\int d\{\mathbf{N}\}\, U_p \exp[-\beta U]\right]_{\lambda=0}, \\ &= \langle U_p\rangle_0 \equiv Q_1 \\ (\partial^2 A/\partial\lambda^2)_{\lambda=0} &= -\beta\left[\langle U_p^2\rangle_0 - \langle U_p\rangle_0^2\right] \equiv -\beta Q_2, \ \ldots\end{aligned}$$

and the angled brackets with subscript 0 denote the average over all configurations of the reference system. The second-order terms, Q_2, account for potential energy fluctuations in the reference system configuration, but for high temperatures or small perturbations, only the first-order term is usually kept,

$$(\beta A/N) = (\beta A_0/N) + \int_0^1 d\lambda \frac{\beta\langle U_p\rangle_\lambda}{N}.$$

If U_p is limited to pairwise interactions $u(r)$, then from the definition of the pair distribution function,

$$\frac{\beta\langle U_p\rangle_\lambda}{N} = \frac{1}{2}\beta\int dr\ 4\pi r^2 g(r;\lambda)u_p(r),$$

where the radial distribution function generally depends upon λ. For high enough densities or where repulsive forces dominate, only the first-order term is important: $g(r;\lambda) \simeq g_0(r)$. Thus the utility of TPT methods depends upon the extent to which the radial distribution function for the reference fluid is known.

For hard sphere potentials, the PY solution for $g_0(r)$ is known analytically [55], but for more realistic potentials, where repulsive forces are described by power law or exponential terms, the choice of the reference system is much less straightforward. Numerous approaches exist, like those of Weeks, Chandler, and Andersen (WCA) [64] or Barker and Henderson (BH) [65] for roughly spherical, neutral molecules, where the repulsive properties of the reference fluid are determined from a second perturbation expansion about the free energy of a hard

sphere fluid. When attractive interactions become important these theories fail unless a large, component of the attractive potential, typically approximated as a Lennard–Jones interaction, can be included in the reference contribution. The properties of such a reference fluid, however, usually must be determined by computer simulations.

If there exist any weak, anisotropic attraction terms, then they may be treated as a perturbation, although convergence may be slow. In fact, in Chapter 4 we use a simplified version of WCA to treat our reference fluid of hard spheres interacting via weak, long range dispersion forces. For strong, highly anisotropic attractive forces, on the other hand, such as in associating fluids, perturbation theories theories like WCA or BH manifestly fail because of the large internal energy contributions which arise from chemical association like hydrogen bonding. In such cases the strong, highly directional attractive forces must be incorporated into the theory early in the analysis instead of as a perturbation.

In Chapters 4 and 5 we introduce the Wertheim TPT equation of state derived graphically in terms of his partial densities and direct correlation generating functional. By renormalizing the Boltzmann factors in his graphical analysis of βPV in order to directly incorporate strong association effects, we are then able to calculate a system Helmholtz free energy through the simple thermodynamic relation $-PV = A - \mu N$.

2.3.4. Density Functional Theory

Classical density functional theory (DFT) may be considered as a reformulation of statistical mechanics using the language of generating functionals [66], wherein the inhomogeneous free energy is expressed as a functional of the average one-body density $\rho(\mathbf{1})$ that characterizes the inhomogeneity of the system. The DFT approach focuses on functionals of $\rho(\mathbf{1})$ and is therefore perfectly suited for application to the graphical formalism of Wertheim theory. It can be proven [67–70] that for a given total interaction potential U, the Helmholtz free energy $A[\rho]$ of any system at fixed temperature T and external potential $\phi(\mathbf{1})$ is uniquely minimized when a *trial* singlet density $\tilde{\rho}(\mathbf{1})$ is equal to the equilibrium one-body density $\rho(\mathbf{1})$. Functionals are generally denoted by the use of square brackets enclosing their argument functions, *e.g.* $A[\rho] = A[\rho(\mathbf{1})]$. The density profile for the inhomogeneous fluid $\rho(\mathbf{1})$ in DFT is obtained through the usual variational

principle

$$\left[\frac{\delta\Omega[\tilde{\rho}(\mathbf{1})]}{\delta\tilde{\rho}(\mathbf{1})}\right]_{\tilde{\rho}=\rho} = 0 \tag{2.20}$$

applied to the grand canonical potential

$$\Omega[\rho] = A[\rho] - \int d\mathbf{1}\ [\mu - \phi(\mathbf{1})]\,\rho(\mathbf{1})\,, \tag{2.21}$$

where μ is the chemical potential; the resulting Euler–Lagrange equation involves the *intrinsic* free energy $A[\rho]$ describing the constancy of the chemical potential throughout the inhomogeneous fluid,

$$\mu = \frac{\delta A[\rho]}{\delta\rho(\mathbf{1})} + \phi(\mathbf{1})\,. \tag{2.22}$$

Any practical implementation of classical DFT for a particular physical problem therefore requires an explicit form for the functional $A[\rho]$. The exact functional, of course, would require an exact solution of the system partition function, and so more or less complicated approximation schemes for $A[\rho]$ are required in all but a few rare (usually 1-D) cases. There are several routes available for the calculation of the Helmholtz free energy; the typical starting point is a suitably chosen free energy as a function of the homogeneous density ρ, followed by the assumption that the same functional form for the inhomogeneous case is similarly related to the inhomogeneous density $\rho(\mathbf{1})$; boundary conditions then dictate how the inhomogeneous aspects appear while the nonlocal nature of the potential determines how such effects propagate. Once the functional $A[\rho]$ is known, the equilibrium $\rho(\mathbf{1})$ and grand potential Ω are determined for a given T, μ, and $\phi(\mathbf{1})$ by minimizing Eq. (2.21). All equilibrium properties are then available, but it should be kept in mind that when $A[\rho]$ is simply a judiciously chosen functional, there is no guarantee that the resulting properties necessarily correspond to those of an exact solution of *any* Hamiltonian, let alone the original system.

The *intrinsic* Helmholtz free energy functional $A[\rho]$ is commonly split into *ideal* A^{id} and *excess* A^{ex} components,[6]

$$\begin{aligned} A[\rho] &\equiv A^{id}[\rho] + A^{ex}[\rho], \\ &= kT \int d\mathbf{1}\, \rho(\mathbf{1}) \Big\{ \ln\left[\Lambda^3 \rho(\mathbf{1})\right] - 1 \Big\} + A^{ex}[\rho], \end{aligned} \tag{2.23}$$

where $\Lambda = [h^2/(2\pi m k_B T)]^{1/2}$ is the de Broglie wavelength. The excess, or *over ideal*, contribution is the focus of DFT theory for nonuniform fluids and originates from interparticle interactions.

The contribution $A^{ex}[\rho]$ is is unique but unknown functional of the singlet density $\rho(\mathbf{1})$. These excess components are related to the direct correlation function hierarchy through functional derivatives,

$$c(\mathbf{1};[\rho]) \equiv -\frac{\delta \beta A^{ex}[\rho]}{\delta \rho(\mathbf{1})} = \frac{\delta \left(\beta A[\rho] - \beta A^{id}[\rho]\right)}{\delta \rho(\mathbf{1})}, \tag{2.24a}$$

$$c(\mathbf{1},\mathbf{2};[\rho]) \equiv \frac{\delta\, c(\mathbf{1})}{\delta \rho(\mathbf{2})}, \tag{2.24b}$$

or

$$\frac{\delta^2 \beta A[\rho]}{\delta \rho(\mathbf{1}) \delta \rho(\mathbf{2})} = \frac{\delta(\mathbf{1}-\mathbf{2})}{\rho(\mathbf{1})} - c(\mathbf{1},\mathbf{2};[\rho]), \tag{2.24c}$$

where the square brackets in the argument serve as a reminder that these correlations are functionals of the density. Note that $\delta A[\rho]/\delta \rho(\mathbf{1})$ can be regarded as an intrinsic potential, and if $\phi \equiv 0$ then $c(\mathbf{1})$ is proportional to the excess chemical potential, but more generally can be considered as an "additional" effective one-body potential. Using the ideal contribution from Eq. (2.23), the Euler-Lagrange equation becomes

$$\Lambda^3 \rho(\mathbf{1}) = \exp\left[\beta\left\{\mu - \phi(\mathbf{1})\right\} + c(\mathbf{1};[\rho])\right]. \tag{2.25}$$

Wertheim theory, being couched in the direct correlation function hierarchy, is easily amenable to a free energy derived from Eqs. (2.24a) and (2.24b) or (2.24c)

---

[6]This split is general: any thermodynamic function obtained by differentiation of A with respect to thermodynamic fields such as V or T can be split up into ideal and excess parts.

which can be functionally integrated at constant temperature from some initial density $\rho_i(\mathbf{1})$ to the final density of interest $\rho(\mathbf{1})$ via some charging parameter λ. The integrations are path independent [71], and using the standard linear route,

$$\begin{aligned}\rho_\lambda(\mathbf{r}) &\equiv \rho_i(\mathbf{1}) + \lambda\big[\rho(\mathbf{1}) - \rho_i(\mathbf{1})\big]\,, \quad 0 \le \lambda \le 1\,,\\ &= \rho_i(\mathbf{1}) + \lambda\Delta\rho(\mathbf{1})\,,\end{aligned}$$

we obtain

$$\beta A[\rho] = \beta A^{id}[\rho_i] + \beta A^{ex}[\rho_i] - \int d\mathbf{1}\; c(\mathbf{1};[\rho_i])\Delta\rho(\mathbf{1}) + \iint d\mathbf{1}d\mathbf{2}\int_0^1 d\lambda\;(\lambda-1)c(\mathbf{1},\mathbf{2};[\rho_\lambda])\Delta\rho(\mathbf{1})\Delta\rho(\mathbf{2})\,. \quad (2.26)$$

Equation (2.26) will act as the template from which our Wertheim free energy is derived in Chapter 4. Of course, it's solution requires a knowledge of the spatial as well as density dependence of the one– and two-body correlations $c(\mathbf{1};[\rho_\lambda])$ and $c(\mathbf{1},\mathbf{2};[\rho_\lambda])$, generally a nontrivial matter.

The grand potential Ω is also a functional of the pairwise additive energy $u(\mathbf{1},\mathbf{2})$,

$$\begin{aligned}U(\mathbf{1},\mathbf{2},\ldots,\mathbf{N}) &= \frac{1}{2}\sum_{i\neq j}\sum_{j=1}^{N} u(\mathbf{1},\mathbf{2})\\ &= \frac{1}{2}\iint d\mathbf{1}d\mathbf{2}\; u(\mathbf{1},\mathbf{2})\rho(\mathbf{1})\left[\rho(\mathbf{2}) - \delta(\mathbf{1}-\mathbf{2})\right]\,,\end{aligned}$$

which at fixed T and $u(\mathbf{1},\mathbf{2})$ translates into

$$\frac{\delta\Omega}{\delta u(\mathbf{1},\mathbf{2})} = \frac{\mathbf{1}}{2}\rho(\mathbf{1},\mathbf{2})\,.$$

Through Eq. (2.21) this relation implies

$$\frac{\delta A[\rho]}{\delta u(\mathbf{1},\mathbf{2})} = \frac{\mathbf{1}}{2}\rho(\mathbf{1},\mathbf{2})\,, \quad (2.27)$$

and so if the intermolecular potential is pairwise additive a common alternative to Eq. (2.26) can be derived by integrating Eq. (2.27) from a reference fluid interacting via some judiciously chosen reference pairwise potential u_0 to the fluid of interest interacting via the full potential using a charging parameter α,

$$u_\alpha(\mathbf{1},\mathbf{2}) \equiv u_0(\mathbf{1},\mathbf{2}) + \alpha u_p(\mathbf{1},\mathbf{2})\,, \quad 0 \le \alpha \le 1\,, \quad (2.28a)$$

where u_p is the perturbing potential and $\rho(\mathbf{1},\mathbf{2};u_\alpha)$ is the two-body density distribution with the potential u_α.[7] The resulting DFT free energy is

$$\beta A[\rho] = \beta A_r[\rho] + \frac{1}{2}\int d\mathbf{1}d\mathbf{2}\int_0^1 d\alpha\,\rho(\mathbf{1},\mathbf{2};u_\alpha)u_p(\mathbf{1},\mathbf{2})\,, \tag{2.28b}$$

and serves as a basis for all DFT perturbation theories of bulk as well as inhomogeneous fluids. Here the task is to determine $\rho(\mathbf{1},\mathbf{2};u_\alpha)$ for the given potential u_α, but is usually taken as the attractive contribution to $u(\mathbf{1},\mathbf{2})$.

The advantages of using a DFT free energy for inhomogeneous fluids are [72] (i) reasonable accuracy compared to computer simulations for hard spheres, (ii) an origin in the grand potential, which is applicable to a wide spectrum of systems, (iii) an expression in terms of the excess Helmholtz free energy, allowing for direct thermodynamic calculations, and (iv) a relatively economical implementation. Wertheim theory, being based upon generating functionals as well, is easily generalized to DFT methods.

[7] The density $\rho(\mathbf{1})$ must not change while the effective potential changes with α.

3. WERTHEIM THEORY PRIMER

Creativity is not the overstuffed armchair of existence, but the pedestrian leather of door-to-door thought.

— T. Peery

3.1. INTRODUCTION

During the last two decades there has been a concerted effort to association equilibria through a graphical analysis of the system partition functions. The works of Andersen [23, 51], Chandler and Pratt [73, 74], Høye and Olaussen [54], Wertheim [19–22], and Olaussen and Stell [75] all address the characteristic anisotropy and short range of the interaction potentials in associating fluids. How the steric incompatibility effects resulting from the repulsive cores and highly anisotropic attractions are incorporated into the graphical analyses, however, varies widely, although the differences are often intricately buried under confusing rubrics.[1] The central questions are What physical quantity will serve as the "monomer" in the theory? and How will the attraction sites (clusters) be defined graphically such that the site-site correlations can be described properly?

Monomers in diagrammatic expansions may correspond to molecules or to the specific atoms from which they are made. Graph vertices in a "molecular" monomer involve both the translational and orientational coordinates of the atoms in the molecule. In the RISM-style approach of Chandler and Anderson [76] monomers are atoms rigidly bound together into molecules by chemical bonds. Each graph vertex represents a single molecule which incorporates all the intramolecular constraints between interaction sites tied to the atoms. The site-site correlations that enter the integral equations (graphs) are thus separated into intra– and inter-molecular quantities. Stell [77] has extended the RISM method to include all degrees of monomer association, yet the RISM approach is not amenable

---

[1]For example, quantities labeled "atomic" may refer to a molecule (H_2O in our case) or even an entire polymer, and terms like "site–site" may refer to intra– as well as inter-molecular entities that may be dependent or independent of the actual associating molecules or atoms they describe.

to analytical solutions of thermodynamic and structural properites, as well as shows an unphysical dependence upon "auxiliary" sites that do not contribute to the interaction potential. An alternative approach, like that of Chandler and Pratt [73, 74], is based upon the theory of physical clusters and focuses upon the attraction sites themselves, attached to either rigid or flexible molecules. Each molecular diagram is replaced by a larger number of interaction-site diagrams, but these diagrams are mathematically simpler quantities because all orientational coordinates have been integrated out. While the site-site distribution functions are directly related to the structure factors measured in X-ray and neutron-scattering experiments, distribution functions like $g(r)$, and hence system thermodynamics, cannot be reconstructed exactly from any finite set of site-site distributions, limiting the theory.

Like Andersen [23, 51], Wertheim developed a graphical theory during the 1980s which introduced the steric incompatibility effects early in the graphical analysis. Wertheim monomers consist of repulsive cores embedded with highly anisotropic attraction sites, but the sites do not replace the atoms or molecules as the primary entity in the theory. The monomers may correspond to atoms or molecules, but comprise the different "species" of the theory according to the number of attraction sites bonded, a separate *partial* density being introduced for each possible state of bonding. The earlier work of Hoye and Olaussen [54] had suggested that a graphical expansion in terms of several density parameters written in terms of fugacity should be more rapidly convergent the a graphical expansion written in terms of the (total) singlet density ρ, *e.g.* the virial expansion. Unlike the physical cluster theory of Chandler and Pratt [73, 74], the Wertheim theory follows the physical cluster approach of Lockett [24], who modifies the Mayer f-bond in order to define physical clusters —Mayer clusters do not interact— because such an approach maintains the separation of kinetic and potential energies. With "clusters" entirely defined in terms of potential energies, Wertheim theory has the great advantage that it is amenable to the standard methods of liquid-state theory, such as thermodynamic perturbation theory (TPT) and integral equation theories (IETs), like the OZ equation. These theories can be derived from a functional expansion of the Helmholtz free energy A in terms of the singlet density $\rho(\mathbf{1})$, and therefore from the partial densities constructed from it. The following discussion of

graph theory and Wertheim's formalism draws liberally upon the detailed analysis of Hansen [55] and Wertheim [19, 21].

3.2. GRAPH THEORY & TOPOLOGICAL REDUCTION

The utility of linear graphs and generating functionals in the description of classical fluids at equilibrium have long been known, beginning in the 1940s with the work of Mayer and co-workers [78, 79] and Bogoliubov [80]. Later, Morita and Hiroike [81] and, independently, De Dominicis and co-workers [82] introduced a comprehensive formalism that combines the use of generating functionals and a felicitous method of resumming the infinite series of graphs associated with the statistical mechanics of classical fluids. An excellent review of these methods has been given by Stell [83]. The basis of this method consists of the use of *functional differentiation* to define n-particle distribution functions and *topological reduction* to partially resum the graph series representing the infinite set of integrals of the grand partition function. This combination greatly simplifies the combinatorial problems that arise in the statistical mechanical solution of many-body problems, as well as illuminates the approximations often used within TPT and IETs, all of which can be derived from functionals of the number density $\rho(\mathbf{1})$.

The simplest version of this method is characterized by Mayer theory [84, 85], originally developed to describe the condensation of dilute gases. Much later, Chandler and co-workers [86, 73] and Lockett [24] introduced schemes (*physical clusters*) based upon a more realistic definition of molecular clusters in order to treat associating systems. Although Wertheim's subsequent multi-density development is somewhat different, the theoretical progress represented by the work of Mayer and Lockett highlights and sets the context for that of Wertheim. It is with these procedural similarities in mind that we review the graphical analyses of Mayer and Lockett.

3.2.1. Graphs in statistical mechanics

We saw in Chapter 2 that the grand partition function, distribution, and correlation functions are defined as an infinite series of multi-dimensional configu-

rational integrals over particle coordinates, namely

$$\Xi(\mu, V, T) = \sum_{N=0}^{\infty} \frac{1}{N!} \int \cdots \int d\{i\}\, z(\mathbf{1}) \cdots z(\mathbf{N}) \prod_{i<j}^{N} \exp\left[-\beta u(i,j)\right] . \qquad (3.1)$$

The integrals in this infinite sum can be judiciously represented by linear *diagrams* or *graphs*. To each of the integrals in (3.1) there corresponds a *labeled diagram*, which generally consist of N vertices or *circles*, certain pairs of which are linked by lines or *bonds*. Each circle represents some function of the particle coordinates, including the unit function, whereas each *bond* represents some form of interaction between particles located at the given vertex coordinates. Within Eq. (3.1) above, the vertices represent the local fugacity $z(i)$ at space point i, and the bonds between vertices located at sites i and j are $e(\mathbf{1},\mathbf{2})$ or "e-bonds", defined as the Boltzmann factors

$$e(i,j) \equiv \exp[-\beta u(i,j)]\,, \qquad (3.2)$$

where $\beta = (k_B T)^{-1}$ and k_B is Boltzmann's constant. The e-bonds are denoted graphically by dotted lines ····· . The first four terms of (3.1) can be written as

$\boxed{\mathrm{N}=0}$ $\quad 1\,,$

$\boxed{\mathrm{N}=1}$ $\quad \overset{\bullet}{\underset{1}{}} = \int d\mathbf{1}\, z(\mathbf{1})\,,$

$\boxed{\mathrm{N}=2}$ $\quad \overset{\bullet\cdots\bullet}{\underset{1\quad 2}{}} = \frac{1}{2!} \iint d\mathbf{1}d\mathbf{2}\, z(\mathbf{1})z(\mathbf{2})e(\mathbf{1},\mathbf{2})\,,$

$\boxed{\mathrm{N}=3}$ $\quad \overset{3}{\underset{1\quad 2}{\bullet\cdots\bullet}} = \frac{1}{3!} \iint d\mathbf{1}d\mathbf{2}d\mathbf{3}\, z(\mathbf{1})z(\mathbf{2})z(\mathbf{3})e(\mathbf{1},\mathbf{2})e(\mathbf{2},\mathbf{3})e(\mathbf{1},\mathbf{3})\,.$

All black circles • are referred to as *field points* and indicate spatial coordinates which are variables of integration. Later, when defining the n-particle distribution functions, we will need to define white circles ○ or *root points*, which correspond to particle coordinates that are <u>not</u> integration variables.

The labeled diagrams above are examples of *simple* diagrams because no pair of circles is linked by more than one bond. The "value" of such a labeled diagram is the value of the integral that the graph represents: it is a function of the coordinates attached to the root points and a functional of the functions associated with the field points and bonds. Two labeled diagrams are said to be *topologically*

distinct if they are characterized by a different set of bond connections. Note that since the field points carry dummy variables, the manner in which they are labeled is irrelevant and thus may be conveniently omitted altogether, producing an *unlabeled diagram.* The economy of manipulating unlabeled graphs is that they implicitly contain the combinatorial factors related to the topological structure of the diagram. Consider, for example, a labeled diagram that contains m field points. Any of the $m!$ • label permutations leaves the value of the diagram unchanged, yet some subset of those permutations may give rise to topologically distinct graphs. Two unlabeled diagrams are *topologically distinct* if it is impossible to find a permutation of the • labels that a converts a labeled version of the diagram into a labeled version of the other. Diagrams that are topologically distinct represent different integrals; therefore statistical mechanical quantities that are usefully discussed in diagrammatic terms are generally obtained as "sums of all topologically distinct graphs" having particular properties. See Appendix A for more details concerning diagrammatic definitions.

Diagram manipulation itself follows a formal set of rules specified by a series of *lemmas* derived by Morita and Hiroike [81] and Stell [83]. For brevity, these *lemmas* will not be presented here, but instead only a synopsis of the specific *lemmas* used in our topological reduction procedure. A thorough review, including examples and some details of the proofs, is given by Hansen and McDonald [55]. The conventional topological reduction procedure of interest utilizes *Lemmas 1, 2,* and *4*, which, for simple and multipolar fluids involves the resummation of graphs in the fugacity expansion to a sum of more highly connected graphs in terms of the singlet density $\rho(\mathbf{1})$. This reduction generally depends only upon the topological structure of the graphs and the associated relationship between the functions represented by graph vertices, *e.g.* $z(\boldsymbol{i})$ and $\rho(\mathbf{1})$, although Mayer's original derivation does requires translational invariance (*i.e.* a vanishing external field) in order that the cluster integrals factor into products of irreducible graphs.

3.2.2. Topological Reduction and Mayer Theory

As already mentioned, the fugacity expansion (3.1) of Ξ is not immediately useful, even for simple fluids. Not only does the series display convergence difficulties for associating fluids, where the e-bond contributions become large and positive, but because $e(\mathbf{1},\mathbf{2}) \to 1$ as $|\mathbf{r}_2 - \mathbf{r}_1| \to \infty$, the contribution from the Nth

term is of order V^N, giving rise to problems in the thermodynamic limit. In a first step towards a renormalization of the e-bond, Mayer and co-workers introduced what has been called the "Mayer f-bond", defined simply as

$$f(i,j) \equiv e(i,j) - 1 . \tag{3.3}$$

Unlike the e-bond, the Mayer f-bond is everywhere bounded and rapidly approaches zero with increasing inter-particle distance r. Apart from renormalizing the configurational partition function, Q_N, the f-bond allows for the interaction potential to vanish between particles, and this leads directly to the partition function for free particles, $Z_N(V,T) = [Q_N(V,T)/(N!\,\Lambda^{3N})] \to (zV)^N/N!$, an important limit for any theory. Introducing the f-bond into the infinite sum Ξ above simply means replacing each of the $N(N-1)/2$ e-bonds in the expansion with a "1-bond" and an f-bond, *i.e.*

$$\begin{aligned}\Xi \;=\; 1 \;+\; \int d\mathbf{1}\, z(\mathbf{1}) \;+\; \frac{1}{2!}\iint d\mathbf{1}d\mathbf{2}\; z(\mathbf{1})z(\mathbf{2})\,[1+f(\mathbf{1},\mathbf{2})] \\ +\; \frac{1}{3!}\iiint d\mathbf{1}d\mathbf{2}d\mathbf{3}\; z(\mathbf{1})z(\mathbf{2})z(\mathbf{3})\Big[1+3f(\mathbf{1},\mathbf{2})+3f(\mathbf{1},\mathbf{2})f(\mathbf{2},\mathbf{3}) \\ +\, f(\mathbf{1},\mathbf{2})f(\mathbf{1},\mathbf{3})f(\mathbf{2},\mathbf{3})\Big] \;+\; \cdots\end{aligned} \tag{3.4}$$

The 1-bond describes non-interacting particles and so 1-bonded vertices are represented graphically by disconnected circles. Equation (3.4) is known as a *cluster expansion* because the first term involves single molecules, the second pairs of molecules, and so on. A Mayer cluster of size L is thus defined as a diagram with L circles that are all connected via f-bonds, these bonds being indicated graphically by solid lines —— . A diagram with m disconnected circles, of course, will contribute a term proportional to V^m to the expansion. Armed with the graphical prescriptions discussed above, we can write down Eq. (3.4) in diagram form:

$$\Xi \;=\; \left\{\begin{array}{l}1 \;+\; \text{sum of all simple diagrams, connected and unconnected,} \\ \text{which consist of one or more black } z(i)\text{-circles and zero or more} \\ f\text{-bonds between field points.}\end{array}\right\}$$

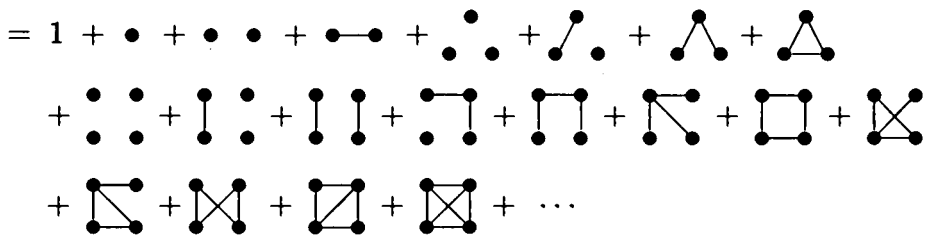

(3.5)

Already the great economy of dealing with unlabeled diagrams is obvious. Enumerating all permutations of f-bonds on N vertices is far more easy than enumerating all labeled graphs with all the appropriate combinatorial factors. However, these combinatorial factors can be relatively easily reproduced. For $N = 3$ and one f-bond, for example, we need only list one generic graph, *i.e.*

the three possible arrangements of the f-bond

(3.6)

all being equivalent. It is then relatively easy to write down the pertinent combinatorial factors, and hence the value of, a given generic diagram from a topological perspective, namely

$$\Xi \propto \frac{1}{3!}\left\{3\,\right\} = \frac{1}{2}\iiint d\mathbf{1}d\mathbf{2}d\mathbf{3}\; z(\mathbf{1})z(\mathbf{2})z(\mathbf{3})\; f(\mathbf{1},\mathbf{2}),$$

where the labeling of $\bullet$ points implied in the integral above is arbitrary. The prefactor of $1/2$ here is $1/S$, where S is the diagram *symmetry number*. The value I of any diagram containing n white and m black vertices can be obtained from

$$I = \frac{1}{S}\left\{\begin{array}{l}\text{any one of the diagrams obtained by attaching}\\ \text{labels } n+1,\ldots,n+m \text{ to the black circles.}\end{array}\right\}. \tag{3.7}$$

Directly determining the symmetry number of a graph with N field points involves arbitrarily labelling all field point coordinates and subsequently enumerating all possible permutations of those labels which leaves the f-bond connectivity of the graph *unchanged*. Using the same $N = 3$ example, we find two possible permutations:

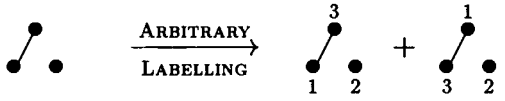

$\Longrightarrow \quad S = 2\,.$

Moreover, the number of these equivalent graphs in our expansion [see Eq. (3.6)] is defined as $N!/S = 3!/2 = 3$, from which we arrive at the same result

$$\Xi \propto \frac{1}{3!}\left\{3\,\right\} = \cdots$$

as above.

So far all we have done is drawn some rather formal pictures of an infinite series in fugacity, little aid in actually evaluating the equation of state βPV or number density $\rho(\mathbf{1})$. In fact, looking at $\Xi(\mu, V, T)$, Eq. (3.5), it would seem that matters are worse. There are many more diagrams which we now have to sum, and for any given N the largest term is the one with *no* f-bonds: it grows like V^N, while a fully f-bonded graph only grows like V (with all other partially bonded graphs lying somewhere between). In the thermodynamic limit, $V \to \infty$ but $z(\boldsymbol{i})$ remains finite, so the cluster terms become negligible compared to the non-interacting terms. The real benefit of graphs lies in the resummation made possible through the judicial application of *topological reduction* procedures, as well as in the physical illumination they provide concerning approximations commonly made upon one– and two-body correlation functions within IETs. The basic topological process, outlined below, can be illustrated by deriving the virial expansion from Eq. (3.5) and will serve to motivate the modifications taken within Wertheim's multi-density theory.

TOPOLOGICAL REDUCTION IN A NUTSHELL

(1) Apply *Lemma 1* to the generating functional Ξ in order to eliminate all unconnected graphs in the expansion.

(2) Apply *Lemma 2* to $\ln \Xi$ in order to generate the one– and two-body distribution functions: *e.g.* $\rho(\mathbf{1})$, $\rho(\mathbf{1}, \mathbf{2})$.

(3) Apply *Lemma 1* to the series $\rho(\mathbf{1})/z(\mathbf{1})$ in order to eliminate all white articulation circles ○ .

(4) Apply *Lemma 4* to the $c(\mathbf{1}) = \ln[\rho(\mathbf{1})/z(\mathbf{1})]$ in order to eliminate all black articulation circles ● by converting fugacity vertices to density vertices, leaving only topologically irreducible graphs in the sum.

By application of *Lemma 1*, or the "exponentiation theorem", we can evaluate the natural logarithm of the graph sum Ξ. For diagrams which contain only field points, this simply translates into the elimination of all *unconnected* graphs in the

series, hence

$$\ln \Xi = \left\{ \begin{array}{l} \text{sum of all simple, topologically distinct connected graphs} \\ \text{consisting of one or more black } z(i)\text{-circles and one or} \\ \text{more } f\text{-bonds.} \end{array} \right\}$$

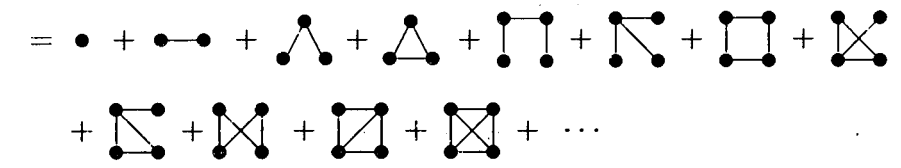

(3.8)

If the external potential $\phi(i)$ contained in $z(i)$ vanishes,[2] which we will assume to be true in Chapters 4 and 5, then from the fundamental relation $\beta PV = \ln \Xi$ we obtain the familiar fugacity expansion

$$\beta P = \sum_{L=1}^{\infty} b_L z^L , \tag{3.9}$$

where the fugacity coefficient b_L is the sum of all possible cluster integrals of f-bonds connecting L vertices (see Ref. [24] for a detailed discussion). These coefficients, which are a function of temperature only, serve as an equilibrium constant for the "chemical" reaction which converts L monomers into a *cluster* of size L; they are not, however, automatically positive definite and this can lead to a physically unreasonable negative equilibrium number density. This unphysical nature of Mayer clusters can be seen by looking at the average number density ρ_L of Mayer clusters of size L. From Eq. (3.9) the equilibrium number density is

$$\rho = z\frac{\partial \beta P}{\partial z} = \sum_{L=1}^{\infty} L b_L z^L , \tag{3.10}$$

and the conservation of particles demands that

$$\rho = \sum_{L=1}^{\infty} L\rho_L ,$$

---

[2]While $\phi(1) = 0$ in those chapters, a local fugacity $z(i)$ will still be present, the inhomogeneity there being a result of the "field" from a particle fixed at the origin, a method developed by Percus [87–89].

where $\rho_L \equiv b_L z^L$. Yet the first fugacity coefficient b_1 is unity, and so the equilibrium monomer density ρ_1 in Mayer theory is just the fugacity, $\rho_1 = z$, which means that monomers do not interact with each other or with clusters. In addition

$$\rho_L = b_L \rho_1^L, \quad \beta P = \sum_{L=1}^{\infty} \rho_L ,$$

meaning Mayer clusters do not interact with each other either, each vertex of one cluster being unconnected or 1-bonded to the vertices of another cluster.

It was precisely the unphysical nature of the Mayer clusters that motivated the development of "physical" cluster theories, which started with the work of Bijl [90], Band [91], and Frenkel [92] (see also Refs. [93–95]). As *every* cluster definition entails some arbitrary partitioning of phase space, independent of nature, there are many possible approaches, including many choices as to what should constitute a monomer. Determining a reasonable yet simple definition is indeed no trivial matter, for the relationship between cluster-specific quantities like the equilibrium number densities ρ_L and physical system quantities like Ξ, ρ, P, μ, *etc.* is unclear at best. One obvious choice, and that taken by Hill [93], is that the total energy of a "cluster" should be negative, *i.e.* the monomers contained therein are bound together, but this involves both kinetic and potential energies and leads to complicated cluster integrals with mixed momentum and spatial-dependent expressions. Nonetheless, similar physical cluster theories have been applied to study the chemical equilibrium and intramolecular of non-rigid polyatomic molecules [86, 73]. The separation of phase space assumed by Mayer-like theories, on the other hand, involve only the potential energy, and this simplifies the application to intermolecular interactions like hydrogen bonding.

Lockett [24] was one of the first to recognize that a physical cluster theory could be developed entirely within the diagrammatic framework of Mayer theory. By separating the Mayer f-bond into two components, $f(\mathbf{1},\mathbf{2}) \rightarrow f_R(\mathbf{1},\mathbf{2}) + f_A(\mathbf{1},\mathbf{2})$ [see Section 3.4 for details], physical clusters could still be defined by potential energy arguments alone, retaining the useful diagrammatic analysis outlined above by which physical quantities of interest could be determined —thereby mitigating ambiguities often encountered in standard cluster theories when separating off the center of mass contributions to the partition function [96]. In traditional cluster theories, for example, letting the interaction potential vanish does not directly lead to the correct free-particle limiting behavior of the approx-

imate partition functions typically derived, as it intrinsically does in Mayer type theories. While the Wertheim theory utilizes Lockett's modified Mayer f-bond, the topological reduction steps (2)–(4) listed above are more easily described in terms of Mayer's original f-bond. As such, we shall first describe those remaining steps, and then present the f-bond modifications introduced by Lockett, from which Wertheim's partial densities will naturally emerge as the next logical step in the diagrammatic analysis of associating fluids.

These remaining topological reduction steps begin to address the interaction limitations inherent in the fugacity expansion of $\ln \Xi$. Returning to Eq. (3.8), which acts as our generating functional, we can obtain the one-body distribution function or singlet density

$$\rho(\mathbf{1}) \;=\; z(\mathbf{1})\frac{\delta \ln \Xi}{\delta z(\mathbf{1})} \tag{3.11}$$

graphically with the aid of *Lemma 2*:

$$\frac{\delta \ln \Xi}{\delta z(\mathbf{1})} \;=\; \left\{ \begin{array}{l} \text{sum of all graphs obtained from } \ln \Xi \text{ by taking all} \\ \text{distinct ways of turning a } \bullet \; z(\boldsymbol{i})\text{-circle into a 1-} \\ \text{circle or root point } \circ \text{ labeled 1; the unit function 1} \\ \text{is associated with this root point } \underset{1}{\circ}\,. \end{array} \right\}, \tag{3.12}$$

which, when applied to Eqs. (3.8) and (3.11), gives

$\rho(\mathbf{1}) =$ 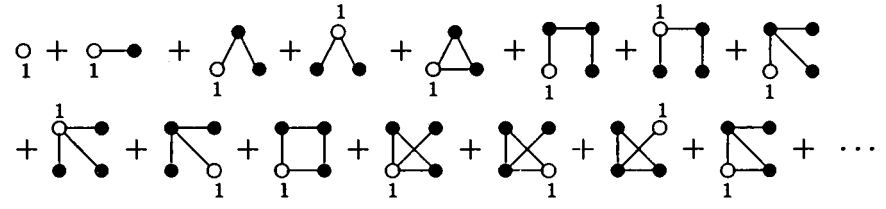 (3.13)

Again, a white circle $\circ$ represents particle coordinates that are *not* integration variables, *e.g.*

$$\underset{1}{\circ}\!\!-\!\!\bullet \;=\; \int d\mathbf{2}\; z(\mathbf{2}) f(\mathbf{1},\mathbf{2})\,.$$

The "1" label on the root point $\underset{1}{\circ}$ here denotes the spatial dependence, $\mathbf{r}_1$, and not the function associated with that vertex, which, by nature of functional differentiation, happens to be the unit function. This is why $\underset{1}{\circ}$ is called a 1-circle, not because it carries the spatial label "1". That is, root points like $\underset{1}{\circ}$ may be

associated with any function, such as $z(\mathbf{1})$ or $\rho(\mathbf{1})$, even though it carries the spatial label 1; the actual function associated with the vertices is usually evident from the context of the analysis and so rarely indicated directly in the diagrams. For example, the $z(\mathbf{1})$ factor in Eq. (3.11) means that the root points $\underset{1}{\circ}$ in the $\rho(\mathbf{1})$ expansion (3.13) are associated with the local fugacity $z(\mathbf{1})$. For convenience the spatial labels on the white circles are also usually omitted, $\underset{1}{\circ} \rightarrow \circ$, with the caveat that all topologically distinct permutations of white circles must be included in the graph sums.

The graph expansion $\rho(\mathbf{1})$ contains both irreducible and reducible graphs. Looking at the reducible graphs, we notice a degree of self-similarity, hinting at a partial resummation scheme. Each reducible graph contains one or more it articulation circles, and these circles mark the points where the diagram factorizes as a product of graphs that have already appeared at lower order in the expansion. Therefore all such graphs with articulation circles can be eliminated, resummed into a "least common denominator" as it were, leaving a series of irreducible diagrams. This resummation is effected by rewriting all fugacity vertices as density vertices and is carried out using Eq. (3.13), which relates $\rho(\mathbf{1})$ to $z(\mathbf{1})$. If we divide Eq. (3.13) by $z(\mathbf{1})$, such that the root points are 1-circles, we see that the resulting series contains both white and black articulation circles, a few examples (marked by arrows) are shown below:

$\rho(\mathbf{1})/z(\mathbf{1}) \propto$ 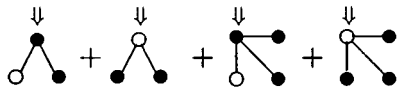 .

By taking the logarithm of $\rho(\mathbf{1})/z(\mathbf{1})$ and applying *Lemma 1*, all white articulation 1-circles are resummed, leaving

$\ln \dfrac{\rho(\mathbf{1})}{z(\mathbf{1})} =$ 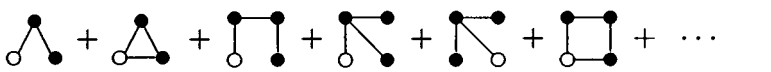 (3.14)

All remaining graphs in (3.14) are either irreducible or diagrams which would be irreducible except for the "hair" growing from the • articulation circles. The subset of reducible diagrams representing all possible diagrams or "hair" that can attached to the • articulation circle can likewise be resummed into lower order diagrams and thus eliminated. To carry out this topological reduction procedure out, we first identify the *maximal, irreducible subdiagram*, Γ_m say, of each reducible

graph in the subset of (3.14). The subdiagram Γ_m must contain the one white circle in the graph, but *maximal* should not necessarily be equated with "largest"; for example,

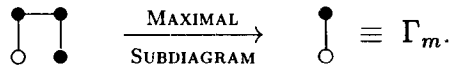

$\equiv \Gamma_m$.

Using this same example, we see that many higher-order graphs will contain this same maximal subdiagram Γ_m. From each unique Γ_m in the set (3.14), we can generate all those higher-order, reducible graphs with that common maximal subdiagram by consecutively "decorating" all • points in Γ_m with the graphs in $\rho(\mathbf{1})$, Eq. (3.13). This process of "decorating" Γ_m, according to *Lemma 4*, means superimposing the ○ $z(i)$-circle in a graph of $\rho(\mathbf{1})$ on all the • $z(i)$-circles of Γ_m, blackening that white circle after attachment. Taking the same Γ_m as above, we see that by attaching the second and third graphs in $\rho(\mathbf{1})$ [Eq. (3.13)] to Γ_m,

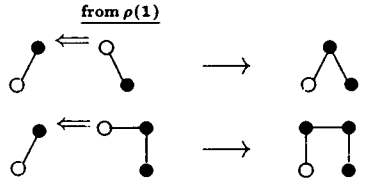

we obtain the second and fourth fugacity graphs in Eq. (3.14) for $\ln[\rho(\mathbf{1})/z(\mathbf{1})]$. Hence by eliminating the • articulation circles we have effectively rewritten the $z(i)$-vertices as $\rho(\mathbf{1})$-vertices, and resummed $\ln[\rho(\mathbf{1})/z(\mathbf{1})]$ into the set of all irreducible density graphs:

$$\ln\frac{\rho(\mathbf{1})}{z(\mathbf{1})} = \left\{\begin{array}{l}\text{sum of all topologically distinct, irreducible graphs}\\ \text{consisting of one white 1-circle ○ and one or more}\\ \rho(i)\text{-circles •, some of which are connected by } f\text{-}\\ \text{bonds.}\end{array}\right\},$$

$$= \text{○—•} + \triangle + \square + \boxtimes + \boxtimes + \boxtimes + \boxtimes + \cdots \tag{3.15}$$

Equation (3.15) marks the culmination of the topological reduction procedure within the Mayer theory, and can be used to derive the familiar virial expansion by setting the external potential ϕ to zero as before, giving

$$\ln z = \ln\rho - \sum_{i=1}^{\infty} \beta_i \rho^i, \tag{3.16}$$

where the coefficients β_i are the irreducible *Mayer cluster integrals*, such as

$$\beta_1 \;=\; \circ\!\!-\!\!\bullet \;=\; \int d\mathbf{1}\, f(\mathbf{1},\mathbf{2})\,.$$

Manipulation of $\beta PV = \ln \Xi$ allows the equation of state to be written as[3]

$$\beta P \;=\; \int_0^{\rho} d\rho'\, \rho' \frac{d \ln z}{d\rho'}\,, \tag{3.17a}$$

which can easily be evaluated using (3.16) to obtain the virial equation of state

$$\beta P \;=\; \rho \;+\; \sum_{i=1}^{\infty} B_i(T)\, \rho^{i+1}\,, \tag{3.17b}$$

where the temperature-dependent *virial coefficients* $B_i(T)$ are related to the Mayer coefficients β_i according to

$$B_1 \;=\; 1\,, \quad B_{i+1} \;=\; -\frac{i}{i+1}\beta_i \qquad \text{for } i \geq 1\,.$$

Particle interactions are now, albeit indirectly, accounted for by the sum on the right-hand side of Eq. (3.17b); dimer formation, for example, is automatically taken care of by B_2. Evaluation of higher order terms, even for hard sphere systems, is difficult because the number of diagrams that contribute to the ith coefficient increases rapidly with i. As the density increases these complications become even worse, requiring higher and higher order terms must be considered. In the liquid-density case it is preferable to make physically reasonable approximations which allow for the density expansion to be summed. Wertheim theory is just such an approach, based upon Lockett's modified Mayer f-bond, with Eq. (3.14) serving as the foundation for an alternative topological reduction procedure, written in terms of *partial densities* which reflect the bonded status of the monomers. In fact, Eq. (3.14) provides the link to system correlations and structure.

3.3. GRAPHICAL DISTRIBUTION FUNCTIONS

While the partial densities in Wertheim theory will be derived from the one-body correlation function $c(\mathbf{1})$, their solution will require a graphical analysis

---

[3]This last step in the derivation is slightly more complicated in the presence of an external potential, but has been treated by Morita and Hiroike [81].

of the background correlation function $y(\mathbf{1},\mathbf{2})$. In addition, solution of the fluid structure via the Ornstein–Zernike equation will require a graphical analysis of the direct $c(\mathbf{1},\mathbf{2})$ and total $h(\mathbf{1},\mathbf{2})$ correlation functions. Their graphical expansions in terms of the singlet density $\rho(\mathbf{1})$ follow from the relation

$$c(\mathbf{1}) \;=\; \ln[\rho(\mathbf{1})/z(\mathbf{1})] \tag{3.18}$$

and the graphical series Eq. (3.15). It should be noted that hereafter, unless specified otherwise, all external fields ϕ will be assumed to be absent. We adopt, instead, the approach taken by Percus [87, 97], wherein a particle is fixed at the origin and all other particles are then free to move around in the "external" force field of that central particle; hence the remaining spatial dependence in $\rho(\mathbf{1})$ and $z(\mathbf{1})$ in Eq. (3.18) above.

The direct correlation function hierarchy, Eqs. (2.24a)–(2.24b) on page 38, used in conjunction with *Lemma 2*, now allows us to immediately write down the diagrammatic expansion for the direct correlation function:

$c(\mathbf{1},\mathbf{2}) \;=\;$ { sum of all topologically distinct diagrams that consist of two white 1-circles ○ labeled 1 and 2, zero or more $\rho(\boldsymbol{i})$-circles ● , one or more f-bonds, and are free of connecting circles. } ,

$$= \;\circ\!\!-\!\!\circ \;+\; \triangle \;+\; \square \;+\; \boxtimes \;+\; \boxtimes \;+\; \boxtimes \;+\; \boxtimes \;+\; \boxtimes \;+\; \cdots \tag{3.19}$$

Recall that when attaching the spatial labels 1 and 2 to the 1-circles ○, all distinct permutations must be included, *e.g.*

$$\boxtimes \;\longrightarrow\; \boxtimes_{1\;2} + \boxtimes_{1\;2} .$$

To lowest order in ρ, the expansion (3.19) shows that $c(1,2) \simeq f(1,2)$, and so at large separations r, $c(1,2) \simeq -\beta u(1,2)$, an indication that the range of $c(1,2)$ is roughly that of the potential. All higher order graphs are at least doubly connected, meaning that their contribution to $c(r)$ decays at least as fast as $[f(1,2)]^2$, making them negligible in the limit $r \to \infty$ compared to the leading term.

The graph expansions for the other pair functions can be obtained systematically by following topological reduction steps similar to those in the derivation

of the virial equation. The fugacity expansion of the truncated distribution $\hat{\rho}(\mathbf{1},\mathbf{2})$ can be found by functional differentiation of $\rho(\mathbf{1})$, evaluated graphically by application of *Lemma 2* to Eq. (3.13) on page 51. Combining these results with the defining relation

$$h(\mathbf{1},\mathbf{2}) \equiv \frac{\hat{\rho}(\mathbf{1},\mathbf{2})}{\rho(\mathbf{1})\rho(\mathbf{2})}$$

yields the fugacity expansion for the total correlation function $h(\mathbf{1},\mathbf{2})$. Evaluation of the ratio above is motivated by noting that $\hat{\rho}(\mathbf{1},\mathbf{2})$ contains $\rho(\mathbf{1})$ and $\rho(\mathbf{2})$ as factors; hence the ratio $\hat{\rho}(\mathbf{1},\mathbf{2})/\rho(\mathbf{1})$, for example, consists of all diagrams that remain connected when all bonds incident at $\mathbf{1}$ are broken. Finally, application of *Lemma 4* leads to the desired density expansion

$$h(\mathbf{1},\mathbf{2}) = \left\{ \begin{array}{l} \text{sum of all connected, topologically distinct dia-} \\ \text{grams that consist of two white 1-circles } \circ \text{ labeled} \\ \text{1 and 2, zero or more } \rho(\boldsymbol{i})\text{-circles } \bullet \text{ and } f\text{-bonds} \\ \text{between some circles, and are free of articulation} \\ \text{circles.} \end{array} \right\},$$

$$= \circ\!\!-\!\!\circ + \cdots \qquad (3.20)$$

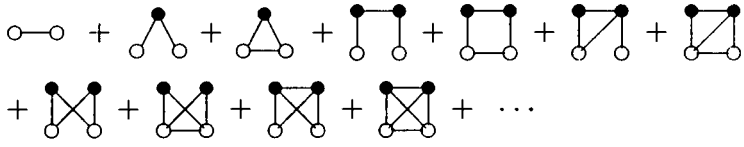

Compared to Eq. (3.19) for $c(\mathbf{1},\mathbf{2})$, Eq. (3.20) contains more diagrams at every order in density beyond the zeroth-order term. The additional diagrams all contain at least one nodal circle. Examining those extra diagrams we note that for every diagram without a direct f-bond between the two white circles, there is one with such a bond. Using $e(\mathbf{1},\mathbf{2}) = f(\mathbf{1},\mathbf{2}) + 1$ then, we can sum of each pair of such diagrams as a single diagram in which the two white circles are connected by an e-bond, all other bonds being f-bonds. Although the zeroth-order diagram $\circ\ \circ$ is absent from $h(\mathbf{1},\mathbf{2})$, it is included in the pair distribution function, $g(\mathbf{1},\mathbf{2}) = h(\mathbf{1},\mathbf{2}) + 1$, allowing for the e-bond to be completely factored out of the series for

$g(\mathbf{1},\mathbf{2})$,

$$g(\mathbf{1},\mathbf{2}) = \left\{ \begin{array}{l} \text{sum of all topologically distinct, irreducible diagrams} \\ \text{that consist of two white 1-circles } \circ \text{ labeled 1 and 2} \\ \text{and connected by an } e\text{-bond, one or more } \rho(i)\text{-circles} \\ \bullet\text{, and two or more } f\text{-bonds between } \bullet \text{ circles but not} \\ \text{directly between the two } \circ \text{ circles.} \end{array} \right\},$$

$$= e(\mathbf{1},\mathbf{2})\Big[\, 1 + \quad + \quad + \quad + \quad + \quad + \cdots \,\Big]. \qquad (3.21)$$

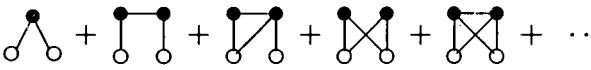

We can see directly from the form of this series that $g(r)$ behaves as $\exp[-\beta u(r)]$ as $\rho \to 0$ as expected; in the same limit, $h(r)$ and $c(r)$ both behave like $f(r)$. The series expansion for the background correlation function then trivially follows from (3.21),

$$y(\mathbf{1},\mathbf{2}) \equiv \frac{g(\mathbf{1},\mathbf{2})}{e(\mathbf{1},\mathbf{2})},$$

$$= 1 + \quad + \quad + \quad + \quad + \cdots \qquad (3.22)$$

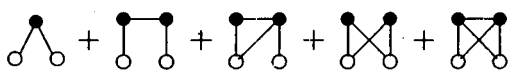

It is obvious that $y(\mathbf{1},\mathbf{2})$ is a continuous function of r, even for discontinuous potentials, because the discontinuity in $g(\mathbf{1},\mathbf{2})$ at $r = R$ is wholly contained in the e-bond factor $\exp[-\beta u(\mathbf{1},\mathbf{2})]$, which has been removed in $y(\mathbf{1},\mathbf{2})$.

3.4. GRAPH THEORY À LA WERTHEIM

Wertheim's multi-density formalism begins back at the fugacity expansion of the logarithm of the grand partition function, step (2) in our topological reduction list on page 48. The remaining topological reduction steps in the Wertheim formalism, however, differ from the standard recipe in that steric incompatibility effects and partial densities are introduced into the analysis, as is Lockett's modification to the Mayer f-bond. In the following general review of these changes for the multi-site case we shall rely heavily upon the detailed discussions given by Wertheim (see Refs. [19] and [21]), limiting the discussion to the single-site or four-site case where helpful. Further details about the single– and four-site models will be discussed in Chapters 4 and 5 respectively, where those models are addressed in full.

According to Wertheim [21], by writing down the pair potential as a sum of *core–core* and *site–site* potentials and introducing Mayer f-bonds into each term, the fugacity graphs "become a very flexible instrument, because they incorporate the relevant information concerning the geometry of the interactions in a form which is accessible and susceptible to physically motivated manipulations." Using $\beta PV = -\ln \Xi$, along with Eq. (3.8) on page 49, we therefore begin with

$$\beta PV = \left\{ \begin{array}{l} \text{sum of all simple, topologically distinct connected} \\ \text{graphs consisting of one or more black } z(\boldsymbol{i})\text{-circles} \\ \text{and one or more } f\text{-bonds.} \end{array} \right\}, \tag{3.23}$$

$$\rho(\mathbf{1}) = \left\{ \begin{array}{l} \text{sum of all graphs obtained from } \beta PV \text{ by taking} \\ \text{all distinct ways of turning } \bullet\ z(\boldsymbol{i})\text{-circles into a} \\ z(\mathbf{1})\text{-circle or root point } \circ \text{ labeled 1.} \end{array} \right\}. \tag{3.24}$$

The separation of the interaction potential $u(\mathbf{1},\mathbf{2})$ mentioned by Wertheim alludes to Lockett's [24] separation of the Mayer f-bond into two components by splitting the pair potential into repulsive $u^R(\mathbf{1},\mathbf{2})$ and attractive $u^A(\mathbf{1},\mathbf{2})$ parts, namely

$$\begin{aligned} f(\mathbf{1},\mathbf{2}) &= e^{-\beta(u^R + u^A)} - 1 \\ &= \left[e^{-\beta u^R} - 1\right] + e^{-\beta u^R}\left[e^{-\beta u^A} - 1\right] \\ &= f^R(\mathbf{1},\mathbf{2}) + e^R(\mathbf{1},\mathbf{2})\, f^A(\mathbf{1},\mathbf{2}) \\ &\equiv f^R(\mathbf{1},\mathbf{2}) + f_A(\mathbf{1},\mathbf{2}). \end{aligned} \tag{3.25}$$

In Lockett's notation f_A contains the e^R bond, whereas f^A does not. By associating f_R with the 1 instead of the f_A in the e-bond,

$$\begin{aligned} e(\mathbf{1},\mathbf{2}) &= \left[1 + f^R(\mathbf{1},\mathbf{2})\right] + f_A(\mathbf{1},\mathbf{2}), \\ &= e^R(\mathbf{1},\mathbf{2}) + f_A(\mathbf{1},\mathbf{2}), \end{aligned} \tag{3.26}$$

the unphysical aspects of Mayer clusters —expansion coefficients b_L of indeterminate sign and non-interacting clusters— are resolved. The $e_R(\mathbf{1},\mathbf{2})$ bonds not only serve as an excluded volume mechanism but within a physical cluster they also ensure that the modified cluster integrals are positive. Figure 3.1 shows (a) Mayer's e-bond separation and (b) the modified general prescription of Lockett. The utility of such a modification is evident by the large number of subsequent works it prompted [98–100, 52, 77, 101–103]. Kalyuzhnyi *et. al.* [102] classify these

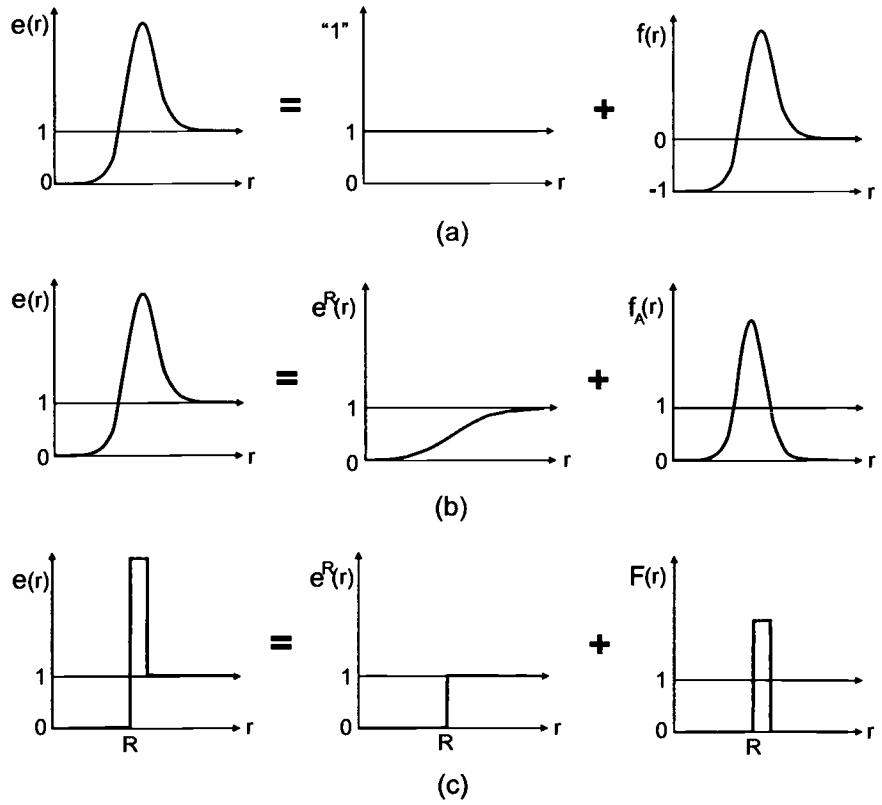

FIGURE 3.1. Graphical representation of the Mayer f-bond and it's modification of for associating fluids. Mayer's original split of the Boltzmann factor $e(r)$ is shown in (a), with Lockett's [24] modification to that factor, $e(r) = e_R(r) + f_A(r)$, defined in (b). The equivalent e-bond modification for the sticky-spot model is given in (c).

---

simple models of chemical association according to the physical implementation of their repulsive and attractive potentials. The repulsive potentials $u^R(\mathbf{1},\mathbf{2})$ typically used are of the hard sphere type, although not necessarily sphereical, and some models allow for core interpenetration or employ soft cores. A large number of attraction potentials exist which mimic, to some degree, the short-ranged, highly directional attractive interactions in associating fluids. Models within Wertheim theory generally fall into the *site–site* classification of Kalyuzhnyi *et. al.*, including the single-site model we use in Chapter 4 to discuss dimerization and the four-site model we use to describe water in Chapter 5, which involve the singular *sticky-spot limit* of a discontinuous, anisotropic potential $u^A(\mathbf{1},\mathbf{2})$. The discontinuity in our attractive potential is evident in the resulting e-bond, shown in Fig. 3.1(c).

Current model singularity notwithstanding, the subtle refinement in Wertheim's formalism begins with the inclusion of the $u^A(\mathbf{1},\mathbf{2})$ potential anisotropy in the modified Mayer f-bond F(**1**,**2**),

$$\begin{aligned} f(\mathbf{1},\mathbf{2}) &= f^R(\mathbf{1},\mathbf{2}) + e^R(\mathbf{1},\mathbf{2})\, f^A(\mathbf{1},\mathbf{2}) \\ &\equiv f^R(\mathbf{1},\mathbf{2}) + F(\mathbf{1},\mathbf{2}), \end{aligned} \tag{3.27}$$

in contrast to Lockett's sterically uninhibited $f_A(\mathbf{1},\mathbf{2})$ bond. For molecular models consisting of repulsive cores and multiple attraction sites which interact via orientationally-dependent, attractive potentials $u^A_{ij}(\mathbf{1},\mathbf{2})$, the Wertheim F-bond becomes a sum of attractive $f^A_{ij}(\mathbf{1},\mathbf{2})$ bonds between site i at point 1 and j at point 2 that reflect the particular association constraints of a given system. If each monomer contains M attraction sites, the set of which is denoted by Γ, then the general F-bond sum can be written as

$$F(\mathbf{1},\mathbf{2}) \equiv e^R(r)\left(\left\{\prod_{i\in\Gamma}\prod_{j\in\Gamma}\left[1 + f^A_{ij}(\mathbf{1},\mathbf{2})\right]\right\} - 1\right). \tag{3.28}$$

The resulting sum includes all possible $f^A_{ij}(\mathbf{1},\mathbf{2})$ bond combinations consistent with the set of attractive sites Γ, including multiply-bonded sites. For the single-site model, of course, the sum reduces to a single $f^A(\mathbf{1},\mathbf{2})$ or $F(\mathbf{1},\mathbf{2})$ bond. All the site–site potentials $u^A_{ij}(\mathbf{1},\mathbf{2})$ are assumed to be purely attractive or, if interactions between certain sites is not allowed, zero.[4] In this way, for example, f-bonds between like sites can be made to vanish: $f^A_{ii}(\mathbf{1},\mathbf{2}) = 0$. More importantly, steric effects —discussed in Section 3.4.1— will eliminate many more terms in $F(\mathbf{1},\mathbf{2})$, particularly those corresponding to graphs with multiply-connected sites.

While such a model is based upon site-site interactions, the sites do not replace the molecules as the primary units in the theory.[5] Nor is the opposite ap-

---

[4]Another possibility, not treated in this work, is that like sites (*e.g.* electron lone pair sites) repel each other, in which case $u^A_{ii}(\mathbf{1},\mathbf{2}) > 0$ and the resulting $f^A_{ii}(\mathbf{1},\mathbf{2})$ contribution no longer vanishes.

[5]The rubric "site–site" used in the context of Wertheim theory should not be confused with that in conjunction with other physical cluster–type theories [76] where interaction sites, not particles, act as primary units in the theory. Nor should the "site–site" quantities that arise in RISM-like molecular models be confused with those in Wertheim theory.

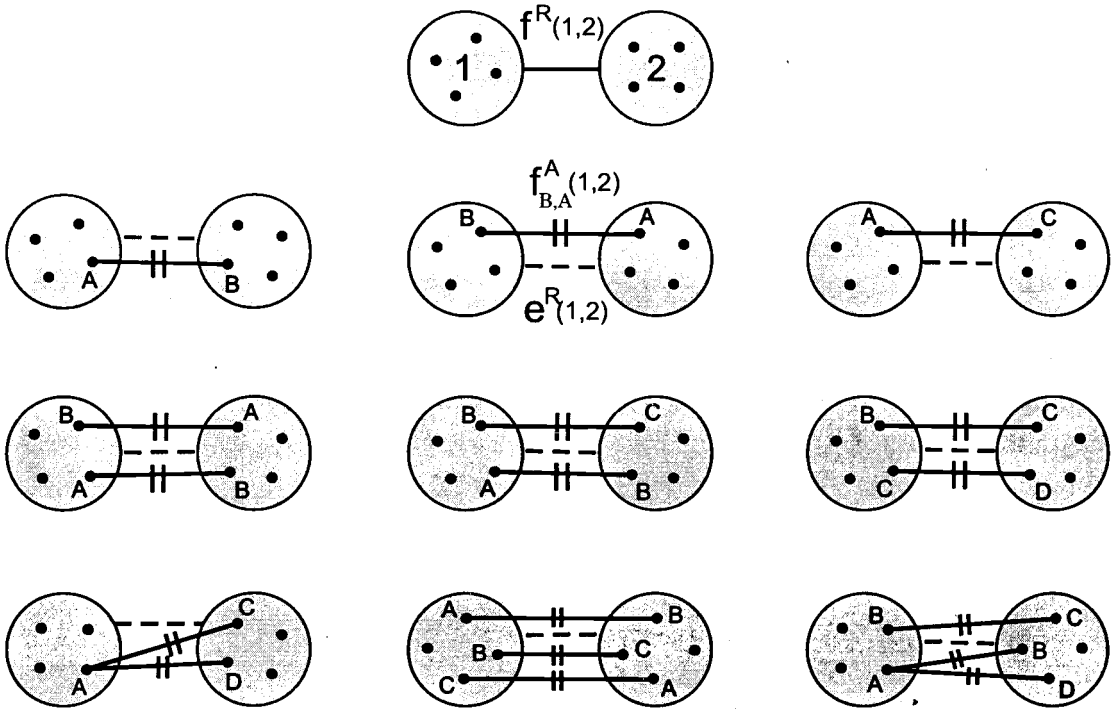

FIGURE 3.2. Several possible hyperpoint bonding states between a pair of identical monomers located at space points 1 and 2 with four attraction sites. Bonding between like sites is not allowed. Hyperpoints are considered directly connected if their is either an f^R bond —— or any number of f_{ij}^A bonds $\dashv\vdash$ between them, the latter also being connected via an e^R bond - - - - .

---

proach taken, where all association products are treated as molecules with internal degrees of freedom, which prohibitively complicates the theory. Instead, Wertheim theory treats each species as a monomeric unit in which some particular set of the M attraction sites is bonded. Given this approach, graph vertices are represented by large open circles called *hyperpoints*, wherein the M attraction sites are represented by small, solid dots, labeled by the type of site when necessary. A site is *bonded* if one or more f_{ij}^A bonds are incident. The $f_{ij}^A(\mathbf{1},\mathbf{2})$ bonds are graphically represented by $\dashv\vdash$ lines, as are the $F(\mathbf{1},\mathbf{2})$ bonds, which make no reference to specific sites but which contain an $e^R(\mathbf{1},\mathbf{2})$ bond. The $e^R(\mathbf{1},\mathbf{2})$ bonds are represented as - - - - lines between hyperpoints, but are not shown when the $\dashv\vdash$ bond is an $F(\mathbf{1},\mathbf{2})$ bond. Finally, $f^R(\mathbf{1},\mathbf{2})$ bonds between hyperpoints are shown graphically as —— lines.

As with Lockett's formalism, the decomposition of the Mayer f-bond according to Eqs. (3.27) and (3.28) results in the replacement of each $f(\mathbf{1},\mathbf{2})$ bond in the graph sum βPV, Eq. (3.23), by an $f^R(\mathbf{1},\mathbf{2})$ bond and subsequently by an $F(\mathbf{1},\mathbf{2})$ bond, which is further decomposed into various $f^A_{ij}(\mathbf{1},\mathbf{2})$ bonds in parallel with an $e^R(\mathbf{1},\mathbf{2})$ bond. Some representative bonding states between identical hyperpoints with four attraction sites each are shown in Fig. 3.2; bonding between like sites is not allowed. Two hyperpoints are considered "bonded" if they are connected by either f^R or f^A_{ij} bonds; that is, if they get sufficiently close enough such that $f^R(\mathbf{1},\mathbf{2})$ is non-negligible or if their attractive sites get close enough such that $f^A_{ij}(\mathbf{1},\mathbf{2})$ is non-negligible. For discontinuous models the "formation" of a bond is more clear-cut. With these bond replacements the pressure and singlet density graph series become

$$\beta PV = \left\{ \begin{array}{l} \text{sum of all topologically distinct connected graphs} \\ \text{composed of one or more black } z(\boldsymbol{i})\text{-hyperpoints} \\ \text{and one or more bonds. Each bonded pair 1, 2} \\ \text{has either an } f^R \text{ bond, or an } e^R \text{ bond and one or} \\ \text{more site–site } f^A_{ij} \text{ bonds.} \end{array} \right\}, \tag{3.29}$$

$$\rho(\mathbf{1}) = \left\{ \begin{array}{l} \text{sum of all graphs obtained from } \beta PV \text{ by taking} \\ \text{all distinct ways of turning field hyperpoints into} \\ \text{a root hyperpoint labeled 1.} \end{array} \right\}. \tag{3.30}$$

Borrowing the terminology of chemistry, we can now define all F– or f^A_{ij}-connected graphs on 1, 2, 3, ..., s hyperpoints as monomer, dimer, trimer, ..., s-mer graphs. For example, going back to the single site case (hyperpoints $\rightarrow$ points) but still allowing for multiple bonding of monomers, the s-mer graphs for s = 1, 2, and 3, along with a representative group from s = 4, look like

$\beta PV \propto$ 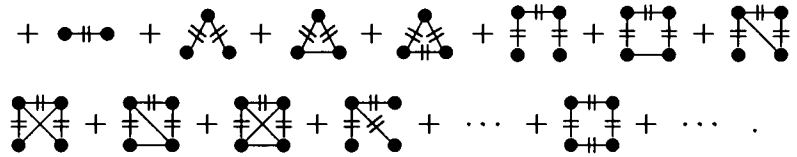 (3.31)

These s-mer graphs represent a subset of the diagrams in (3.29) above, but are of central interest because physically-motivated approximation schemes are all couched in terms of restrictions upon s-mers. Moreover, the low density, high association limit (wherein s-mers form but rarely interact) will also reduce to a fugacity description of s-mers.

It is precisely at this stage, therefore, that Wertheim introduces the steric incompatibility (SI) effects such that vanishing or negligible s-mer graphs (based upon those SI effects) can be combined into graphically irreducible forms that will not broken up or "decomposed" into lower order graphs which may be non-negligible or which are mixed with non-negligible graphs during the topological reduction process. Making these vanishing or negligible s-mer graphs irreducible involves "filling" them with e^R bonds, yet before describing this process it is first important to identify which s-mer graphs vanish or are negligible, and this requires knowledge of the SI effects.

3.4.1. Steric Incompatibility

The highly directional, short-ranged nature of attractive bonds in associating fluids, *i.e.* the interaction geometry, leads to steric incompatibility effects wherein certain bond configurations are physically negligible or absent. These steric incompatibility effects are easily manifest by appropriately tailoring the interaction range and anisotropy and greatly simplify the evaluation of the graph sums βPV and $\rho(\mathbf{1})$. Wertheim identifies three types of steric incompatibility (SI) that are important in associating fluids [21]: SI-1, SI-2, and SI-3. The first type concerns one attraction site per monomer, while the last two depend upon the presence of two or more attraction sites on each monomer. A sketch of the first two types is shown in Fig. 3.3.

3.4.1.1. Basic SI Effects

The first SI type, SI-1, involves three monomers and one attraction site on each. When an attraction site on monomer 1 approaches another site on monomer 2 such that the pair form an $F(\mathbf{1},\mathbf{2})$ or $f_{ij}^{A}(\mathbf{1},\mathbf{2})$ bond, then those two sites i and j become *saturated*, the repulsive cores of 1 and 2, along with that of a third monomer 3, prevent any attraction site on 3 from coming close enough to form a bond with the saturated sites i and j. This precludes any one site from bonding to more than one monomer. By limiting the range and angle of the attraction sites, the presence of the combined e^R bond, $e^R(\mathbf{2},\mathbf{3})$ say, creates a vanishing graph if

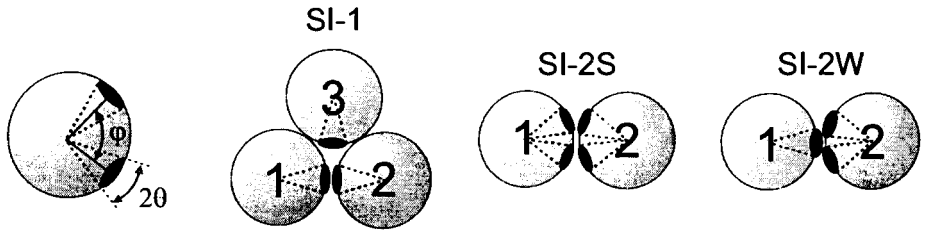

FIGURE 3.3. Sketch of steric incompatibility effects SI-1, SI-2S, and SI-2W for the sticky spot model. The shaded spheres represent the hard core, while the sticky spots are shown as dark disks on the surface. At left, the bond angle φ and the cone angle θ are defined.

---

an $f_{jk}^{A}(\mathbf{2},\mathbf{3})$ bond were to form between sites j and k because $e^{R}(\mathbf{2},\mathbf{3})$ is zero for the required hard core overlap.

The second SI type comes in two forms, SI-2S and SI-2W, and involves pairs of monomers and the interrelationship between the bond angle φ, the cone angle θ, and the attraction site range —which is infinitesimal in the sticky spot limit. Depending upon the attraction range and cone angle θ, a sufficiently small value of φ will allow for double bonding between monomers. One possibility is that two attraction sites on one monomer form f_{ij}^{A} bonds with two sites on another monomer (see Fig. 3.3). The limitation of such bond formation on physical grounds is known as the strong form of SI-2 or SI-2S. For even smaller bond angles φ, a single attraction site on one monomer could form a "double bond" with *two* sites on another monomer. Given the typical range and anisotropy of attractive forces in associating fluids, such double bonding is physically improbable and its prohibition is referred to as the weak form of SI-2 or SI-2S.

Together, the SI-1 and SI-2W effects constitute the *single bonding condition* (SBC) [21], and corresponds to omitting all graphs with multiple bonding of an attraction site. The SBC is meant to reflect the saturation of chemical bonds and vastly simplifies the graphical analysis of βPV.

The third type of SI effect, SI-3, involves two or more attraction sites per monomer in s-mers with s $\geq$ 3, but is much more complicated and difficult to apply. If the bond angle φ is fixed, such that the s-mer is a rigid structure, the addition of f^{R} bonds between hyperpoints inconsistent with the s-mer structure will produce a vanishing graph. As an example, consider the tetrameric (s = 4)

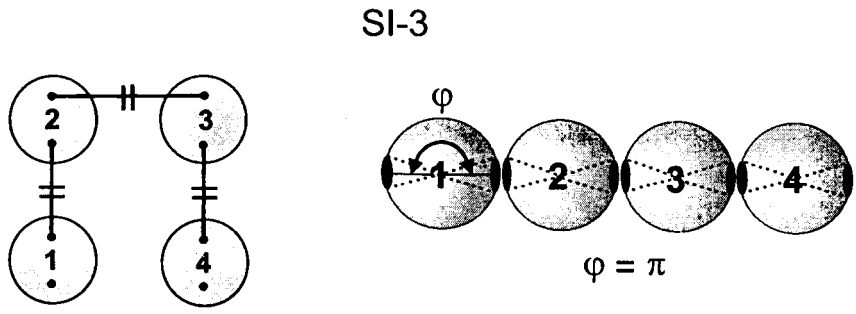

FIGURE 3.4. Illustration of an SI-3 effect for a two-site sticky spot model. If the angle φ is fixed, say at π, then the F-bonded diagram at left is nonvanishing for the rigid chain configuration sketched at right. The addition of any possible f^R bonds between these hyperpoints, however, produces a vanishing graph.

---

graph shown at left in Fig. 3.4 with no f^R bonds. If the bond angle is fixed at $\varphi = \pi$ then this diagram is non-negligible for the monomer configuration sketched at right. Yet because of the hard cores and short range of the attraction sites, the addition of any one of the three possible f^R bonds, *viz.* $f^R(\mathbf{1},\mathbf{4})$, $f^R(\mathbf{1},\mathbf{3})$, or $f^R(\mathbf{2},\mathbf{4})$, produces a vanishing graph; the hard core overlap dictated by the f^R bond is incompatible with the requirement of neither breaking an f^A bond nor violating hard core exclusion. Whenever the rigidity of the s-meric structure, *i.e.* bond angles, prevents monomers in the structure from encountering each other, there is necessarily an absence of "steric self-hindrance", meaning an absence of f^R bonds. Clearly self-hindrance also depends upon the attraction site range and angle limits —in our model the cone angle θ.

The difficulties in the implementation of SI-3 effects are two-fold. First, enforcing rigid bond angles vastly complicates evaluation of the cluster integrals, even under the SBC. Second, rigid bond angles not only disturb the topological reduction procedure by complicating the process of making s-mer graphs irreducible, thereby losing the optimal SI results, but also complicate the solution of integral equations (like the OZ). Before describing this, as yet, vague process of rewriting s-mer graphs as irreducible diagrams in order to optimize the topological reduction process, we might be tempted to simply relax this bond angle restriction in hopes of eliminating these problems. In fact, this is exactly what we have done in order to obtain analytical results for our sticky spot model: our cluster integrals will be

averaged over bond angles φ such that the attraction sites are effectively randomly located on the hard core surface, each acting independently of the other sites. As will be seen in Chapter 5, such a scheme simplifies the analysis in many ways, but the omission of fixed bond angles carries its own serious consequences as far as the capabilities of the theory.

3.4.1.2. s-mer Bond-Combining Rule

Armed with the SI effects described above, we now have physically-motivated criteria by which to judge the size of the contribution of s-mer graphs in the sum βPV or $\rho(\mathbf{1})$. Some subset of the s-mer graphs in these sums will be zero or negligible due to SI effects. Yet some subset of *those* graphs will be reducible, and therefore broken up or "decomposed" into lower-order graphs or mixed with lower-order graphs which may or may not be negligible. In this manner negligible diagrams erroneously contribute to the graph sum βPV. In order to keep any negligible s-mer graphs from being split up in the remaining topological reduction steps, Wertheim combines subsets of s-mer graphs such that they become irreducible, and hence left untouched by topological reduction. Specifically, given a set of fugacity graphs on s points with F and f^R bonds, a subset of them is the set in which all s points are distinctly connected by paths of F bonds, and this subset can be constructed in two steps: (1) construct all connected graphs on s points with all F bonds; (2) for any pair of points not directly connected by an F bond, insert an e^R bond.

As a simple example, consider for the moment a single-site model and the representative s-mer graphs in Eq. (3.31). The *bare* s-mer graph

is reducible, and so will be split up in steps (2) and (3) of the topological reduction procedure, even though SI-1 dictates that this is a vanishing diagram. We can make this diagram irreducible, however, by "filling" it with e^R bonds

(3.32)

which, according to $e^R = 1 + f^R$, simply corresponds to combining the bare s-mer graph with all possible combinations of f^R-bonds:

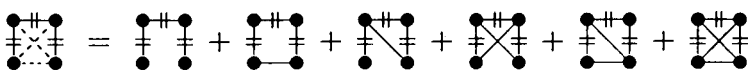

(3.33)

According to Wertheim [21]:

> *The regrouping effected by adoption of the combined e^R-bond insures that incompatible bond configurations which are killed by SI-1 stay together when topological reduction is used to eliminate articulation points. This allows us to carry out the reduction in all generality without forgoing the chance to apply the single bonding condition [or other SI effects] later.*

For interaction potentials like the single-site, sticky spot model, all s-mer graphs for s $\leq$ 2 vanish due to the SI-1 condition, leading to a model of dimerization. Such a system will be discussed in detail in Chapter 4.

Filling s-mer graphs with e^R bonds is not so straightforward for multi-site attraction models however, because bonding information concerning individual sites is lost in the process. That information is important not only in terms of SI-3 effects, but also in defining the partial densities —which are introduced in the next section. In order maintain this connectivity information we must refine our definition of connectivity and the process of e^R bond filling.

First, hyperpoint connectivity must be clarified. Following Wertheim, we define the subset of all graphs which contain networks of $F-$ or f_{ij}^A-bond connected hyperpoints as $\{S\}$. Since the hyperpoints in this subset are already connected, an $f^R(k,l)$ bond may or may not be present between any pair of hyperpoints k, l. By considering a bare graph in this subset, *i.e.* absent of any f^R bonds, we can identify two kinds of *connectedness* between hyperpoints, mediated by the attraction sites. Label two sites A and B and define:

(1) Two sites A and B as *bond-connected* if and only if there is a path consisting of attraction bonds and attraction sites from A to B.

(2) Two sites A and B are *constraint-connected* if and only if they are located on the same hyperpoint.

Any graph in $\{S\}$ may contain some or no unbonded sites and one or more bond-connected networks. If two or more networks of bond-connected sites exist, then

they must contain hyperpoints k wherein the connectedness is supplied by constraint connections between sites belonging to different networks. All such hyperpoints k are defined as *constraint-articulation points* (c-APs); deleting the constraint connection at k (without deleting any sites or bonds) and any f^R or e^R bonds incident at k will cause the s-mer graph to split into two or more connected, but not mutually connected graphs. A bond-connected articulation point (b-AP) can also be defined in a fashion analogous to the single-site case.

The question at hand now is: Considering any pair of hyperpoints k and l in $\{S\}$ not directly connected by an f_{ij}^A bond, to what extent should the absence and presence of an $f_{ij}^A(k,l)$ bond be combined into an $e^R(k,l)$ bond? Wertheim's rule for e^R bond filling is that

Rule 1

If any site A in hyperpoint k is bond-connected to any site B in hyperpoint l then a combined $e^R(k,l)$ bond is adopted.

With this e^R–bond filling scheme, all hyperpoints spanned by a bond-connected network become irreducible because e^R bonds are never to be split up into their constituent 1– and f^R-bonds; in addition all b-APs have been eliminated in the process. Why not incorporate e^R bonds between constraint-connected hyperpoints? This limited adoption of e^R bonds between hyperpoints with bond-connected sites can, in part, be understood in terms of the difficulties associated with the SI-3 effects discussed in the last section. The wholesale addition of f^R bonds between hyperpoints not directly bond-connected —implied in e^R-bond filling— is not an effective strategy because non-negligible and negligible graphs may be mixed in the execution: the addition of an f^R bond may be inconsistent with bond angle constraints and lead to a vanishing graph due to SI effects. Filling e^R bonds between hyperpoints is only effective when negligible or vanishing graphs are combined in the process. Moreover, the addition of e^R bonds between hyperpoints without direct connection by F or f_{ij}^A bonds leads to more highly connected graphs, which reduces the solution possibilities of integral equations, like the OZ. Such relations generate graphs by composition of lower-order graphs that share one or two labeled hyperpoints. For a more detailed exposition, see Ref. [21].

Of course, more than one such e^R-filled network of hyperpoints may exist within an s-mer graph, and it is convenient to classify them as s-mer *subgraphs*.

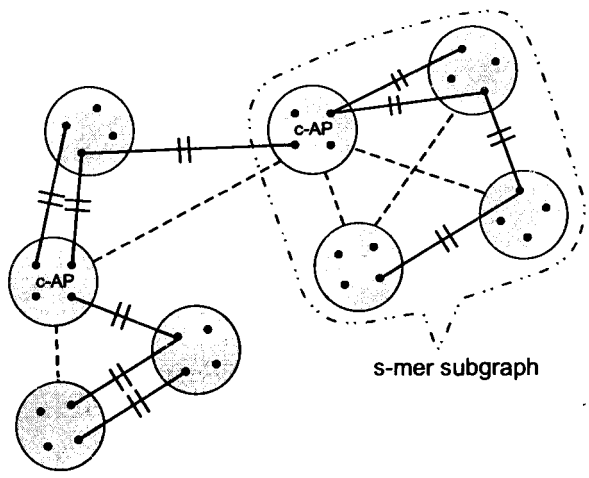

FIGURE 3.5. General filling of s-mer *subgraphs* with e^R-bonds inside a Wertheim s-mer *graph* for a four-site model. All hyperpoints spanned by a bond-connected network of F-bonded sites (three subgraphs in this case) are filled with e^R-bonds - - - - ; recall that F-bonds ⊣⊢ contain an e^R factor. Constraint articulation points (c-APs) define the boundaries of the subgraphs, between which no e^R-bonds are inserted [21].

An example of an s-mer graph with three subgraphs is shown in Fig. 3.5. The s-mer subgraphs, under Wertheim's scheme, are filled with e^R bonds, two c-APs being clearly evident. Note that the attractive sites (black dots) in this s-mer are not labeled, such labels being irrelevant to the current point, thus making the attractive bonds ⊣⊢ F-bonds; if specific site labels are attached, turning all attractive bonds into f_{ij}^A-bonds, then all possible site-site combinations consistent with the given SI effects must be considered. Thus, for brevity, we shall omit site-specific labels whenever possible, and instead perform our graphical analysis using generic, site-independent graphs such as the one shown in Fig. 3.5. The great economy of this approach will be seen in Chapter 5 where we treat a four-site, water-like system.

The addition of f^R bonds between s-mer subgraphs, *i.e.* steric self-hindrance, is a an important issue for multi-site models, but, as already alluded to, must be considered on an individual basis. As such it is convenient to characterize the graph sum in terms of s-mer graphs and subgraphs. Using the notation of Wertheim, consider the subset of $\{S\}$ that consists of all diagrams of F-bond

connected hyperpoints without any f^R bonds, and call it $\{B\}$ for "bare" graphs. This leaves the subset $\{H\}$, defined as $\{H\} \equiv \{S\} - \{B\}$, and consists of all "hindered" graphs in $\{S\}$, obtained by taking all ways of adding f^R bonds between hyperpoints not already connected by F or e^R bonds. Both sets $\{B\}$ and $\{H\}$ contain irreducible diagrams and trees of irreducible diagrams connected by c-APs. The hindered s-mer graphs in $\{H\}$ account for the steric self-hindrance effects of s-meric structures. In order to obtain analytic results in Chapter 5 for our four-site model, all of these hindered graphs will be neglected. Inclusion of these graphs without enforcing fixed bond angles and properly treating SI-3 effects can lead to non-physical results.[6]

3.4.2. Partial Densities & Correlations

With the s-mer conventions defined in the last section, as well as the general SI effects in mind, we are now prepared to re-examine the topological reduction process, steps (2) and (3) on page 48. The pressure and singlet density, written in terms of the graph set $\{S\}$ are

$$\beta PV = \left\{ \begin{array}{l} \text{sum of all topologically distinct, connected s-mer} \\ \text{graphs, including the monomer hyperpoint, where} \\ \text{s} = 1, 2, \ldots, \infty, \text{ and all possible combinations of} \\ f^R \text{ bonds between hyperpoints in distinct s-mers.} \end{array} \right\}, \tag{3.34}$$

$$\rho(\mathbf{1}) = \left\{ \begin{array}{l} \text{sum of all graphs obtained from } \beta PV \text{ by taking} \\ \text{all distinct ways of turning field hyperpoints into} \\ \text{root hyperpoints labeled 1.} \end{array} \right\}. \tag{3.35}$$

As before, the analysis begins with singlet density $\rho(\mathbf{1})$, but the application of *Lemma 1*, the removal of white articulation points (APs), must be modified because there is more than one type of white AP, and we do not wish to lose hyperpoint bonding information in the process. The bonding information is examined by classifying the diagrams in $\rho(\mathbf{1})$ according to the connectivity at each labeled

---

[6] A preliminary analysis [104] of the four-site, sticky spot model with some hindered graphs incorporated into the theory suggests that unphysical results can occur when rigid bond angles are not included as well.

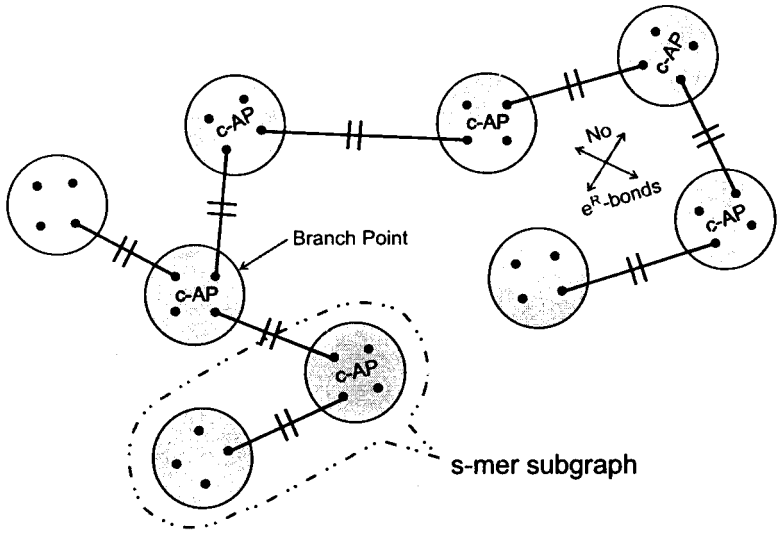

FIGURE 3.6. Representative bare s-mer graph in the four-site model under the water-like SI conditions: SI-1, SI-2S, and SI-2W. These conditions effectively turn all hyperpoints into c-APs, thereby limiting s-mer *subgraphs* to dimers (*cf.* Fig. 3.5) and eliminating all e^R-bonds except those embedded in the F-bonds.

---

hyperpoint. For simplicity we use the four-site, sticky-spot model examined in Chapter 5 to model water as a template for our remaining graphical analysis, and thus impose the SI conditions consistent with that system: SI1, SI-2W, and SI-2S. Wertheim discusses the general case, assuming none of the SI effects [21]. The SI conditions adopted here confine s-mer *subgraphs* to dimers, effectively turning every hyperpoint into a c-AP. A representative s-mer graph is shown in Fig. 3.6. Under the SBC no b-APs exist, preempting the need to fill s-mer subgraphs with e^R-bonds; the F bond directly connecting every dimer subgraph already contains an e^R bond. The four attraction sites on a "water" monomer represent the two hydrogen sites, H_a and H_b say, and the two electron lone pair sites, L_a and L_b. Under the SI conditions, the general $F(\mathbf{1},\mathbf{2})$ bond, Eq. (3.28) on page 60, simplifies to

$$F(\mathbf{1},\mathbf{2}) \equiv e^R(r)\sum_{i=H_a}^{H_b}\sum_{j=L_a}^{L_b}\left[f_{ij}^A(\mathbf{1},\mathbf{2}) + f_{ji}^A(\mathbf{1},\mathbf{2})\right], \tag{3.36}$$

where no like-site bonding is allowed, *e.g.* $f_{H_aH_a}^A(\mathbf{1},\mathbf{2}) = f_{L_aL_b}^A(\mathbf{1},\mathbf{2}) = 0$. The $F(\mathbf{1},\mathbf{2})$ bond then contains eight equal site-site terms reflecting the proper con-

nectivity constraints on the individual $f_{ij}^{A}(\mathbf{1},\mathbf{2})$ bonds between site i on monomer 1 and site j on monomer 2.

Much of this site-specific information, however, can be subsumed into the graphical analysis by working with generic quantities instead, *e.g.* $F(\mathbf{1},\mathbf{2})$. This means that our inspection of all graphs in $\rho(\mathbf{1})$ mentioned above can be carried out in terms of generic, F-bond connected graphs instead of site-specific $f_{ij}^{A}(\mathbf{1},\mathbf{2})$ graphs; there is no need to explicitly show hyperpoints with separate attraction sites, and so we use the same graph formalism as for the single-site case (hyperpoints $\rightarrow$ points).

Using the simplifications and the SI conditions mentioned above, we now examine the fugacity graph sum $\rho(\mathbf{1})$,

$\rho(\mathbf{1}) =$ 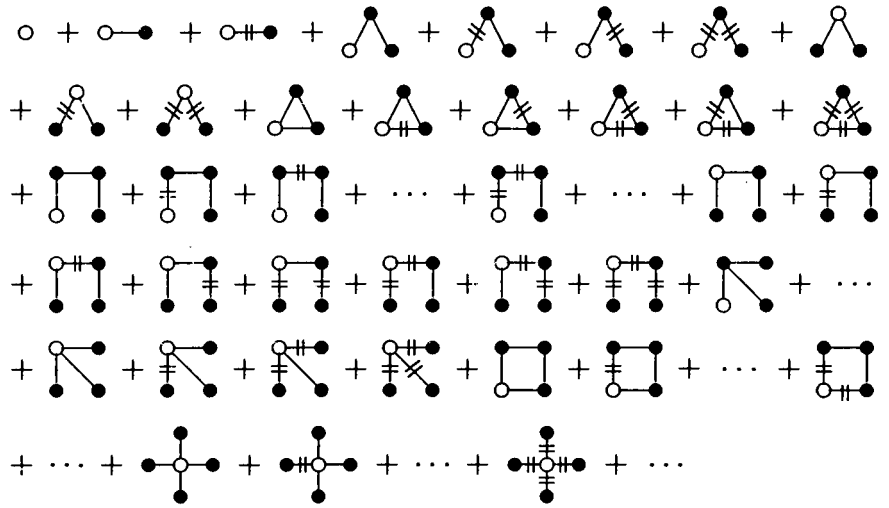 (3.37)

obtained from Eqs. (3.30) and (3.36). Again, the vertices in these graphs are hyperpoints, but the site-specific information is subsumed into the F-bond. We now classify these graphs according to the number of F bonds incident upon the labeled root point o . Obviously, the current model limits the maximum number incident at any one root point to four. The singlet density $\rho(\mathbf{1})$ therefore trivially splits into a sum of four *partial densities* $\rho^{(m)}(\mathbf{1})$, *viz.*

$$\rho(\mathbf{1}) \equiv \sum_{m=0}^{4} \rho^{(m)}(\mathbf{1}), \tag{3.38}$$

each partial density reflecting the number of incident F bonds through its index m. Wertheim's graphical formalism is thus a first-order theory in density. All graphs

with no incident F bonds, for example, are included in the monomer density $\rho^{(0)}(\mathbf{1})$,

$\rho^{(0)}(\mathbf{1}) =$ 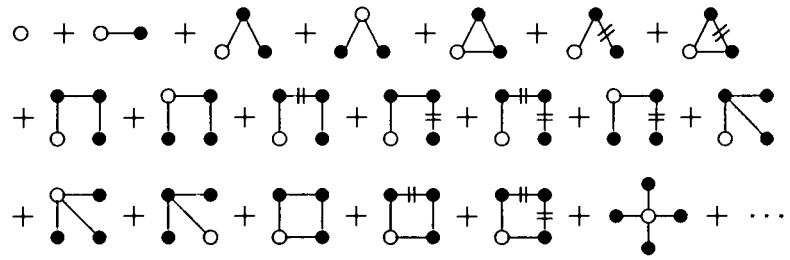 (3.39a)

while a representative set of graphs for each of the remaining partial densities is:

$\rho^{(1)}(\mathbf{1}) =$ 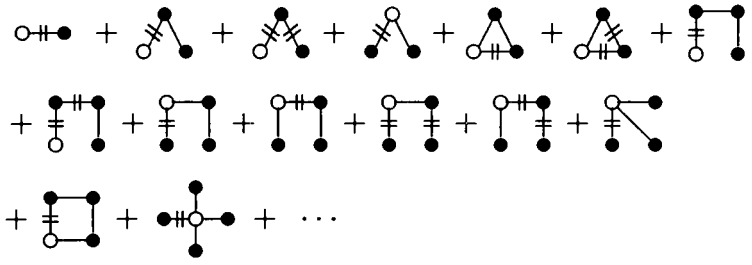 (3.39b)

$\rho^{(2)}(\mathbf{1}) =$ 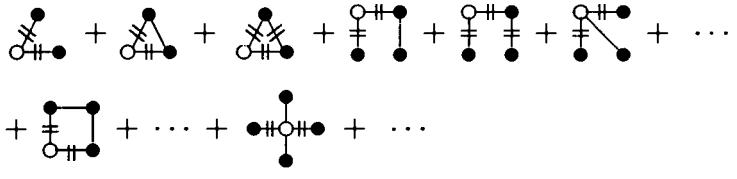 (3.39c)

$\rho^{(3)}(\mathbf{1}) =$ 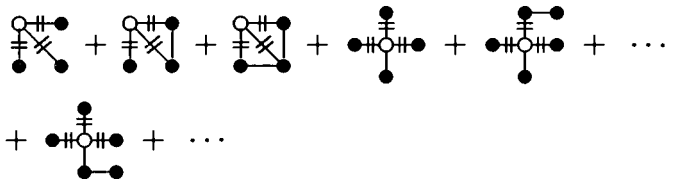 (3.39d)

$\rho^{(4)}(\mathbf{1}) =$ 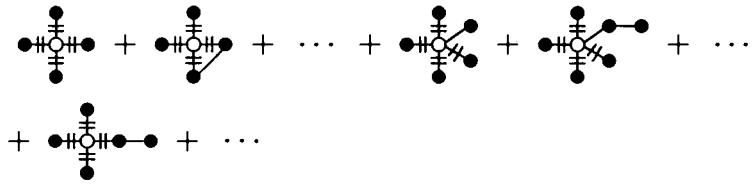 (3.39e)

While $\rho^{(0)}(\mathbf{1})$ is the monomer density, the $\rho^{(m)}(\mathbf{1})$ for $m \geq 1$ do not correspond to the "m-mer" densities, but instead the number density of monomers with m incident F bonds: a quick glance, for example, at the graphs included in $\rho^{(1)}(\mathbf{1})$ clearly shows why this is true.

In order to apply *Lemma 1* we now analyze the root points $\circ$ in each $\rho^{(m)}(\mathbf{1})$. Recall that the single bonding condition (SBC) precluded the possibility of any, let alone white, bond-connected articulation points or b-APs. There are,

however, still (Mayer) white APs as well as white c-APs in the partial densities. After a quick glance at the representative graphs above, it is clear that all white APs are contained in $\rho^{(0)}(\mathbf{1})$. We therefore apply *Lemma 1* to the graphs in $\rho^{(0)}(\mathbf{1})/z(\mathbf{1})$, step (3) in the topological reduction list, to obtain the subset of graphs for which the root point $\circ$ is not an AP; this defines the one-body correlation function $c^0(\mathbf{1})$,

$$c^0(\mathbf{1}) \;=\; \ln\left[\rho^{(0)}(\mathbf{1})/z(\mathbf{1})\right] \,, \tag{3.40}$$

analogous to the $c(\mathbf{1})$ correlation function defined in Mayer theory. The superscript 0 indicates that no F-bonds are incident upon the labeled point 1. Looking closely at the other partial densities, we also note that each $\rho^{(m)}(\mathbf{1})$ for $m \geq 1$ contains $\rho^{(0)}(\mathbf{1})$ as a factor. That is, the root point in each graph of $\rho^{(m)}(\mathbf{1})$ can be "decorated" by the graph sum $\rho^{(0)}(\mathbf{1})$ in a *star product*[7] in order to generate some higher-order graphs in $\rho^{(m)}(\mathbf{1})$. As an example, the star product of the first graph in $\rho^{(1)}(\mathbf{1})$, , and the first four graphs in $\rho^{(0)}(\mathbf{1})$ from Eq. (3.39a) gives

where all four graphs on the right-hand side are seen from Eq. (3.39b) to belong to $\rho^{(1)}(\mathbf{1})$. We may therefore factor out $\rho^{(0)}(\mathbf{1})$ from the partial densities in order to simplify the topological reduction method. Returning, for the moment, to the general case where none of the SI conditions are imposed (see Fig. 3.5 on page 69), the ratio $\rho^{(m)}(\mathbf{1})/\rho^{(0)}(\mathbf{1})$ generally contains diagrams such that the root point $\circ$ is *not* a c-AP and diagrams where $\circ$ *is* a c-AP. All those diagrams in which $\circ$ is *not* a c-AP Wertheim assigns to the *partial* one-body correlation functions $\mathrm{c}^m(\mathbf{1})$, whereas all diagrams in which $\circ$ *is* a c-AP are products of graphs in the single-body $c^\gamma(\mathbf{1})$ functions, where γ is a partition of m into nonempty subsets. In the absence of SI effects then, the general density relation is

$$\rho^{(m)}(\mathbf{1}) \;=\; \rho^{(0)}(\mathbf{1}) \sum_{P(m)=\{\gamma\}} \prod_{\gamma} c^\gamma(\mathbf{1}) \,, \tag{3.41}$$

---

[7]The process of "decorating" the root points $\circ$ in $\rho^{(m)}(\mathbf{1})$ with the graphs in $\rho^{(0)}(\mathbf{1})$ refers to the formation of a *star product*; for more details see Appendix A in this work or Section 4.4 of Hansen and McDonald's text [55].

where $P(m) = \{\gamma\}$ denotes the partition of m into subsets with index γ; the improper partition of the single set $\gamma = m$ is included. In our generic notation of F-bonded structures, the partial densities according to Eq. (3.41) are[8]

$$\rho^{(1)}(\mathbf{1}) = \rho^{(0)}(\mathbf{1})\, c^1(\mathbf{1}), \tag{3.42a}$$

$$\rho^{(2)}(\mathbf{1}) = \rho^{(0)}(\mathbf{1}) \left\{ c^2(\mathbf{1}) + \frac{1}{2!}\left[c^1(\mathbf{1})\right]^2 \right\}, \tag{3.42b}$$

$$\rho^{(3)}(\mathbf{1}) = \rho^{(0)}(\mathbf{1}) \left\{ c^3(\mathbf{1}) + \frac{1}{3}\, c^2(\mathbf{1}) c^1(\mathbf{1}) + \frac{1}{3!}\left[c^1(\mathbf{1})\right]^3 \right\}, \tag{3.42c}$$

$$\rho^{(4)}(\mathbf{1}) = \rho^{(0)}(\mathbf{1}) \left\{ c^4(\mathbf{1}) + \frac{1}{4}\, c^3(\mathbf{1}) c^1(\mathbf{1}) + \frac{1}{3}\, c^2(\mathbf{1}) c^2(\mathbf{1}) + \frac{1}{4!}\left[c^1(\mathbf{1})\right]^4 \right\}. \tag{3.42d}$$

The higher-order partial correlations, *i.e.* $c^m(\mathbf{1})$ for $m > 1$, correspond to multiple F-bonds incident at the hyperpoint, and as such incorporate more complex correlations between highly connected graphs. Self-consistently solving this nonliner set of partial density equations is impossible analytically. Numerical solutions are possible, but these higher-order correlations involve orientational effects that are not easily approximated; their inclusion, in fact, can lead to worse results than even a first-order treatment. Under the SI conditions adopted here however, specifically the SBC where all subgraphs are limited to dimers, *every* hyperpoint is a c-AP, and so all $c^m(\mathbf{1})$ vanish for $m > 1$.

We are now left with partial densities defined in terms of the one-body partial correlation function $c^1(\mathbf{1})$:

$$\rho^{(1)}(\mathbf{1}) = \rho^{(0)}(\mathbf{1})\, c^1(\mathbf{1}), \tag{3.43a}$$

$$\rho^{(2)}(\mathbf{1}) = \rho^{(0)}(\mathbf{1}) \frac{1}{2!}\left[c^1(\mathbf{1})\right]^2, \tag{3.43b}$$

$$\rho^{(3)}(\mathbf{1}) = \rho^{(0)}(\mathbf{1}) \frac{1}{3!}\left[c^1(\mathbf{1})\right]^3, \tag{3.43c}$$

$$\rho^{(4)}(\mathbf{1}) = \rho^{(0)}(\mathbf{1}) \frac{1}{4!}\left[c^1(\mathbf{1})\right]^4. \tag{3.43d}$$

Note that all incident F-bonds are accounted for directly through the $c^1(\mathbf{1})$ functions. The only other bonds which may be incident upon the labeled point o in the graph sum $c^1(\mathbf{1})$ are f^R-bonds. All such possible repulsive interactions with other

---

[8]Compare our generic density relations to the much more complicated site-specific quantities of Vakarin *et. al.* [105].

s-mers are accounted for by the implicit star product $\rho^{(0)}(\mathbf{1}) * c^1(\mathbf{1})$ in Eqs. (3.43a)–(3.43d). The fugacity graph series $c^1(\mathbf{1})$, however, still contains black articulation points, *i.e.* both reducible and irreducible graphs. Following step (4) in the topological reduction list on page 48, we can generate all fugacity graphs in $c^1(\mathbf{1})$ from the subset irreducible graphs by rewriting the fugacity vertices of those irreducible graphs as partial density vertices. That is, at each field point • of an irreducible graph "attach" nothing, or any allowable graph sum $\rho^{(m)}(\mathbf{1})$ consistent with the connectivity constraints (max of 4 incident F-bonds). A few such representative irreducible graphs for $\rho^{(1)}(\mathbf{1})$ are

$\rho^{(1)}(\mathbf{1}) =$ 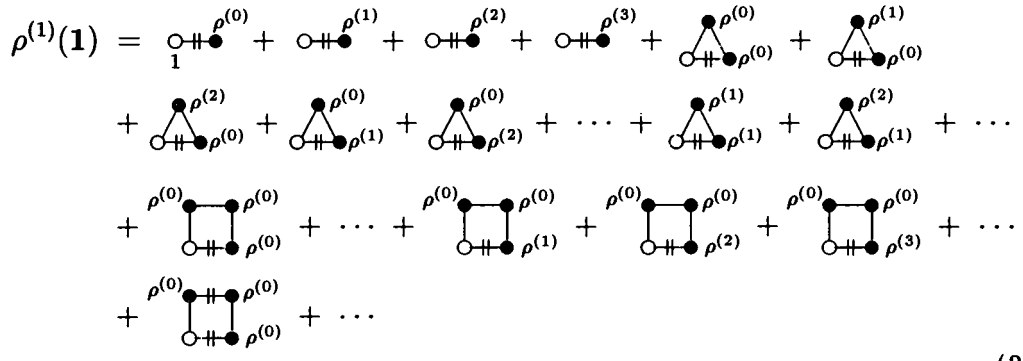

(3.44)

where the labeled point 1 carries the function $\rho^{(0)}(\mathbf{1})$, but is not shown.

Future manipulation of these partial density graph sums is made more economical through the definition of a set of generic, *complementary* density parameters $\sigma^{(n)}(\mathbf{1})$, each representing a sum of $\rho^{(m)}(\mathbf{1})$ graphs with at least m available bonding sites:

$$\sigma^{(0)}(\mathbf{1}) = \rho(\mathbf{1}), \tag{3.45a}$$

$$\sigma^{(1)}(\mathbf{1}) = \rho^{(0)}(\mathbf{1}) + \rho^{(1)}(\mathbf{1}) + \rho^{(2)}(\mathbf{1}) + \rho^{(3)}(\mathbf{1}), \tag{3.45b}$$

$$\sigma^{(2)}(\mathbf{1}) = \rho^{(0)}(\mathbf{1}) + \rho^{(1)}(\mathbf{1}) + \rho^{(2)}(\mathbf{1}), \tag{3.45c}$$

$$\sigma^{(3)}(\mathbf{1}) = \rho^{(0)}(\mathbf{1}) + \rho^{(1)}(\mathbf{1}), \tag{3.45d}$$

$$\sigma^{(4)}(\mathbf{1}) = \rho^{(0)}(\mathbf{1}). \tag{3.45e}$$

These density parameters are similar to those of Wertheim, but differ in two respects. First, our density parameters $\sigma^{(n)}(\mathbf{1})$ are generic, not making any references to specific interaction sites. Second, the index m in our case is *complementary* to the density index m in $\rho^{(m)}(\mathbf{1})$, meaning that n refers to the *minimum* number

of sites not bonded at the labeled vertex. The density indices in the standard multi-site notation [105], in contrast, indicate subsets of *bonded* sites. The density parameters further resum the allowed graphs. Take, for example, the first-order graphs in $\rho^{(1)}(\mathbf{1})$,

$$\rho^{(1)}(\mathbf{1}) \propto \underset{1}{\circ}\!\!=\!\!\overset{\rho^{(0)}}{\bullet} + \circ\!\!=\!\!\overset{\rho^{(1)}}{\bullet} + \circ\!\!=\!\!\overset{\rho^{(2)}}{\bullet} + \circ\!\!=\!\!\overset{\rho^{(3)}}{\bullet} \equiv \circ\!\!=\!\!\overset{\sigma^{(1)}}{\bullet} .$$

With only one attractive bond $F(\mathbf{1},\mathbf{2})$ incident at space point 2, we are free to attach any partial density except the total density, which is equivalent to attaching a single factor of $\sigma^{(1)}(\mathbf{1})$. The general rule for expressing $c^1(\mathbf{1})$ in terms of irreducible graphs is:

Rule 2

With each field hyperpoint k of an irreducible graph we associate a factor of $\sigma^{(n)}(k)$ where the $4-n$ is the number of bonded sites at k.

We have now expressed $c^1(\mathbf{1})$, and hence the $\rho^{(m)}(\mathbf{1})$, as irreducible diagrams written in terms of the complementary density parameters. The partial densities are not free parameters however, but must instead be found self-consistently through the nonlinear recursive relations (3.43a)–(3.43d). In Chapter 5 we shall invoke the *ideal network approximation*, greatly simplifying the self-consistent solution of these partial correlation functions. Of course, in the single-site model the density parameters are unnecessary because only $\rho^{(0)}(\mathbf{1})$ and $\rho^{(1)}(\mathbf{1})$ are defined, $\rho^{(1)}(\mathbf{1})$ being defined by Eq. (3.43a). Rule 2 in this case should be appropriately modified to reflect the single bonding site.

It will also be useful to define a generating functional $c^{(0)}$, based upon the direct correlation function hierarchy, from which the general one-body $c^m(\mathbf{1})$ and

two-body $c^{mn}(\mathbf{1},\mathbf{2})$ correlation functions can be derived. Specifically,

$$c^{(0)} = \left\{ \begin{array}{l} \text{sum of all irreducible s-mer graphs (including} \\ \text{monomer hyperpoints) and } f^R \text{ bonds; all hyperpoints} \\ \text{are field hyperpoints and carry } \sigma^{(n)}\text{-factors according} \\ \text{to the SI connectivity rules.} \end{array} \right\} \tag{3.46}$$

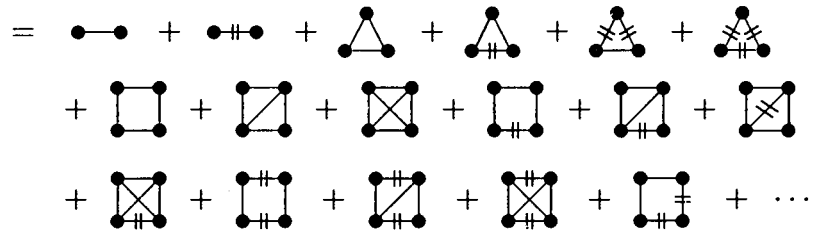

As per the direct correlation function hierarchy, the partial one-body correlations are obtained by functional differentiation,

$$c^{m}(\mathbf{1}) = \frac{\delta c^{(0)}}{\delta \sigma^{(m)}(\mathbf{1})}, \tag{3.47}$$

and translates into all ways of turning a field hyperpoint that carries a factor of $\sigma^{(m)}(\mathbf{1})$ into a labeled hyperpoint that carries the unit function: the factor $\sigma^{(m)}(\mathbf{1})$ is deleted. Under the SBC, the generating functional $c^{(0)}$ vertices only carry factors of $\sigma^{(0)}(\mathbf{1})$ or $\sigma^{(1)}(\mathbf{1})$ in the four-site model. Thus, by Eq. (3.47), the only nonzero one-body correlations are $c^{0}(\mathbf{1})$ and $c^{1}(\mathbf{1})$, as expected. The partial two-body correlation function is derived via a second functional derivative,

$$c^{mn}(\mathbf{1},\mathbf{2}) = \frac{\delta c^{(0)}}{\delta \sigma^{(n)}(\mathbf{2}) \delta \sigma^{(m)}(\mathbf{1})}, \tag{3.48}$$

where the superscripts m and n refer to the number of F-bonds incident upon labeled points 1 and 2 respectively. The generating functional $c^{(0)}$, as well as the functional hierarchy above, plays a central role in defining the TPT equation of state and Helmholtz free energy in Wertheim theory.

3.4.3. Wertheim TPT

The partial densities derived in the last section are the focus of Wertheim's graphical formalism, in part because many of the approximation schemes within the standard theory for dealing with simple liquids are couched in terms of the

two-body correlation functions. These same functions are directly related to the one-body correlations we saw arise in the definition of the partial densities above. Because the graphical analysis of those partial densities is derived from that of βPV, which acts as a generating functional, the thermodynamics of the theory follow in a somewhat reverse fashion from that usually encountered: an equation of state is formulated in terms of the system interactions first, from which the chemical potential, free energy, and other thermodynamic quantities then follow. As such, the route to system thermodynamics is rather indirect and complicated. The Wertheim multi-density equation of state, analogous to that derived on page 54 for the virial pressure, Eqs. (3.17a) and (3.17b), will be motivated in this section, while the subsequent derivation of the Helmholtz free energy will be given in Chapter 5. We shall, however, state the general free energy result here because we shall use it for our dimeriziation model in Chapter 4.

In the last section we derived the partial densities $\rho^{(m)}(\mathbf{1})$ from the fugacity series expansion of βPV through functional derivatives and the process of topological reduction. Yet, in the end, there is still the nontrivial task of relating the pressure to the final results of that analysis, *viz.* to the partial densities and correlations, such that the pressure can be evaluated. Rather than directly deriving such a relation, we shall follow Wertheim and assert the *ansatz* that, for an M-site system

$$\beta PV = \int d\mathbf{1} \left[\rho(\mathbf{1}) - \sum_{i=0}^{M} \sigma^{(i)}(\mathbf{1}) c^{i}(\mathbf{1})\right] + c^{(0)}, \tag{3.49}$$

which originates from Morita and Hiroika's [81] desire to rewrite $\ln \Xi$ as a functional of $\rho(\mathbf{1})$ and the Mayer f-bond. Their derivation begins with the statistical mechanical relation

$$\rho(\mathbf{1}) = \frac{z(\mathbf{1})}{\Xi} \frac{\delta \Xi}{\delta z(\mathbf{1})}, \tag{3.50}$$

and is summarized by Stell [83] for the singlet density $\rho(\mathbf{1})$ case. For brevity we shall instead simply motivate this equation of state by verifying that Eq. (3.49) satisfies the thermodynamic relation

$$\left(\frac{\partial P}{\partial \mu}\right)_{T,V} = \rho, \tag{3.51}$$

where ρ is the homogeneous number density. We again limit our analysis to the four-site model under the same three SI conditions: the SBC and SI-2S.

Start by taking the variation of βPV (keeping β and V constant), which becomes

$$\beta\delta PV = \int d\mathbf{1}\left[\delta\rho(1) - \sum_{i=0}^{M}\{\delta\sigma^{(i)}(\mathbf{1})\,c^i(\mathbf{1}) + \sigma^{(i)}(\mathbf{1})\,\delta c^i(\mathbf{1})\}\right] + \delta c^{(0)}. \quad (3.52)$$

Using the functional derivative definition of the $c^m(\mathbf{1})$ we can evaluate the variation of the generating functional $c^{(0)}$,

$$\delta c^{(0)} = \int d\mathbf{1}\left[c^0(\mathbf{1})\delta\sigma^{(0)}(\mathbf{1}) + c^1(\mathbf{1})\delta\sigma^{(1)}(\mathbf{1})\right], \quad (3.53)$$

where we have imposed the four-site model SI conditions, wherein only two density parameters in $c^{(0)}$ are nonzero, namely

$$\sigma^{(0)}(\mathbf{1}) = \rho(\mathbf{1}), \qquad \sigma^{(1)}(\mathbf{1}) = \rho(\mathbf{1}) - \rho^{(4)}(\mathbf{1}). \quad (3.54)$$

Substituting Eq. (3.53) into the variation of our pressure (3.52) for $i = 0, 1$ and cancelling terms, we have

$$\beta\delta PV = \int d\mathbf{1}\left[\delta\rho(\mathbf{1}) - \sum_{i=0}^{1}\sigma^{(i)}(\mathbf{1})\,\delta c^i(\mathbf{1})\right]. \quad (3.55)$$

Now construct $\delta\rho(\mathbf{1})$ from Eqs. (3.38) and (3.43a)–(3.43d), which combined can be written as

$$\rho(\mathbf{1}) = \rho^{(0)}(\mathbf{1})\Big\{1 + c^1(\mathbf{1}) + \frac{1}{2!}\left[c^1(\mathbf{1})\right]^2 + \frac{1}{3!}\left[c^1(\mathbf{1})\right]^3 + \frac{1}{4!}\left[c^1(\mathbf{1})\right]^4\Big\}. \quad (3.56)$$

Taking the variation of (3.56) and using Eq. (3.54),

$$\begin{aligned}
\delta\rho(\mathbf{1}) &= \frac{\rho(\mathbf{1})}{\rho^{(0)}(\mathbf{1})}\,\delta\rho^{(0)}(\mathbf{1}) \\
&\quad + \rho^{(0)}(\mathbf{1})\Big\{1 + c^1(\mathbf{1}) + \frac{1}{2!}\left[c^1(\mathbf{1})\right]^2 + \frac{1}{3!}\left[c^1(\mathbf{1})\right]^3\Big\}\,\delta c^1(\mathbf{1}), \\
&= \frac{\rho(\mathbf{1})}{\rho^{(0)}(\mathbf{1})}\,\delta\rho^{(0)}(\mathbf{1}) + \left[\rho(\mathbf{1}) - \rho^{(4)}(\mathbf{1})\right]\delta c^1(\mathbf{1}), \\
&= \frac{\rho(\mathbf{1})}{\rho^{(0)}(\mathbf{1})}\,\delta\rho^{(0)}(\mathbf{1}) + \sigma^{(1)}(\mathbf{1})\,\delta c^1(\mathbf{1}). \qquad (3.57)
\end{aligned}$$

The density variation $\delta\rho^{(0)}(\mathbf{1})$ can be rewritten with the aid of the relation $c^0(\mathbf{1}) = \ln[\rho(\mathbf{1})/z(\mathbf{1})]$, from which it follows that

$$\frac{\delta\rho^{(0)}(\mathbf{1})}{\rho^{(0)}(\mathbf{1})} = \frac{\delta z(\mathbf{1})}{z(\mathbf{1})} + \delta c^0(\mathbf{1}), \tag{3.58}$$

Inserting this result into (3.57) the variation $\delta\rho(\mathbf{1})$ becomes

$$\delta\rho(\mathbf{1}) = \frac{\delta z(\mathbf{1})}{z(\mathbf{1})}\rho(\mathbf{1}) + \rho(\mathbf{1})\,\delta c^0(\mathbf{1}) + \sigma^{(1)}(\mathbf{1})\,\delta c^1(\mathbf{1}), \tag{3.59}$$

such that the total variation of the pressure, Eq. (3.55), is

$$\begin{aligned}\beta\delta PV &= \int d\mathbf{1}\left[\frac{\delta z(\mathbf{1})}{z(\mathbf{1})}\rho(\mathbf{1}) + \rho(\mathbf{1})\,\delta c^0(\mathbf{1}) + \sigma^{(1)}(\mathbf{1})\,\delta c^1(\mathbf{1}) - \right.\\ &\qquad \left.\left\{\sigma^{(0)}(\mathbf{1})\,\delta c^0(\mathbf{1}) + \sigma^{(1)}(\mathbf{1})\,\delta c^1(\mathbf{1})\right\}\right],\\ &= \int d\mathbf{1}\,\frac{\delta z(\mathbf{1})}{z(\mathbf{1})}\rho(\mathbf{1}),\end{aligned} \tag{3.60}$$

and with the relation $z(\mathbf{1}) = \Lambda\exp[\beta\mu]$, the ratio

$$\frac{\delta z(\mathbf{1})}{z(\mathbf{1})} = \beta\delta\mu$$

can be substituted into Eq. (3.60) to give

$$\beta\delta PV = \beta\int d\mathbf{1}\,\rho(\mathbf{1})\delta\mu. \tag{3.61}$$

For a homogeneous system at constant temperature and volume, this functional equation finally is seen to satisfy the required thermodynamic relation

$$\left(\frac{\partial P}{\partial\mu}\right)_{T,V} = \rho. \tag{3.62}$$

Having established at least the consistency of Eq. (3.49), we now have our desired relation between the pressure and the partial densities and one-body correlations determined by the model. We use this equation of state in Chapter 5 to derive the properties of our water-like model, including a derivation of the multi-density TPT Helmholtz free energy. Yet in Chapter 4, where we examine a dimerizing fluid, it is more efficient to derive the Helmholtz free energy first, from general DFT considerations. We do not, however, derive the Wertheim TPT free

energy contribution in that chapter, but instead simply use Wertheim's previous result. We therefore state the general result here, without derivation, in anticipation of its use in Chapter 4. For an M-site model the TPT free energy can be derived from $\beta A = \beta\mu N - \beta PV$ and the DFT result

$$\beta\mu N = \int d\mathbf{1}\, \rho(\mathbf{1}) \left\{ \ln[\rho^{(0)}(\mathbf{1})\Lambda^3] - c^0(\mathbf{1}) \right\} , \tag{3.63}$$

which is a direct result of Eq. (3.40). The generic Helmholtz free energy is then

$$\beta A = \int d\mathbf{1} \left\{ \rho(\mathbf{1}) \ln[\rho^{(0)}(\mathbf{1})\Lambda^3] - \rho(\mathbf{1}) + \sum_{i=0}^{M} \sigma^{(i)}(\mathbf{1}) c^i(\mathbf{1}) \right\} - c^{(0)} . \tag{3.64}$$

For the single-site model we use in Chapter 4, under the SI-1 condition, the dimerization contribution to the TPT free energy simplifies to

$$\frac{\beta A}{N} = \ln X - \frac{1}{2}(1 - X) . \tag{3.65}$$

The free energy for the four-site model differs slightly from this and is derived in Chapter 5.

3.4.4. Wertheim IET

Through the use of graph theory the entire formalism of s-particle correlation functions can be transferred directly to the multi-density formalism. The topological reduction procedure affects bonds, but not points or hyperpoints. The standard methods of eliminating APs and replacing fugacity vertices with density parameters according to Rule 2 remains unchanged when writing down the two-body distribution functions necessary for the integral equation theories.

As implied earlier, the s-particle *partial direct correlation functions* follow from a functional hierarchy analogous to that for the singlet density case, namely

$$c^{mn\cdots\alpha}(\mathbf{1}, \mathbf{2}, \ldots, \boldsymbol{s}) = \frac{\delta^s c^{(0)}}{\delta\sigma^{(m)}(\mathbf{1})\delta\sigma^{(n)}(\mathbf{2})\cdots\delta\sigma^{(\alpha)}(\boldsymbol{s})} , \tag{3.66}$$

where the superscripts denote the number of incident F-bonds at the labeled points, m at hyperpoint $\mathbf{1}$, n at $\mathbf{2}$, ..., and α at $\boldsymbol{s}$. The generating functional $c^{(0)}$ is generally defined by Eq. (3.74), where Rule 2 is used in rewriting fugacity vertices in terms of density parameters consistent with the appropriate SI conditions. The remaining multi-density correlation functions are derived from the

truncated s-particle distribution functions $\hat{\rho}(\mathbf{1},\mathbf{2},\ldots,s)$, Eq. (2.10). The same topological reduction procedure described in Section 3.3 is used here, which converts each graph sum $\hat{\rho}(\mathbf{1},\mathbf{2},\ldots,s)$ into its subset free of articulation points where each hyperpoint carries a density parameter consistent with Rule 2; then from Eq. (2.13)

$$\hat{\rho}(\mathbf{1},\ldots,s) \;=\; \sum_{m=0}^{M}\cdots\sum_{\alpha=0}^{M}\sigma^{(m)}(\mathbf{1})\cdots\sigma^{(\alpha)}(s)\,h^{m\cdots\alpha}(\mathbf{1},\ldots,s)\,. \tag{3.67}$$

This graphical relation serves to define the *partial total correlation functions* $h^{m\cdots\alpha}(\mathbf{1},\ldots,s)$, where the superscripts denote the number of incident F-bonds as stated before.

Using a pair theory approach only the one– and two-body correlation functions enter the theory. Assuming the SBC and SI-2W conditions, the key graphical relation of the theory is

$$\begin{aligned}\hat{\rho}(\mathbf{1},\mathbf{2}) \;&=\; \sum_{m=0}^{1}\sum_{n=0}^{1}\sigma^{(m)}(\mathbf{1})h^{mn}(\mathbf{1},\mathbf{2})\sigma^{(n)}(\mathbf{2})\,,\\ &=\; \rho(\mathbf{1})h(\mathbf{1},\mathbf{2})\rho(\mathbf{2})\,,\end{aligned} \tag{3.68}$$

which relates the partial correlations $h^{mn}(\mathbf{1},\mathbf{2})$ to the total correlation function $h(\mathbf{1},\mathbf{2})$. Equations (2.12) and (2.11) further show that

$$\begin{aligned}\rho(\mathbf{1},\mathbf{2}) \;&\equiv\; \sum_{m=0}^{1}\sum_{n=0}^{1}\sigma^{(m)}(\mathbf{1})g^{mn}(\mathbf{1},\mathbf{2})\sigma^{(n)}(\mathbf{2})\,,\\ &=\rho(\mathbf{1})g(\mathbf{1},\mathbf{2})\rho(\mathbf{1})\,,\end{aligned} \tag{3.69}$$

with the partial correlations being related by

$$h^{mn}(\mathbf{1},\mathbf{2}) \;=\; g^{mn}(\mathbf{1},\mathbf{2}) \;-\; \delta_{m,0}\delta_{n,0}\,, \tag{3.70}$$

where $\delta_{m,n}$ is the Kronecker delta function. The graphical descriptions of the correlation functions $c(\mathbf{1},\mathbf{2})$, $h(\mathbf{1},\mathbf{2})$ and $g(\mathbf{1},\mathbf{2})$ in Section 3.3 provide the link by which the corresponding partial correlations defined above can be graphically analyzed. Moreover, Eqs. (3.68) and (3.69) will also serve as the connection between the partial quantities of the theory with the two-body correlations $h(\mathbf{1},\mathbf{2})$ and $g(\mathbf{1},\mathbf{2})$; these quantities play a pivotal role in determining the system structure and thermodynamics within standard liquid state theories.

One of the major tools for determining these correlation functions in the singlet density formalism is the Ornstein-Zernike equation,

$$h(\mathbf{1},\mathbf{2}) \;=\; c(\mathbf{1},\mathbf{2}) \;+\; \int d\mathbf{3}\; c(\mathbf{1},\mathbf{3})\rho(\mathbf{3})h(\mathbf{3},\mathbf{2})\,. \tag{3.71}$$

A completely analogous relation can be derived for the multi-density formalism of Wertheim. The graphs in $h(\mathbf{1},\mathbf{2})$ are free of APs, but may contain bridge points. After examining the bond connectivity at the bridge points, we note that these diagrams are composed of (irreducible) graphs free of both APs and bridge points and with some particular set of bonded attraction sites. These sums of irreducible graphs can be obtained from the generating functional $c^{(0)}$ by taking all ways of turnilng 2 points with that particular bonding into labeled points, thereby deleting the $\sigma^{(m)}$ factors. These specific graph sums happen to correspond to those of the two-body partial correlation function $c^{mn}(\mathbf{1},\mathbf{2})$. This graphical analysis effectively "decomposes" $h(\mathbf{1},\mathbf{2})$ into simple chains of irreducible graphs, giving a matrix analog of the Ornstein-Zernike equation,

$$h^{mn}(\mathbf{1},\mathbf{2}) \;=\; c^{mn}(\mathbf{1},\mathbf{2}) \;+\; \int d\mathbf{3}\; c^{mk}(\mathbf{1},\mathbf{3})\sigma^{kl}(\mathbf{3})h^{ln}(\mathbf{3},\mathbf{2})\,, \tag{3.72}$$

known as the *associated* Ornstein-Zernike or AOZ equation. For an M-site model the AOZ is an $(M+1)\times(M+1)$ matrix equation, with an upper triangular generic density parameter matrix $\boldsymbol{\sigma}$. For the four-site model under the SBC and SI-2W conditions, only two density parameters enter the theory and so the only nonzero elements σ^{kl} in the sparse (5×5) matrix are $\sigma^{00}=\sigma^{(0)}=\rho$, $\sigma^{01}=\sigma^{10}=\sigma^{(1)}$, and $\sigma^{11}=0$ —see Section 5.4.1. For the single-site model the triangular (2×2) matrix is simply

$$\boldsymbol{\sigma} \;=\; \begin{pmatrix} \rho & \rho^{(0)} \\ \rho^{(0)} & 0 \end{pmatrix}. \tag{3.73}$$

Solution of Eq. (3.72) is nontrivial even for the single-site model because the AOZ, like the OZ equation, is a recursive convolution equation. A factorization method derived by Baxter [106] $h^{mn}(\mathbf{1},\mathbf{2})$ and $c^{mn}(\mathbf{1},\mathbf{2})$ can be used to separate and solve (under a closure condition) the AOZ. We give a detailed overview of the factorization procedure in Chapter 5.

As noted by Wertheim, the type of closure condition used in order to solve the OZ or AOZ equation critically depends upon the situation at hand. At high enough temperatures or low enough association strengths the equation of state is

determined largely by the repulsive forces; if an "exact" knowledge of a reference system interacting only through the repulsive potential u^R but at the same ρ and T as the associating fluid can be acquired somehow, then the high density and temperature results of the theory will be vastly improved by using the reference pair distribution function $g^{ref}(\mathbf{1},\mathbf{2})$ to solve the AOZ as compared to a treatment without such a reference system.[9] For lower temperatures or higher association strengths the task of obtaining a $g^{ref}(\mathbf{1},\mathbf{2})$ is even more problematic, and so for many associating systems it is necessary to adopt a closure relation without a reference system.

Since the Percus-Yevick (PY) approximation works well for hard sphere systems and is amenable to analytical solution, the most reasonable AOZ closure condition for us to adopt for our sticky-spot model is one that reduces to the PY equation when the site-site attraction vanishes: $F \to 0$. The PY-like integral equations suggested by Wertheim [20] begin with the fugacity expansion

$$y^{mn}(\mathbf{1},\mathbf{2}) \;=\; \delta_{m,0}\delta_{n,0} \;+\; \left\{\begin{array}{l}\text{sum of all graphs with no}\\ \text{direct } e^R(\mathbf{1},\mathbf{2}) \text{ bond.}\end{array}\right\}. \tag{3.74}$$

Using the defining equation for $y^{mn}(\mathbf{1},\mathbf{2})$,

$$g^{mn}(\mathbf{1},\mathbf{2}) \;=\; e^R(\mathbf{1},\mathbf{2})y^{mn}(\mathbf{1},\mathbf{2})\,, \tag{3.75}$$

we can split the partial background correlation function into reducible and irreducible parts,

$$y^{mn}(\mathbf{1},\mathbf{2}) \;=\; [g^{mn}(\mathbf{1},\mathbf{2}) \;-\; c^{mn}(\mathbf{1},\mathbf{2})] \;+\; Z^{mn}(\mathbf{1},\mathbf{2})\,, \tag{3.76}$$

where the quantity in square brackets contains the reducible diagrams while $Z^{mn}(\mathbf{1},\mathbf{2})$ contains the irreducible diagrams. The graphical PY approximation, briefly discussed in Appendix C, ignores the more highly connected graphs because of the small integral values they represent. The analogous PY condition here is to ignore all irreducible graphs in $y^{mn}(\mathbf{1},\mathbf{2})$:

$$Z^{mn}(\mathbf{1},\mathbf{2}) \;=\; 0\,. \tag{3.77}$$

---

[9]No unique relation between an interaction potential $u(\mathbf{1},\mathbf{2})$ and $g(\mathbf{1},\mathbf{2})$ exists, so determining a reference pair distribution function for a given model is nontrivial, even when experimental data is available.

The *associative* PY-like relations are thus given by

$$g^{mn}(\mathbf{1},\mathbf{2}) \;=\; e^{R}(1,2)\left[y^{mn}(\mathbf{1},\mathbf{2}) \;+\; \delta_{m,0}\delta_{n,0}F(\mathbf{1},\mathbf{2})y^{00}(\mathbf{1},\mathbf{2})\right]\,, \tag{3.78}$$

or, eliminating the $y^{mn}(\mathbf{1},\mathbf{2})$ functions, finally yields our desired AOZ closure equations:

$$e^{R}(\mathbf{1},\mathbf{2})c^{mn}(\mathbf{1},\mathbf{2}) \;=\; f^{R}(\mathbf{1},\mathbf{2})g^{mn}(\mathbf{1},\mathbf{2}) \;+\; \delta_{m,0}\delta_{n,0}F(\mathbf{1},\mathbf{2})g^{00}(\mathbf{1},\mathbf{2})\,. \tag{3.79}$$

There is a simple relation between the PY $c(\mathbf{1},\mathbf{2})$ and $h(\mathbf{1},\mathbf{2})$ graphs and the PY-like $c^{mn}(\mathbf{1},\mathbf{2})$ and $h^{mn}(\mathbf{1},\mathbf{2})$ graphs above. The conversion is accomplished by taking all ways of replacing each $f(\mathbf{1},\mathbf{2})$ bond by either $f^{R}(\mathbf{1},\mathbf{2})$ or $F(\mathbf{1},\mathbf{2})$ such that the number of incident F-bonds at each vertex is consistent with the SI conditions adopted. Then relabel those vertices with the density parameters $\sigma^{(m)}$ according to Rule 2. Each graph is then assigned to $c^{mn}(\mathbf{1},\mathbf{2})$ and $h^{mn}(\mathbf{1},\mathbf{2})$ according to the number of F-bonds incident at labeled points 1 and 2, m and n respectively. We use the PY-like approximation described above in Chapters 4 and 5 in order to obtain analytical results.

4. INTERFACE PROFILES IN A DIMERIZING SYSTEM

Reading made Don Quixote a gentleman, but believing what he read made him mad.

—George Bernard Shaw

4.1. INTRODUCTION

Predicting the behavior of complex fluids at interfaces remains a challenging goal in theoretical and applied research alike [107, 108]. It has long been recognized that attractive as well as repulsive intermolecular forces are important in determining liquid properties near the critical and triple points [109], but a clear understanding of their influence in the phase behavior of complex fluids has not yet been reached. The delicate interplay between structural energy and entropy which characterizes associating fluids creates a rich variety of spontaneous structural and thermodynamic transitions. Yet interfacial statistical mechanics has lagged behind bulk theories of complex fluids [110–112], in part because of the need to match bulk properties while accounting for the inhomogeneous interface correlations.

4.1.1. The Liquid–Vapor Interface

In the analysis of inhomogeneous density profiles for multi-component, self-assembling systems, the theory typically begins with a free energy parameterized to contain the proper number of minima —equal to the number of phases present— and the appropriate set of Laplacians to smoothly connect the density profile from one bulk phase to the other [113–115]. The profiles of the mesoscopic to macroscopic scale structures that emerge from these phenomenological studies, however, are complicated, with extraordinary topologies, and therefore are difficult to decipher in terms of the role of specific intermolecular forces.

Nonetheless, recent progress in interfacial theories of simple fluids, coupled with advances in bulk theories of complex liquids and computer simulation capabilities, has rejuvenated research in interfacial fluid behavior [108, 107], specifically concerning fluids with complex interactions. A sufficient understanding of association and simple interface physics exists such that some fundamental questions

concerning the influence of molecular association on interface structure can be addressed. In particular, the study of dimerization and association equilibria has undergone a recent renaissance, catalyzed in large part by the work of Wertheim [116, 117, 19, 20]. Equilibrium constants, free energies, and structural information (such as pair distribution functions and direct correlation functions) can now be determined for associating fluids at liquid densities [118–128].

Many primitive models of dimerization have been formulated (see [102, 129] and references therein), using both density functional theory (DFT) and integral equation theory (IET) methods in their description, but most of these studies involve such associating fluids near walls or confined in pores —systems of obvious industrial import. Treating these systems in an analytical fashion is problematic however. Short range correlations in liquids near substrates can lead to density profile oscillations which simple DFT approaches, like square gradient theory, cannot handle: packing effects due to both the repulsive and attractive parts of a substrate potential can cause the local density $\rho(z)$ to exceed even close-packed values. Under such circumstances the homogeneous Helmholtz free energy density $f(\rho)$ diverges. In order to treat these wall–particle correlation effects, as well as to account for wetting or layering transitions [130, 131], more complicated methods are required, such as weighted density approximations (WDA). These methods "renormalize" the true density $\rho(\mathbf{r})$ over a local volume —determined by the range of the forces— into a smoothed density $\bar{\rho}(\mathbf{r})$ using a coarse-graining procedure. The large $\rho(\mathbf{r})$ values near the substrate are thus smoothed out, eliminating the divergences in the excess free energy density by making it a *local* function of $\bar{\rho}(\mathbf{r})$. Numerous versions of WDAs exist (see Ref. [131] for an overview), each corresponding to a different recipe for calculating $\bar{\rho}(\mathbf{r})$. Yet, while these WDA approaches are non-perturbative, *i.e.* do not correspond to a finite-order density expansion of the excess Helmholtz free energy, analytical results are not possible, greatly limiting their ability to highlight the fundamental influence of highly anisotropic attractive forces in the interfacial region.

Since many basic questions concerning the direct effects of complex forces upon interfacial boundaries are, as yet, unclear, a model system which allows for an analytical treatment within the framework of statistical mechanics would be useful. There has been some recent interest in exploring the phase behavior of pure fluids with both isotropic [132, 133] and anisotropic [134, 135] interactions,

opening many questions about possible fluid–fluid, liquid–liquid, fluid–solid, or liquid–solid structural and thermodynamic transitions, but none using Wertheim's multi-density formalism. Therefore, we move to the simplest of cases in order to obtain a clear picture of the effects of dimerization upon a planar liquid-gas interface using Wertheim theory. The well-known planar liquid–vapor interface has a relatively simple number density profile $\rho(z)$ [115, 72, 68], changing from the high density liquid ρ_ℓ to the low density gas ρ_g according to

$$\rho(z) = \rho_\ell - \frac{(\rho_\ell - \rho_g)}{1 + \exp[z/\xi]}, \tag{4.1}$$

where ξ is the bulk correlation length and $\rho(z) \to \rho_g$ as $z \to -\infty$ and $\rho(z) \to \rho_l$ as $z \to \infty$, with the coordinate origin at the Gibbs (*equimolar*) dividing surface. Equation (4.1) emerges from a Landau-Ginzburg theory of an interface (the so-called square gradient theory) and has a firm theoretical foundation [72, 68]. Our use of the simple square gradient theory with a well-known profile allows us to completely focus upon the influence of short-ranged, highly anisotropic attraction, *i.e.* dimerization, upon the planar interface properties, such as density profile, surface tension, coexistence densities, *etc.* .

4.1.2. Chapter 4 Focus

The system of interest here is therefore a classical fluid of spherical monomers which interact via weak dispersion forces, and which can assemble into dimers. Our approach is in a sense the simplest of possible theories: the associating fluid consists of hard core particles with a sticky patch to mimic dimerization, along with long range attraction that is treated perturbatively [136]. The plan is to calculate density profiles $\rho(z)$ for both monomers and dimers, the bulk correlation length ξ, and the surface tension γ in order to assess the effects of association on the planar liquid-vapor interface. We draw heavily upon the previous theories of the liquid-gas interface and dimerization equilibria. Sticky-spot models can be used to describe the dimers formed in fluids of carboxylic acids, alkanols, and secondary amines, [137],

carboxylic acids	alkanols	secondary amines
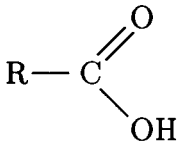	R — OH	R_2—NH

where R represents an *alkyl group* (R may also represent H in the carboxylic acid group). Such fluid interfaces should exhibit the behavior to be detailed here. In fact, Wertheim theory has been widely applied to chain-forming or polymerizing fluids [138–141], in large part because the only information required to construct an approximation equation of state for a chain fluid is the equation of state and the pair correlation function at contact of the monomer fluid.

4.2. THEORY

After a description of the primitive, single-site model for our dimerizing fluid, we derive analytical results for the system thermodynamics using Wertheim's (first-order) thermodynamic perturbation theory (TPT) for the association contribution and square-gradient density functional theory (DFT) for the dispersion contribution to the free energy. The theory is written in terms of the direct correlation function, solved through Baxter's factorization of the *associated* Ornstein–Zernike (AOZ) equation using a Percus–Yevick-like closure condition and the *mean spherical approximation* (MSA). The interface density profile is obtained by the DFT minimization of the square-gradient free energy. The final numerical evaluation of the analytical results requires implementation of the sticky-spot limit, which will be discussed in Section 4.3.

4.2.1. The Model

4.2.1.1. Interaction Potentials

Here our thermodynamic system consists of a fluid of N rigid, *spherical* particles of diameter R in a volume V and at a temperature T with a bulk density $\rho = N/V$. These rigid monomers interact via a pairwise potential u containing

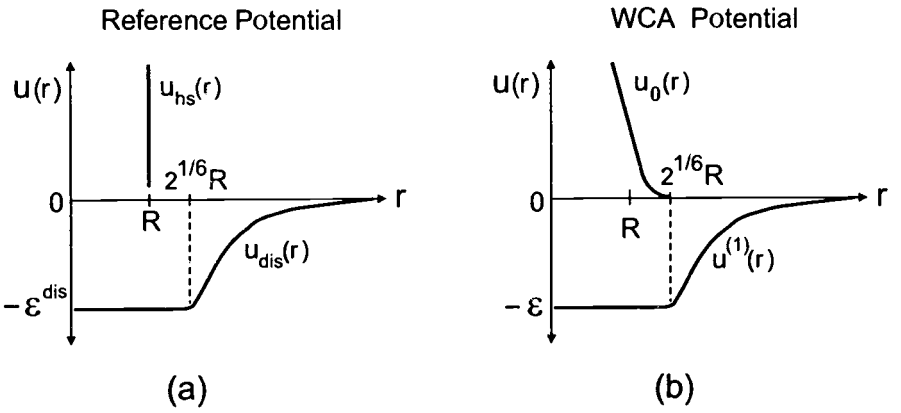

FIGURE 4.1. Comparison of the present reference potential with the standard WCA potential. In the standard WCA method, shown in (b), the potential is split into a soft (repulsive) reference term $u_0(r)$ and the attractive perturbation term $u^{(1)}(r)$. The present model, in (a), replaces the soft repulsive term $u_0(r)$ with a hard sphere term $u_{dis}(r)$.

---

three parts: (1) hard core repulsion u_{hs}, (2) long range dispersion u_{dis}, and (3) short range, highly anisotropic attraction,

$$u(\mathbf{r}) = \Big[u_{hs}(r) + u_{dis}(r)\Big]_{ref} + u_{dim}(\mathbf{r})\,, \tag{4.2}$$

where $\mathbf{r}$ denotes the vector separation between the centers of monomers 1 and 2, with a magnitude of $r = |\mathbf{r}_2 - \mathbf{r}_1|$. We split our spherically symmetric "reference" potential (square brackets above) into purely repulsive and purely attractive contributions in the spirit of Weeks-Chandler-Anderson (WCA) theory [142, 136]; their argument being that molecules do not "know" the sign of their mutual potential energy, but rather the sign of the force. See Fig. 4.1 for a comparison of our reference potential to the standard WCA potential. For simplicity, we replace the *soft* repulsion of WCA theory with that of the hard sphere,

$$u_{hs}(r) = \begin{cases} \infty & r < R, \\ 0 & r \geq R, \end{cases} \tag{4.3}$$

but keep the longer-ranged isotropic dispersion contribution, approximated by a Lennard–Jones 6-12 potential with well depth ε^{dis}. With only one anisotropic, short-ranged attraction site per monomer, the largest bond-connected cluster will

be the dimer, which interacts only through hard core repulsion; hence the absence of a liquid–gas transition and our inclusion of the longer-ranged dispersion interaction above.[1]

$$u_{dis}(r) = \begin{cases} -\varepsilon^{dis} & r < 2^{1/6}R, \\ 4\varepsilon^{dis}\left[(R/r)^{12} - (R/r)^{6}\right] & r \geq 2^{1/6}R. \end{cases} \tag{4.4}$$

4.2.1.2. Anisotropy and Steric Effects

The form of the dimerizing potential u_{dim} is slightly more complicated because of its anisotropic nature. This angular dependence is incorporated through a *conical well* or *reactive cone*, with a depth of ε^{dim} and a range of l^{dim}:

$$u_{dim}(\mathbf{r}) = \begin{cases} -\varepsilon^{dim} & \text{if } \begin{cases} R < |\mathbf{r}| < (R + l^{dim}) \\ \cos|\theta_{max}| \leq \hat{\mathbf{r}} \cdot \hat{\mathbf{e}}_1 \leq 1 \\ \cos|\theta_{max}| \leq -\hat{\mathbf{r}} \cdot \hat{\mathbf{e}}_2 \leq 1 \end{cases} \\ 0 & \text{otherwise}. \end{cases} \tag{4.5}$$

The model geometry is shown in Fig. 4.2 on the next page. Each monomer contains an associating cone A, oriented along some direction $\hat{e}_n$, the subscript n referring to the particular monomer label. The cone angle θ_n extends from the cone's central axis $\hat{e}_n$ up to some maximum angle θ_{max} dictated by the physical steric constraints. In order to limit association products to dimers, for example, the required constraint between θ_{max} and l^{dim} in Eq. (4.5) above is $\sin(\theta_{max}) = R\left[2\,(R+2\,l^{dim})\right]^{-1}$. This constraint equation is the mathematical description of Wertheim's SI-1 steric effect, shown in Fig. 4.3 on page 94.

Once two monomers are bound to form a dimer, their hard core repulsion prevents any third monomer site from approaching close enough to form a 3-way bond, thus saturating the original bond. For our (pure) unary system $\theta_1 = \theta_2 \leq \theta_{max}$. Since l^{dim} is typically very small compared to the hard sphere diameter R, that part of the reactive cone available for bonding is usually characterized as a "sticky spot" (see Fig. 4.2 on the next page).

---

[1]See, for example, Sear and Gelbart [132], Velasco *et. al.* [143] for more discussion on the role of repulsive forces in fluid phase behavior.

4.2.2. DFT Free Energy and Thermodynamics

Any practical implementation of classical density functional theory (DFT) requires some explicit approximation for the intrinsic Helmholtz free energy functional $A[\rho]$. Once given, minimization of the grand potential $\Omega[\rho] = A[\rho] - \int d\mathbf{1}\, \rho(\mathbf{1})\,[\mu - \phi(\mathbf{1})]$ for a given T, μ, and external potential $\phi(\mathbf{1})$ determines the equilibrium density $\rho(\mathbf{1})$. The reliability and accuracy of the results reflect the skill with which $A[\rho]$ is constructed for a particular system. In the analysis of inhomogeneous, self-assembling systems, theories commonly begin with a gradient expansion of the Landau–Ginzburg free energy [144], which, for the simplest case of a single, scalar order parameter φ looks like

$$A[\varphi] = \int d\mathbf{1} \Big[a_0 + a_1\varphi(\mathbf{1}) + a_2\varphi(\mathbf{1})^2 + a_3\varphi(\mathbf{1})^3 + a_4\varphi(\mathbf{1})^4 + \cdots + c_1|\nabla\varphi(\mathbf{1})|^2 + c_2|\Delta\varphi(\mathbf{1})|^2 + \cdots + \varphi(\mathbf{1})^2|\nabla\varphi(\mathbf{1})|^2 + \cdots \Big]. \quad (4.6)$$

Within a thermodynamic approach, φ represents an extensive thermodynamic variable or its density and distinguishes the various phases present. The gradient term with a negative coefficient $c_1 < 0$ tends to create the interface, whereas the Laplacian term with a positive coefficient $c_2 > 0$ stabilizes the interface. The number of terms used and the values of the coefficients are "chosen" such that the free energy displays the proper number of minima (one for each phase) and the appropriate set of Laplacians to smoothly connect the density profile from one phase to another

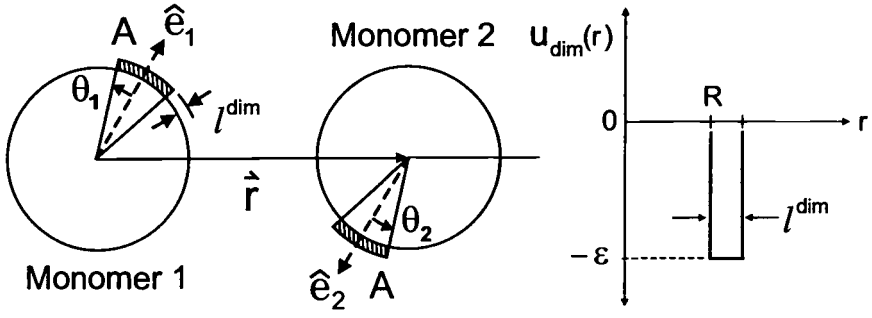

FIGURE 4.2. The reactive cone geometry and potential for the "sticky-spot" model. The shaded region corresponds to the sticky spot. Note that typically the range $l^{dim} < 0.15R$, but is shown enlarged for clarity.

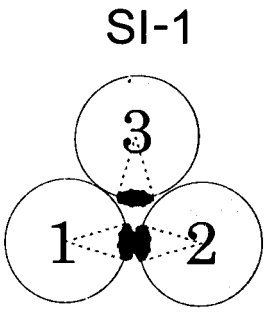

FIGURE 4.3. Wertheim's SI-1 steric constraint. Once two attractive sites A on monomers 1 and 2 have bonded together they become saturated; the hard core repulsion from those monomers prevents a third monomer from approaching close enough to form a 3-way bond.

---

[113]. Actually determining those coefficients, however, means imposing additional requirements upon $A[\rho]$.

For complex fluids like self-assembling colloids the field $\varphi(\mathbf{1})$ usually represents some difference in concentrations (*e.g.* between oil and water) such that $\varphi(\mathbf{1}) = 0$ describes the (surfactant) interface between phases. In such cases the extra conditions necessary for the specification of expansion coefficients are often taken from interface curvature considerations [114]. The profiles that emerge from such phenomenological studies, however, are complicated because of the multicomponent nature of the fluid and the extraordinary interface topologies involved.[2] Given our much more fundamental focus —analytical look at the planar liquid–vapor interface of a pure, dimerizing hard sphere fluid— it is reasonable to compose our free energy functional in accord with the simplest of DFT approaches: the *square-gradient approximation* [107].

Since association in Wertheim theory is manifest within the correlation functions, it is appropriate to construct our free energy functional by integrating the

---

[2]At high concentrations, for example, surfactant and lipid dispersions can form an ordered *mesophase*, a normal phase in the thermodynamic sense, but one that is more structurally complex than a simple liquid or solid. A mesophase may contain numerous small, monodisperse or polydisperse molecular aggregates, or convoluted lamellar or tubular structures that link up to form periodic, three-dimensional networks that extend indefinitely throughout the phase, *e.g.* a bicontinuous phase.

direct correlation function hierarchy. Recall from Section 2.3.4 that functionally integrating the direct correlation function $c(\mathbf{1},\mathbf{2})$ from some initial density $\rho_i(\mathbf{1})$ to a final density of interest $\rho(\mathbf{1})$ at the same temperature T led to [68, 145]

$$\beta A[\rho] = \beta A^{id}[\rho_i] + \beta A^{ex}[\rho_i] - \int d\mathbf{1}\; c(\mathbf{1};[\rho_i])\Delta\rho(\mathbf{1}) + \iint d\mathbf{1}d\mathbf{2} \int_0^1 d\lambda\; (\lambda-1)c(\mathbf{1},\mathbf{2};[\rho_\lambda])\Delta\rho(\mathbf{1})\Delta\rho(\mathbf{2})\,, \tag{4.7}$$

where the charging parameter λ is defined by the linear path $\rho_\lambda(\mathbf{r}) = \rho_i(\mathbf{1}) + \lambda\Delta\rho(\mathbf{1})$, and $\Delta\rho \equiv \big[\rho(\mathbf{1}) - \rho_i(\mathbf{1})\big]$. For our purposes we can choose $\rho_i(\mathbf{1}) = 0$ and let all external potentials ϕ vanish —the interface will be imposed through boundary conditions on our density. The first three terms on the right-hand side of Eq. (4.7) then vanish as well, giving

$$\beta A[\rho] = \int d\mathbf{1}\; \rho(\mathbf{1}) \ln\big[\rho(\mathbf{1})\Lambda^3/e\big] + \iint d\mathbf{1}d\mathbf{2} \int_0^1 d\lambda\; (\lambda-1)\rho(\mathbf{1})\rho(\mathbf{2})c(\mathbf{1},\mathbf{2};[\lambda\rho])\,, \tag{4.8}$$

which becomes the starting point for our derivation of the system thermodynamics. The logarithmic term in (4.8) is the ideal contribution to our free energy, and so the inherently non-local[3] second term on the RHS must account for all *excess* contributions. While exact, Eq. (4.8) requires a knowledge of the density dependence in $c(\mathbf{1},\mathbf{2};[\lambda\rho])$ in order to carry out the integration over the charging parameter λ, a nontrivial task. A full knowledge of the two-body correlation function $c(\mathbf{1},\mathbf{2})$, even in a homogeneous regime, requires information about higher-order correlations (evident by the direct correlation function hierarchy) and so some means of approximating $c(\mathbf{1},\mathbf{2};[\lambda\rho])$ is necessary.

In the absence of attractive forces, *e.g.* hard spheres near hard walls, the dependence of $c(\mathbf{1},\mathbf{2};[\lambda\rho])$ on the charging parameter λ can often be neglected all together, and $\rho_\lambda(\mathbf{1})$ is simply replaced by the bulk density ρ_b in Eq. (4.7). This

---

[3]The range over which the non-locality should be considered essentially corresponds to the correlation length ξ of the fluid, which is a measure of the range of the relevant intermolecular forces. An accurate description of the vanishing of the surface tension as the critical point is approached, for example, requires an accurate incorporation of non-local effects.

prescription describes the characteristic oscillatory density profile near the wall, but, with no attraction, cannot predict phase transitions, such as macroscopically thick wetting (or drying) at the wall-fluid interface or critical adsorption [146, 147]. In order to predict liquid–gas coexistence, either higher order terms in this scheme must be included [*e.g.* $c(\mathbf{1},\mathbf{2},\mathbf{3};\rho_b)$], or some better account of the density dependence in $c(\mathbf{1},\mathbf{2};[\lambda\rho])$ must be found so that the charging integration can be evaluated. When attractive forces are included in the description of confined fluids or fluids near walls, pronounced peaks occur in the oscillatory profile, where the local density may exceed that for close-packing. In such cases more complex schemes like the weighted-density approximations (WDA) are adopted, wherein coarse-graining procedures smooth or average the true density $\rho(\mathbf{1})$ profile over a local volume determined by the interaction range. The excess free energy can then be well approximated by a *local* function of the smoothed density . The many different versions of WDA correspond to different recipes for calculating $\bar{\rho}(\mathbf{1})$.

Given our simple interface topology and boundary conditions upon the density $\rho(\mathbf{1})$, there is no need to employ such complex methods in order to evaluate our charging integration. As a first step towards an analytical theory of association, we implement the simplest of DFT approaches, the well-known *square-gradient theory* (SGT), which corresponds to truncating the gradient expansion of $A[\rho]$ at second order. We therefore construct the *excess* contribution to $A[\rho]$ arising from $c(\mathbf{1},\mathbf{2};[\rho_\lambda])$ as a sum of three components: (1) a hard sphere term using the Carnahan–Starling representation, (2) a van der Waals or dispersion term, and (3) a Wertheim TPT term arising from dimerization. The representation of the free energy as a sum of parts in the context of self-assembly has been discussed before [42]. Of course, close to the critical point the local density $\rho(\mathbf{1})$ may take on values that lie within the bulk two-phase region, which, in the SGA involves some extrapolation of $c(\mathbf{1},\mathbf{2};[\rho_\lambda])$ into the two-phase region. In the square-gradient approximation proper, the whole of the direct correlation function is delta function-like, but use of the *mean spherical approximation* (MSA) to account for the longer-ranged dispersion contribution to $c(\mathbf{1},\mathbf{2})$ essentially makes SGA equivalent to van der Waals theory.

Whatever the particular density dependence taken for $c(\mathbf{1},\mathbf{2};[\lambda\rho])$, however, care must be exercised when calculating the other thermodynamic functions since they involve derivatives of $A[\rho]$, and will therefore generally carry a different

dependence upon the charging parameter λ. For this reason it is useful to functionally derive the other thermodynamic functions in terms of the charging parameter λ first, and so it is to this task that we now turn.

The chemical potential and pressure can be determined in the standard fashion,

$$\beta\mu = \left(\frac{\partial\beta A}{\partial N}\right)_{V,T,d(\mathbf{1})}, \quad \beta P = \left(\frac{\partial\beta A}{\partial V}\right)_{N,T,d(\mathbf{1})},$$

where the distribution $d(\mathbf{1})$, defined by $\rho(\mathbf{1}) \equiv \frac{N}{V}d(\mathbf{1})$, is to be held constant, but the volume derivative of A is difficult to evaluate. It is easier to functionally differentiate the *intrinsic* chemical potential with respect to $\rho(\mathbf{1})$,

$$\beta\mu(\mathbf{1}) = \frac{\delta\beta A[\rho]}{\delta\rho(\mathbf{1})},$$

and then, using

$$\beta\mu N = \int d\mathbf{1}\, \beta\mu(\mathbf{1})\rho(\mathbf{1}) \tag{4.9}$$

determine the form of the pressure through the identity $\beta PV = \beta(\mu N - A)$. Begin with the functional derivative of (4.8),

$$\begin{aligned}\frac{\delta\beta A[\rho]}{\delta\rho(\mathbf{a})} = \ln\left[\rho(\mathbf{a})\Lambda^3\right] &+ \int d\mathbf{2}\int_0^1 d\lambda\,(\lambda-1)\rho(\mathbf{2})c(\mathbf{a},\mathbf{2};[\lambda\rho]) \;+ \\ &\int d\mathbf{1}\int_0^1 d\lambda\,(\lambda-1)\rho(\mathbf{1})c(\mathbf{1},\mathbf{a};[\lambda\rho]) \;+ \\ &\iint d\mathbf{1}d\mathbf{2}\int_0^1 d\lambda\,(\lambda-1)\rho(\mathbf{1})\rho(\mathbf{2})\frac{\delta c(\mathbf{1},\mathbf{2};[\lambda\rho])}{\delta\rho(\mathbf{a})},\end{aligned} \tag{4.10}$$

where $\mathbf{a}$ simply stands for a generic space point $\mathbf{r}_a$. Since the direct correlation function is symmetric (see Eq. (2.24b) on page 38) $c(\mathbf{a},\mathbf{2};[\lambda\rho]) = c(\mathbf{1},\mathbf{a};[\lambda\rho])$, the second and third terms in (4.10) can be combined. The last term is more complicated since it means evaluating $\delta c(\mathbf{1},\mathbf{2};[\lambda\rho])/\delta\rho(\mathbf{a})$. For this, represent the density dependence in $c(\mathbf{1},\mathbf{2};[\lambda\rho(\mathbf{2})])$ with an infinite series,

$$c(\mathbf{1},\mathbf{2};[\lambda\rho(\mathbf{2})]) \equiv \sum_{n=0}^{\infty} c_n(\mathbf{1},\mathbf{2})[\lambda\rho(\mathbf{2})]^n,$$

where the coefficients $c_n(\mathbf{1},\mathbf{2})$ contain the direct spatial dependence. Then

$$\frac{\delta c(\mathbf{1},\mathbf{2};[\lambda\rho(\mathbf{2})])}{\delta\rho(\mathbf{a})} = \sum_{n=0}^{\infty}\delta(\mathbf{a}-\mathbf{2})c_n(\mathbf{1},\mathbf{a})\,n\lambda[\lambda\rho(\mathbf{a})]^{n-1},$$

but

$$\rho(\mathbf{a})\frac{\delta c(\mathbf{1},\mathbf{2};[\lambda\rho(\mathbf{2})])}{\delta\rho(\mathbf{a})} = \sum_{n=0}^{\infty}\delta(\mathbf{a}-\mathbf{2})\,n\,c_n(\mathbf{1},\mathbf{a})[\lambda\rho(\mathbf{a})]^n$$
$$= \delta(\mathbf{a}-\mathbf{2})\,\lambda\,\frac{dc(\mathbf{1},\mathbf{a};[\lambda\rho(\mathbf{a})])}{d\lambda}$$

means that we can rewrite the last term in (4.10) as

$$\int d\mathbf{1}d\mathbf{2}\int_0^1 d\lambda\,(\lambda-1)\rho(\mathbf{1})\rho(\mathbf{2})\frac{\delta c(\mathbf{1},\mathbf{2};[\lambda\rho])}{\delta\rho(\mathbf{a})} =$$
$$\int d\mathbf{1}d\mathbf{2}\,\rho(\mathbf{1})\rho(\mathbf{2})\delta(\mathbf{a}-\mathbf{2})\underbrace{\int_0^1 d\lambda\,(\lambda^2-\lambda)\frac{dc(\mathbf{1},\mathbf{a};[\lambda\rho(\mathbf{a})])}{d\lambda}}_{\text{Integrate by parts}},$$

such that an integration by parts (as indicated above) changes Eq. (4.10) to

$$\frac{\delta\beta A[\rho]}{\delta\rho(\mathbf{a})} = \ln\left[\rho(\mathbf{a})\Lambda^3\right] + \int d\mathbf{2}\int_0^1 d\lambda\,(2\lambda-2)\rho(\mathbf{2})c(\mathbf{a},\mathbf{2};[\lambda\rho]) +$$
$$\int d\mathbf{1}d\mathbf{2}\,\rho(\mathbf{1})\rho(\mathbf{2})\delta(\mathbf{a}-\mathbf{2})\int_0^1 d\lambda\,(1-2\lambda)c(\mathbf{1},\mathbf{a};[\lambda\rho(\mathbf{a})])\,. \quad (4.11)$$

The chemical potential now follows from Eq. (4.9) on the page before,

$$\beta\mu N = \int d\mathbf{a}\,\rho(\mathbf{a})\ln\left[\rho(\mathbf{a})\Lambda^3\right] + \int d\mathbf{a}d\mathbf{2}\,\rho(\mathbf{a})\rho(\mathbf{2})\int_0^1 d\lambda\,(2\lambda-2)c(\mathbf{a},\mathbf{2};[\lambda\rho]) +$$
$$\int d\mathbf{1}d\mathbf{a}\,\rho(\mathbf{1})\rho(\mathbf{a})\int_0^1 d\lambda\,(1-2\lambda)c(\mathbf{1},\mathbf{a};[\lambda\rho(\mathbf{a})])\,.$$

Since the spatial coordinates, like $\mathbf{a}$, are just dummy variables, the symmetry of the direct correlation function allows us to combine the last two (excess) terms such that

$$\beta\mu N = \int d\mathbf{1}\,\rho(\mathbf{1})\ln\left[\rho(\mathbf{1})\Lambda^3\right] - \int d\mathbf{1}d\mathbf{2}\,\rho(\mathbf{1})\rho(\mathbf{2})\int_0^1 d\lambda\,c(\mathbf{1},\mathbf{2};[\lambda\rho])\,. \quad (4.12)$$

The pressure relation $\beta PV = \beta\,(\mu N - A)$ immediately follows:

$$\beta PV = \int d\mathbf{1}\,\rho(\mathbf{1}) - \int d\mathbf{1}d\mathbf{2}\,\rho(\mathbf{1})\rho(\mathbf{2})\int_0^1 d\lambda\,\lambda c(\mathbf{1},\mathbf{2};[\lambda\rho])\,. \quad (4.13)$$

Now the dependence upon the charging parameter is known explicitly for all thermodynamic functions and we can consistently implement some approximation for

the direct correlation function. Often integral equations or perturbation theory is used to obtain an approximation for the homogeneous case which is then extrapolated into the two-phase region.

Since the Carnahan–Starling [148] approximation gives hard sphere results that are nearly indistinguishable from those of molecular dynamics (MD) and Monte Carlo (MC) calculations, we will use it to obtain the density dependence of $c(\mathbf{1},\mathbf{2};[\lambda\rho])$.[4] Specifically, for a homogeneous fluid, we find that

$$\begin{aligned} c^{hs}(\rho) &\equiv \int d\mathbf{r}\; c(r;[\rho])\,, \\ &= -2v_0\,\frac{(4-\eta)}{(1-\eta)^4}\,, \end{aligned} \tag{4.14}$$

where $r = |\mathbf{r}_2 - \mathbf{r}_1|$ and v_0 is the molecular volume $\pi R^3/6$. The charging parameter integrations over λ in Eqs. (4.8), (4.12), and (4.13) can now be carried out. Upon inserting this density-dependent contribution $c^{hs}(\rho)$ and integrating we obtain, respectively,

$$c_A^{hs}(\rho) \equiv \int_0^1 d\lambda\;(1-\lambda)c^{hs}(\lambda\rho) = -v_0\frac{(4-3\eta)}{(1-\eta)^2}\,, \tag{4.15a}$$

$$c_\mu^{hs}(\rho) \equiv \int_0^1 d\lambda\; c^{hs}(\lambda\rho) = -v_0\frac{(8-9\eta+3\eta^2)}{(1-\eta)^3}\,, \tag{4.15b}$$

$$c_p^{hs}(\rho) \equiv \int_0^1 d\lambda\;\lambda c^{hs}(\lambda\rho) = -2v_0\frac{(2-\eta)}{(1-\eta)^3}\,. \tag{4.15c}$$

With the charging integrations complete, we can return to our calculation of the system thermodynamics, *i.e.* to the determination of the non-ideal contributions to the free energy arising from $c(\mathbf{1},\mathbf{2};[\lambda\rho])$ in Eq. (4.8) on page 95. The (Carnahan–Starling) hard sphere contribution therein, when combined with Eq. (4.15a), immediately follows as

$$\frac{\beta A^{hs}}{N} = \eta\,\frac{4-3\eta}{(1-\eta)^2}\,, \tag{4.16}$$

---

[4]The attractive dispersion interaction here, being treated in the van der Waals limit, does not contribute to the structure of our reference fluid, as does the hard sphere repulsion; hence our reliance upon the Carnahan–Starling approximation to determine the density dependence of $c(\mathbf{1},\mathbf{2};[\lambda\rho])$.

where the packing fraction $\eta = \rho v_o$ and v_o is the monomer volume ($\pi R^3/6$).

The attractive part of the dispersion contribution enters through the mean spherical approximation (MSA) [136], represented by

$$\begin{aligned} g(r) &= 0 && r < R, \\ c^{dis}(r) &= -\beta u_{dis}(r) && r > R, \end{aligned} \tag{4.17}$$

where $r \equiv |r_2 - r_1|$. Furthermore, using the relation $\rho(\mathbf{2}) = g(\mathbf{1},\mathbf{2})\,\rho(\mathbf{1})$ derived by Percus [89], density functional theory maintains that the free energy contribution in question can be written as

$$\beta A^{dis} = -\frac{\beta}{2}\iint d\mathbf{1}d\mathbf{2}\;\rho(\mathbf{1})^2 g(\mathbf{1},\mathbf{2})\,u_{dis}(\mathbf{1},\mathbf{2})\,, \tag{4.18}$$

where often the radial distribution function $g(\mathbf{1},\mathbf{2})$ is approximated as that of a uniform hard sphere reference fluid, $g(\mathbf{1},\mathbf{2}) \approx g^{hs}(r)$. This is equivalent to assuming that pairwise correlations arise primarily from excluded volume effects, and for uniform dense liquids, like L–J fluids for example, this is known to be an accurate approximation [55, 64]; yet since our radial distribution function in (4.18) applies only to the relatively weak, isotropic dispersion component of our uniform reference fluid, we go one step further to the van der Waals limit by setting $g(\mathbf{1},\mathbf{2}) = 1$ outside the hard core —excluded volume effects are accounted for by the Carnahan–Starling scheme βA^{hs} above. Inserting $u_{dis}(r)$, Eq. (4.4), into the integral (4.18) and evaluating

$$\begin{aligned} \rho N\int_\sigma^\infty d\mathbf{r}\; u_{dis}(r) &= -4\pi\rho N\int_R^{2^{1/6}R} dr\; r^2\varepsilon^{dis} + 4\pi\rho N\int_{2^{1/6}R}^\infty dr\; r^2 4\,\varepsilon^{dis}\left[(R/r)^{12} - (R/r)^6\right], \\ &= -\frac{8}{3}v_o\rho N\varepsilon^{dis}\left(8\sqrt{2} - 3\right), \end{aligned}$$

we have, using $\eta = \rho v_o$,

$$\frac{\beta A^{dis}}{N} = -\frac{1}{2}\beta\varepsilon^{dis}\nu\eta\,, \quad \nu = \frac{8}{3}\left(8\sqrt{2} - 3\right) \simeq 22.170\,. \tag{4.19}$$

Use of the van der Waals limit not only allows for analytic density profile results, but also for the bulk correlation length and surface tension as well.

Finally, according to Wertheim's thermodynamic perturbation theory (TPT) results [19] (see Section 3.4.3), the dimerization contribution to the free energy is

$$\frac{\beta A^{dim}}{N} = \ln X + \frac{1}{2}(1 - X)\,, \tag{4.20}$$

where N is the total number of monomeric units (bound or free) and the mole fraction of *free* monomers

$$X \equiv \frac{\rho^{(0)}(\mathbf{1})}{\rho(\mathbf{1})}$$

is completely defined by the density of *free* monomers $\rho^{(0)}(\mathbf{1})$ and the total density of monomers and dimers $\rho(\mathbf{1}) = \rho^{(0)}(\mathbf{1}) + \rho^{(1)}(\mathbf{1})$. Notably, the density $\rho^{(1)}(\mathbf{1})$ does not enter the calculation for X, and is therefore absent from the thermodynamic results as well. The monomer density $\rho^{(0)}(\mathbf{1})$ is not a free parameter like $\rho(\mathbf{1})$, but is instead determined self-consistently within the theory. For dimerizing systems, where all s-mer graphs with $s \geq 2$ vanish, the theory greatly simplifies; all F-bonds consist of only one site-site term, $e^R f^A$, and the one-body correlation

$$c^1(\mathbf{1}) \;=\; \rho^{(1)}(\mathbf{1})/\rho^{(0)}(\mathbf{1})$$

is then easily seen to be the graph sum

$$c^1(\mathbf{1}) \;=\; \int d\mathbf{2}\, F(\mathbf{1},\mathbf{2})\, y(\mathbf{1},\mathbf{2})\, \rho^{(0)}(\mathbf{2})\,.$$

Now the fundamental relation

$$\rho(\mathbf{1})/\rho^{(0)}(\mathbf{1}) \;=\; 1 + c^1(\mathbf{1})$$

becomes our *mass action law* of association,

$$\rho(\mathbf{1}) = \rho^{(0)}(\mathbf{1}) + \rho^{(0)}(\mathbf{1}) \int d\mathbf{2}\, F(\mathbf{1},\mathbf{2})\, y(\mathbf{1},\mathbf{2})\, \rho^{(0)}(\mathbf{2})\,, \tag{4.21}$$

which can be inverted to give the desired monomer density $\rho^{(0)}(\mathbf{1})$. The dimer density immediately follows from $\rho(\mathbf{1}) = \rho^{(0)}(\mathbf{1}) + \rho^{(1)}(\mathbf{1})$.

The Mayer-F bonds

$$F(\mathbf{1},\mathbf{2}) = \exp\bigl[-\beta u^{hs}(r)\bigr]\bigl(\exp\bigl[-\beta u^{dim}(\mathbf{1},\mathbf{2})\bigr] - 1\bigr)\,, \tag{4.22}$$

responsible for system dimerization, are all explicitly accounted for in this case. Their evaluation, however, requires details of the pair potentials, particularly $u_{dim}(\mathbf{r})$ in Eq. (4.5) on page 92. For an analytical evaluation of the mass action law, (4.21), $F(\mathbf{1},\mathbf{2})$ must be replaced with a pseudo-potential and angle-averaged; this is the so-called "sticky-spot limit" and is discussed in detail in Section 4.3.1. In that limit, only the contact value of the background (or cavity) distribution

function $y(\mathbf{1},\mathbf{2})$ is required. Since $y(r) = g(r)\exp[\beta u(r)]$, it is not very sensitive to the intermolecular potential and the WCA method thus approximates it for the reference fluid by that of an appropriate hard-sphere system.[5] The value of the hard sphere diameter R is chosen by requiring that the compressibility of the reference system equal that of the hard-sphere system, wherein R becomes a unique function of both temperature and density —a simple algorithm for $R(\beta,\rho)$ is given by Verlet and Weis [149]. For simplicity and consistency, we ignore the T and ρ dependence of R and simply approximate $y(R)$ using the Carnahan–Starling form

$$y(R) \approx y^{hs}(R) = \frac{1-\frac{1}{2}\eta}{(1-\eta)^3}, \tag{4.23}$$

which can be derived from the virial equation of state (EOS) for hard spheres, namely

$$\begin{aligned}\frac{\beta P}{\rho} &= 1 - \frac{2\pi}{3}\beta\rho\int_0^\infty dr\, r^3 u'(r)\exp\left[-\beta u(r)\right] y(r;\rho)\,,\\ &= \frac{1+\eta+\eta^2-\eta^3}{(1-\eta)^3} \qquad \text{(Carnahan–Starling EOS)}\,.\end{aligned}$$

All the contributions to the homogeneous free energy, Eqs. (4.16), (4.19), and (4.20), can now be collected, giving [42]

$$\frac{\beta A}{N} = \ln\left[\rho\Lambda^3/e\right] + \eta\left[\frac{4-3\eta}{(1-\eta)^2} - \frac{1}{2}\beta\epsilon\nu\right] + \ln X + \frac{1}{2}(1-X)\,. \tag{4.24}$$

The compressibility and chemical potential follow from the functional forms Eqs. (4.12) and (4.13) on page 98, along with the charging integrals for $c^{hs}(\lambda\rho)$, Eqs. (4.15b) and (4.15c) [42]:

$$\frac{\beta P}{\rho} = \frac{1+\eta+\eta^2-\eta^3}{(1-\eta)^3} - \frac{1}{2}\beta\epsilon\nu\eta - \frac{1}{2}(1-X)\left[1+\eta\, d_\eta \ln y^{hs}(R)\right]\,, \tag{4.25}$$

$$\beta\mu = \ln\left[\eta_0\Lambda^3\right] + \eta\frac{(8-9\eta+3\eta^2)}{(1-\eta)^3} - \beta\epsilon\nu\eta - \frac{1}{2}(\eta-\eta_0)\, d_\eta \ln y^{hs}(R)\,, \tag{4.26}$$

---

[5]This assumes that the structure of the fluid is primarily determined by repulsive (reference) forces: when averaged over typical fluid configurations (mean-field), the vector sum of long-ranged attractive forces on a given molecule in a *homogeneous* liquid tend to cancel out through pairs of oppositely situated neighbors. This cancellation argument fails at low densities and for *inhomogeneous* fluids, where "unbalanced" attractive forces exist.

where η_0 is the *free* monomer packing fraction and d_η denotes the total derivative with respect to η. Full evaluation of these thermodynamic results requires evaluation of the monomer density $\rho^{(0)}$, or X, and hence the implementation of the pseudo-potential approximation for $F(\mathbf{1},\mathbf{2})$, which will be done in Section 4.3.1.

4.2.3. DFT of the Liquid-Gas Interface

Equilibrium theories of the liquid–vapor interface have a long and lively history [72, 150], in part because two types of fluctuations can be said to occur simultaneously in the interface: (i) bulk fluctuations, which are present even in the absence of the interface and cause the temperature dependence in the fluid density, and (ii) collective surface excitations or capillary waves of the (2-D) interface position. The spatial extension of the bulk fluctuations, of course, extend from the molecular diameter R to the bulk correlation length ξ. The wavelengths of capillary waves —which have no bulk counterpart— roughly span from ξ to a (macroscopic) capillary length $l_c = \sqrt{\gamma/[(\rho_\ell - \rho_g)g]}$, where γ is the surface tension and g is the acceleration due to gravity. A proper account of the liquid-vapor interface should incorporate both types of fluctuation, and some work has been done to reconcile these two views into one consistent theory,[6] but no rigorous theory yet exists. The usual approach taken —and in particular the theory which underpins the classical profile Eq. (4.1)— is that originally developed by van der Waals, who described an "intrinsic" density profile which smoothly varies between the two bulk phase densities. The capillary wave approach, put forth by Buff, Lovett, and Stillinger [151], describes the smooth density profile as a thermal average of a fluctuating step-function-like interface between phases. The van der Waals (vdW) theory neglects microscopic fluctuations[7] in the attractive interactions which arise

---

[6]Buff *et. al.* [151] and Sengers and van Leeuwen [152], for example, have treated semi-infinite liquids possessing thermally excited capillary waves superimposed upon the intrinsic bulk density profile.

[7]The thermodynamic functions produced by mean-field theories correspond to (hypothetical) fluids constrained to be uniform over distances greater than the range of the attractive forces. The approximation is that within the range of the attractive forces of every molecule there is *assumed* to be the same number of neighboring molecules. That approximation is reasonable so long as the unconstrained fluctuations have a short

from correlations in number-density fluctuations [153]. The lowest-order vdW theory can be generalized to nonuniform fluids [154, 88, 72], giving the familiar square gradient theory. External forces, like gravity, play no direct role in square gradient theory (SGT), which leads to well-defined density profiles for the planar liquid–vapor interface, which is why we choose SGT for our analysis. In order to connect with the direct correlation functions, which, in the context of Wertheim theory, carry the details of the potentials, we provide a short review of square gradient theory (see *e.g.* Safran [115]).

Generally, the derivation of the interface profile begins with the Helmholtz free energy $A[\rho]$, which is functionally minimized with respect to the singlet density $\rho(\mathbf{1})$, subject to the constraint of constant N, T, and V. The so-called "square gradient" free energy (the cornerstone of the theory of interfaces) arises out of a specific implementation of the N-constraint on the free energy.

That is, since the Landau–Ginzberg free energy is commonly expressed as an analytic gradient expansion about the critical point, the minimization must be performed with the constraint that the density $\rho(\mathbf{1})$, when averaged over *both* coexisting phases, is held fixed at the critical value ρ_c.[8] Since this (minimization) corresponds to fixing the chemical potential at $\mu = [\partial\psi/\partial\rho]_{\rho_c}$, where ψ is the Helmholtz free energy density, the conditions for coexistence —equality of chemical potentials and osmotic pressures— imply that the two coexisting phases are, in fact, determined by minimization of the grand potential $\Omega = A - \mu N$.

4.2.3.1. Grand Potential Derivation

Minimizing the grand potential at constant chemical potential then requires the functional expansion $A[\rho] - A[\rho_c]$, wherein the homogeneous reference density ρ_c shifts to the inhomogeneous final density $\rho(\mathbf{1})$. As before, we choose a linear

---

correlation length ξ. Yet very close to the critical point the coherence length diverges, and the mean-field approximation therefore becomes less and less accurate [72].

[8]With the *average* density equal to the critical density ρ_c, the fluid may remain in a single phase or phase separate into two coexisting phases whose relative volumes are such that the average density is still ρ_c.

path with charging parameter λ,

$$\rho_\lambda(\mathbf{1}) = \rho_c + \lambda\,\phi(\mathbf{1})\,, \tag{4.27a}$$

$$d\rho_\lambda(\mathbf{1}) = \phi(\mathbf{1})\,d\lambda\,, \tag{4.27b}$$

where $\phi(\mathbf{1}) \equiv [\rho(\mathbf{1}) - \rho_c]$. To simplify the expansion and its λ dependence, start with the functional equivalent of the fundamental theorem of the integral calculus,

$$A[\rho] - A[\rho_c] = \int d\mathbf{1} \int_0^1 d\lambda\; \phi(\mathbf{1})\, \frac{\delta A[\rho_\lambda]}{\delta\rho(\mathbf{1})}\,. \tag{4.28}$$

Iterating once again we obtain

$$\frac{\delta A[\rho_\lambda]}{\delta\rho(\mathbf{1})} = \mu(\rho_c) + \int d\mathbf{2} \int_0^\lambda d\lambda'\; \phi(\mathbf{2})\, \frac{\delta^2 A[\rho'_\lambda]}{\delta\rho(\mathbf{1})\delta\rho(\mathbf{2})}\,. \tag{4.29}$$

Furthermore, to connect the theory to the direct correlation function, which, in the Wertheim context carries all of the details of the interaction potential, we need only recall a general property of the second derivative [72], namely

$$\frac{\delta^2 A[\rho]}{\delta\rho(\mathbf{1})\delta\rho(\mathbf{2})} = k_B T \left[\frac{\delta(\mathbf{1},\mathbf{2})}{\rho(\mathbf{1})} - c\big(\mathbf{1},\mathbf{2};\rho(\mathbf{2})\big) \right]. \tag{4.30}$$

The difference $A[\rho] - A[\rho_c]$ is exact at this point [72], but becomes a Taylor expansion when we evaluate the derivatives (4.29) and Eq. (4.30) at the critical density ρ_c, in which case all the λ dependence becomes isolated in the coefficients of ϕ. Inserting these derivatives then gives, up to fourth order in ϕ,

$$\begin{aligned} A[\rho] - A[\rho_c] = {} & \int d\mathbf{1}\; \mu(\rho_c)\phi(\mathbf{1}) \\ & + \frac{1}{2!}\, k_B T \int d\mathbf{1}d\mathbf{2}\; \phi(\mathbf{1})\phi(\mathbf{2}) \left[\frac{\delta(\mathbf{1},\mathbf{2})}{\rho(\mathbf{1})} - c(\mathbf{1},\mathbf{2};\rho) \right]_{\rho_c} \\ & + \frac{1}{3!}\, k_B T \int d\mathbf{1}d\mathbf{2}\; \phi^2(\mathbf{1})\phi(\mathbf{2}) \left[-\frac{\delta(\mathbf{1},\mathbf{2})}{\rho^2(\mathbf{1})} - \frac{\partial c(\mathbf{1},\mathbf{2};\rho)}{\partial\rho} \right]_{\rho_c} \\ & + \frac{1}{4!}\, k_B T \int d\mathbf{1}d\mathbf{2}\; \phi^3(\mathbf{1})\phi(\mathbf{2}) \left[2\,\frac{\delta(\mathbf{1},\mathbf{2})}{\rho^3(\mathbf{1})} - \frac{\partial^2 c(\mathbf{1},\mathbf{2};\rho)}{\partial\rho^2} \right]_{\rho_c} \\ & + \cdots \quad . \end{aligned} \tag{4.31}$$

Because the direct correlation function is of relatively short range (roughly the range of the intermolecular potential) we can simplify the non-local density depen-

dence in the relation above by expanding $\phi(\mathbf{2})$ in a series about point $\mathbf{1}$,

$$\begin{aligned}\phi(\mathbf{2}) &= \left[1 + \mathbf{r}_{12}\cdot\nabla + \frac{1}{2}(\mathbf{r}_{12}\cdot\nabla)^2 + \cdots\right]\phi(\mathbf{1}),\\ &\simeq \phi(\mathbf{1}) + \frac{1}{6}r^2(d/dz)^2\phi(z),\end{aligned} \tag{4.32}$$

where the planar interface is taken to be located in the x-y plane and only even terms in $\mathbf{r}$ are retained. Now define w_2 through the relation

$$w_2(T) \equiv \int d\mathbf{2}\left[\frac{\delta(\mathbf{1},\mathbf{2})}{\rho(\mathbf{1})} - c(\mathbf{1},\mathbf{2};\rho)\right] = \frac{\beta}{\rho}\left(\frac{\partial P}{\partial \rho}\right)_T, \tag{4.33}$$

such that we can approximate the grand potential energy excess $W[\rho]V$ as

$$\beta W[\rho]V \equiv \beta\Big\{A[\rho] - A[\rho_c] - \mu_c V(\rho - \rho_c)\Big\}, \tag{4.34a}$$

$$\begin{aligned}\simeq \int d\mathbf{1}\Big[&\frac{1}{2!}\phi^2(\mathbf{1})w_2(T) + \frac{1}{3!}\phi^3(\mathbf{1})w_3(T) + \frac{1}{4!}\phi^4(\mathbf{1})w_4(T)\\ &+ \cdots - \frac{1}{2}m^2(T)\phi(\mathbf{1})\big(d^2\rho(\mathbf{1})/dz^2\big)\Big],\end{aligned} \tag{4.34b}$$

where we have defined

$$m^2(T)v_o = \frac{1}{3!}\int d\mathbf{r}\, r^2 c(r;\rho_c), \tag{4.35}$$

$$w_n(T) = (d/d\rho)^{n-2} w_2(T) \qquad \forall\, n \geq 2. \tag{4.36}$$

Recall that v_o is the molecular volume, and $c(r;\rho_c)$ is the direct correlation function of a (hypothetical) uniform fluid held at density ρ_c, which lies somewhere between the liquid ρ_ℓ and gas ρ_g densities. In the original vdW theory, $m(T)$ does not carry any density dependence, and so (4.35) represents the simplest extension of the vdW square gradient theory into nonuniform fluids. Other methods include approximating the direct correlation function in the (inhomogeneous) interface region through interpolation between correlations evaluated in the homogeneous phases [155].

Evaluation of the $w_n(T)$ terms in our expansion, Eq. (4.34b), can be physically motivated by rewriting these Landau terms in a more convenient form [115]:

$$\beta WV \propto -\frac{a}{2}\phi^2 + \frac{b}{3}\phi^3 + \frac{c}{4}\phi^4 + \cdots. \tag{4.37}$$

When $b \neq 0$ we have a first-order transition, with $\phi = 0$ for a large and negative, but jumps (discontinuously) to some nonzero value ϕ_o as a is increased. If $b = 0$,

however, the two coexisting phases have compositions which now approach the critical value smoothly, *i.e.* $\phi \to 0$ and $a \to 0$ at the critical point —evident by minimizing (4.37) with $b = 0$. The value of the system composition ρ_o at which $b = 0$ when $a = 0$ is the critical density ρ_c. Our expansion of βWV around ρ_c, with μ equal to its critical value μ_c, then yields a free energy of the form of Eq. (4.37), but with $b = 0$. Minimization of βWV when $\mu = \mu_c$ (equivalent to holding the composition fixed at ρ_c) implies that $\phi_\ell = -\phi_g$, or, using Eq. (4.27a), that $(\rho_\ell + \rho_g) = 2\rho_c$.

We can, of course, relate the coefficients a, b, and c to the functions $w_2(T)$, $w_3(T)$, and respectively. In our vdW-like mean field theory then, the condition $b = 0$ corresponds to evaluating $w_3(T)$ at the critical temperature as well as the critical density, where it identically vanishes. The "analytical continuation" our free energy into the two-phase region is then typically accomplished by evaluating $w_2(T)$ at an arbitrary temperature, but all higher-order terms, like $w_4(T)$, at the critical temperature T_c. Imposing these conditions and keeping terms to fourth order, we have

$$\beta W[\rho]V = \int d\mathbf{1} \left[\frac{1}{2} w_2(T)\phi^2(\mathbf{1}) + \frac{1}{4} w_4(T_c)\phi^4(\mathbf{1}) + \frac{1}{2} m^2(T) v_o \left(d\phi(\mathbf{1})/dz\right)^2 \right], \tag{4.38}$$

which is known as a Landau-Ginzberg expansion.

Minimization of the fourth-order equation (4.38) will yield two solutions, ρ_ℓ and ρ_g, in terms of temperature-dependent constants and ρ_c. What we really want is an equilibrium density profile $\rho(\mathbf{1})$ written in terms of the coexistence densities, and so we rewrite our Landau-Ginzberg equation above in terms of ρ_ℓ and ρ_g instead of ρ_c,

$$W_1 \propto a(\rho - \rho_c)^2 + b(\rho - \rho_c)^4 \quad \longrightarrow \quad W_2 \propto b(\rho - \rho_g)^2(\rho_\ell - \rho)^2 . \tag{4.39}$$

By equating the derivatives of W_1 and W_2 and using the relation $(\rho_\ell + \rho_g) = 2\rho_c$, we find that

$$\beta W[\rho]V \equiv \int d\mathbf{1} \Big[\frac{1}{4!} w_4(T_c) \left[\rho(\mathbf{1}) - \rho_g\right]^2 \left[\rho_\ell - \rho(\mathbf{1})\right]^2 + \frac{1}{2} m^2(T) v_o \left(d\phi(\mathbf{1})/dz\right)^2 \Big], \tag{4.40}$$

which is the familiar square gradient theory equation [115, 72, 68].

4.2.3.2. Minimization and Density Profile

Finally, to obtain our semi-infinite density profile $\rho(z)$ we functionally minimize Eq. (4.40), giving the Euler-Langrange relation

$$\frac{\delta W[\rho]}{\delta \rho(z)} = \frac{dW(\rho(z))}{d\rho(z)} - k_B T m^2(T) v_o \nabla^2 \rho(z) = 0, \tag{4.41a}$$

which we multiply by $d\rho(z)/dz$ in order to obtain

$$\frac{dW(\rho(z))}{dz} - \frac{1}{2} k_B T m^2(T) v_o \frac{d}{dz} \left(\frac{d\rho(z)}{dz} \right)^2 = 0. \tag{4.41b}$$

This equation can be written in terms of total derivatives,

$$dW(\rho(z)) - \frac{1}{2} k_B T m^2(T) v_o \, d\left(d\rho(z)/dz\right)^2 = 0, \tag{4.41c}$$

and integrated to yield

$$W(\rho(z)) - \frac{1}{2} k_B T m^2(T) v_o \left(d\rho(z)/dz\right)^2 + const. = 0. \tag{4.41d}$$

Since $W(\rho)$, according to Eq. (4.39), happens to be the square of a function, as is $(d\rho(z)/dz)^2$, we can up to an additive constant take the square root of Eq. (4.41d),

$$\sqrt{\frac{w_4(T_c)}{4!}} \left(\rho - \rho_g\right)\left(\rho_\ell - \rho\right) = \pm \sqrt{\tfrac{1}{2} k_B T m^2(T) v_o} \, \frac{d\rho(z)}{dz}, \tag{4.42}$$

which, by defining the new constant

$$\omega \equiv \sqrt{\frac{\beta w_4(T_c)}{12 v_o}}, \tag{4.43}$$

where $\beta = (k_B T)^{-1}$, allows us to rewrite (4.42) in the simple form

$$\frac{d\rho(z)}{dz} = \pm \frac{\omega}{m(T)} \left(\rho - \rho_g\right)\left(\rho_\ell - \rho\right). \tag{4.44}$$

Integrating this separable equation with the Gibbs dividing surface —which we are free to choose— set at $z = 0$ or vanishing adsorption, we obtain

$$\left(\rho_\ell - \rho_g\right)^{-1} \ln \left[\frac{\left(\rho(z) - \rho_g\right)}{\left(\rho_\ell - \rho(z)\right)} \right] = \pm \frac{\omega}{m(T)} z. \tag{4.45}$$

Choosing the plus sign above we place the liquid phase in the positive half plane, *i.e.* $\rho(z) \to \rho_\ell$ as $z \to +\infty$ and $\rho(z) \to \rho_g$ as $z \to -\infty$, and our profile $\rho(z)$ becomes

$$\rho(z) = \rho_\ell - \frac{(\rho_\ell - \rho_g)}{1 + \exp[z/\xi]}, \tag{4.46}$$

with microscopic defining relations for all parameters. The bulk correlation length ξ, which is a measure of the van der Waals "intrinsic" interface thickness, is defined by the right-hand side of Eq. (4.45). For convenience, we recast ξ into a dimensionless form

$$\frac{\xi(T)}{R} = \frac{[m(T)/R]}{(\eta_\ell - \eta_g)(\omega/v_o)}, \tag{4.47}$$

where η is the packing fraction $\eta = \rho v_o$, v_o the molecular volume, and ω/v_o, from Eq. (4.48), can be written as

$$\omega \equiv \sqrt{\frac{\beta w_4(T_c)}{12 v_o}} = v_o \sqrt{\frac{1}{12\,\eta_c}\left(\frac{\partial^3 \beta P v_o}{\partial \eta^3}\right)_c}, \tag{4.48}$$

where the subscript c denotes evaluation at the full critical point.

The full interface width d in our theory is really twice the bulk correlation length $2\xi(T)$, which can be seen by rewriting Eq. (4.46) in its more familiar hyperbolic tangent form,

$$\rho(z) = \frac{1}{2}(\rho_\ell + \rho_g) - \frac{1}{2}(\rho_\ell - \rho_g)\tanh[z/2\xi]. \tag{4.49}$$

The standard measure of interface width, however, is not d but the "10–90" thickness t, defined as distance Δz between which $(\rho(z) - \rho_\ell)/(\rho_g - \rho_\ell)$ varies from 0.1 to 0.9. For the hyperbolic tangent profile, or Eq. (4.46), t is related to ξ by the equation

$$t = 2\,\xi(T)\ln 9 \approx 4.394\,\xi(T).$$

4.2.3.3. Surface Tension

The surface tension γ can be written either in terms of the excess free energy or pressure associated with the interface. Generally, for an inhomogeneous fluid the grand potential can be written as

$$\Omega = -PV + \gamma A,$$

where γ is the surface tension and A is the surface area. Since each bulk phase α carries an energy of $\Omega^\alpha = -PV^\alpha$, the surface tension or surface free energy Ω^S per unit area is

$$\gamma = \frac{\Omega^S}{\mathrm{A}}.$$

For our mean-field, planar profile we defined a free-energy-density excess of $W(\rho)$, which suggests the surface tension relation

$$\gamma = \int_{-\infty}^{\infty} dz\, W(\rho(z)). \tag{4.50}$$

We need not, moreover, be concerned here with the position of our dividing surface, for $W(\rho(z))$ does, in fact, correspond to the excess pressure associated with the interface. Defining the Helmholtz free-energy density $\psi[\rho(z)] = A(\rho)/V$ and dividing Eq. (4.34a) by βV, we obtain

$$W(\rho(z)) = \psi[\rho(z)] - \mu_c\rho(z) - (\psi(\rho_c) - \mu_c\rho_c), \tag{4.51}$$

which, when coupled with $A - \mu N = -PV$, or

$$\psi(\rho) - \mu\rho = -P,$$

shows that

$$-W(\rho) = [P_{\mu_c} - P_{\rho_c}] \tag{4.52}$$

is the negative of the pressure excess, where P_{μ_c} is the equilibrium pressure of the system with its chemical potential fixed at μ_c (equivalent to an *average* composition of ρ_c), and P_{ρ_c} is the pressure of the homogeneous system with density ρ_c. Shown in Fig. 4.4(a) is a plot of the mean-field Helmholtz free energy density $\psi(\rho, T)$ as a function of ρ for fixed T in the phase coexistence region. The equilibrium liquid ρ_ℓ and gas ρ_g densities are defined by the common tangent to the curve (dashed line), $\psi^{(2)}(\bar{\rho})$, which is the free energy density of the two-phase system at mean density $\bar{\rho}$. If $\psi(\rho)$ is the single-phase Helmholtz free energy density, then $\psi[\rho(z)]$ is its analytic continuation through the two-phase region, and $\psi(z)$ is the van der Waals approximation to the actual free energy density at height z,

$$\psi(z) = \psi[\rho(z)] + \frac{1}{2}\big(d\rho(z)/dz\big)^2 m^2\big(T, \rho(z)\big). \tag{4.53}$$

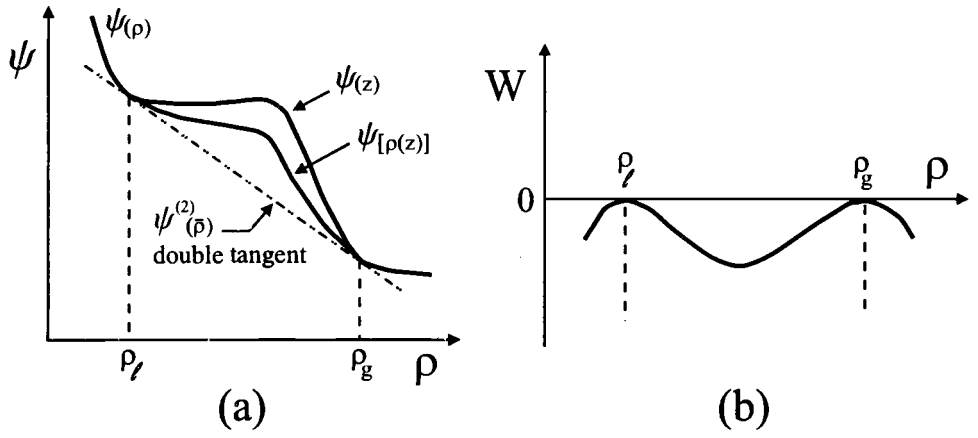

FIGURE 4.4. Isotherms defining the excess free-energy-density $W(\rho)$. In (a) are isotherms of the Helmholtz free energy density ψ, and (b) the free energy density $-W(\rho)$, which equals the negative of the excess of the formal pressure $\mu\rho - \psi[\rho(z)]$.

The function $-W(\rho)$, shown in Fig. 4.4(b), is then seen as the height of the $\psi[\rho(z)]$ isotherm above the double tangent,

$$-W(\rho(z)) = \psi[\rho(z)] - \psi^{(2)}(\bar{\rho})\,. \tag{4.54}$$

Inserting Eq. (4.53) into (4.54), and recognizing the difference $\Psi(z) = \psi(z) - \psi^{(2)}(\bar{\rho})$ as the excess Helmholtz free energy, we have

$$-W(\rho(z)) \;=\; \Psi(z) - \frac{1}{2}\big(d\rho(z)/dz\big)^2\, m^2\big(T, \rho(z)\big)\,. \tag{4.55}$$

The N constraint upon our minimization of the free energy then corresponds to the second term on the right-hand side of Eq. (4.55), which imposes a characteristic length in the fluid through its dependence upon the direct correlation function, Eq. (4.35). Free energy minimization without that term would lead to a step-function profile $\rho(z)$ instead of the hyperbolic tangent one, Eq. (4.49), which smoothly transitions from the bulk gas phase ρ_g at $-\infty$ to the bulk liquid phase at $+\infty$.

The resulting free energy minimization shows that [see Eq. (4.41d)]

$$W\left(\rho(z)\right) \;=\; \frac{1}{2}\, k_B T m^2(T) v_o \left(d\rho(z)/dz\right)^2\,, \tag{4.56}$$

such that the surface tension can be evaluated from

$$\begin{aligned}\gamma &= \int_{-\infty}^{\infty} dz\, W(\rho(z))\,, \\ &= k_B T v_o \int_{-\infty}^{\infty} dz\, \left(d\rho(z)/dz\right)^2 m^2\left(T, \rho_c(z)\right)\,, \end{aligned} \tag{4.57}$$

which is the standard square gradient result [72]. The density dependence is shown in $m(T)$ is reminder that it must be evaluated at the critical density.

4.2.4. Evaluation of Parameters

The interface for our model is defined by the correlation length ξ, which has three important contributions: (i) the liquid and gas densities, ρ_ℓ and ρ_g respectively; (ii) the volume term ω, Eq. (4.48), specified by the third density derivative of the pressure; and (iii) the characteristic length $m(T)$, Eq. (4.35), which requires the direct correlation function $c(r;\rho_c)$ or simply $c(r)$. It is to this function that we now turn our attention.

The direct correlation function was approximated as a sum of two terms: $c^{hs+dim}(r)$ from the solution of the *associated* Ornstein-Zernike (AOZ) equation in the presence of both hard-sphere and dimerization potentials [19, 20] and $c^{dis}(r)$ from the *mean spherical approximation* (MSA) theory of van der Waals interactions [136],

$$c(r) \simeq c^{hs+dim}(r) + c^{dis}(r)\,. \tag{4.58}$$

The quantity $c^{hs+dim}(r)$ was determined by solution of the Percus-Yevick (PY) equation for a dimerizing fluid, using the methods of Wertheim [156] and later, Kalyuzhnyi [98, 102], which were adapted from the factorization methods of Wertheim [157] and Baxter [158]. The factorization method will be discussed in more detail in Chapter 5 where it is applied to a four-site, water-like model; here we simply state the integral equation results for the direct correlation function. If no F-bonded rings are allowed, Wertheim theory maintains that the short-range correlations can be written as

$$c^{hs+dim}(r) = c^{00}(r) + 2\left(\eta_0/\eta\right) c^{01}(r) + \left(\eta_0/\eta\right)^2 c^{11}(r)\,. \tag{4.59}$$

Recall that a superscript 0 denotes that no F-bonds are incident at the labelled point, whereas a superscript 1 denotes the presence of an F-bond incident upon

the labelled point. Inside the hard core factorization results for the $c^{ij}(x)$ give

$$c^{00}(x) = c^{hs}(x) + \frac{1}{2}(\eta - \eta_0)(1-x)\left[\frac{5+\eta-(x^2+x)(1+2\eta)}{(1-\eta)^3}\right], \tag{4.60a}$$

$$c^{01}(x) = c^{10}(x) = \frac{(\eta-\eta_0)}{4\eta_0}\left[\frac{2+\eta-x(1+2\eta)}{(1-\eta)^2}\right], \tag{4.60b}$$

$$c^{11}(x) = 0, \tag{4.60c}$$

where $x \equiv r/R < 1$ and $c^{hs}(x)$ is the usual PY result [159, 160], *i.e.*

$$c^{hs}(x) = -\left[(1+\frac{1}{2}\eta x^3)\lambda_1 + 6\eta\lambda_2 x\right] \qquad x < 1\,,$$
$$\lambda_1 = \frac{(1+2\eta)^2}{(1-\eta)^4}, \quad \lambda_2 = -\frac{(1+\frac{1}{2}\eta)^2}{(1-\eta)^4}\,.$$

Note that, due to the convolution in the AOZ, association effects from the sticky spot show up *inside* the hard core: second term in (4.60a) for $c^{00}(x)$ as well as $c^{01}(x)$ and $c^{10}(x)$ in Eq. (4.60b). The pre-factor $(\eta - \eta_0)$ ensures that these contributions vanish in the limit of no association. Outside the hard core, only $c^{11}(x)$ is non-zero,

$$c^{11}(x) = F(x)\, y^{00}(x) \simeq F(x)\, y^{hs}(x) \qquad x \geq 1\,. \tag{4.61}$$

Armed with the solution for $c(r)$, we can now calculate an analytical solution for $m(T)$ and hence for the bulk correlation length ξ, Eq. (4.47), and the surface tension γ, Eq. (4.57). Inserting $c(x)$ into Eq. (4.35) on page 106 and carrying out the spatial integration gives

$$\frac{m^2(T)}{R^2} \simeq -\frac{1}{20}\left[\frac{16-11\eta+4\eta^2}{(1-\eta)^4}\right] + 13.9\,\beta\varepsilon^{dis} + \frac{1}{60}(\eta-\eta_0)\left[\frac{10-2\eta+\eta^2}{(1-\eta)^3\eta^2}\right], \tag{4.62}$$

where η is to be evaluated at $\frac{1}{2}(\eta_\ell + \eta_g) \simeq \eta_c$. The characteristic length $m(T)$ has origins similar to those of the elastic constants for liquid crystals [161] and involves precisely the same type of integral, with contributions from repulsion as well as attraction.

The surface tension follows from Eqs. (4.57) and (4.62). After a change of integration variables in (4.57) from z to ρ, the resulting density integral can be

approximated using the mean value theorem such that

$$\beta R^2\gamma \simeq \frac{3}{2}\frac{(\eta_\ell - \eta_g)^2}{(\xi/R)}\left[\frac{m(T)}{R}\right]^2 . \tag{4.63}$$

Apart from minor notational differences, Eq. (4.63) is the same as that found in the literature [72, 162].

4.3. APPLICATIONS AND RESULTS

4.3.1. Sticky-Spot Potential Limit

Numerical predictions of the thermodynamics from the present results can be derived, provided that additional details of the dimerizing potential are specified. If the dimerization potential u^{dim} is very short-ranged and large in magnitude, *i.e.* $l^{dim} \ll R$ and $\varepsilon^{dim} \gtrsim 10\, k_B T$, then $F(\mathbf{1},\mathbf{2})$ may be approximated by a pseudo-potential,

$$F(\mathbf{1},\mathbf{2}) \to l^{dim}\,\delta(r-R)\Big[\exp\big(\beta\varepsilon^{dim}\big) - 1\Big], \tag{4.64}$$

subject to the same orientational (steric) restrictions of Eq. (4.5). This replacement corresponds to the "sticky-spot limit" of $u^{dim}(r)$, wherein the conical well depth ε^{dim} goes to infinity while the width l^{dim} goes to zero,[9] analogous to the adhesive sphere sticky limit of Baxter [106, 158, 163, 164]. In this limit the attractive site effectively becomes an infinitesimally-ranged "sticky spot" or patch located on the hard core surface (*i.e.* at R^+).

In a spatially homogeneous system, Eq. (4.21) gives the relation between the density of free monomers $\rho^{(0)}$ and the total monomer density ρ,

$$\rho = \rho^{(0)} + \Delta_A\left[\rho^{(0)}\right]^2 , \tag{4.65}$$

$$X = \frac{\rho^{(0)}}{\rho} = \frac{2}{1+\sqrt{1+4\rho\Delta_A}} , \tag{4.66}$$

where

---

[9]This limit is often constrained such that the second virial coefficient $B_2(T)$ for the association potential remains constant.

$$\Delta_A = \int d\mathbf{r}\, \frac{1}{(4\pi)^2} \iint d\hat{e}_1 d\hat{e}_2\, F(\mathbf{1},\mathbf{2})\, y(\mathbf{1},\mathbf{2}),$$

$$= 24\, v_0\, s_{dim}^2 \frac{l^{dim}}{R} \left[\exp\left(\beta\varepsilon^{dim}\right) - 1\right] y^{hs}(R), \tag{4.67}$$

$$= 4\pi\, K_A \left[\exp\left(\beta\varepsilon^{dim}\right) - 1\right] y^{hs}(R). \tag{4.68}$$

The steric restrictions

$$s_{dim} = \frac{1}{2}\left[1 - \cos(\theta_c)\right] \tag{4.69}$$

are contained in the unweighted angle average $\langle F(\mathbf{1},\mathbf{2})\rangle_{\hat{e}_1\hat{e}_2}$ and the volume available for bonding is identified as

$$K_A = R^3 s_{dim}^2 \frac{l^{dim}}{R}. \tag{4.70}$$

Recall that $y^{hs}(R)$ is approximated by the Carnahan-Starling result, Eq. (4.23) on page 102. The above calculations show that *all* of the density dependence in Δ_A is contained in $y^{hs}(R)$, while *all* of the temperature dependence is contained in $\beta\varepsilon^{dim}$ —unlike the WCA approximation, our molecular diameter R in Eqs. (4.3) and (4.4) on page 92 is temperature and density independent.

In this work we approximate the systems discussed by Jackson *et. al.* [42] and Chapman [165] by choosing a maximum cone angle of $\theta_c = 27°$ and an effective association range of $l^{dim} = 0.01R$ (see Fig. 4.2). These values not only guarantee that association is limited to dimer formation (SI-1), but are also consistent with our pseudo-potential evaluation of $F(\mathbf{1},\mathbf{2})$ in Eq. (4.64). The above conical association parameters produce a bonding volume of $K_A = 2.970 \times 10^{-5} R^3$. With ε^{dim} and K_A now given, Δ_A proceeds from Eq. (4.68) and thereby determines the extent of dimerization. When discussing the results of the theory it will be useful to define the following dimensionless quantities: the reduced association strength $\varepsilon^* \equiv \varepsilon^{dim}/\varepsilon^{dis}$ and the reduced temperature $T^* \equiv k_B T/\varepsilon^{dis}$, where k_B is Boltzman's constant.

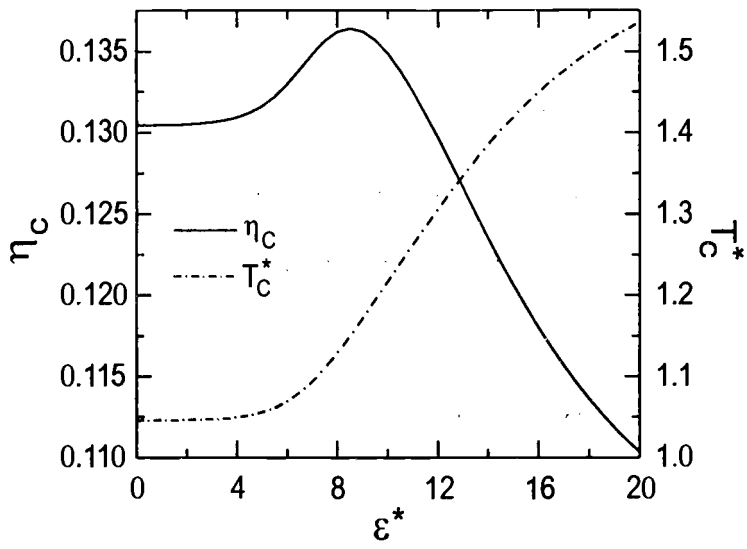

FIGURE 4.5. Critical packing fraction η_c and temperature T_c as a function of reduced association strength ε^* for a single site system with $K_A = 2.970 \times 10^{-5} R^3$. Note that while T_c^* (plotted at right) displays a monotonic increase with ε^*, η_c (plotted at left) shows decidedly non-monotonic behavior, peaking around $\eta_c \approx 0.1364$ at $\varepsilon^* \approx 8.5$ and $T_c^* \approx 1.15$.

4.3.2. Critical Point and Coexistence

A model hard sphere system with only one anisotropic, short-ranged attraction site per monomer (1-D association) does not exhibit a critical point.[10] Inclusion of longer-ranged van der Waals–like interaction $-u^{dis}(r)$ in our case, however, guarantees the usual liquid–gas phase equilibria. Nonetheless, system critical constants and coexistence curves are affected by the varying degrees of (short-ranged) association present in he fluid. For our model of single-site association, the liquid–gas critical points and coexistence densities had to be found numerically from Eqs. (4.25) and (4.26) on page 102.

[10]The *necessary* geometrical conditions (*e.g.* interaction range and degree of anisotropy) required for the existence of a critical point, in terms of intermolecular interactions, are not yet fully understood. As will be shown in Chapter 5, four tetrahedrally-arranged "sticky spots" are enough to generate a critical point, even when those spots are infinitesimally ranged.

For a one-component system, the inflection point of the pressure isotherm defines the critical point: $(\partial P/\partial\rho)_{N,T} = (\partial^2 P/\partial\rho^2)_{N,T} = 0$. Solving these simultaneous conditions (using the K_A value above) gives the critical packing fractions and temperatures (denoted by a subscript c), which are shown in Fig. 4.5. While T_c^* increases monotonically with ε^*, our model consistently underestimates the critical temperatures of Chapman [165] by roughly 20%. This discrepancy arises from our use of the van der Waals limit, $g(\mathbf{1},\mathbf{2}) = 1$, in Eq. (4.18) on page 100 and our simplified treatment of Δ_A in Eq. (4.68); Chapman, while making the same assumption that the structure of the reference fluid is determined by repulsive forces, incorporates a "complete" WCA treatment (see Fig. 4.1) of the mean-field potential for $r < 2^{1/6}R$ when approximating the pair correlation function $g^{ref}(r)$. Müller *et. al.* [166], in fact, have pointed out the sensitivity of Wertheim theory to the accuracy with which Δ_A is calculated, Δ_A itself being sensitive to the approximations used for $g^{ref}(r)$. Comparison of both T_c^* and η_c with the theoretical results of Jackson *et. al.* [42] shows agreement to within 1%–2% after properly scaling the van der Waals contributions to the free energy. In the non-associating limit ($\varepsilon^* = 0$), there is exact agreement: $\eta_c = 0.130444$ and $T_c^* = 1.04563$. As ε^* is increased η_c increases to a maximum around 0.1364 at $\varepsilon^* \approx 8.5$ and $T_c^* \approx 1.15$, but then decreases as ε^* increases further. As Fig. 4.7 suggests this initial increase in η_c at moderate association values seems to correspond to the initial increase in dimer formation in the liquid phase, with the maximum occurring approximately when the fraction of monomers X in the gas phase begins to drop sharply.

The mean-field liquid and gas coexistence densities ρ_ℓ and ρ_g were determined using the equality of pressures and chemical potentials at constant temperature in the distinct phases,

$$P(\rho_\ell) = P(\rho_g), \qquad \mu(\rho_\ell) = \mu(\rho_g)$$

Coexistence curves were calculated using a Newton-Raphson iterative method, wherein $P(\rho)$ and $\mu(\rho)$ are expanded about two initial guesses, ρ_ℓ^o and ρ_g^o, for the equilibrium densities ρ_ℓ and ρ_g and then iterated until they stabilize at the ρ_ℓ and ρ_g values. For a simple, one-dimensional case, the Newton-Raphson method consists of geometrically extending the tangent line at the current point x_i until it crosses zero, *i.e.* $f(x) = 0$, and then sets the next guess x_{i+1} to the abscissa of that zero-crossing. The function is expanded in a Taylor series in a neighborhood

about some point

$$f(x+\delta) \approx f(x) + f'(x)\delta + \frac{f''(x)}{2}\delta^2 + \cdots .$$

If $f(x)$ is "well-behaved" and δ is small enough,[11] terms beyond the linear one are negligible and thus $f(x+\delta) = 0$ implies that

$$\begin{aligned} x_{i+1} &= x_i + \delta , \\ &= x_i - \frac{f(x_i)}{f'(x_i)} . \end{aligned}$$

For N functional relations involving N variables,

$$F_i(x_1, x_2, \ldots, x_N) = 0 , \qquad i = 1, 2, \ldots, N ,$$

the generalization is simply

$$F_i(\mathbf{x} + \delta\mathbf{x}) \approx F_i(\mathbf{x}) + \sum_{j=1}^{N} \frac{\partial F_i}{\partial x_j}\,\delta x_j + \mathcal{O}(\delta\mathbf{x}^2) ,$$

which, with the identifications $F_1(\rho_\ell^o, \rho_g^o) \equiv P(\rho_\ell^o) - P(\rho_g^o)$ and $F_2(\rho_\ell^o, \rho_g^o) \equiv \mu(\rho_\ell^o) - \mu(\rho_g^o)$, gives for our case the set of simultaneous equations

$$\begin{aligned} P(\rho_\ell^o) + \left.\frac{\partial P}{\partial \rho_\ell}\right|_{\rho_\ell^o} (\rho_\ell - \rho_\ell^o) &= P(\rho_g^o) + \left.\frac{\partial P}{\partial \rho_g}\right|_{\rho_g^o} (\rho_g - \rho_g^o) , \\ \mu(\rho_\ell^o) + \left.\frac{\partial \mu}{\partial \rho_\ell}\right|_{\rho_\ell^o} (\rho_\ell - \rho_\ell^o) &= \mu(\rho_g^o) + \left.\frac{\partial \mu}{\partial \rho_g}\right|_{\rho_g^o} (\rho_g - \rho_g^o) . \end{aligned}$$

The identity $(\partial\mu/\partial\rho)_T = \rho^{-1}\,(\partial P/\partial\rho)_T$ allows us to rewrite the chemical potential derivative in terms of the pressure derivative,

$$\beta\frac{\partial}{\partial\rho}\Big[P - \big(P^{hs} + P^{dis}\big)\Big]_T = -\frac{1}{2}\,(\eta - \eta_0)\Big[\frac{q}{(\eta - \frac{1}{2}\eta_0)} + \eta\, d_\eta^2 \ln y^{hs}(\eta)\Big] , \qquad (4.71)$$

where

$$q \equiv 1 + 2\,\eta\, d_\eta \ln y^{hs}(\eta) + \frac{1}{2}\,\eta\,\eta_0\big[d_\eta \ln y^{hs}(\eta)\big]^2$$

---

[11] Starting close to the critical point, δ can be made arbitrarily small by choosing $\delta \approx |\rho_{\ell,g}^o - \rho_c| \ll 1$.

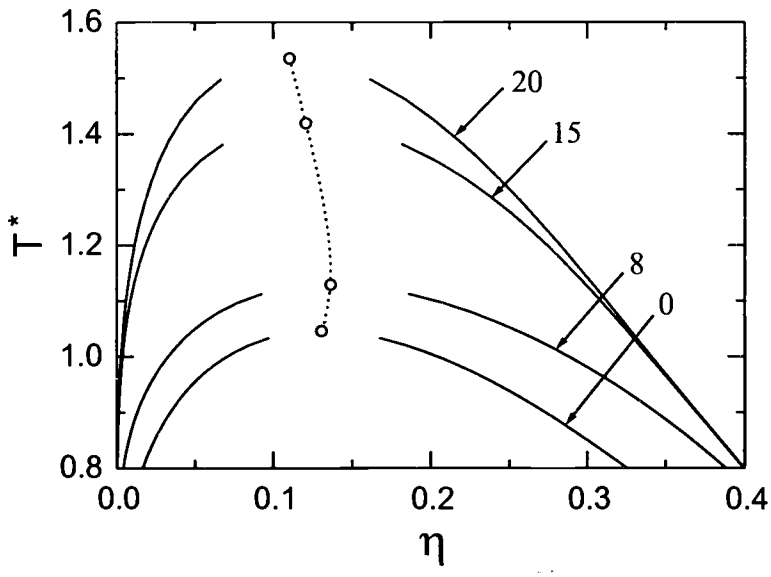

FIGURE 4.6. Liquid–gas coexistence curves for association strengths $\varepsilon^* = 0$, 8, 15, and 20. The locus of the critical point is indicated by the dashed line, with circles marking the actual points for the given association strengths.

---

and $d_\eta = d/d\eta$. With bonding volume differences of a factor of 2, our coexistence densities η_ℓ and η_g, shown in Fig. 4.6 for four association strengths, are within approximately 10% of the values of Jackson *et. al.* [42].

The mole fractions of monomers X in the coexisting phases for five values of association strength are shown in Fig. 4.7 as a function of reduced temperature. In the absence of bonding both liquid and gas phases are entirely composed of monomers, $X = 1$, at all temperatures. As ε^* increases the liquid phase undergoes the more extensive dimerization, as expected, due to its greater density. As ε^* increases further the gas phase begins to appreciably dimerize as well, such that when $\varepsilon^* \gtrsim 20$ both phases are nearly completely dimerized . The *increase* with temperature of the monomer mole fraction X at moderate to high association strengths in both liquid and vapor phases is much more surprising. Particularly striking is the rapid increase in free monomers in the liquid as T^* increases when $\varepsilon^* = 10$. For $\varepsilon^* \gtrsim 10$ temperature effects upon X seem to dominate those of density, except near the critical point where the sharp increase in η_g overpowers the temperature dominance in the gas phase, decreasing X.

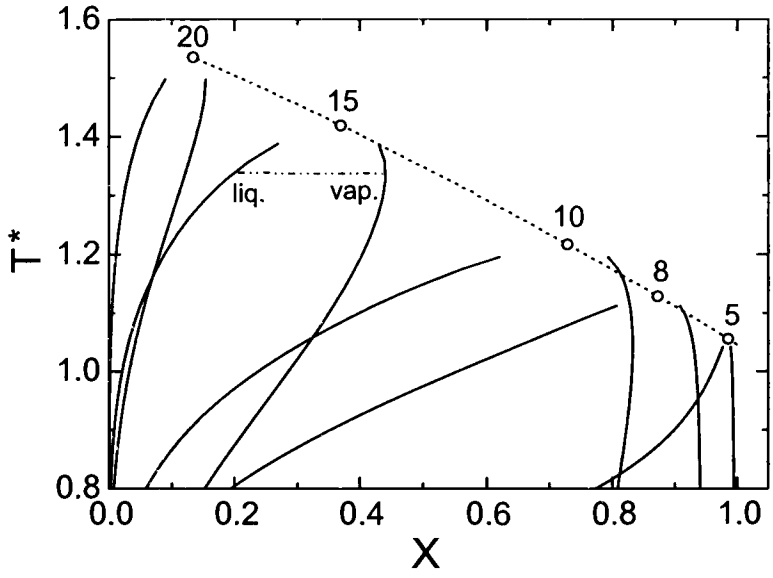

FIGURE 4.7. Monomer mole fraction X along the liquid–gas coexistence curve for association strengths $\varepsilon^* = 5$, 8, 10, 15, and 20. Each value is listed above the circle marking the critical point of the curve. The right-hand side of each curve corresponds to gas X values while those on the left to liquid X values: the horizontal dashed line indicates equilibrium values for a given T^*.

4.3.3. Interface Properties

These comparisons aside, our intent is to explore any signature dimerization may have upon the planar liquid-vapor interface, not to recalculate critical points and coexistence curves already known from simulations. The most obvious change related to association occurs in the direct correlation function, Eq. (4.58), which is shown in Fig. 4.8 for reduced association strengths $\varepsilon^* = 0$, 8, and 20 at $T/T_c = 0.85$ and $\eta = \eta_c = 0.130444$. Inside the hard core $c(x)$ is negative for all association strengths, yet becomes less so as association increases. Outside the hard core $c^{hs+dim}(x) = 0$ when $\varepsilon^* = 0$, but develops a small peak (inset in Fig. 4.8) at $x = 1$ with width $\delta x = l^{dim} = 0.1$ as ε^* increases corresponding to the reactive cone contribution $c^{11}(x)$. In the "sticky-spot" limit this contribution becomes a delta-function located at $x = 1^+$. The MSA contribution $c^{dis}(x)$ to $c(x)$ outside the hard core is a positive constant for $1 < x \leq 2^{1/6}$, but tapers off to zero as $x \to \infty$.

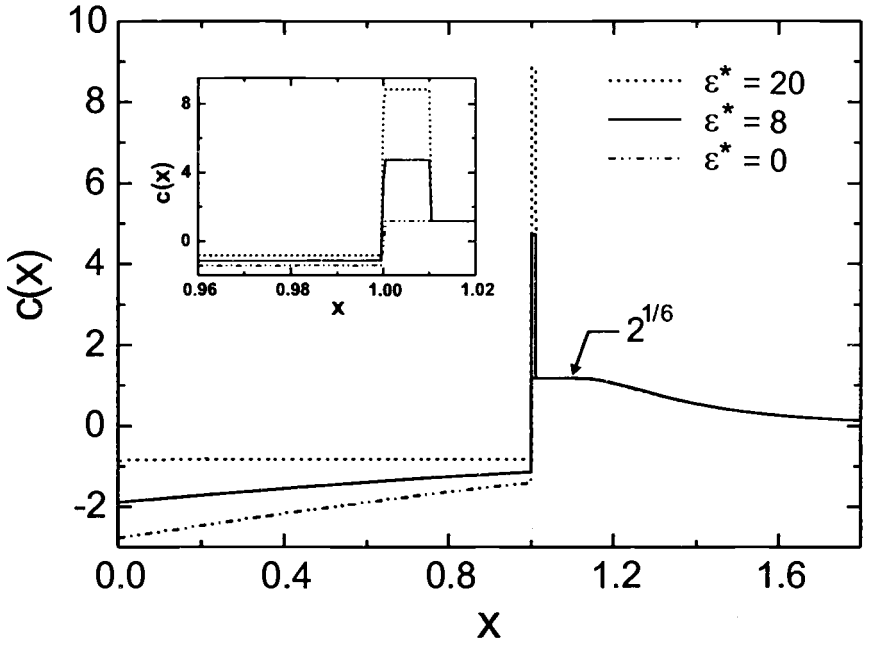

FIGURE 4.8. Variation of the direct correlation function $c(x)$ with association ε^*. All curves, $\varepsilon^* = 0$, 8, and 20, correspond to $T/T_c = 0.85$ and $\eta = \eta_c = 0.130444$. The inset graph amplifies the associative contribution at $x = 1$ with a width of $l^{dim} = 0.01R$ arising from $c^{11}(x)$. The MSA contribution $c^{dis}(x) > 0$ tapers off to zero for $x > 2^{1/6}$.

With these changes to $c(x)$ as ε^* increases, Eq. (4.35) on page 106 would seem to suggest that the characteristic length $m(T)$ will increase as well, but for fixed T/T_c the volume integral of $r^2c(r;\rho_c)$ in (4.35) actually *decreases* with increasing association strength. This decrease in $m(T)$ with ε^* can be seen in Fig. 4.9 and highlights a subtle point: the large shift in η_c tends to overwhelm the positive yet small increase in $c(r;\rho_c)$ as the reduced association strength ε^* increases, evident from Figs. 4.5 and 4.8. The quantities η_c, $(\eta_\ell - \eta_g)$, and $\frac{1}{2}(\eta_\ell + \eta_g)$ all depend non-monotonically upon ε^*, further complicating the behavior of ξ and γ. The effects of these nontrivial changes on the bulk correlation length ξ, Eq. (4.47), can be seen in Fig. 4.10 as R/ξ versus T/T_c. Interestingly, ξ initially *decreases* with association, reaching a minimum for $\varepsilon^* \approx 8$ to 10 (values around which the critical density peaks as well), and then *increases* until it nearly reaches its original value for a non-associating fluid at around $\varepsilon^* \approx 20$. At intermediate T/T_c values the

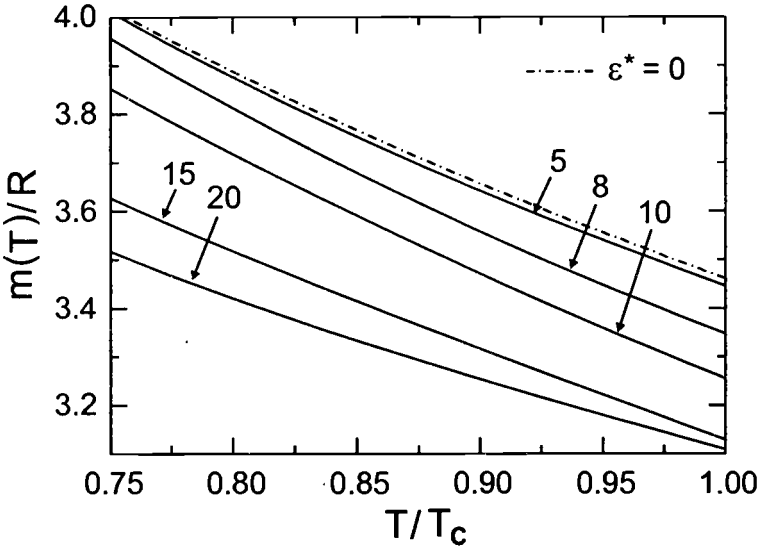

FIGURE 4.9. Variations in the characteristic length $m(T)$ with association. The zero-association reference values of $m(T)$ are displayed as the dashed curve, while the non-zero association curves, with strengths $\varepsilon^* = 5$, 8, 10, 15, and 20, are labeled with arrows.

---

approximate shift below the zero-association reference value is approximately 14%, tapering off slightly as $T/T_c \to 0.7$ but going to zero as $T/T_c \to 1$.

Association, as it introduces attractive forces, would seem to increase ξ, but here the non-monotonic factors in Eq. (4.47) become important. The density dependence of ω in Eq. (4.48), the third derivative of the pressure, has small contributions from association and no contribution from van der Waals attractions, and thus can be approximated by its hard body component. So while ω does display some non-monotonic behavior, its change with ε^* is relatively small: $\sim 5\%$. The density difference $\eta_\ell - \eta_g$, however, can shift with ε^* by as much as $\pm 15\%$ of its zero-association value, and is responsible for the divergence of ξ as $T \to T_c$ since $m(T)$ and ω are both finite and non-zero at the critical point. The small, non-monotonic behavior of ξ with association then is merely a reflection of the behavior of $\eta_\ell - \eta_g$.

A similar non-monotonic behavior is found for the surface tension, plotted in Fig. 4.11 in reduced form as $\beta R^2 \gamma$. According to Eq. (4.57), $\gamma \propto \xi^{-1} (\eta_\ell - \eta_g)^2$, so such behavior is expected with variation in association. For a given T/T_c, γ increases with association until $\varepsilon^* \simeq 8$, and then drops (unlike ξ) below its

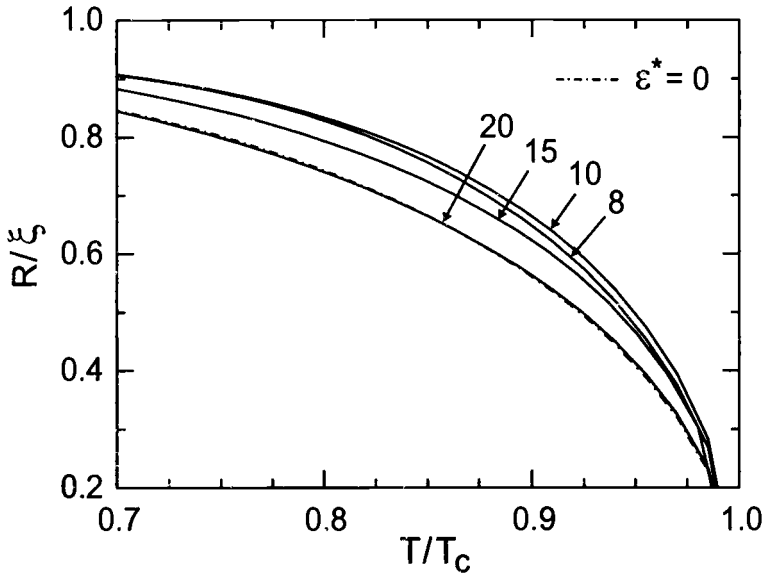

FIGURE 4.10. Variation of the inverse reduced correlation length R/ξ with T/T_c. Numbers with arrows corresponding to the association strengths ε^* label the curves, with the dashed curve (barely visible below the $\varepsilon^* = 20$ line) showing the zero-association reference value. Note the non-monotonic behavior. The apparent discontinuous behavior for $R/\xi \lesssim 0.25$ is an artifact of the inability of the Newton-Raphson iterative method to converge to two distinct coexistence densities as $T/T_c \to 1$.

---

non-associating value as ε^* increases further. As $T/T_c \to 0.7$ these changes in γ represent a 25%−40% shift in value.

To assess the accuracy of our interface predictions, we compare our results in the zero-association limit with the theoretical, simulation, and experimental results of others. Generally, our (non-associating) surface tension values agree to within 10% of the DFT results of Iatsevitch and Forstmann [155], the molecular dynamics (MD) of Mecke *et. al.* [167], and the mean-field theory of Lu *et. al.* [168]. Not surprisingly, our γ values underestimate those of Iatsevitch and Forstmann, who account for some of the interface inhomogeneity by approximating $c(\mathbf{1},\mathbf{2};[\rho])$ within the interfacial region using a *weighted density approximation* (WDA) method. Their better account of interface correlations leads to surface tension values which agree more closely with the MD results of Mecke *et. al.* Our 10–90 interfacial thickness t overestimates that of Iatsevitch and Forstmann by 20%−30%, in accord with our lower γ values. Alternately, our surface tension

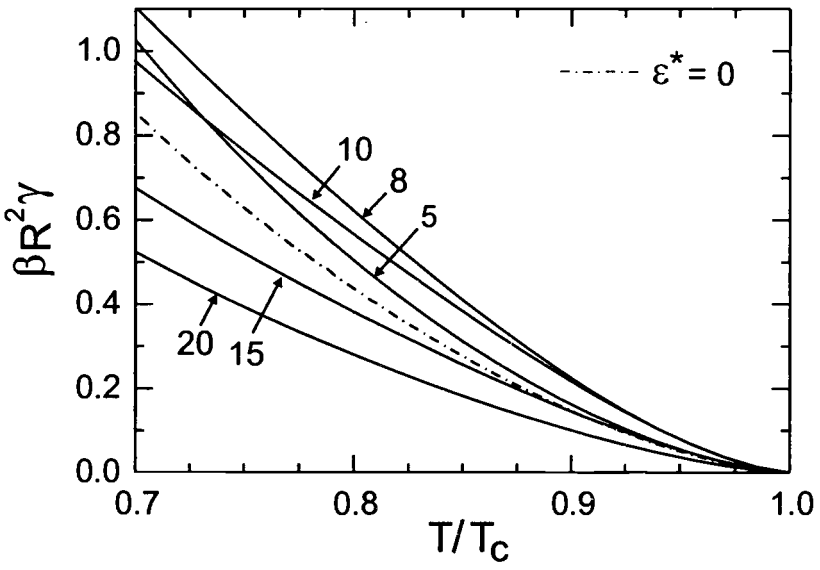

FIGURE 4.11. Temperature dependence of the reduced surface tension $\beta R^2\gamma$ for association strengths $\varepsilon^* = 0$, 5, 8, 10, 15, and 20 (labelled with arrows). The dashed curve represents the non-associating reference value. As with η_c and R/ξ there is significant non-monotonic behavior.

---

values slightly overestimate the mean-field results of Lu *et. al.*, with agreement improving to around 6% as $T/T_c \to 1$. Correspondingly, our 10–90 interfacial widths t are smaller than their values, with differences ranging from roughly 19% at $T/T_c = 0.9$ to approximately 4% at $T/T_c = 0.7$. Similar agreement is anticipated for fluids of associating monomers, although why agreement between γ values should improve as $T/T_c \to 1$ while that for t values as $T/T_c \to 0$ is unknown.

Accompanied by the non-monotonic behavior of ξ and γ is a relatively strong demixing of monomers and dimers for "intermediate" association strengths at temperatures well below T_c, evident by the monomer mole fraction $\eta_0(z)/\eta(z)$ across the interface plotted in Figs. 4.12(a) and (b) for $T/T_c = 0.7$ and $T/T_c = 0.925$ respectively. As expected at lower temperatures [Fig. 4.12(a)] association effects begin in the liquid phase first because of it's higher density; the fraction of free monomers η_o in the liquid is drastically reduced even for small ε^* values. Maximal demixing occurs when ε^* approaches 8 to 10, where the liquid η_o composition

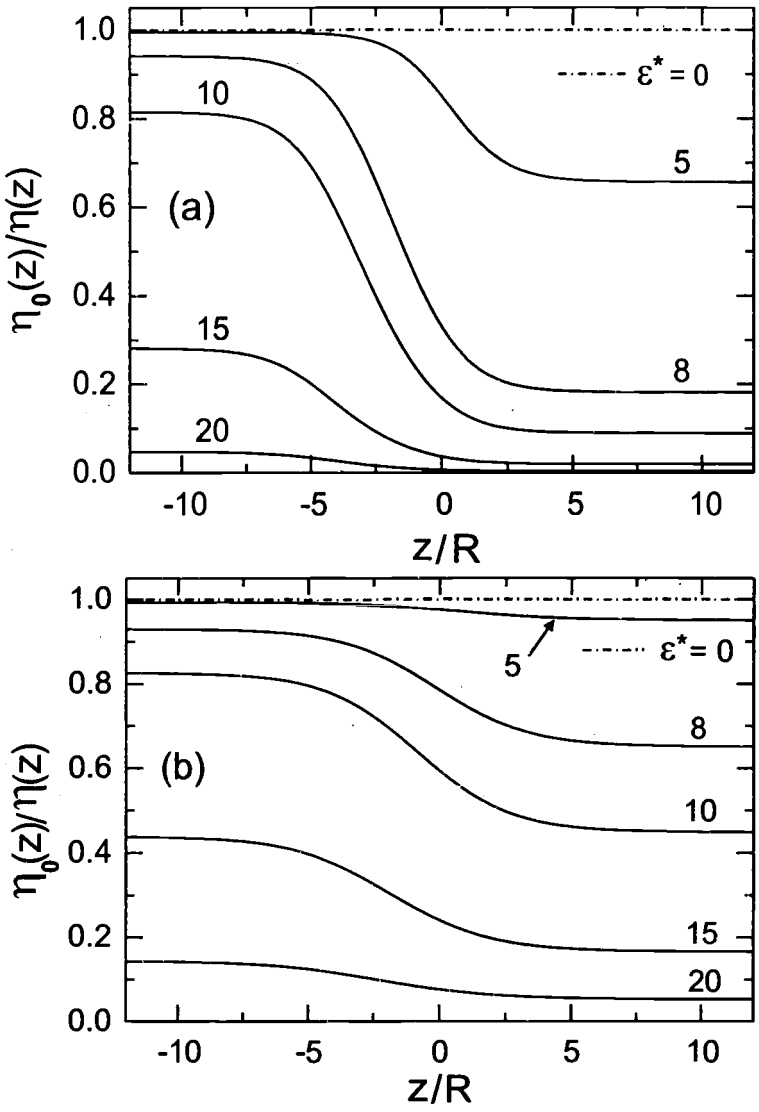

FIGURE 4.12. Variation of the monomer mole fraction profile $\eta_0(z)/\eta(z)$ with association strength for $T/T_c = 0.7$ and $T/T_c = 0.925$. Zero-association values are given by the dashed line, while all other association strengths ε^* are indicated just above their corresponding curve. Figure (a) gives the $T/T_c = 0.7$ results while (b) those for $T/T_c = 0.925$.

---

is only 9%–18% while that of the gas remains at $\sim 82\%-95\%$. The monomer mole fraction X is entrained by Eq. (4.66), and this preferential concentration of monomers in the gas phase is a consequence of LeChatelier's principle. When $\varepsilon^* \approx 20$, however, the attractive strength is large enough to overcome density effects and virtually all monomers in both phases become completely dimerized. At

higher temperatures [Fig. 4.12(b)] the overall extent of dimerization has obviously decreased. At $\varepsilon^* = 20$ and $T/T_c = 0.925$, for example, monomer concentrations in both phases are increased by roughly a factor of three as compared to the $T/T_c = 0.7$ values. The extent of demixing also decreases with temperature since the difference between equilibrium densities η_ℓ and η_g goes to zero as $T \to T_c$.

Given these significant yet subtle changes above, it is somewhat surprising that association produces only negligible effects in the total density profile $\eta(z)/\eta_\ell$. As indicated by Fig. 4.13(a), the liquid-gas interface at $T/T_c = 0.7$ sharpens slightly as ε^* passes through a value of ~ 8, but expands again nearly to its original position as dimerization continues. These shifts are very small indeed, probably lying outside experimental and simulation sensitivity. At $T/T_c = 0.925$ the intrinsic interface is much more flat, as shown in Fig. 4.13(b), but the non-monotonic behavior remains much the same, although the shift is slightly more pronounced than before because the gas density is $\sim 20\%$ that of the liquid at this temperature. It may be that highly anisotropic, short-ranged attraction has more of an effect upon the formation of the interface (*viz.* the liquid–gas transition itself) than on the overall density profile. Interestingly, a single-site, "sticky-spot" hard sphere model satisfying the SI-1 steric condition is not capable of inducing a liquid–gas phase transition, but a four-site model can —we will discuss such a model in Chapter 5. Moreover, recent work on dipolar hard spheres [135, 134] has opened questions about the possibility of chain formation preempting the liquid–gas transition, and further suggests the onset of fluid–fluid structural transitions. While, issues of structural transitions are limited for a single-site model, there are compositional changes related to association which occur in the interface region.

The total density profile $\eta(z)$ may remain relatively unchanged by association, but the monomer–dimer composition of the interface itself does not. This is perhaps the most interesting yet subtle effect in our simple system and is a function of both association strength and temperature. Recall that $z/R = 0$ marks the Gibbs equimolar surface. The partial demixing of monomers and dimers thus creates a "crossover point" in the interface where the fluid is equally composed of free monomers and dimers. This crossover point is ε^* and T dependent; Figure 4.14 plots several simultaneous compositional profiles, namely $\eta(z), \eta_0(z)$, and $\eta_{dim}(z)$, as association strength (left column) and temperature (right column) are increased, each calculated using $K_A = 2.969 \times 10^{-5}$ and normalized by η_ℓ. Specif-

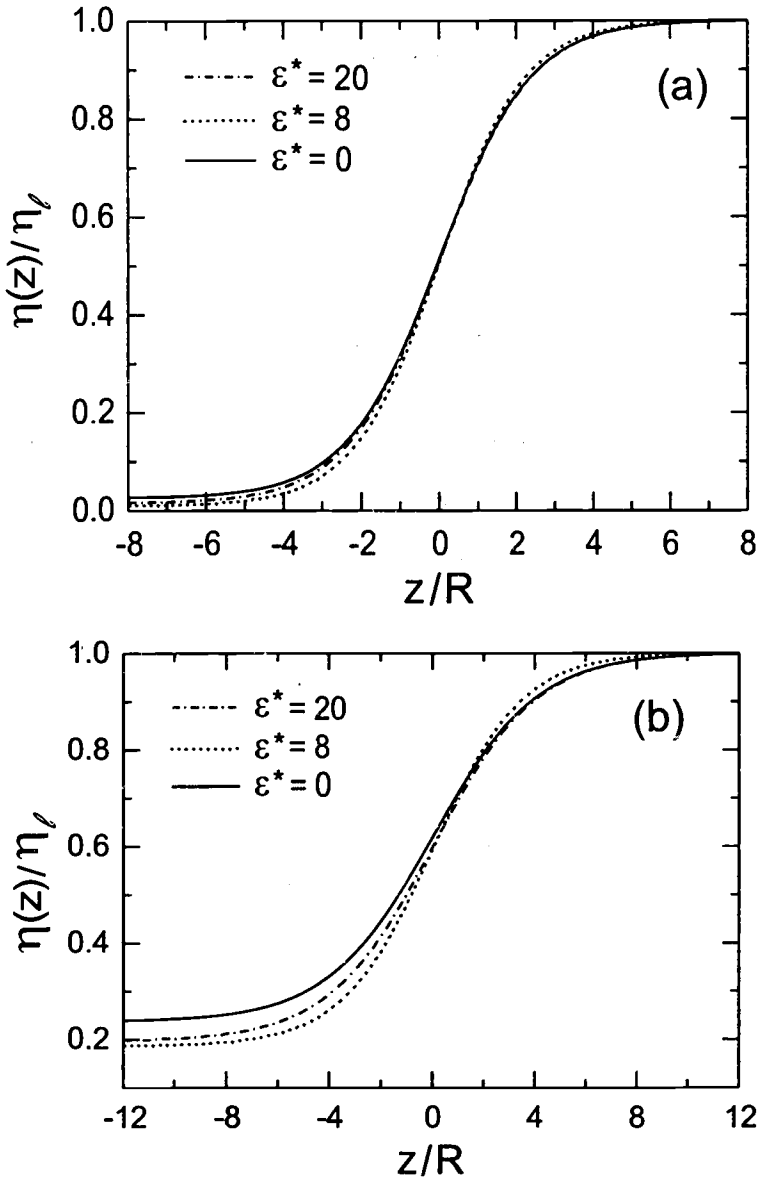

FIGURE 4.13. Variation of the normalized interface density profile $\eta(z)/\eta_\ell$ with association strength for $T/T_c = 0.7$ and $T/T_c = 0.925$. Figure (a) shows the variation at $T/T_c = 0.7$ as ε^* changes from 0, to 8, to 20; Figure (b) shows the same variation except at $T/T_c = 0.925$.

---

ically, Figs. 4.14(a)–(c) display the shift of the compositional crossover point for $T/T_c = 0.7$ as ε^* changes from 8, to 10, and finally to 20 respectively. For $\varepsilon^* = 8$ in (a), dimers persist just past the equimolar surface even at the low gas phase densities, with the crossover point located at $z/R \simeq -1.4$. As ε^* increases further,

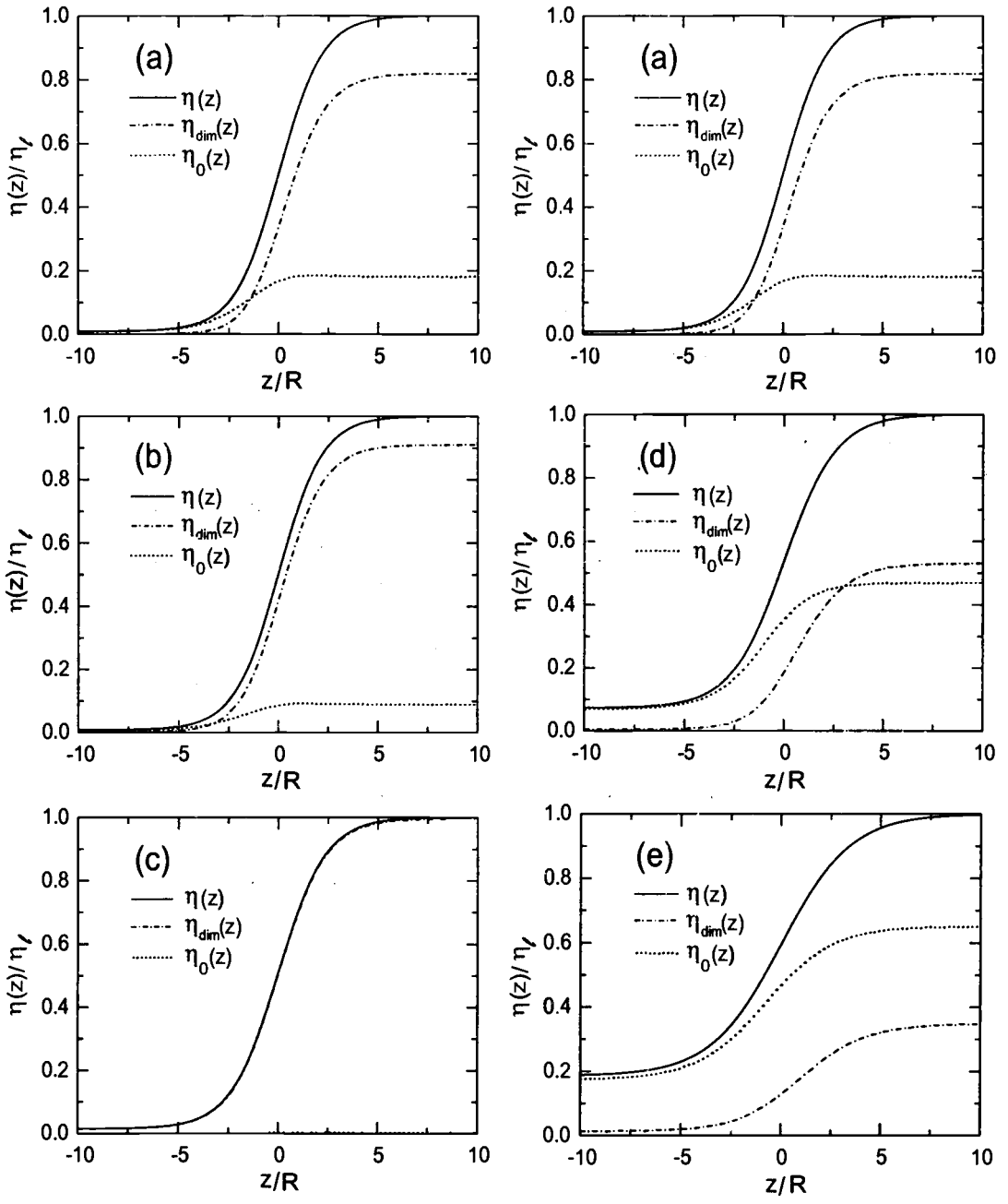

FIGURE 4.14. Variation of interface composition profiles $\eta(z)/\eta_\ell$, $\eta_{dim}(z)/\eta_\ell$, and $\eta_0(z)/\eta_\ell$ with association strength and temperature. Figures (a)–(c) in the left column display compositional changes for $T/T_c = 0.7$ as ε^* varies from 8, to 10, to 20 respectively. In the right column, Figs.(a), (d), and (e) show the compositional changes for $\varepsilon^* = 8$ as T/T_c shifts from 0.7, to 0.85, and to 0.925 respectively. $K_A = 2.969 \times 10^{-5}$ for all curves.

to 10 and 20, we see the crossover point shift well into the gas phase and finally disappear as the bulk gas becomes fully dimerized.

The opposite process occurs when the association strength is held fixed and the temperature is varied. For $\varepsilon^* = 8$, Figs. 4.14(a), (d), and (e) show the crossover point shift *into* the liquid as T/T_c progresses from 0.7, to 0.85, to 0.925 respectively. As before, the crossover point begins at approximately $z/R \simeq -1.4$, but as the temperature increases to $T/T_c = 0.85$, in (d), conditions favor free monomers and the bulk liquid begins to lose dimers; this shifts the crossover point well into the liquid phase at $z/R \simeq 3.2$. Here, not only is the interface largely composed of free monomers, but even the bulk liquid composition is split nearly 50/50 between monomers and dimers. Finally, in (e) at $T/T_c = 0.925$, the crossover point has vanished, leaving the interface and the system composed predominantly of free monomers. The small fraction of dimers still present in gas phase and interface, however, are enough to sharpen the interface width a small amount [see Fig. 4.13(b)].

4.4. DIMERIZATION CONCLUSIONS

Our primitive model of dimerization incorporated additive hard-sphere, van der Waals, and associative contributions to the Helmholtz energy, and in doing so, is reminiscent of many previous theories of associating fluid thermodynamics [137, 42] inspired by Wertheim. Because of our mean-field treatment of the dispersioin forces, there are errors of $\sim 20\%$ in the critical temperature and density predicted by our model fluid. Our cavalier assessment of the system critical point did not, however, detract from our focus on the effects of association anisotropy upon the liquid–vapor interface. Our theory of the interface was a simple extension of the well-documented square gradient, mean-field theory which ignores the complications of capillary waves and, to some extent, the true three-dimensional nature of the liquid–gas interface, including more realistic topologies. Yet, even within the square gradient theory, some approximation for the direct correlation function is required in order to predict the properties of the interface. The direct link between the partial densities and direct correlation function hierarchy within a Wertheim approach made it optimally suited to treat the separate contributions of short-ranged repulsion and attraction from those of longer-ranged dispersion inter-

actions in order to determine the structure and thermodynamics of our dimerizing model.

The effects of short-ranged, anisotropic association upon interfacial properties appear to be minor, but non-trivial nonetheless. Correlation lengths as well as surface tensions become non-monotonic functions of $\varepsilon^* = \varepsilon^{dim}/\varepsilon^{dis}$. As the strength of the intermolecular attractions increases, *a priori* one would expect that the surface tension would increase monotonically as well, but this turns out to be false. Initially, as association strength increases, so too does γ, but as dimerization becomes more prominent (at around $\varepsilon^* \sim 8$) the difference between the coexistence densities η_ℓ and η_g decreases and this leads to a *diminution* in the the surface tension at a fixed value of T/T_c. The interface profiles $\eta(z)$, when expressed as functions of T/T_c, appear nearly independent of the extent of association, and yet the monomer and dimer fractions are sensitive to the strength of the sticky-spot potential responsible for dimerization. Perhaps the most significant result of this work was that the thermodynamics (critical points, surface tension, *etc.*) were more sensitive measures of association than the density profile, at least for the simple case of a dimerizing system.

5. ASSOCIATION IN A FOUR–COORDINATED, WATER–LIKE FLUID

I'm having deja-vu and amnesia at the same time.
It's like I think I've forgotten this before.

—Unknown

5.1. INTRODUCTION

Of all known associating fluids, water is perhaps the most widely studied because of its importance in many areas of science, especially biology [2]. Despite that import, as well as its ubiquity and seemingly simple molecular structure, accurately predicting the unique thermodynamic and structural properties of water over a wide range of temperatures and densities remains a central challenge in liquid state theory. The physical and chemical properties of water, of course, are well known and documented [2–4], but analytical approaches are seriously limited by a lack of symmetry and the complexity of the interaction potentials involved in the dense liquid state. Nonetheless, water acts as an key paradigm for associating fluids because of its two special interactions: the hydrogen bond and the hydrophobic effect.

In contrast to the orientationally smooth attractive forces characteristic of simple fluids, associating fluids involve strongly orientation-dependent attractive forces. The hydrogen bond is the prototypical example of such a force, and the unique properties of water are certainly related to the highly directional nature of the bond. Both quantum and classical descriptions of the hydrogen bond exist [40], but the intrinsic nature of the bond itself is, as yet, only imperfectly understood. The water–water intermolecular potential cannot be measured directly in the liquid state, and although some components of the potential can be mapped or even tested via computer simulations, there is still large uncertainty in the definition of an effective potential. Furthermore, it is not clear whether an effective potential will be able to explain the unique properties of hydrogen bonded fluids like water. It is clear, however, that the highly anisotropic, short range character of the hydrogen bond promotes localized order and open structures in the liquid phase, and for water, with its peculiar ability to form four hydrogen bonds per

molecule, this translates into the formation of complex, tetrahedrally-coordinated network structures which greatly influence its bulk thermodynamic properties. [4]

5.1.1. Water Models

A large number of molecular models for water have been proposed in the literature, based upon empirical or quantum methods, varying from rigid to flexible models with or without polarization effects included [35, 65, 169, 170, 60, 171]. Jorgensen *et. al.* [169] provide a comparative review of pure water models. Although numerous models of hydrogen bonding fluids have been constructed, their focus is generally upon providing a detailed description of particular aspects of specific hydrogen-bonding fluids, often over limited temperature or density ranges. As a consequence such models tend to be rather complicated and difficult to interpret in any qualitative sense.

High level *ab initio* and semi-empirical quantum calculations [172–176] can determine interaction energies as well as equilibrium structures for small, isolated water clusters, but extending predictions into liquid densities is difficult at best. Effective potentials based upon the point charge model of Bjerrum [177] typically employ anywhere from three to seven point charges in rigid and flexible geometries, some including polarization and limited many-body effects. The most commonly used potentials, such as the SPC [178], SPC/E [179], ST2 [180], TIP3P, TIP4P [181], and MCY [174] reproduce many of the structural and thermodynamic properties of water under normal temperatures and pressures. These models are, not surprisingly, still far too complex for current statistical mechanical theories to treat analytically, and thus Monte Carlo (MC) or Molecular Dynamics (MD) computer simulations must be used to evaluate bulk properties. Integral equation theories, based upon interaction site models applicable to both rigid [76] and flexible [73] models also provide a useful approach to obtain atom-atom correlations for molecular fluids like water [182]. Although generally successful in predicting short range correlations in fluids, the RISM and RISM-like interaction site methods are also not readily adaptable to analytical calculations.

Unlike the case for simple fluids, as yet there are no simple models which simultaneously embody the intrinsic qualitative features of association and are amenable to analytical analysis. Any simple association model which can elucidate

the salient features of hydrogen-bonded fluids in the same fashion that the hard-sphere and nonspherical hard-body models have captured the essential features of many simple fluids would be invaluable in extending liquid state theory as well as in judiciously directing computer simulations of more complex systems, like associating mixtures. The hard-sphere model has, arguably, contributed more to the advancement of liquid state theory than any other model.

Based upon the successes and widespread use of the hard-sphere model, coupled with the relatively short-ranged attraction characteristic in hydrogen bonding, there is hope that a similarly simple, short-ranged interaction potential might represent some of water's salient features while allowing for an analytical description; such a model could provide a more qualitative assessment of the theory than usually possible. A hard-sphere potential with contact attraction, for example, might provide a reference system (*e.g.* in perturbative expansions) in much the same way as the hard sphere and Lennard Jones models have for simple liquids. Wertheim's multi-density theory of association [19–22] is one of the few approaches that elegantly incorporates such short-ranged, highly anisotropic forces within a rigorous, graph-based statistical mechanical formalism. Moreover, it can be systematically generalized to the standard methods applied to simple liquids, like perturbation and integral equation theories.

Wertheim's multi-density formalism has been widely studied for tangent [98, 128] as well as fused [102] dimerizing and polymerizing systems [103]. The theory has been extended to various mixtures of associating spherical, non-spherical molecules and chain molecules [183] [including *statistical associating fluid theory* (SAFT)], providing correlations in the thermodynamics of aromatics, esters, ketones, amines, and polymers [137, 122, 123]. While the predicted fluid structure and thermodynamics of Wertheim's theory compare well to simulation results for molecules with one or two interaction sites, the theory has not been fully tested for associating systems with more than two bonding sites per molecule, *i.e.* when branched chains or networks are allowed to form. This latter case is exactly that required to treat water.

There are numerous water-like simple models which combine a hard core with four, short-ranged attraction sites. In 1982 Bol [184] used Monte Carlo (MC) techniques to determine the free energy and equation of state for a system of hard spheres with tetrahedral adhesion interactions. A few years later Bratko *et. al.* [60]

and Cummings and Blum [50] compared MC simulations with integral equation theory methods on a system composed of hard sphere particles with a embedded dipole and an encircling tetrahedral square well. This class of models —involving tetrahedral surface adhesion in a molecular Ornstein-Zernike equation coupled with a mean spherical approximation (MSA) to treat the long-range multipolar energy contributions— has been found to provide an impressive rendering of the atom–atom pair correlation functions in water [185, 170]. In many regards, the Blum methods represent a more complicated approach than the methods of Wertheim to be addressed here.

5.1.2. Chapter 5 Focus

Wertheim's multi-density theory has, in fact, already been applied precisely to the four-site, sticky-spot model we consider in this work. Nezbeda *et. al.* [186–188] found that Wertheim's thermodynamic perturbation theory (TPT) accurately represented the MC simulation results for system internal energy and pressure. Ghonasgi and Chapman [47] modified that TPT work by adapting the reference fluid to include Lennard-Jones interactions and discovered that, yet again, the pressures, internal energies, and average number of hydrogen bonds per particle were treated accurately. Structural properties such as the pair correlation function $g(r)$ and structure factors $S(k)$ were considered by Vakarin, Duda, and Holovko [105, 189, 190, 121], who solved the *associated* Ornstein-Zernike integral equations using a Percus-Yevick-like closure condition and calculated liquid-vapor coexistence and critical behavior from $S(k)$.

The purpose of this work is two-fold: (i) to derive all possible thermodynamic and structural properties of the four-site, sticky-spot model using Wertheim theory, and (ii) to judge the successes and failures of the theory in its description of water-like properties, especially concerning the role or influence of four-fold connectivity constraints —which the Wertheim formalism treats exactly. We follow Baxter in taking the sticky hard-sphere limit [163] of the four-site model, as did Kolafa [191] and Duda [121], but with a different and perhaps simpler analysis of the graphs. Our work reproduces the TPT results of Ghonasgi and Chapman and the integral equation methods of Duda. Yet we extend those previous works by calculating the direct correlation functions, a simplified form of the structure factor S(k), and we also test the applicability of this model as a template for

hydrogen-bonding fluids like water. Obviously, the omission of long range forces and permanent dipole moment, coupled with the inability of the theory to enforce any rigid tetrahedral coordination of attraction sites inhibits the model from quantitatively representing real water. The goal of such a primitive model, rather, is the economical reproduction of the qualitative, essential features of a hydrogen bonding system.

5.2. THEORY

In this section we derive numerous thermodynamic and structural results for a four-site, sticky-spot hard sphere model meant to mimic the properties of water using the Wertheim multi-density formalism. As such, water-like steric incompatibility (SI) effects are implemented within the theory, as is the *ideal network approximation* (INA) [47, 105, 121] in order to simplify not only the self-consistent solution of the *partial* densities, but also the system correlation functions. With the aid of the sticky-spot limit introduced introduced in Chapter 4, analytical results for the first-order thermodynamic perturbation theory (TPT) and *associated* Ornstein-Zernike (AOZ) equations is possible. Equal energetics in the model allows us to subsume the site-specific details of the theory into generic density and correlation functions, greatly reducing the dimensions of the TPT and AOZ equations. The economy of these generic quantities vastly simplifies the overall analysis.

5.2.1. The Four-Site Model

Our primitive, water-like model consists of hard core monomers of diameter R, each containing four interaction sites located incrementally exterior to the hard core surface. These association sites can be thought of in terms of the conical wells described in Chapter 4 (see Fig. 4.2 in Section 4.2.1.2). The four sites are nominally located in a tetrahedral fashion about the hard core, two representing the hydrogens, labeled H_a and H_b, and the other two the electron lone pairs, labelled L_a and L_b. A sketch of this model is shown in Fig. 5.1. Mimicking real water, our model exhibits site–site (hydrogen) bonding between H and L sites, but not between like sites, which do not interact. The intermolecular pair potential, as usual, is composed of isotropic hard-sphere repulsion $u^R(r)$ and a short-ranged, anisotropic attraction $u_{ij}^A(\mathbf{1},\mathbf{2})$ between unlike sites i and j on different monomers,

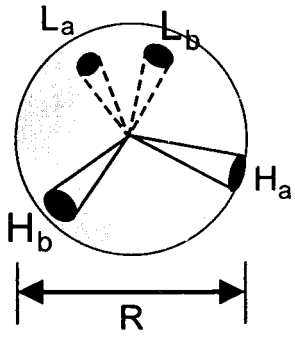

FIGURE 5.1. Sketch of the current primitive model of water with four attractive sites, H_a, H_b, L_a, and L_b, nominally oriented in a of diameter R. The hard core is represented by the gray sphere, with the four labeled attraction sites shown as black circles on the surface. In the sticky-spot limit these sites become infinitesimally-ranged sticky "spots" located randomly on the surface of the hard core.

$$u(\mathbf{1},\mathbf{2}) = u^R(r) + \sum_{i=H_a}^{H_b} \sum_{j=L_a}^{L_b} \left[u_{ij}^A(\mathbf{1},\mathbf{2}) + u_{ji}^A(\mathbf{1},\mathbf{2}) \right] . \tag{5.1}$$

The superscripts R and A indicate repulsive and attractive interactions respectively. The notation $\mathbf{1}$ represents both the center of mass position $\mathbf{r}_1$ and the orientation of the monomer located at space point 1 relative to the vector $\mathbf{r}$, where r is the center of mass separation $r \equiv |\mathbf{r}_2 - \mathbf{r}_1|$ between monomers 1 and 2.

The attractive forces responsible for association, *i.e.* hydrogen bonding, are short-ranged and highly anisotropic, leading to the steric incompatibility (SI) effects characteristic of associating fluids. Some of the SI effects are manifest by the bonding potentials $u_{ij}^A(\mathbf{1},\mathbf{2})$. Apropos of a water-like fluid, the *single bonding condition* (SBC), described in Section 3.4.1, is adopted such that once a hydrogen bond is formed, the participating sites become saturated or unavailable for further bonding. In terms of the conical well potential defined in Chapter 4, Eq. (4.5), this corresponds to imposing limitations between the maximum cone angle θ_c and range l^{dim} as before, but with multiple attraction sites these limits depend upon the bond angle φ as well (see Fig. 3.3). We further adopt the SI-2S condition because experimental and *ab initio* work [192, 193] suggests that such structures are energetically unstable.

While these SI conditions account for the particular attraction site anisotropy, they do not address the real tetrahedral orientation of the four at-

traction sites on the monomer. Enforcing fixed bond angles requires the incorporation of SI-3 effects, and for reasons discussed in Chapter 3, these effects are extremely difficult to deal with in a wholesale fashion, specifically when dealing with the topological reduction procedure. Sterically incompatible bond angles for a given monomer configuration must be treated on a rather individual basis, and this complicates the entire topological reduction process, *i.e.* the evaluation of the self-consistent density relations as well as the TPT and AOZ equations.

In order to obtain analytical results for our primitive model, we therefore relax the tetrahedral bond angle requirement and let the interaction sites move randomly over the hard sphere surface. The theory is thus one of fully flexible, branched chains or networks of freely jointed tangent hard spheres. This relaxation of tetrahedral orientation may appear to preempt all efforts to describe the water-like nature of our model, but this turns out not to be the case. The partial densities intrinsic to the theory, along with the SBC and SI-2S conditions, are able to account for many of the important steric features inherent in water, *e.g.* the four-fold connectivity constraints of each water molecule.

On the basis of the steric considerations above, as well as the additivity of the interaction potential, the Mayer f-bond

$$f(\mathbf{1},\mathbf{2}) \;=\; \exp\left[-\beta u(\mathbf{1},\mathbf{2})\right] - 1 \;\equiv\; e(\mathbf{1},\mathbf{2}) - 1$$

separates rigorously according to Lockett's [24] scheme, into a purely repulsive f^R-bond and an "attractive" F-bond

$$f(\mathbf{1},\mathbf{2}) \;=\; f^R(r) + e^R(r) f^A(\mathbf{1},\mathbf{2}) \;\equiv\; f^R(r) + F(\mathbf{1},\mathbf{2})\,, \tag{5.2}$$

which is a sum of purely attractive $f_{ij}^A(\mathbf{1},\mathbf{2})$ hydrogen bonds,

$$F(\mathbf{1},\mathbf{2}) \;\equiv\; e^R(r) \sum_{i=H_a}^{H_b} \sum_{i=L_a}^{L_b} \Big[f_{ij}(\mathbf{1},\mathbf{2}) + f_{ji}(\mathbf{1},\mathbf{2}) \Big]\,. \tag{5.3}$$

As usual, $\beta = (k_B T)^{-1}$ and k_B is Boltzmann's constant. The $F(\mathbf{1},\mathbf{2})$ bond, which becomes a site-projection operator, contains eight equal site-site terms reflecting the proper connectivity constraints on the individual $f_{ij}^A(\mathbf{1},\mathbf{2})$ bonds between site i on monomer 1 and site j on monomer 2. For convenience the $e^R(r)$ bond between hyperpoints will be subsumed into the $f_{ij}^A(\mathbf{1},\mathbf{2})$ bonds hereafter as well.

Since all attraction sites on a monomer act independently, we spherically average the $f_{ij}(\mathbf{1},\mathbf{2})$ bonds as was done in Chapter 4,

$$f_{ij}(r) \;=\; \Omega^{-2}\int d\hat{e}_{1i}\, d\hat{e}_{2j}\; f_{ij}(\mathbf{1},\mathbf{2})\,,$$

where $\hat{e}_{1i}$ and $\hat{e}_{2j}$ denote respectively the orientation of sites i and j on monomers 1 and 2, and Ω is the normalization constant.[1] While this orientation averaging eliminates the angular dependence of the pairwise f_{ij}^{A} bonds, the steric incompatibility and partial densities still reflect the highly anisotropic nature of the attractive interactions.

An analytical evaluation of $f_{ij}^{A}(r)$ still requires taking the sticky limit of the interaction potential $u_{ij}^{A}(\mathbf{1},\mathbf{2})$, where we once again follow Baxter [163]. The attraction sites become sticky spots located infinitesimally outside the hard core at R^{+} and the orientation-averaged $f_{ij}^{A}(r)$ bonds are replaced by the pseudopotentials,

$$f_{ij}^{A}(r) \;\longrightarrow\; \frac{\delta(r-R^{+})}{4\pi R^{2}}\,\bar{f}\,, \tag{5.4}$$

where $\bar{f}$ is a measure of the association strength, *vide infra*.

5.2.2. Wertheim Partial Densities

The Wertheim multi-density formalism permits the explicit elimination of all s-mer graphs from βPV that are inconsistent with water-like connectivity constraints. The connectivity constraints contained in the model determine the graph types which contribute to βPV, and, via functional derivatives, to $\rho(\mathbf{1})$. For the four-site model under the SBC and SI-2S conditions, all s-mer subgraphs are limited to dimers, and βPV consists of all combinations of chains, branched chains, and rings such that no vertex can have more than four incident F-bonds. As usual, all the graphs in $\rho(\mathbf{1})$ are categorized by the number of incident F-bonds at each labelled vertex, so we can immediately express $\rho(\mathbf{1})$ in terms of the *partial* densities $\rho^{(m)}(\mathbf{1})$ contributing to to the sum,

$$\rho(\mathbf{1}) \;=\; \rho^{(0)}(\mathbf{1}) + \rho^{(1)}(\mathbf{1}) + \rho^{(2)}(\mathbf{1}) + \rho^{(3)}(\mathbf{1}) + \rho^{(4)}(\mathbf{1})\,, \tag{5.5}$$

---

[1] Integration over the orientations of the two monomers is equivalent to the integration over the orientations of the sites themselves since they are independent of each other.

where each $\rho^{(m)}(\mathbf{1})$ represents all labeled vertices with m incident F-bonds. These partial densities are *not* free parameters, but are instead determined self-consistently once $\rho(\mathbf{1})$ and β are given. Since we know what s-mer graph types are consistent with the connectivity constraints of the model, we know what graph types are allowed in the generating functional $c^{(0)}$, and through functional derivatives, those in $c^{1}(\mathbf{1})$. Now, using the defining relation for $c^{1}(\mathbf{1})$, Eq. (3.41), we can directly enumerate and self-consistently solve the partial densities through the recursive set of nonlinear equations

$$\rho^{(1)}(\mathbf{1}) = \rho^{(0)}(\mathbf{1})\, c^{1}(\mathbf{1}), \tag{5.6a}$$

$$\rho^{(2)}(\mathbf{1}) = \rho^{(0)}(\mathbf{1})\frac{1}{2!}\left[c^{1}(\mathbf{1})\right]^{2}, \tag{5.6b}$$

$$\rho^{(3)}(\mathbf{1}) = \rho^{(0)}(\mathbf{1})\frac{1}{3!}\left[c^{1}(\mathbf{1})\right]^{3}, \tag{5.6c}$$

$$\rho^{(4)}(\mathbf{1}) = \rho^{(0)}(\mathbf{1})\frac{1}{4!}\left[c^{1}(\mathbf{1})\right]^{4}. \tag{5.6d}$$

Again, since all site–site interactions involve equal energetics, we need not label individual attraction sites in the graph sums $c^{1}(\mathbf{1})$, which affords the great economy of manipulating *unlabelled* diagrams[2] in the ensuing graphical analysis: appropriate multiplicity factors can be subsumed into generic quantities that reflect only the complete state of bonding at the given vertex. A careful, systematic approach leads to a particularly concise mathematical listing of all the generic, irreducible

---

[2]See Appendix B for information concerning graph labels.

graphs contributing to each $\rho^{(m)}(\mathbf{1})$, namely

$$\rho^{(1)}(\mathbf{1}) = \sum_{n=0}^{3} \int d2\, F(\mathbf{1},2)\rho^{(0)}(\mathbf{1})y^{0n}(\mathbf{1},2)\sigma^{(n+1)}(2)\,, \tag{5.7a}$$

$$\rho^{(2)}(\mathbf{1}) = \sum_{n=0}^{3} \int d2\, F(\mathbf{1},2)\left[\rho^{(0)}(\mathbf{1})y^{1n}(\mathbf{1},2) + \rho^{(1)}(\mathbf{1})y^{0n}(\mathbf{1},2)\right]\sigma^{(n+1)}(2)\,, \tag{5.7b}$$

$$\rho^{(3)}(\mathbf{1}) = \sum_{n=0}^{3} \int d2\, F(\mathbf{1},2)\left[\rho^{(0)}(\mathbf{1})y^{2n}(\mathbf{1},2) + \rho^{(1)}(\mathbf{1})y^{1n}(\mathbf{1},2) + \rho^{(2)}(2)y^{0n}(\mathbf{1},2)\right]\sigma^{(n+1)}(2)\,, \tag{5.7c}$$

$$\rho^{(4)}(\mathbf{1}) = \sum_{n=0}^{3} \int d2\, F(\mathbf{1},2)\left[\rho^{(0)}(\mathbf{1})y^{3n}(\mathbf{1},2) + \rho^{(1)}(\mathbf{1})y^{2n}(\mathbf{1},2) + \rho^{(2)}(\mathbf{1})y^{1n}(\mathbf{1},2) + \rho^{(3)}(\mathbf{1})y^{0n}(\mathbf{1},2)\right]\sigma^{(n+1)}(2)\,. \tag{5.7d}$$

Note that the direct F-bond between hyperpoints 1 and 2 in each dimer subgraph is enumerated explicitly, while all other incident F-bonds, up to a maximum of four, are accounted for by "appending" $\rho^{(m)}(\mathbf{1})$, $\sigma^{(n)}(\mathbf{1})$, or $y^{mn}(\mathbf{1},2)$ functions at the hyperpoints 1 and 2. Recall the defining relations for the set of generic, *complementary* density parameters $\sigma^{(n)}(\mathbf{1})$, each representing a sum of $\rho^{(m)}(\mathbf{1})$ graphs with at least m *available* bonding sites:

$$\sigma^{(0)}(\mathbf{1}) = \rho(\mathbf{1})\,, \tag{5.8a}$$

$$\sigma^{(1)}(\mathbf{1}) = \rho^{(0)}(\mathbf{1}) + \rho^{(1)}(\mathbf{1}) + \rho^{(2)}(\mathbf{1}) + \rho^{(3)}(\mathbf{1})\,, \tag{5.8b}$$

$$\sigma^{(2)}(\mathbf{1}) = \rho^{(0)}(\mathbf{1}) + \rho^{(1)}(\mathbf{1}) + \rho^{(2)}(\mathbf{1})\,, \tag{5.8c}$$

$$\sigma^{(3)}(\mathbf{1}) = \rho^{(0)}(\mathbf{1}) + \rho^{(1)}(\mathbf{1})\,, \tag{5.8d}$$

$$\sigma^{(4)}(\mathbf{1}) = \rho^{(0)}(\mathbf{1})\,. \tag{5.8e}$$

The partial density relations (5.7a)–(5.7d) are exact within the limits of the model, although graph symmetry numbers in have been omitted for convenience; they will be systematically included later when needed.

5.2.3. Ideal Network Approximation

Solution of Eqs. (5.7a)–(5.7d), of course, requires some approximations. Typically, the approximations made involve the neglect of higher-order $y^{mn}(\mathbf{1},2)$

correlations. The simplest such approximation is to ignore all $y^{mn}(\mathbf{1},\mathbf{2})$ graphs with F-bonds incident at the labelled points 1 and 2,

$$y^{mn}(\mathbf{1},\mathbf{2}) \longrightarrow y^{00}(\mathbf{1},\mathbf{2})\,\delta_{m,0}\,\delta_{n,0}\,, \qquad \forall\, n,m\,, \tag{5.9}$$

where $\delta_{n,0}$, $\delta_{m,0}$ are Kronecker delta functions. The replacement (5.9) is the *ideal network approximation* (INA), whose simplifications we adopt early in our analysis. Physically, Eq. (5.9) means that (i) all F-bonded ring structures are eliminated, and (ii) all interactions between non-bonded segments or branches in a given aggregate are ideal: no repulsive f^R bonds between non-adjacent (intramolecular) vertices are included. Hard core overlap of *adjacent*, F-bonded vertices, however, is prohibited by the presence of the e^R factors in the F-bonds [see Eq. (5.3)]. The use of Eq. (5.9) then limits the sums in (5.7a)–(5.7d) such that only two density parameters remain in the theory: $\sigma^{(0)}(\mathbf{2})$ and $\sigma^{(1)}(\mathbf{2})$.

Effectively, all chains and branched chains are then generated by the mass action law, wherein the density parameters $\sigma^{(0)}(\mathbf{2})$ and $\sigma^{(1)}(\mathbf{2})$ are appended to graph vertices according to the proper connectivity constraints of the model. Attaching density graphs (through topological reduction), however, can never close loops between labeled points, as they represent chain graphs. This can be seen by expanding a representative graph in the $\rho^{(1)}(\mathbf{1})$ sum, Eq. (5.7a), in terms of fugacity vertices. If we ignore, for the moment, the *intermolecular* graph components associated with $y^{00}(\mathbf{1},\mathbf{2})$ and focus instead upon the *intramolecular* interactions associated with the densities, we see that

$$\rho^{(0)}(\mathbf{1})F(\mathbf{1},\mathbf{2})\rho^{(1)}(\mathbf{2}) \;\propto\; \overset{\rho^{(0)}\ \rho^{(1)}}{\underset{1\quad 2}{\circ\!\!=\!\!\bullet}} \;\propto\; \underset{1\quad 2}{\bullet\!\!=\!\!\bullet\atop \circ\!\!=\!\!\bullet}\,,$$

where the field points $\bullet$ in last graph carry fugacity functions $z(i)$. Contrast this with an equivalent description of the underlying graph when *intramolecular* F-bonds are included through the $y^{mn}(\mathbf{1},\mathbf{2})$ functions:

$$y^{01}(\mathbf{1},\mathbf{2}) \;\propto\; \underset{1\quad 2}{\bullet\!\!=\!\!\bullet\atop \circ\quad\ \ \circ} \;\Longrightarrow\; \rho^{(0)}(\mathbf{1})F(\mathbf{1},\mathbf{2})y^{01}(\mathbf{1},\mathbf{2})\rho^{(0)}(\mathbf{2}) \;\propto\; \underset{1\quad 2}{\bullet\!\!=\!\!\bullet\atop \circ\!\!=\!\!\bullet}\,,$$

where, again, the last graph carries $z(i)$ vertices. It is apparent that the INA also corresponds to ignoring *intramolecular* f^R interactions between chain branches, the so called Cayley Tree approximation. It is important to note that hard core or f^R interactions between adjacent monomers in a given aggregate are not ignored

because of the repulsive contribution e^R contained in the F-bond. Moreover, unlike the hard sphere approximation $y_{hs}(\mathbf{1},\mathbf{2})$, the remaining correlation function $y^{00}(\mathbf{1},\mathbf{2})$ includes graphs with any number of F-bonds,

$$y^{00}(\mathbf{1},\mathbf{2}) \propto$$ 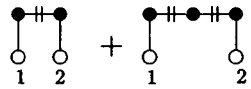 $$+ \cdots$$

just not F-bonds incident upon points 1 or 2. Hence *intermolecular* repulsive interactions between aggregates are still accounted for.

The importance of ring structures for a two-site model as well as a two-site chain (polymer) model[3] has been addressed by Sear and Jackson [125]. They made approximations for pertinent ring graphs in order to obtain an analytical free energy within the Wertheim formalism, and found that rings had a large effect on phase behavior far from the critical point, especially in the vapor phase. The vapor phase was predicted to contain a high proportion of ring structures, whose omission leads to an underestimation of the gas pressure, whereas the liquid was dominated by chains structures. Evans and Vaida [194] have also investigated ring structures within the boundaries of Wertheim theory, specifically concerning water vapor in the atmosphere. In such a low density environment, the direct enumeration of the relatively small, pertinent ring structures and their subsequent evaluation is much more feasible than at liquid densities.

The INA, Eq. (5.9), allows us to iteratively solve Eqs. (5.7a)–(5.7d) for the partial densities $\rho^{(m)}(\mathbf{1})$, which is carried out in Section 5.2. However, in terms of the simplifications that will arise in the TPT and AOZ solutions, the INA is better

---

[3]Such models are useful in the description of, for example, fluids of HF and Sulfur, along with organic compounds which exhibit intramolecular bonding.

expressed in terms of the generating functional $c^{(0)}$, defined as [21]

$$c^{(0)} = \left\{ \begin{array}{l} \text{all irreducible s-mer graphs (including monomer points) and} \\ f^R \text{ bonds; all vertices are field points and carry } \sigma\text{-factors} \\ \text{according to the SI connectivity rules.} \end{array} \right\} \tag{5.10}$$

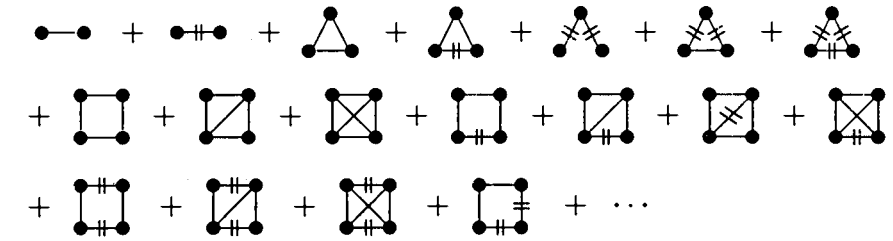

The one- and two-body correlations follow from the fundamental graph sum (5.10) through functional differentiation according to the direct correlation function hierarchy, namely

$$c^m(\mathbf{1}) = \frac{\delta c^{(0)}}{\delta \sigma^{(m)}(\mathbf{1})}, \tag{5.11a}$$

$$c^{mn}(\mathbf{1},\mathbf{2}) = \frac{\delta c^m(\mathbf{1})}{\delta \sigma^{(n)}(\mathbf{2})}. \tag{5.11b}$$

The correlation $c^m(\mathbf{1})$, for example, is generated from $c^{(0)}$ by enumerating all possible ways of turning a field point $\bullet$ carrying a factor of $\sigma^{(m)}$ into a 1-circle $\circ$, thereby eliminating integration over that coordinate.

In these terms the INA corresponds to ignoring all graphs in $c^{(0)}$ which contain *intramolecular* subgraphs corresponding to $s \geq 3$; the last graph in (5.10), for example, contains an $s = 3$ subgraph and so is excluded by the INA. All monomer field points of the remaining graphs in $c^{(0)}$ then carry a factor of $\sigma^{(0)}$, whereas all field points with one incident F-bond carry a factor of $\sigma^{(1)}$; all other field points vanish:

$$\text{INA} \Longrightarrow \left\{ \begin{array}{rll} c^n(\mathbf{1}) &= 0 & \forall\ n \geq 2\,, \\ c^{0n}(\mathbf{1},\mathbf{2}) &= c^{m0}(\mathbf{1},\mathbf{2}) = 0 & \forall\ m \geq 2\,. \\ c^{mn}(\mathbf{1},\mathbf{2}) &= h^{mn}(\mathbf{1},\mathbf{2}) = 0 & \end{array} \right. \tag{5.12}$$

The restrictions (5.12) are generally referred to as the "single bonding condition" in the literature [139], but should not be confused with the SI single bonding approximation described in Section 3.4.1.

5.2.4. Density Solutions

Under the *ideal network approximation* [139] the partial density relations Eqs. (5.7a)–(5.7d) reduce to

$$\rho^{(n)}(\mathbf{1}) = \frac{1}{n}\int d\mathbf{2}\, \rho^{(n-1)}(\mathbf{1})F(\mathbf{1},\mathbf{2})\sigma^{(1)}(\mathbf{2})y^{00}(\mathbf{1},\mathbf{2}), \quad n \in \{1,2,3,4\}, \tag{5.13}$$

where the factor n^{-1} accounts for the particular graph symmetry numbers. Because all four attraction sites act independently and have equal bond energies, Eq. (5.13) can be successively solved for each partial density.

Evaluation of the integrals in (5.13) means specifying the site details. Each generic partial density $\rho^{(n)}(\mathbf{1})$ represents a sum over specific attraction sites, subject to the proper connectivity constraints. The site-specific densities are denoted by subscripts listing the particular bonded sites:

$$\begin{aligned}
\rho^{(1)}(\mathbf{1}) &= \rho^{(1)}_{H_a}(\mathbf{1}) + \rho^{(1)}_{H_b}(\mathbf{1}) + \rho^{(1)}_{L_a}(\mathbf{1}) + \rho^{(1)}_{L_b}(\mathbf{1}), \\
&= 4\rho^{(1)}_{H_a}(\mathbf{1}), && (5.14a)\\
\rho^{(2)}(\mathbf{1}) &= \rho^{(2)}_{H_aH_b}(\mathbf{1}) + \rho^{(2)}_{H_aL_a}(\mathbf{1}) + \rho^{(2)}_{H_bL_a}(\mathbf{1}) + \rho^{(2)}_{H_bL_b}(\mathbf{1}) + \rho^{(2)}_{L_aL_b}(\mathbf{1}), \\
&= 6\rho^{(2)}_{H_aH_b}(\mathbf{1}), && (5.14b)\\
\rho^{(3)}(\mathbf{1}) &= \rho^{(3)}_{H_aH_bL_a}(\mathbf{1}) + \rho^{(3)}_{H_aH_bL_b}(\mathbf{1}) + \rho^{(3)}_{H_aL_aL_b}(\mathbf{1}) + \rho^{(3)}_{H_bL_aL_b}(\mathbf{1}), \\
&= 4\rho^{(3)}_{H_aH_bL_a}(\mathbf{1}), && (5.14c)\\
\rho^{(4)}(\mathbf{1}) &= \rho^{(4)}_{H_aH_bL_aL_b}(\mathbf{1}). && (5.14d)
\end{aligned}$$

By treating the $F(\mathbf{1},\mathbf{2})$ bond in Eq. (5.13) as a site projection operator which eliminates specified attraction sites from the density parameters $\sigma^{(1)}(\mathbf{2})$, we can determine all the site-specific densities using Eqs. (5.13) and (5.14a)-(5.14d).

For the density of molecules with one incident hydrogen bond, site H_a say, we obtain by application of the site projector $F(\mathbf{1},\mathbf{2})$ operator

$$\rho^{(1)}_{H_a}(\mathbf{1}) = \int d\mathbf{2}\, \rho^{(0)}(\mathbf{1})\left[f_{H_aL_a}(\mathbf{1},\mathbf{2})\sigma^{(1)}_{L_a}(\mathbf{2}) + f_{H_aL_b}(\mathbf{1},\mathbf{2})\sigma^{(1)}_{L_b}(\mathbf{2})\right] y^{00}(\mathbf{1},\mathbf{2}), \tag{5.15a}$$

$$= 2\,\rho^{(0)}(\mathbf{1})\,\sigma^{(1)}_{L_a}\bar{f}, \tag{5.15b}$$

where, for example, $\sigma^{(1)}_{L_a}(\mathbf{2})$ is defined as the sum of all densities at space point 2 with *no* F-bond incident at the L_a site. Both terms in Eq. (5.15a) are equal, and the integral is evaluated using Eq. (5.4) for $f_{H_aL_a}(\mathbf{1},\mathbf{2})$.

For the density of molecules with two incident hydrogen bonds, sites H_a and H_b for example, application of $F(\mathbf{1},\mathbf{2})$ gives

$$\begin{aligned} 2\,\rho^{(2)}_{H_aH_b}(\mathbf{1}) &= \rho^{(1)}_{H_a}(\mathbf{1}) \int d\mathbf{2} \left[f_{H_bL_a}(\mathbf{1},\mathbf{2})\sigma^{(1)}_{L_a}(\mathbf{2}) + f_{H_bL_b}(\mathbf{1},\mathbf{2})\sigma^{(1)}_{L_b}(\mathbf{2}) \right] y^{00}(\mathbf{1},\mathbf{2}) \\ &\quad + \rho^{(1)}_{H_b}(\mathbf{1}) \int d\mathbf{2} \left[f_{H_a,L_a}(\mathbf{1},\mathbf{2})\sigma^{(1)}_{L_a}(\mathbf{2}) + f_{H_aL_b}(\mathbf{1},\mathbf{2})\sigma^{(1)}_{L_b}(\mathbf{2}) \right] y^{00}(\mathbf{1},\mathbf{2}), \\ &= 4\rho^{(1)}_{H_a}(\mathbf{1})\,\sigma^{(1)}_{L_a}\bar{f}, \end{aligned} \tag{5.16}$$

where the last line follows from the same arguments as those used for $\rho^{(1)}_{H_a}(\mathbf{1})$. Subsequent calculations for $\rho^{(3)}_{H_aH_bL_a}$ and $\rho^{(4)}_{H_aH_bL_aL_b}$ show that a general recursive relation exists,

$$\rho^{(n)}_{ij\ldots}(\mathbf{1})/\rho^{(n-1)}_{ij\ldots}(\mathbf{1}) = 2\sigma^{(1)}_{La}\bar{f}, \quad n \in \{1,2,3,4\} \tag{5.17}$$

where the subscript $ij\ldots$ represents the list of n or $n-1$ specific bonded sites. These equations imply that

$$\begin{aligned} \sigma^{(1)}_{L_a}(\mathbf{1}) &= \rho^{(0)}(\mathbf{1}) + 3\rho^{(1)}_{H_a}(\mathbf{1}) + 3\rho^{(2)}_{H_aH_b}(\mathbf{1}) + \rho^{(3)}_{H_aH_bL_b}(\mathbf{1}), \\ &= \rho^{(0)}(\mathbf{1}) \left(1 + 2\bar{f}\sigma^{(1)}_{L_a}\right)^3, \end{aligned} \tag{5.18}$$

and

$$\begin{aligned} \rho(1) &= \rho^{(0)}(\mathbf{1}) + 4\rho^{(1)}_{H_a}(\mathbf{1}) + 6\rho^{(2)}_{H_aH_b}(\mathbf{1}) + 4\rho^{(3)}_{H_aH_bL_a}(\mathbf{1}) + \rho^{(4)}_{H_aH_bL_aL_b}(\mathbf{1}), \\ &= \rho^{(0)}(\mathbf{1}) \left(1 + 2\bar{f}\sigma^{(1)}_{L_a}\right)^4. \end{aligned} \tag{5.19}$$

Equations (5.18) and (5.19) are precisely the density relations found in the standard Wertheim TPT approach, and upon combining them we obtain

$$\rho = \left(1 + 2\bar{f}\sigma^{(1)}_{L_a}\right)\sigma^{(1)}_{L_a} \tag{5.20}$$

or

$$\sigma^{(1)}_{L_a} = \frac{2\rho}{1 + \sqrt{1 + 8\bar{f}\rho}}. \tag{5.21}$$

The monomer density follows from Eqs. (5.19) and (5.20) as

$$\rho^{(0)}(1) = \left[\sigma^{(1)}_{L_a}/\rho\right]^4 \rho \equiv (X_{L_a})^4 \rho, \tag{5.22}$$

where X_{L_a}, for example, is the fraction of molecules that are *not* bonded at site L_a. Clearly, once ρ and $\bar{f}$ are given, Eq. (5.21) subsequently determines all partial

densities $\rho^{(n)}(1)$ through Eqs. (5.22) and (5.17). These relations for the partial densities are equivalent to Eqs. (32)–(36) of Ghonasgi and Chapman once the purely notational replacement $X_{L_a} \rightarrow X_A$ is made.

All higher order density parameters $\sigma^{(n)}$ can be written in terms of $\sigma^{(1)}_{L_a}$, although under the INA only $\sigma^{(1)}(\mathbf{1})$ and $\sigma^{(2)}(\mathbf{1})$ are required in order to determine all thermodynamic and structural properties of the model. Recall that $\sigma^{(2)}(\mathbf{1})$ represents all combinations of densities with two sites that are *unavailable* for bonding,

$$\sigma^{(2)}(\mathbf{1}) = \sigma^{(2)}_{H_aH_b}(\mathbf{1}) + \sigma^{(2)}_{H_aL_a}(\mathbf{1}) + \sigma^{(2)}_{H_aL_b}(\mathbf{1}) + \sigma^{(2)}_{H_bL_a}(\mathbf{1}) + \sigma^{(2)}_{H_bL_b}(\mathbf{1}) + \sigma^{(2)}_{L_aL_b}(\mathbf{1}) . \quad (5.23)$$

All terms in (5.23) are equal, so only one term need be evaluated; the first term is

$$\begin{aligned} \sigma^{(2)}_{H_a,H_b}(\mathbf{1}) &= \rho^{(0)}(\mathbf{1}) + \rho^{(1)}_{La}(\mathbf{1}) + \rho^{(1)}_{Lb}(\mathbf{1}) + \rho^{(2)}_{LaLb}(\mathbf{1}) , \\ &= \rho^{(0)}(\mathbf{1}) + 2\rho^{(1)}_{Ha}(\mathbf{1}) + \rho^{(2)}_{LaLb}(\mathbf{1}) , \\ &= \rho^{(0)}(\mathbf{1}) \left(1 + 2\bar{f}\sigma^{(1)}_{La}\right)^2 . \end{aligned} \quad (5.24)$$

Using Eqs. (5.19) and (5.20), we arrive at

$$\sigma^{(2)}_{H_aH_b} = \frac{\left[\sigma^{(1)}_{L_a}\right]^2}{\rho} , \quad (5.25)$$

which, through (5.21), is self-consistently determined.

Much of the system bonding information follows directly from Wertheim's multi-density formalism. Perhaps one of the most fundamental, the average number of hydrogen bonds per water molecule

$$N_{hb} \equiv \frac{\sum_{n=1}^{4} n\, \rho^{(n)}(\mathbf{1})}{\sum_{n=1}^{4} \rho^{(n)}(\mathbf{1})}$$

can now easily be written in terms of the association strength and total density:

$$N_{hb} = 8\sigma^{(2)}_{H_a,H_b}\bar{f} \quad (5.26)$$

$$= \frac{32\, \bar{f}\rho}{\left(1 + \sqrt{1 + 8\bar{f}\rho}\right)^2} . \quad (5.27)$$

The simplicity of this result for N_{hb} is matched only by its ubiquity within the Wertheim theory: nearly all thermodynamic and correlation functions can be expressed as relatively simple functions of N_{hb}. It is important to point out, however,

that all temperature dependence in N_{hb} comes from $\bar{f}$, as ρ carries no inherent T dependence in the theory (see Section 5.5 for details on $\bar{f}$).

While N_{hb} naturally falls out of the formalism, the mean cluster size or cluster distribution does not when three or more attraction sites are included. For the two site case one can uniquely determine the chain size distribution given the connectivity information provided by the partial densities $\rho^{(j)}(\mathbf{1})$. With three or more sites per monomer, the chains can now branch and even a statistical analysis of the $\rho^{(j)}(\mathbf{1})$ cannot provide a unique distribution of aggregate sizes. That is, we know how many monomers are singly bonded, doubly bonded, *etc.* , but that is not the same as knowing the number of dimers, trimers, and so on: a singly bonded monomer may be part of a dimer or the end of a long branched chain for example. The connectivity information is expressed by the average monomer mole fraction X_j, where j equals the number of incident hydrogen bonds,

$$X_j = \rho^{(j)}(\mathbf{1})/\rho(\mathbf{1}) . \tag{5.28}$$

Also note that X_{L_a} is related to X_j via Eq. (5.22):

$$X_{L_a} = (X_0)^{1/4} . \tag{5.29}$$

This will be important when discussing the equation of state and the percolation threshold.

5.3. THERMODYNAMIC FUNCTIONS

No matter what method is used to determine system thermodynamics, some approximations are required. These approximations are typically expressed in terms of one- and two-body correlation functions, which, through Eqs. (5.11a) and (5.11b), dictates the form of Wertheim's generating functional $c^{(0)}$. The graphical description of this functional [19–21] in terms of partial densities $\rho^{(i)}(\mathbf{1})$ proves useful in characterizing those standard approximations in terms of the SI constraints pertinent to the physical system.

Within thermodynamic perturbation theory (TPT) these constraints enter through Wertheim's graphical analysis of the pressure, which he asserts [19–21] can be written as

$$\beta PV = \int d\mathbf{1} \left[\rho(\mathbf{1}) - \sum_i \sigma^{(i)}(\mathbf{1}) c^i(\mathbf{1})\right] + c^{(0)} . \tag{5.30}$$

As suggested by the functional relation between βPV and ρ, *viz.* $\rho \propto \delta(\beta PV)/\delta\rho$, Eq. (5.30) can be shown to satisfy the thermodynamic relation $\beta(\partial P/\partial\mu)_{V,T} = \rho$ (for details see Ref. [19–21]). With βPV written in this fashion, the four-fold connectivity and correlation restrictions —imposed by the INA— are relatively transparent: all graph vertices in $c^{(0)}$ are limited to density factors of $\sigma^{(0)}(\mathbf{1})$ or $\sigma^{(1)}(\mathbf{1})$ [*cf.* Section 5.2.3], limiting the sum over i in (5.30) to 0 and 1 only.

We are now in a position to calculate the Helmholtz free energy using the thermodynamic relation $\beta A = \beta(\mu N - PV)$. The chemical potential term can be found by recognizing the one-body correlation function $c^0(\mathbf{1})$ as the non-ideal adjustment to the chemical potential,

$$\beta\mu \;=\; \ln\left[\rho^{(0)}(\mathbf{1})\Lambda^3\right] \;-\; c^0(\mathbf{1})\,,$$

which, coupled with the ansatz (5.30), gives

$$\beta A \;=\; \int d\mathbf{1}\Big[\rho(\mathbf{1})\ln\left[\rho^{(0)}(\mathbf{1})\Lambda^3\right] - \rho(\mathbf{1}) + \sigma^{(1)}(\mathbf{1})c^1(\mathbf{1})\Big] \;-\; c^{(0)}\,. \tag{5.31}$$

The hard sphere contribution

$$\beta A_{hs} \;=\; \int d\mathbf{1}\Big[\rho(\mathbf{1})\ln\left[\rho(\mathbf{1})\Lambda^3\right] \;-\; \rho(\mathbf{1})\Big] \;-\; c_{hs}^{(0)}$$

can be subtracted from (5.31) to give

$$\beta(A - A_{hs}) \;=\; \int d\mathbf{1}\Big[\rho(\mathbf{1})\ln\left[\rho^{(0)}(\mathbf{1})/\rho(1)\right] + \sigma^{(1)}(\mathbf{1})c^1(\mathbf{1})\Big] \;-\; \left(c^{(0)} - c_{hs}^{(0)}\right)\,. \tag{5.32}$$

Evaluation of the last term in Eq. (5.32) requires analysis of the generating functional and TPT:

$$c^{(0)} - c_{hs}^{(0)} \;=\; \frac{1}{2}\int d\mathbf{1}d\mathbf{2}\;\sigma^{(1)}(\mathbf{1})F(\mathbf{1},\mathbf{2})\sigma^{(1)}(\mathbf{2}) \;=\; \frac{1}{2}\int d\mathbf{1}\;\sigma^{(1)}c^{(1)}(\mathbf{1})\,. \tag{5.33}$$

As a result,

$$\begin{aligned}\beta(A - A_{hs}) &= \int d\mathbf{1}\;\Big[\rho(\mathbf{1})\ln\left[\rho^{(0)}(\mathbf{1})/\rho(\mathbf{1})\right] \;+\; \frac{1}{2}\sigma^{(1)}(\mathbf{1})c^1(\mathbf{1})\Big]\,,\\ &= \int d\mathbf{1}\;\Big[\rho(\mathbf{1})\ln\left[\rho^{(0)}(\mathbf{1})/\rho(\mathbf{1})\right] \;+\; \frac{1}{2}\sigma^{(1)}(\mathbf{1})\rho^{(1)}(\mathbf{1})/\rho^{(0)}(\mathbf{1})\Big]\,,\end{aligned} \tag{5.34}$$

where we have used the definition $c^1(\mathbf{1}) \equiv \rho^{(1)}(\mathbf{1})/\rho^{(0)}(\mathbf{1})$. The generic product $\sigma^{(1)}(\mathbf{1})\rho^{(1)}(\mathbf{1})$ can be evaluated in site specific terms,

$$\begin{aligned}\sigma^{(1)}(\mathbf{1})\rho^{(1)}(\mathbf{1}) &= \rho_{H_a}^{(1)}(\mathbf{1})\sigma_{H_a}^{(1)}(\mathbf{1}) \;+\; \cdots \;+\; \rho_{L_b}^{(1)}(\mathbf{1})\sigma_{L_b}^{(1)}(\mathbf{1})\,,\\ &= 4\rho_{L_a}^{(1)}(\mathbf{1})\sigma_{L_a}^{(1)}(\mathbf{1})\,,\end{aligned} \tag{5.35a}$$

and with $\sigma_{L_a}^{(1)}$ given by Eq. (5.18),

$$\frac{\rho_{L_a}^{(1)}\sigma_{L_a}^{(1)}}{\rho^{(0)}\rho} = 1 - \left(\frac{\rho^{(0)}}{\rho}\right)^{1/4}. \tag{5.35b}$$

Substitution of (5.35a) and (5.35b) into Eq. (5.34) finally gives the our model TPT free energy:

$$\mathcal{A} \equiv \beta(A - A_{hs})/N = \ln\left[\rho^{(0)}/\rho\right] + 2\left(1 - [\rho^{(0)}/\rho]^{1/4}\right). \tag{5.36}$$

This agrees with the TPT free energy of Ghonasgi and Chapman (see Eqs. (14)and (17) in Ref. [47]).

Having determined the Helmholtz energy difference $\mathcal{A}$, the other thermodynamic properties follow by the standard methods. Both the pressure and the internal energy are simple sums of hard sphere (HS) and attractive parts:

$$P_{tpt} = P_{hs} - \frac{1}{2}\rho^2 k_B T N_{hb}\left[\frac{d\ln(\rho\bar{f})}{d\rho}\right]_T, \tag{5.37}$$

$$\frac{E}{N} = 3k_BT - \frac{1}{2}N_{hb}\left[\frac{d\ln\bar{f}}{d\beta}\right]_\rho. \tag{5.38}$$

Complete evaluation of these results requires the determination of $\bar{f}$, and hence the specifics of the associating system in question.

5.4. LIQUID STRUCTURE

Apart from the TPT route above, Wertheim's formalism allows for thermodynamic as well as structural data to be determined from standard integral equation methods. Therein an *associated* Ornstein-Zernike (AOZ) equation can be solved using an *associated* Percus–Yevick-like (APY) closure condition [98]. This route not only permits determination of the usual thermodynamic quantities, but also three methods by which to derive an equation of state: a virial path, based upon $g(r)$ at contact, and two compressibility paths, one based upon the structure factor and the other upon the direct correlation function. Consequently, thermodynamic self-consistency can be directly analyzed.

5.4.1. Associated Ornstein-Zernike Relation

Even for a pure fluid the AOZ relation for a four-site model typically involves a (16 × 16) matrix equation [105, 121]

$$\boldsymbol{h}(\mathbf{1},\mathbf{2}) \;=\; \boldsymbol{c}(\mathbf{1},\mathbf{2}) + \int d\mathbf{3}\; \boldsymbol{c}(\mathbf{1},\mathbf{3})\boldsymbol{\sigma}(\mathbf{3})\boldsymbol{h}(\mathbf{3},\mathbf{2})\,, \tag{5.39}$$

where bold typeface indicates a matrix quantity. Use of our generic densities and correlation functions, on the other hand, simplifies that relation to a (5 × 5) partitioned matrix equation. The matrix of density parameters $\boldsymbol{\sigma}$ assumes a triangular form

$$\boldsymbol{\sigma} \;=\; \begin{pmatrix} \sigma^{(0)} & \sigma^{(1)} & \sigma^{(2)} & \sigma^{(3)} & \sigma^{(4)} \\ \sigma^{(1)} & \sigma^{(2)} & \sigma^{(3)} & \sigma^{(4)} & 0 \\ \sigma^{(2)} & \sigma^{(3)} & \sigma^{(4)} & 0 & 0 \\ \sigma^{(3)} & \sigma^{(4)} & 0 & 0 & 0 \\ \sigma^{(4)} & 0 & 0 & 0 & 0 \end{pmatrix} \tag{5.40}$$

with generic elements $\sigma^{(m)}$ defined as before by Eqs. (5.8a)–(5.8e). Both the direct $\boldsymbol{c}$ and total $\boldsymbol{h}$ correlation functions, referred to collectively as $\boldsymbol{s}$, follow the general form

$$\boldsymbol{s} \;=\; \begin{pmatrix} s^{00} & s^{01} & s^{02} & s^{03} & s^{04} \\ s^{10} & s^{11} & s^{12} & s^{13} & s^{14} \\ s^{20} & s^{21} & s^{22} & s^{23} & s^{24} \\ s^{30} & s^{31} & s^{32} & s^{33} & s^{34} \\ s^{40} & s^{41} & s^{42} & s^{43} & s^{44} \end{pmatrix}. \tag{5.41}$$

Here superscript matrix element indices also denote the total number of incident F-bonds at the indicated space point in the same fashion as for the background correlation functions $y^{mn}(\mathbf{1},\mathbf{2})$ described earlier. Since the F-bonds are assumed to act independently and are arranged randomly about the monomer, all correlation functions can be orientation averaged, $\boldsymbol{s}(\mathbf{1},\mathbf{2}) \rightarrow \boldsymbol{s}(r)$, where r is the one-dimensional center–to–center separation. The orientation-averaged version of the APY closure relation[4] [19, 20, 156] under the INA becomes

$$h^{mn}(r) \;=\; -\,\delta_{m,0}\,\delta_{n,0}\,, \qquad\qquad r < R, \tag{5.42a}$$

---

[4]See Kalyuzhnyi *et. al.* [98] for an example of a solution to the associative Percus–Yevick approximation for an n-component mixture of associating hard spheres.

$$\left.\begin{aligned} c^{00}(r) &= f_R(r)y^{00}(r) \\ c^{01}(r) = f_R(r)y^{01}(r), \quad c^{10}(r) &= f_R(r)y^{10}(r) \end{aligned}\right\} \quad r < R, \tag{5.42b}$$

$$c^{11}(r) = f_R(r)y^{11}(r) + e_R(r)y^{00}(r)F(r), \qquad r > R, \tag{5.42c}$$

where $\delta_{m,0}$, $\delta_{n,0}$ are the Kronecker delta function.

5.4.2. AOZ Factorization Solution

The AOZ matrix relation (5.39), the APY closure conditions (5.42a)–(5.42c), and the partial density equations (5.17) and (5.21), all form a closed set of equations. For an infinitesimally short-ranged attractive potential, analytical solutions for the correlation functions $c(r)$ and $h(r)$ can be obtained using Baxter's factorization method, [163]. This method has been widely used for adhesive models in conjunction with Wertheim theory [105, 121, 139]; nonetheless, a brief synopsis follows.

Despite the closed set of equations appropriate to our system, the AOZ is a convolution and hence difficult to separate and solve for the correlations $c(r)$ and $h(r)$. Nevertheless, Baxter demonstrated that the Fourier transform of the AOZ

$$\tilde{\boldsymbol{h}}(k) = \tilde{\boldsymbol{c}}(k) + \tilde{\boldsymbol{c}}(k)\boldsymbol{\sigma}\tilde{\boldsymbol{h}}(k)$$

can be factorized in terms of one-dimensional auxiliary functions $q^{mn}(r)$. The factorization procedure effectively separates the functions $\tilde{h}(k)$ and $\tilde{c}(k)$, which can then be individually solved in terms of the auxiliary functions. By rewriting the above transform as

$$\left[\boldsymbol{\sigma}^{-1} - \tilde{\boldsymbol{c}}(k)\right]\left[\boldsymbol{I} + \boldsymbol{\sigma}\tilde{\boldsymbol{h}}(k)\right] = \boldsymbol{\sigma}^{-1}$$

it can be —in a mathematical *tour de force*— factorized[5] according to

$$\left[\boldsymbol{\sigma}^{-1} - \tilde{\boldsymbol{c}}(k)\right] = \boldsymbol{q}^T(-k)\boldsymbol{\sigma}\boldsymbol{q}(k), \tag{5.43a}$$

$$\left[\boldsymbol{I} + \boldsymbol{\sigma}\tilde{\boldsymbol{h}}(k)\right] = \left[\boldsymbol{\sigma}\boldsymbol{q}^T(-k)\boldsymbol{\sigma}\boldsymbol{q}(k)\right]^{-1}, \tag{5.43b}$$

---

[5]Unlike the case for a one-component system, there is no formal theory for the Wiener–Hopf factorization of matrices; see Ref. [106] for a discussion of the factorization procedure as it applies to mixtures or associating fluids.

where $\boldsymbol{I}$ is the identity matrix and $\boldsymbol{q}^T(-k)$ is the complex conjugate and transpose of the auxiliary function matrix $\boldsymbol{q}(k)$, with elements

$$q^{mn}(k) \;=\; (\sigma^{-1})^{mn} \;-\; 2\pi \int_0^R dr\; e^{ikr} q^{mn}(r)\,.$$

After an analysis of these matrices in the complex plane, their real space solution results in a decoupling of the partial correlation functions into the following integro-differential equations:

$$rh^{mn}(r) \;=\; -\frac{dq^{mn}(r)}{dr} \;+\; 2\pi \sum_{k,l} \int_0^R dt\; (r-t) q^{mk}(t) \sigma^{kl} h^{ln}(|r-t|)\,, \tag{5.44}$$

$$rc^{mn}(r) \;=\; -\frac{dq^{mn}(r)}{dr} \;+\; 2\pi \sum_{k,l} \frac{d}{dr} \int_0^{R-r} dt\; q^{km}(t) \sigma^{kl} q^{ln}(r+t)\,. \tag{5.45}$$

Superscripts refer to the matrix elements given by Eqs. (5.40) and (5.41), with the independent sums over k and l generally running from 0 to 4 for a four site model. As with the density parameters, the INA here limits that sum to 0 and 1, such that the only nonzero (generic) auxiliary functions will be $q^{00}(r)$, $q^{10}(r)$ and $q^{11}(r)$.

Solutions to the decoupled Eqs. (5.44) and (5.45) for the auxiliary functions $q^{mn}(r)$ are obtained, in part, by imposing the APY closure conditions, Eqs. (5.42a)–(5.42c), along with the $q^{mn}(r)$ boundary conditions that arise in the factorization process:

$$q^{mn}(R^-) \;=\; 0 \tag{5.46a}$$

$$q^{mn}(0) \;=\; q^{nm}(0) \quad \text{for } m \neq n\,. \tag{5.46b}$$

Given the form of the APY conditions inside the hard core [see Eq. (5.47)], it is easiest to find the auxiliary functions by solving (5.44) first.

5.4.2.1. The q^{0n} Solutions

Inside the hard core the APY conditions translate into

$$h^{00}(r) \;=\; -1 \quad \forall\, r < R^-\,, \tag{5.47}$$

and since all other correlations $h^{mn}(r)$ vanish inside the hard core, all $q^{0n}(r)$ terms follow trivially from Eq. (5.44):

$$q^{0n}(r) \;=\; 0 \quad \forall\, r \text{ and } n > 0\,, \tag{5.48}$$

where the boundary condition (5.46a) was used.

5.4.2.2. The q^{00} Solution

With all $q^{0n}(r)$ known, the hard sphere term $q^{00}(r)$ easily follows as

$$q^{00}(r) \;=\; \frac{1}{2}\,a^{00}\left(r^2 - R^2\right) \;+\; b^{00}\,(r - R)\,, \tag{5.49a}$$

where the coefficients

$$a^{00} \;=\; \frac{1+2\eta}{(1-\eta)^2} \tag{5.49b}$$

$$b^{00} \;=\; \frac{-3R\eta}{2(1-\eta)^2} \tag{5.49c}$$

are functions of the packing fraction η, defined in terms of the molecular volume v_0 as $\eta = \rho v_0$. Note that $q^{00}(r)$ goes smoothly to zero at the boundary $r = R$.

5.4.2.3. The q^{11} Solution

The remaining contributions from association are much more difficult to determine, and so a more detailed solution will be given. Immediately outside the hard core, the generic correlation function $h^{11}(r)$ can be written as

$$h^{11}(r) \;=\; F(r)y^{00}(r)\,, \tag{5.50}$$

which, in the sticky-spot limit, corresponds to a *site-specific* pseudopotential replacement

$$h^{11}_{Ha,La}(r) \longrightarrow \frac{\delta(r - R^+)\bar{f}}{4\pi R^2}\,. \tag{5.51}$$

The particular form of this replacement insures that the volume integral of $h^{11}_{Ha,La}(r)$ is exactly $\bar{f}$, which includes the background correlation function $y^{00}(R)$ evaluated at contact. Evaluation of Eq. (5.44) in this case, however, requires care, for there are numerous, equal pseudopotential replacements $h^{11}_{i,j}(r)$, where

$i,j \in \{H_a, H_b, L_a, L_b\}$. Substitution of an $h^{11}_{i,j}(r)$, *e.g.* Eq. (5.51), into Eq. (5.44) then transforms that generic integro-differential relation into a set of *site-specific* equations; all generic auxiliary functions [except $q^{00}(r)$] thus represent a set of site-specific auxiliary functions and all the attendant combinatoric factors of that transformation must be accounted for. Yet, unlike the simple relation among the generic and site-specific densities, the analogous relation among the total correlation functions is complex: these correlations not only involve the site projection operators $F(1,2)$ but also *background* site-site correlations such as $h_{H_a,H_a}(r)$ or $h_{H_a,H_b}(r)$, for example. Hence, although $h^{11}(1,2)$ consists of eight equal, site-specific terms that are not necessarily zero, $h^{11}(r) \neq 8h^{11}_{H_a,L_a}(r)$! Thankfully, under the INA all higher-order generic correlations $h^{mn}(r)$, *e.g.*

$$h^{22}(r) \;=\; y^{11}(r)F(r)\,, \quad h^{32}(r) \;=\; y^{21}(r)F(r)\,, \;\ldots$$

are neglected because they depict ring structures between vertices 1 and 2 —closed by the $y^{11}(r)$, $y^{21}(r)$ functions and $F(r)$ bonds.

According to Eq. (5.52a) then, the generic $q^{11}(r)$ auxiliary function satisfies the relation

$$rh^{11}(r) \;=\; -\,\frac{dq^{11}(r)}{dr} \;+\; 2\pi \sum_k \int_0^R dt\;(r-t)q^{1k}(t)\sigma^{k1}h^{11}(|r-t|)\,, \qquad (5.52a)$$

where only the $l = 1$ term contributes to the first sum. The integral term on the right-hand side is a well behaved function which contributes some finite constant across the infinitesimal interval $[R^-, R^+]$,

$$rh^{11}(r) \;=\; -\,\frac{dq^{11}(r)}{dr} + const\,. \qquad (5.52b)$$

Upon substituting Eq. (5.51) into the left-hand side of (5.52b) and integrating, we obtain the site-specific relation

$$q^{11}_{H_a,L_a}(R^+) \;-\; q^{11}_{H_a,L_a}(R^-) \;=\; -\int dr\; r\;\frac{\delta(r-R^+)}{4\pi R^2}\,\bar{f}\,, \qquad (5.52c)$$

or, using Eq. (5.46a),

$$q^{11}_{H_a,L_a}(R^-) \;=\; \frac{\bar{f}}{4\pi R}\,, \qquad q^{11}_{H_a,L_a}(R^+) \;=\; 0\,. \qquad (5.53)$$

There are eight such equal, non-zero constant terms associated with the proper connectivity constraints, whereas all other possible terms (combinations) are zero

since they depict improper bonding, an H site directly bonded to another H site, for example, making $q^{11}(r)$ therefore a 4×4 matrix. It should be noted that the connectivity exclusions $q^{11}_{H_a,H_b}(R^+) = q^{11}_{L_a,L_b}(R^+) = \cdots = 0$ arise solely because equations like (5.51) only account for the *direct* F–bonds between vertices 1 and 2. This does *not* mean that same-site background correlations like $h_{H_a,H_a}(r)$ or $h_{H_a,H_b}(r)$ necessarily vanish (in fact they do not).

5.4.2.4. The q^{10} Solution

The generic $q^{10}(r)$ follows from Eq. (5.44) in an analogous fashion:

$$rh^{10}(r) \;=\; -\frac{dq^{10}(r)}{dr} \;+\; 2\pi \sum_{k,l} \int_0^R dt\,(r-t) q^{1k}(t) \sigma^{kl} h^{l0}(|r-t|) \;=\; 0\,. \qquad (5.54a)$$

This generic relation corresponds to four equal, site-specific terms; choosing one of these and labelling the sites,

$$\frac{dq^{10}_{H_a}(r)}{dr} \;=\; 2\pi\rho \int_0^R dt\,(t-r) q^{10}_{H_a}(t) \;+\; 2\pi\sigma^{(1)}_{H_a} \int_0^R dt\,(t-r)\left[q^{11}_{H_a,L_a}(t) + q^{11}_{H_a,L_b}(t)\right].$$

Since $q^{11}_{H_a,L_a}(t) = q^{11}_{H_a,L_b}(t) = (4\pi R)^{-1}\bar{f}$ is a constant, inside the hard core the last integral on the right-hand side can be evaluated to give

$$\begin{aligned} \frac{dq^{10}_{H_a}(r)}{dr} \;&=\; 2\pi\rho \int_0^R dt\,(t-r) q^{10}_{H_a}(t) \;+\; 4\pi\sigma^{(1)}_{Ha}\left[\tfrac{1}{2}R^2 - Rr\right] q^{11}_{H_a,L_a}(R^-)\,, \\ &\equiv\; ar \;+\; b\,, \end{aligned} \qquad (5.54b)$$

where

$$a \;=\; -2\pi\rho \int_0^R dt\, q^{10}_{H_a}(t) \;-\; 4\pi\sigma^{(1)}_{H_a} R\, q^{11}_{H_a,L_a}(R^-)\,, \qquad (5.54c)$$

$$b \;=\; 2\pi\rho \int_0^R dt\, t\, q^{10}_{H_a}(t) \;+\; 2\pi\sigma^{(1)}_{H_a} R^2\, q^{11}_{H_a,L_a}(R^-)\,. \qquad (5.54d)$$

Solving these relations we obtain

$$q^{10}_{H_a}(r) \;=\; \frac{1}{2}\,a^{10}(r^2 - R^2) + b^{10}(r-R)\,, \qquad (5.55a)$$

$$a^{10} \;=\; \frac{-4\pi\sigma^{(1)}_{H_a} R\, q^{11}_{H_a,L_a}(R^-)}{1-\eta} \;=\; -\frac{\sigma^{(1)}_{H_a}\bar{f}}{1-\eta}\,, \qquad (5.55b)$$

$$b^{10} \;=\; -\frac{R\,a^{10}}{2}\,. \qquad (5.55c)$$

This solution satisfies both boundary conditions Eqs. (5.46a) and (5.46b) as required.

5.4.3. Correlation Function Contact Properties

Once all the auxiliary functions $q^{mn}(r)$ are known, the contact values of the total correlation functions $h^{mn}(R)$ and hence the radial distribution function $g(R)$ immediately follow. At contact we note from Eq. (5.44) that all dq^{mn}/dr terms vanish since they are to be evaluated in the region where all $q^{mn}(r) \equiv 0$. Insertion of the appropriate $q^{mn}(r)$ and $h^{mn}(r)$ functions inside the hard core then allows for evaluation of the integrals in Eq. (5.44); some resulting site-specific contact values are

$$h^{00}(R) = \frac{1}{2}\frac{\eta(5-2\eta)}{(1-\eta)^2}, \tag{5.56a}$$

$$h^{01}_{H_a}(R) = h^{10}_{H_a}(R) = -\frac{2\pi R\sigma^{(1)}_{H_a} q^{11}_{H_aL_b}(R^-)}{1-\eta} = -\frac{1}{2}\frac{\sigma^{(1)}_{H_a}\bar{f}}{(1-\eta)}, \tag{5.56b}$$

$$h^{11}_{H_aL_a}(R) = \frac{\sigma^{(2)}_{H_aH_b}\bar{f}^2}{2\pi R^3} = 2h^{11}_{H_aH_a}(R). \tag{5.56c}$$

Results like $h^{11}_{H_aL_a}(R) = 2h^{11}_{H_aH_a}(R)$, which relate (direct) F-bonded correlations to background (same-site) correlations, ensue from a careful assessment of (5.44) and confirms that the same-site correlations are non-zero, even though the same-site auxiliary functions are.

These total correlations may now be used to determine the contact value of the radial distribution function through the relation $g^{mn}(r) = h^{mn}(r) - \delta_{m,0}\delta_{n,0}$ where $\delta_{m,n}$ is the Kronecker delta function. By means of Wertheim's formalism, $g(r)$ is a graphical superposition of partial correlations $g^{mn}(r)$,

$$\rho^2 g(1,2) \equiv \sum_{m=0}^{4}\sum_{n=0}^{4} \sigma^{(m)}(1) g^{mn}(1,2)\sigma^{(n)}(2), \tag{5.57}$$

$$\rho^2 g(r) = \rho g^{00}(r)\rho + 2\,\rho g^{01}(r)\sigma^{(1)} + \sigma^{(1)} g^{11}(r)\sigma^{(1)}, \tag{5.58}$$

here restricted to three terms under the INA. Transforming to site-specific quantities with the appropriate multiplicity factors, we obtain

$$\rho^2 g(r) = \rho^2 g^{00}(r) + 8\,\rho\sigma^{(1)}_{H_a} g^{01}_{H_a}(r) + 8\left[\sigma^{(1)}_{H_a}\right]^2\left[g^{11}_{H_aL_a}(r) + g^{11}_{H_aH_a}(r)\right]. \tag{5.59}$$

It is important to distinguish between $g^{11}_{H_aL_a}(r)$ and $g^{11}_{H_aH_a}(r)$ in the last term on the right-hand side of (5.59): as indicated above they are not equal. Upon insertion of the site-specific $h^{mn}(R)$ functions (5.56a)–(5.56c) along with Eq. (5.26) for N_{hb}, the contact radial distribution function becomes

$$g(R) = \frac{1+\frac{1}{2}\eta}{(1-\eta)^2} - \frac{\frac{1}{2}N_{hb}}{(1-\eta)} + \frac{[N_{hb}]^2}{64\eta}. \tag{5.60}$$

This solution is equivalent to Duda's 1998 result [121] [see Eq. (30)] once various notational differences are taken into account. In both cases, the delta-function contribution to $h^{11}(r) \simeq F(r)$ at $r = R^+$ has been omitted; even though $g(R)$ in Eq. (5.60) involves all contributions at contact apart from the δ-function peak itself, the "secondary" effects of that δ-function are obviously apparent in (5.60).

5.4.4. Direct Correlation Functions

The *partial* direct correlation functions $c^{mn}(r)$ inside the hard core now ensue from Eq. (5.45) because the auxiliary functions $q^{mn}(r)$ are already known in that region. In the final analysis we obtain

$$c^{00}(x) = c^{00}_{hs}(x) + \frac{\eta N_{hb}(1-x)}{4(1-\eta)^3} \times \left[10 + 2\eta - 2(1+2\eta)(x^2+x) + \frac{3}{8}N_{hb}(1-\eta)(x^2+x-2)\right], \tag{5.61a}$$

$$c^{01}_{H_a}(x) = c^{10}_{H_a}(x) = \frac{\bar{f}\sigma^{(1)}_{H_a}}{2(1-\eta)^2} \times \left[2 - x + \eta - 2x\eta + \frac{3}{8}N_{hb}(x-1)(1-\eta)\right], \tag{5.61b}$$

$$c^{11}_{H_aL_a}(x) = 2c^{11}_{H_aH_a}(x) = -\frac{\bar{f}N_{hb}}{16\pi R^3 x}, \tag{5.61c}$$

where $x \equiv r/R$ and $c^{00}_{hs}(x)$ is the PY hard sphere contribution [55],

$$c^{00}_{hs}(x) = -\lambda_1 - 6\eta\lambda_2 x - \frac{1}{2}\eta\lambda_1 x^3, \qquad x < 1$$
$$\lambda_1 = \frac{(1+2\eta)^2}{(1-\eta)^4}, \quad \lambda_2 = -\frac{(1+\frac{1}{2}\eta)^2}{(1-\eta)^4}.$$

Analogous with the total correlation functions, $c^{11}_{H_aL_a}(x) = 2c^{11}_{H_aH_a}(x)$, both being odd results but which reflect the pedestrian manner in which aggregates

are "constructed" in pairwise fashion. Equations (5.61a)–(5.61c) also satisfy the proper boundary conditions at the hard core surface, namely $\lim_{r\to R^-} c^{mn}(r) = -y^{mn}(R)$.

While there is no generalized relation between the direct correlation function $c(r)$ and the *partial* functions $c^{mn}(r)$ in Wertheim theory, as exists for $g(r)$ and $h(r)$, the exclusion of ring-bonded structures under the INA permits just such a relation (see Section 4.1 in Ref. [20]): $c(r)$ can be written as a density-weighted superposition of $c^{mn}(r)$ functions similar to Eq. (5.57) for $g(r)$:

$$\begin{aligned}\rho^2 c(r) &= \sum_{m=0}^{4}\sum_{n=0}^{4} \sigma^{(m)} c^{mn}(r) \sigma^{(n)} \\ &= \rho^2 c^{00}(r) + 8\rho\sigma_{H_a}^{(1)} c_{H_a}^{01}(r) + 8\left[\sigma_{H_a}^{(1)}\right]^2 \left[c_{H_a L_a}^{11}(r) + c_{H_a H_a}^{11}(r)\right] . \end{aligned} \tag{5.62}$$

The relevant site-specific quantities (5.61a)–(5.61c) can be inserted to give the full direct correlation function, which can then be spatially integrated to give the compressibility relation

$$\begin{aligned}\left(\frac{\partial \beta P_{com}}{\partial \rho}\right)_T &= 1 - \rho \int d\mathbf{r}\, c(r) , \\ &= \frac{\left[1 + 2\eta - \frac{1}{4}N_{hb}(1-\eta)\right]\left[1 + 2\eta - \frac{3}{4}N_{hb}(1-\eta)\right]}{(1-\eta)^4} . \end{aligned} \tag{5.63}$$

With N_{hb} given as a function of density in Eq. (5.27), (5.63) can be numerically integrated to give the compressibility pressure P_{com}.

5.4.5. Virial Equation of State

Within the sticky-spot model limit, only the contact value of $g(r)$ is required in order to determine the virial equation of state, which can be written [55] as

$$\beta P_{vir} = \rho - \frac{2\pi\beta}{3} \int dr\, r^3 \rho^2 g(r) \frac{d}{dr} u(r) . \tag{5.64}$$

Recall that our interaction potential $u(r)$ is separable into repulsive $u^R(r)$ and attractive $u^A(r)$ parts.

5.4.5.1. Hard Sphere Contribution

The hard sphere singularities in (5.64) associated with the discontinuity in $g(r)$ and $u(r)$ can be integrated by rewriting $g(r)$ in terms of the continuous

background correlation function $y(r) = \exp[+\beta u^R(r)]g(r)$, such that

$$\beta P_{vir} = \rho + \frac{2\pi\beta}{3}\int dr\, r^3\rho^2 y(r)\frac{d}{dr}e^{-\beta u(r)}. \tag{5.65}$$

For the hard sphere potential, the Boltzmann factor above is simply the Heaviside step-function, the derivative of which is a Dirac delta-function $-\beta e^R(r)(du^R(r)/dr) = \delta(r - R^+)$; hence

$$\begin{aligned}\beta P_{vir} &= \rho + \frac{2\pi}{3}\rho^2 \lim_{r\to R^+} r^3 y(r) + \beta\delta P^A, \\ &= \rho + \frac{2\pi}{3}R^3\rho^2 g(R^+) + \beta\delta P^A,\end{aligned} \tag{5.66}$$

with the "direct" $u^A(r)$ contributions of (5.65) contained in

$$\beta\delta P^A \equiv \frac{2\pi}{3}\int dr\, r^3\rho^2 g(r)\Big[-\beta\frac{d}{dr}u^A(r)\Big]. \tag{5.67}$$

A closer inspection of Eqs. (5.66) and (5.60) shows that even this nominally hard sphere component of the pressure contains contributions from association in the form of N_{hb} dependence. Isolating the purely hard-sphere (PY virial pressure) contribution P^R, Eq. (5.66) becomes

$$\beta(P_{vir} - P^R) = 2\rho N_{hb}\left(\frac{N_{hb}}{32} - \frac{\eta}{1-\eta}\right) + \beta\delta P^A. \tag{5.68}$$

5.4.5.2. Attractive Contribution

Evaluation of the attractive contribution $\beta\delta P^A$ begins with the relation

$$\rho^2 g(r) = e^R(r)\Big\{\rho^2 y^{00}(r) + 2\sigma^{(1)}\rho y^{01}(r) + \left[\sigma^{(1)}\right]^2\left[y^{11}(r) + y^{00}(r)(e^{-\beta u^A(r)} - 1)\right]\Big\},$$

which follows from Eq. (5.58) and the graphical definition of the $y^{mn}(r)$ functions. The integrand in (5.67) can thus be written as

$$\begin{aligned}&\rho^2 g(r)\Big[-\beta\frac{d}{dr}u^A(r)\Big] \\ &\quad = e^R(r)\Big[\rho^2 y^{00}(r) + 2\sigma^{(1)}\rho y^{01}(r) + \left[\sigma^{(1)}\right]^2 y^{11}(r)\Big]\Big[-\beta\frac{d}{dr}u^A(r)\Big] \\ &\qquad + e^R(r)[\sigma^{(1)}]^2 y^{00}(r)\frac{d}{dr}\left[e^{-\beta u^A(r)} - 1\right].\end{aligned} \tag{5.69}$$

Upon inserting this relation into Eq. (5.67) we note that for a deep, narrow well just outside the hard core the volume integral of $[-\beta du^A(r)/dr]$ in Eq. (5.69) behaves like $\varepsilon\ell$, whereas the volume integral of the last term in (5.69) behaves like $(e^{\beta\varepsilon}-1)\ell$. In the sticky-spot limit then, the contribution from the latter term will greatly exceed that of the former, which can therefore be omitted from Eq. (5.69). An integration by parts of the remaining term in the sticky limit then gives

$$\begin{aligned}\lim_{\substack{\varepsilon\to\infty\\ \ell\to 0}} \beta\delta P^A &= \frac{2\pi}{3}\left[\sigma^{(1)}\right]^2 \int dr\, r^3 y^{00}(r) e^R(r) \frac{d}{dr}\left[e^{-\beta u^A(r)}-1\right] \\ &= -\frac{2\pi}{3}\left[\sigma^{(1)}\right]^2 \int dr\, F(r) \frac{d}{dr}\left[r^3 y^{00}(r)\right] \\ &= -4\rho\bar{f}\,\sigma^{(2)}_{H_a,H_b} \lim_{r\to R}\left[1+\frac{1}{3} r \frac{d}{dr}\ln y^{00}(r)\right], \end{aligned} \tag{5.70}$$

wherein Eq. (5.68) becomes

$$\beta(P_{vir}-P^R) = \rho N_{hb}\left(\frac{N_{hb}}{24} - \frac{2\eta}{1-\eta} - \frac{1}{2}\lim_{r\to R}\left[1+\frac{1}{3} r \frac{d}{dr}\ln y^{00}(r)\right]\right). \tag{5.71}$$

Further evaluation of (5.71) requires specification of $y^{00}(r)$, and hence the model parameters; these will be discussed in Section 5.5.1.

5.4.6. Scattering and Compressibility

The static structure factor, defined in terms of the Fourier transform $\tilde{h}(k)$ of the total correlation function $h(r)$, $S(k) = 1 + \rho\tilde{h}(k)$, can be rewritten in terms of Baxter's auxiliary functions and thus analytically determined. Recall from the AOZ factorization procedure that, in k space,

$$\left[\boldsymbol{\sigma} + \boldsymbol{\sigma}\tilde{\mathbf{h}}(k)\boldsymbol{\sigma}\right] = \left[\tilde{\mathbf{q}}^T(-k)\boldsymbol{\sigma}\tilde{\mathbf{q}}(k)\right]^{-1}. \tag{5.72}$$

Looking at the zeroth matrix element of the left-hand side we find

$$\left\{\left[\boldsymbol{\sigma} + \boldsymbol{\sigma}\tilde{\mathbf{h}}(k)\boldsymbol{\sigma}\right]\right\}^{00} = \sigma^{00} + \sum_{m,n=0}^{4} \sigma^{0m}\tilde{h}^{mn}(k)\sigma^{n0}, \tag{5.73a}$$

$$= \rho + \sum_{m,n=0}^{4} \sigma^{(m)}\tilde{h}^{4-m\,4-n}(k)\sigma^{(n)}, \tag{5.73b}$$

but the last term on the right-hand side of (5.73b) is precisely $\rho^2\tilde{h}(k)$, the graphical sum of partial correlations $\tilde{h}^{mn}(k)$ analogous to that for $\rho^2 g(r)$, Eq. (5.57) on page 156. Hence

$$\left\{\left[\boldsymbol{\sigma} + \boldsymbol{\sigma}\tilde{\mathbf{h}}(k)\boldsymbol{\sigma}\right]\right\}^{00} = \rho + \rho^2\tilde{h}(k)\,, \tag{5.73c}$$

from which it follows that

$$\begin{aligned} S(k) &= \rho^{-1}\left[\rho + \rho^2\tilde{h}(k)\right], \\ &= \rho^{-1}\left\{\left[\boldsymbol{q}^T(-k)\,\boldsymbol{\sigma}\boldsymbol{q}(k)\right]^{-1}\right\}^{00}, \end{aligned} \tag{5.74}$$

where, again, the elements of the matrix $\boldsymbol{q}(k)$ are Fourier transforms of the auxiliary functions $q^{mn}(r)$ arising from Baxter's factorization procedure:

$$\begin{aligned} q^{mn}(k) &= (\boldsymbol{\sigma}^{-1})^{mn} - 2\pi\int_0^R dr\; e^{ikr}q^{mn}(r) \\ &\equiv (\boldsymbol{\sigma}^{-1})^{mn} - w^{mn}(k)\,. \end{aligned} \tag{5.75}$$

Inserting these $q^{mn}(k)$ into Eq. (5.74) and simplifying gives

$$S(k) = \rho^{-1}\left\{\left(\left[\mathbf{I} - \boldsymbol{\sigma}\boldsymbol{w}^T(-k)\right]\left[\mathbf{I} - \boldsymbol{\sigma}\boldsymbol{w}(k)\right]\right)^{-1}\boldsymbol{\sigma}\right\}^{00}; \tag{5.76}$$

evaluation of the matrix inverse requires a $(1 + 4 + 6 + 4 + 1)$ or 21-dimensional vector space, which arises from the site-site details contained in the generic density parameters $\sigma^{(i)}$ $(i = \{1, 2, 3, 4\})$ that comprise the matrix $\boldsymbol{\sigma}$. Luckily, calculation of that 21-dimensional inverse is simplified by the fact that $\boldsymbol{w}$ becomes a sparse matrix in the *ideal network approximation*; the only nonzero integrand elements $q^{mn}(r)$ in (5.75) are given by Eqs. (5.49a), (5.53), and (5.55a). This translates into only three nonzero $w^{mn}(k)$ elements, *viz.*

$$\begin{aligned} w^{00}(\kappa) = \frac{-i\pi R^3}{\kappa^3(1-\eta)^2} \\ \times\left[e^{i\kappa}(2i\kappa - 2 + i\eta\kappa - 4\eta) + (2 + \kappa^2 + 4\eta - \eta\kappa^2 + 3i\eta\kappa)\right] \end{aligned} \tag{5.77a}$$

$$w^{10}(\kappa) = \frac{i\pi R^3\sigma_{H_a}^{(1)}\bar{f}}{\kappa^3(1-\eta)}\left[e^{i\kappa}(i\kappa - 2) + i\kappa + 2\right] \tag{5.77b}$$

$$w^{11}(\kappa) = \frac{(e^{i\kappa} - 1)\bar{f}}{2i\kappa}\,, \tag{5.77c}$$

where $\kappa \equiv kR$. These results, when coupled with the density parameters contained in σ from Section 5.4.1, gives an analytical description of the structure factor,

$$S(\kappa) = \frac{1 + 4\sigma^{(2)}_{H_a,H_b} Re[w^{11}(\kappa)] - 12w^{11}(\kappa)w^{11}(-\kappa)\left[\sigma^{(2)}_{H_a,H_b}\right]^2}{[1 - X(\kappa)][1 - X(-\kappa)]}, \tag{5.78a}$$

where

$$X(\kappa) \equiv \rho w^{00}(\kappa) + 4\sigma^{(1)}_{H_a} w^{10}(\kappa) + 6\sigma^{(2)}_{H_a,H_b} w^{11}(\kappa) + 2\left[\sigma^{(1)}_{H_a}\right]^2 w^{11}(\kappa)w^{00}(\kappa). \tag{5.78b}$$

To our knowledge, no one has yet produced an analytical structure factor before for the hard sphere, four-site model. The symmetry and simplicity of the primitive model is reflected in this, as in other, results: *e.g.* only $\sigma^{(1)}$ and $\sigma^{(2)}$ elements appear.

The isothermal compressibility κ_T immediately follows by evaluating the $\kappa \to 0$ limit of $S(\kappa)$:

$$\kappa_T = (\rho k_B T)^{-1} \lim_{\kappa \to 0} S(\kappa).$$

For the case of hard spheres, that limit leads to

$$\kappa_T^{hs} = (\rho k_B T)^{-1} \frac{(1-\eta)^4}{(1+2\eta)^2} \tag{5.79}$$

as expected: the singularity in κ_T^{hs} associated with the spinodal line is purely density dependent. The $S(\kappa)$–based compressibility pressure P_{com} can also be found by numerical integration of

$$\left(\frac{\partial \beta P_{com}}{\partial \rho}\right)_T = (\rho k_B T \kappa_T)^{-1} = \frac{[1 + 2\eta + \frac{3}{8}(2\eta - 1)N_{hb}]^2}{(1 + \frac{3}{8}N_{hb})(1 - \frac{1}{8}N_{hb})(1-\eta)^4}. \tag{5.80}$$

To first order in N_{hb} this result agrees with that obtained by integration of the direct correlation function, Eq. (5.63) on page 158. Unlike the c(r)–based compressibility pressure, however, the P_{com} derived from Eq. (5.80) is inherently positive because its numerator is a square and $N_{hb} \leq 4$. This fact will have a profound impact at high association strengths or low temperatures (*cf.* Section 5.5).

5.5. APPLICATIONS & DISCUSSION

Our model requires three parameters for its application to any system: (i) a hard sphere diameter R, (ii) a hydrogen bond energy ε, and (iii) the pair "reactive" volume which is the volume available for bonding between two unlike sites. All three of these parameters enter the theory through the integrated association strength $\bar{f}$,

$$\bar{f} \;=\; \delta V\,[\exp(\beta\varepsilon) - 1]\,y^{00}(R)\,, \tag{5.81}$$

where, from Section 4.3.1, we see that $\delta V \propto K_A$ and so contains the steric constraints, although in the four-site model these constraints are much more complicated. The background correlation function at contact immediately follows from our factorization result (5.56a) for $h^{00}(R^+)$,

$$y^{00}(R) \;=\; h^{00}(R^+) + 1 \;=\; \frac{1}{1-\eta} + \frac{3\eta}{2(1-\eta)^2}\,, \tag{5.82}$$

but does not allow us to calculate its radial derivative at contact, necessary for evaluation of the virial pressure (5.71). In order to evaluate that derivative, we use the boundary condition

$$y^{00}(R) \;=\; -\lim_{r\to R^-} c^{00}(r)\,,$$

such that

$$\lim_{r\to R} r\,\frac{dy^{00}(r)}{dr} = -\frac{9\eta(1+\eta)}{2(1-\eta)^3} + \frac{3\eta N_{hb}}{2(1-\eta)^2}\,. \tag{5.83}$$

5.5.1. Application to Water

For application of our primitive four-site model to water we choose parameter values from experiment. While the oxygen–oxygen separation distance varies little with temperature, increasing from roughly 2.8Å at room temperature to only about 2.9Å at 200 °C, the theory is sensitive to small changes in R. We chose a molecular diameter of $R = 2.8$Å which is consistent with X-ray data and the peak in the oxygen–oxygen radial distribution function $g_{OO}(r)$ obtained by Soper and Phillips [195]. An analysis of the dimerization equilibria of water vapor [194]

provides an estimate for the bonding volume and association strength, $\delta V = 1\text{Å}^3$ and $\varepsilon/k_B = 1645\,\text{K}$ respectively. Our interaction energy corresponds to a hydrogen bond strength of $\varepsilon_{hb} \simeq 5.4\,\text{kcal/mol}$ [196] corrected for the differences in the zero-point energies of the monomer and dimer,

$$\begin{aligned} \varepsilon &= \varepsilon_{hb} + \frac{1}{2}\sum_{j=1}^{12} h\nu_j^{\text{dimer}} - \sum_{j=1}^{3} h\nu_j^{\text{monomer}}, \\ &\simeq 3.27\,\text{kcal/mol}, \end{aligned}$$

where h is Planck's constant and the ν_j correspond to the vibrational frequencies given by Xantheas and Dunning [172]. Finally, for comparison purposes we incorporate an empirically-derived temperature-dependent density $\rho(T)$ for water valid at one atmosphere from Kell [197]; deriving any such temperature dependence for ρ within Wertheim theory unfortunately does not seem feasible.

To assess the accuracy afforded by the theory, consider the second virial coefficient,

$$B_2(T) = -\frac{1}{2}\int d\mathbf{1}\, f(\mathbf{1}),$$

where $f(\mathbf{1})$ here is the Mayer f-bond. Since the virial expansion is valid in the low density limit, we expect that the leading correction term to the ideal gas law, *i.e.* $B_2(T)$, should be primarily determined by pair interactions, and therefore act as a good check on our parameter validity.[6] Splitting the Mayer f-function, Eq. (5.2), according to Wertheim theory, the second virial coefficient relation becomes

$$B_2(T) = N\left[\frac{2}{3}\pi R^3 - 8\,\delta V\left(e^{\beta\varepsilon} - 1\right)\right]. \tag{5.84}$$

The model $B_2(T)$ curve using the water-like parameters listed above is shown in Fig. 5.2 along with the experimental results reported by Eisenberg and Kauzmann [4]. The overall trend is captured by (5.84), but the lack of both repulsive softness (important at high T) and long range attraction (important at low T) is also evident. Given that $B_2(T) < 0$ in Fig. 5.2 the attractive part of the interaction potential must dominate the repulsive part, evident from Eq. (5.84) itself. Indeed,

---

[6]For long-range potentials like the Coulomb potential $B_2(T)$ diverges, as do higher-order coefficients, signifying that the equation of state is a non-analytic function of density.

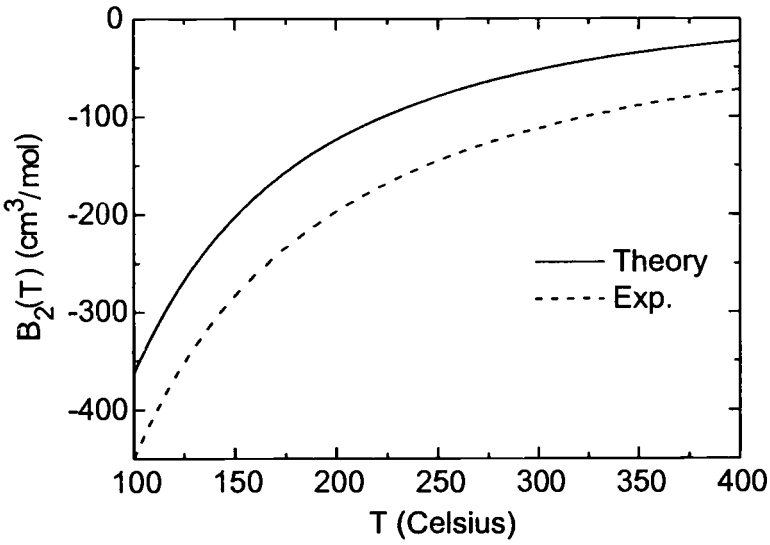

FIGURE 5.2. Second virial coefficient $B_2(T)$ from theory and experiment. The theory curve was determined using $\delta V = 1\text{Å}^3$ and $\varepsilon/k_B = 1645K$, with experimental values reported by Eisenberg [4].

---

the Boyle (reduced) temperature $T_B^* \equiv k_B T_B/\varepsilon$ —where $B_2(T)$ passes through zero— for our model system is roughly 0.5, well above the reduced temperature range in Fig.5.2 ($0.06 \lesssim T^* \lesssim 0.24$), indicating that the largest contribution to the discrepancy in the $B_2(T)$ curves arises from the omission of some attractive forces in our model.

These omissions, made from the outset, would tend to cause an overestimation of the system pressure, but the PY approximation also introduces errors into the equation of state, even for hard sphere fluids. In particular, the PY approximation does not satisfy thermodynamic self-consistency: it predicts differences between the compressibility and virial equations for hard spheres [198, 55], especially for densities greater than $\eta \gtrsim 0.3$. A comparison of the compressibility (C) and virial (P) hard sphere results using the PY and *hypernetted chain* (HNC) approximations is shown in Fig. 5.3. The inconsistency in PY results at large densities is apparent. Nonetheless, for a temperature independent hard core potential the PY approximation is better than the HNC, and is one of the reasons why we use the Percus–Yevick results for our water-like model, although we actually use the more accurate Carnahan–Starling equation for the hard sphere contribution to

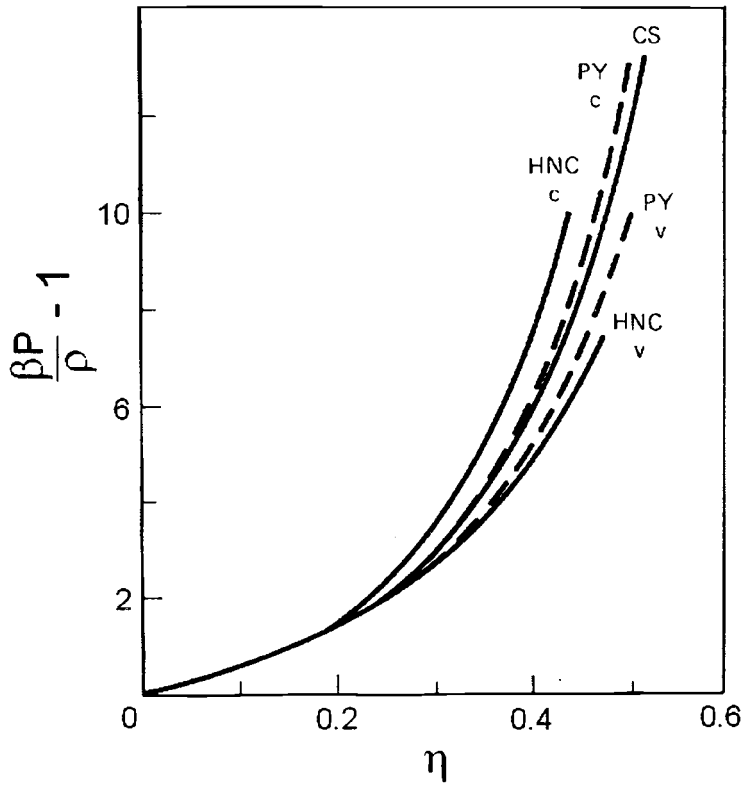

FIGURE 5.3. Comparison of hard sphere equations of state derived from compressibility and virial equations, both using the PY, HNC, and CS approximations. Compressibility curves are labelled with a C, virial curves with a V, and the Carnahan–Starling (CS) curve directly overlays the "exact" MD simulation results [136].

---

our system pressure,

$$\frac{\beta P}{\rho} = \frac{1 + 2\eta + 3\eta^2}{(1-\eta)^2},$$

which is simply a one-third to two-thirds linear combination of the virial (P) and compressibility (C) hard sphere PY results, respectively.

5.5.2. Pressures and Critical Behavior

In a practical sense, the ultimate test of any theory or model involves the equation of state. The generality of the Wertheim formalism allows for pressures

to be calculated through TPT and virial relations, as well as $S(k)$– and $c(r)$–based compressibility equations, providing a direct measure of thermodynamic self-consistency. In some cases model parameters, such as the hard core diameter, are adjusted in order to obtain a self-consistent solution for system properties, but in our case we take the model parameters as fixed values, and therefore thermodynamic self-consistency should not be expected.

5.5.2.1. Equations of State

With $\bar{f}$ determined by our system parameters and $y^{00}(R)$, Eq. (5.82), the density derivative in Eq. (5.37) can be evaluated to determine the TPT pressure P_{tpt}. Similarly, with Eq. (5.83) the spatial derivative in Eq. (5.71) can be evaluated to give the virial pressure P_{vir}. The resulting equations of state are

$$P_{tpt} = \rho k_B T \left[Z_{vir} - \frac{(1+2\eta)N_{hb}}{(1-\eta)(2+\eta)} \right], \tag{5.85}$$

$$P_{vir} = \rho k_B T \left[Z_{vir} - \frac{(1+2\eta)N_{hb}}{(1-\eta)(2+\eta)} + \frac{1}{24}\frac{(2-11\eta)[N_{hb}]^2}{2+\eta} \right], \tag{5.86}$$

where

$$Z_{vir} \equiv \frac{1+2\eta+3\eta^2}{(1-\eta)^2}$$

is the Carnahan–Starling compressibility factor. Surprisingly, both agree to first order in N_{hb}, and are relatively simple in form. This is to be compared to the compressibility-derived pressures P_{com}, which had to be numerically integrated from Eqs. (5.63) and (5.80). Yet, Eqs. (5.85) and (5.86) also show how sensitive the pressures are to association effects: the small differences inside the square brackets are multiplied by the very large factor $\rho k_B T$.

We compare all of our pressure results to the TPT and simulation results of Ghonasgi and Chapman [47], shown in Fig. 5.4. Their NPT Monte Carlo results were consistent with a bonding volume of $\delta V \approx 3.5 \times 10^{-3}\text{Å}^3$, and for this figure alone we use this value of δV. For small association energies, $\varepsilon/k_B T \simeq 2$, all theories give essentially quantitative results at low density values, but as η increases above ~ 0.30 the virial and TPT pressures begin to underestimate the simulation and compressibility values. This is consistent with the inherent omissions of the PY approximation and the similarity between Eqs. (5.85) and (5.86).

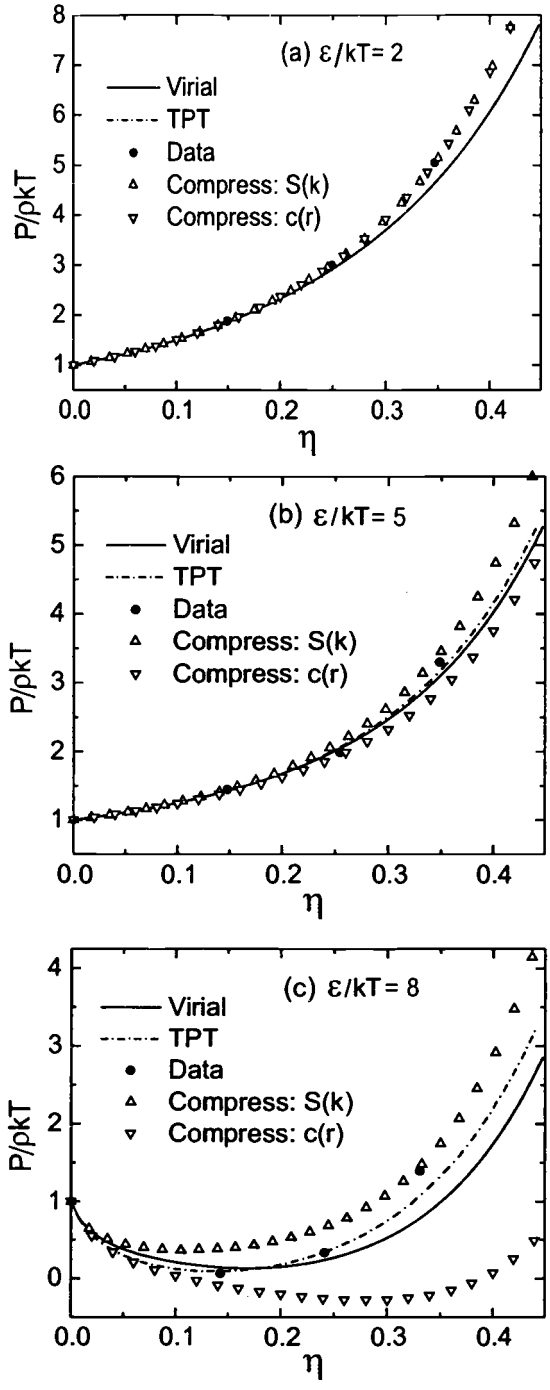

FIGURE 5.4. Reduced pressure $P/(\rho k_B T)$ versus packing fraction η for $\delta V = 3.5 \times 10^{-3}\text{Å}^3$ and association energies $\varepsilon/k_B T = 2$, 5, and 8 in (a), (b), and (c) respectively. The "Data" points • are NPT MC simulations [47], while the Δ and ∇ symbols represent numerically integrated compressibility pressures.

As ε increases further, Fig. 5.4(b), the disagreement between theories at high densities expands, with the largest shift occurring for the $c(r)$–based compressibility pressure; it now underestimates even the virial pressure. The significant increase in N_{hb} with density for $\varepsilon = 5$ shows up in the second-order effects of the virial equation, which now begins to underestimate the TPT and simulation results. Depending upon the representation used (see Table 5.1), this association strength may correspond to near-critical conditions. In the critical region very large fluctuations in the density occur which are manifested in the isothermal compressibility. Such effects could account for the disagreement here between both compressibility pressures and the virial, TPT, and simultion results. The actual split between the $c(r)$– and $S(k)$–derived pressures can be understood by looking at the functional differences between the two results: Eqs. (5.63) and (5.80).

At $\varepsilon/k_BT = 8$, Fig. 5.4(c), association effects are clearly dominant at all but the highest densities. At low densities and high ε/k_BT values —which corresponds to low temperatures, the influence of attractive forces is evident by the decrease in all pressures to values well below unity. None of the theories represent the simulation results quantitatively, although the TPT results clearly approximate them the best. The functional differences between the virial and TPT equations are also evident here, the two curves displaying a cross-over point around $\eta \simeq 0.18$. The compressibility results are the worst, although the $c(r)$–derived pressure is by far the worst of all, grossly underestimating the simulation results at nearly all densities and becoming negative for intermediate η values. The reasons for this "thermodynamic instability", *i.e.* negative pressure, are not entirely clear. For $\varepsilon/k_BT = 8$, the system is well below the critical temperature as calculated from the $c(r)$–based compressibility pressure: $\sim 410K$ (see Table 5.1 below). The negative pressures at intermediate η values may be indicative of a percolation transition —discussed in Section 5.5.6— wherein the fluid contains an infinite cluster instead of a distribution of branched aggregates. Yet the accuracy of the Percus–Yevick (or HNC) equation in the neighborhood of a phase change has been shown to be questionable [199–201, 142]. Figure 5.5 shows similar pressure behavior for an LJ fluid near it's triple point at $k_BT/\varepsilon = 0.72$, along with simulation and experimental results for liquid argon [198]. The large spread between our virial and $c(r)$–based compressibility results is consistent with the PY (V) and PY (C) results shown in the figure, although their PY (C) curve is more negative than ours

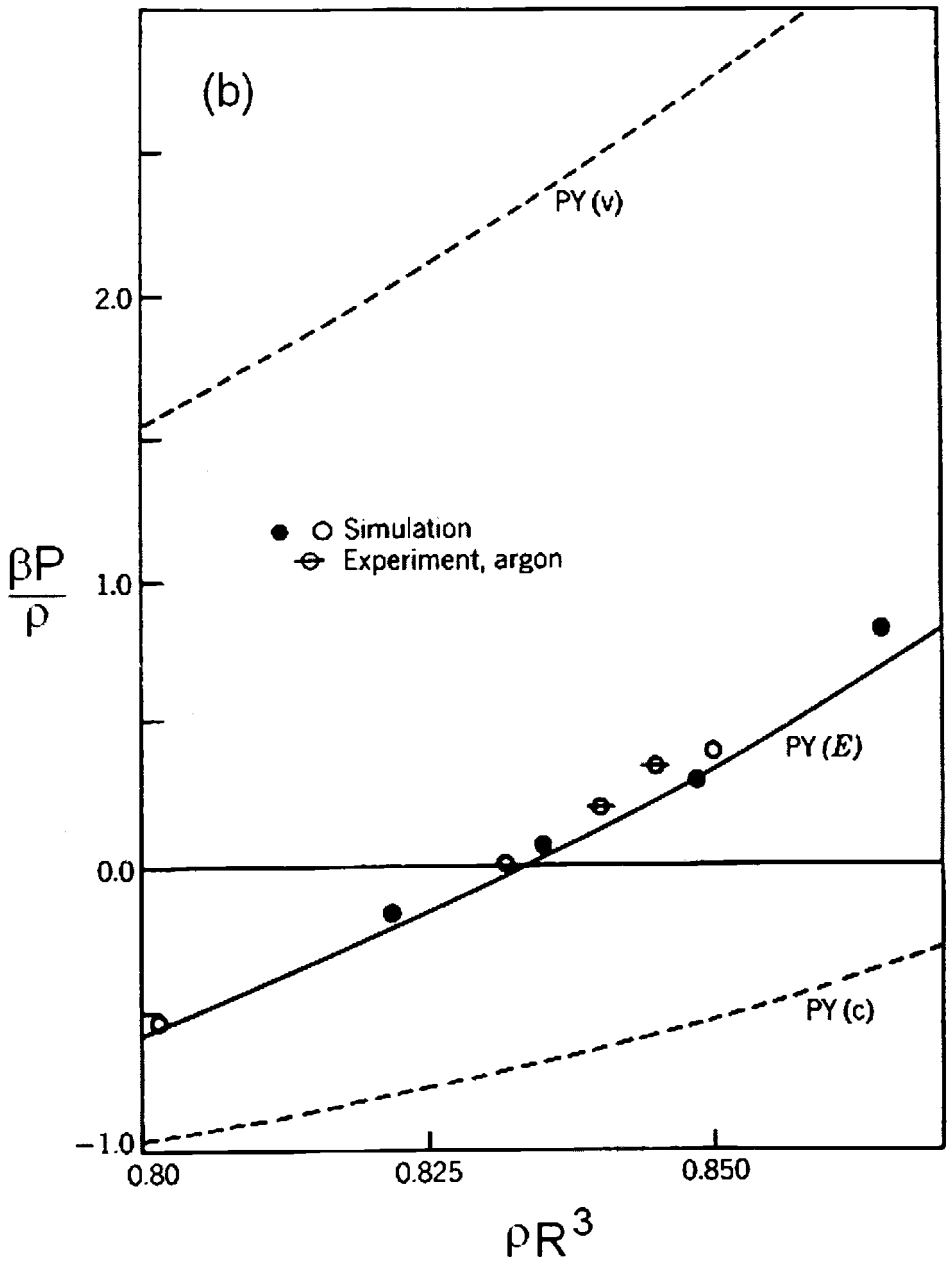

FIGURE 5.5. Percus–Yevick equations of state for an LJ fluid at $k_BT/\varepsilon = 0.72$ along with simulation and experimental results for argon. PY curves shown are from the virial (V), Helmholtz energy (E), and compressibility (C) equations [198].

in the same density range. Our TPT pressure curve most closely corresponds to the Helmholtz energy-derived curve PY (E) in the figure, and seems to confirm the semi-quantitative agreement with simulation suggested therein. The large positive values of the $S(k)$–based compressibility pressure at all densities stands in stark contrast to the $c(r)$–based results, but given the functional form of Eq. (5.80), coupled with the fact that $N_{hb} \leq 4$ at all densities, it is no surprise that this pressure cannot take on negative values, and thus greatly overestimates the simulation results.

It would appear, then, that a more thorough accounting of attractive forces, which we underestimated according to an analysis of $B_2(T)$, would seem to only worsen the thermodynamic instabilities of the equations of state, at least at intermediate association strengths, *e.g.* $\varepsilon \sim 8$. The theoretical equations of state, however, are mathematically correct as far as we can tell; their constituent parts, whether components of $c(r)$ or $g(r)$, illustrate the proper limiting behaviors. The discrepancies shown in Fig. 5.4 would thus seem to be indicators of the flaws inherent in the PY equation rather than arithmetic errors. The applicability of the PY approximation to anisotropic associating fluids is still somewhat unclear. In Section 5.5.6 some comparisons to the (isotropic) adhevise hard-sphere model of Baxter will be made, from which a few comments about the role of anisotropy can be made.

5.5.2.2. Critical Behavior

The isothermal compressibility κ_T for our water-like model was derived from Eq. (5.80), on the basis of the static structure factor, and is presented in Fig. 5.6 using a temperature-dependent density $\rho(T)$, empirically fit to water at 1 atm [197]. The density and temperature are both independent parameters within the theory, which unfortunately contains no obvious physical scaffold upon which a viable functional relation like $\rho(T)$ can be derived. Nevertheless, such a function is essential for an accurate comparison of the model to experimental and simulation results. As such we incorporate the empirical $\rho(T)$ given by Kell for the rest of our results —unless otherwise noted. It is this external $\rho(T)$, in fact, that is responsible for the temperature dependence of the hard sphere κ_T curve in Fig. 5.6 —recall that the hard core diameter R is a constant. The theoretical κ_T values in that

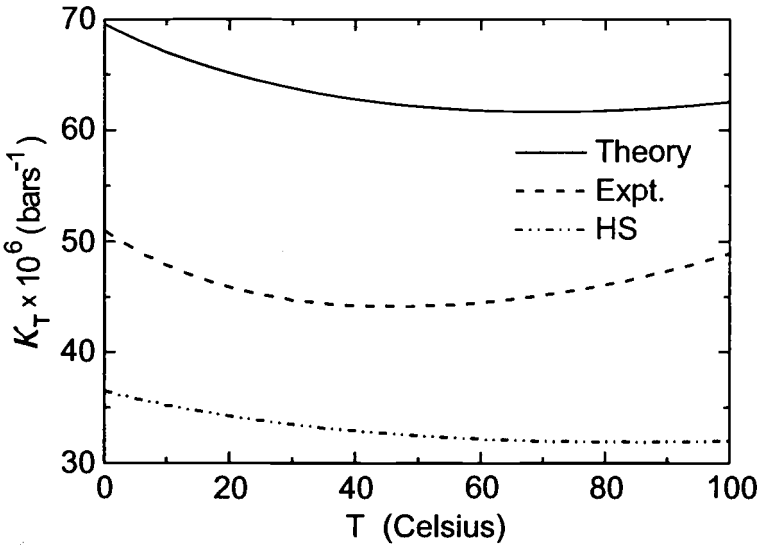

FIGURE 5.6. Variation of the isothermal compressibility κ_T with temperature. The theory includes an empirically-derived temperature dependent density $\rho(T)$ for water at 1 atm given by Kell [197].

---

figure are seen to be nearly twice as large as the hard sphere values over the entire temperature range, and lie well above experiment [4]. While the theory clearly overestimates the attractive contributions to κ_T, it does show the proper functional form, displaying a minimum, albeit shifted to higher temperatures: $T_{min} \simeq 80\,^{\circ}\mathrm{C}$ instead of approximately $47\,^{\circ}\mathrm{C}$. This is in agreement with previous theoretical work [187, 188] on primitive water models [202]. Likewise, κ_T can also be determined from the direct correlation function, Eq. (5.63), but, like the pressure derived from it, gives values in numerical disagreement with the other approaches.

The critical densities η_c and temperatures T_c were determined using the TPT, compressibility, and virial pressures (see Table 5.1 for details). On the basis of the derived T_c values, the liquid phase appears to be stable for temperatures less than $\sim 300\,^{\circ}\mathrm{C} - 350\,^{\circ}\mathrm{C}$ depending upon the representation chosen for the thermodynamic properties. Being that the present model omits dispersion forces, customarily responsible for the formation of the liquid phase, it is consoling that a liquid phase forms at all.

For a three-dimensional system, the PY equation predicts the existence of a critical point, as does our water-like model. In order to characterize the system behavior in this region, critical-point exponents can be derived. Generally, the

critical-point exponent λ for some function $f(\epsilon)$ is defined as

$$\lambda \equiv \lim_{\epsilon \to 0} \frac{\ln f(\epsilon)}{\ln \epsilon},$$

where ϵ serves as a dimensionless variable measuring the proximity to the critical point. For typical thermodynamic functions the actual relationship between f and ϵ can be complicated,

$$f(\epsilon) = A\epsilon^{\lambda}(1 + B\epsilon^{y} + \cdots), \qquad \{A, B, \ldots\} = \text{const.}$$

containing correction terms, but in terms of the limit above are usually written as

$$f(\epsilon) \sim \epsilon^{\lambda}.$$

For our liquid–gas transition the functions ϵ of interest are

$$\epsilon \equiv \frac{T - T_c}{T_c}, \quad \epsilon \equiv \frac{\eta - \eta_c}{\eta_c}, \tag{5.87}$$

and the pertinent critical exponents λ are δ and β, corresponding to the shape of the critical isotherm and coexistence curves respectively.

Along the critical isotherm T_c our pressure relations (5.85) and (5.86) are found to obey the relation

$$\frac{P - P_c}{P_c} \approx A\left(\frac{\eta - \eta_c}{\eta_c}\right)^{3}, \qquad A \simeq \begin{cases} 0.50 & \text{virial Eq.} \\ 0.61 & \text{TPT Eq.} \end{cases} \tag{5.88}$$

wherein $\delta = 3$. In order to derive the coexistence curve exponent β we must minimize the Helmholtz energy $A[\rho]$ subject to the constraint that the overall density

---

TABLE 5.1. Critical packing fractions η_c and temperatures T_c derived through virial, TPT, as well as $S(k)$– and $c(r)$–based compressibilities.

Critical Point Data					
Method:	**Compress.**		**Virial**	**TPT**	**Expt**
	$S(k)$	$c(r)$			
η_c	0.0685	0.166	0.07498	0.0842	0.116
T_c (°C)	197	410	306	355	374.4

is held constant. As discussed in Chapter 4, this is tantamount to minimizing the function W, given by [150]

$$\begin{aligned} W &= \frac{A(\rho,T) - A(\rho_c,T_c)}{V} - \mu_c(\rho - \rho_c)\,, \\ &= \sum_{n=2} \frac{1}{n!}\, w_n(T)(\rho - \rho_c)^n \end{aligned} \tag{5.89a}$$

where

$$w_n(T) \equiv \left(\frac{d}{d\rho}\right)^{n-2} \left[\frac{1}{\rho}\left(\frac{\partial p}{\partial \rho}\right)_T\right]. \tag{5.89b}$$

If we now follow these recipes using the virial equation of state, Eq. (5.86), we obtain

$$\frac{W(T,\eta)}{k_B T} \simeq 1.667\,\tau\left(\frac{\eta - \eta_c}{\eta_c}\right)^2 + 47.75\left(\frac{\eta - \eta_c}{\eta_c}\right)^4 + \cdots \tag{5.90a}$$

where

$$\tau \equiv \frac{\varepsilon}{k_B T_c}\left(\frac{T - T_c}{T_c}\right). \tag{5.90b}$$

Upon minimizing W with respect to density, we find that

$$\left(\frac{\eta - \eta_c}{\eta_c}\right)^2 \simeq -\tau \qquad T < T_c\,, \tag{5.91}$$

wherein $\beta = 1/2$.

These critical exponents $\delta = 3$ and $\beta = 1/2$ agree with the classical, *i.e.* mean-field, values and appear to be consistent with previous work; the PY solution for the adhesive hard sphere model, in fact, gives rise to an equation of state for the compressibility that leads to classical critical exponents [203]. The singular nature of the model does not appear to affect the critical behavior of the fluid. This is not entirely surprising, since as the critical point is approached, and long-range random fluctuations predominate, the specific form of the potential becomes masked in the asymptotic (universal) region of the correlation functions [204]. Moreover, the asymptotic behavior

$$c(r) \longrightarrow -\frac{u(r)}{k_B T}\,, \qquad \text{as } r \to \infty \tag{5.92}$$

has been shown [205] to be inherent to the PY equation

$$c(r) = g(r)\,[1 - \exp(u(r)/k_B T)] \tag{5.93}$$

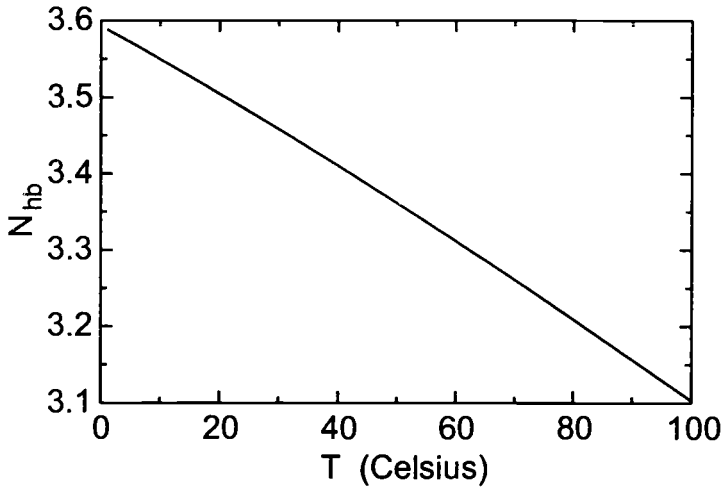

FIGURE 5.7. Average number of hydrogen bonds per paricle N_{hb} as a function of temperature using Kell's empirical $\rho(T)$ [197].

---

at any thermodynamic state. Hence, classical critical exponents associated with our use of the PY equation is not surprising. However, the scaling functions may depend upon the detailed shape of the potential [203]. Specifically, critical amplitudes W_{-}^{+} can be defined along the critical isotherm [206] according to

$$|(P/P_c) - 1| \approx W_{-}^{+}(\nu)^{\delta}, \quad \rho - \rho_c \to 0_{-}^{+},$$

where $\nu = (\rho/\rho_c)^{-1}$ and W^+ and W_- refer to $\nu > 0$ and $\nu < 0$ respectively. The asymmetry of the isotherm is then characterized by W_-/W^+, which for a van der Waals or classical theory is $W_-/W^+ = 1$, but which is found to be $W_-/W^+ = 34$ for the adhesive hard sphere model [203]. A similar asymmetry may be found for the sticky spot model.

5.5.3. Hydrogen Bonding

The bonding structure of our water-like model follows from the system parameters, *i.e.* from $\bar{f}$. As shown in Fig. 5.7, the average number of hydrogen bonds per particle $N_{hb}(T)$, following Eq. (5.27), ranges from about 3.6 at the freezing point to roughly 3.1 at the boiling point. For room temperature (25°C) water, Dang and Chang [207] find $N_{hb} \simeq 3.8$ for their MD simulations of a rigid,

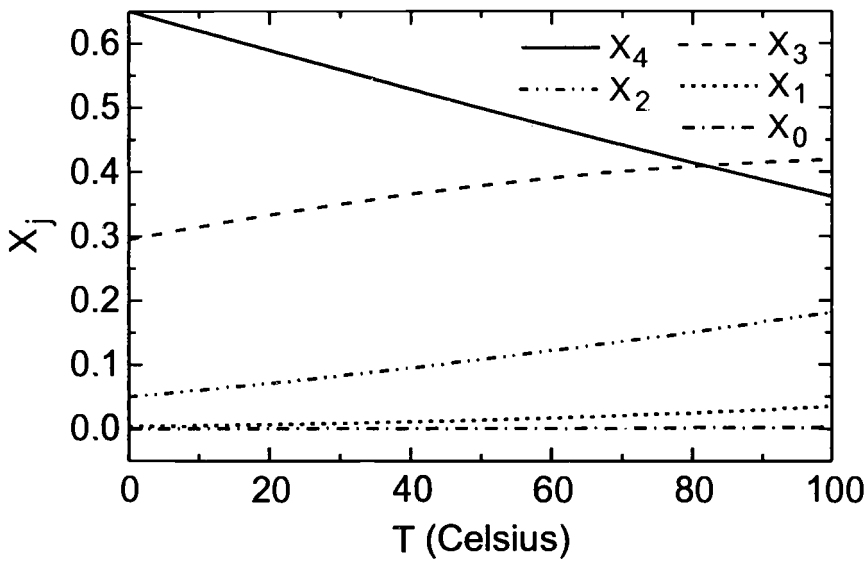

FIGURE 5.8. Average monomer mole fraction X_j with j incident hydrogen bonds as a function of temperature with the empirical $\rho(T)$ [197].

---

four-site polarizable model, in accordance with the neutron diffraction results of Soper and Phillips [195]. Our underestimation of the room-temperature N_{hb} by only $\sim 8\%$ stands as testimony to the elegance of Wertheim theory, especially given the primitive nature of our model compared to that of Dang and Chang, *e.g.* the infinitesimal range of our hydrogen bonding forces. That being said, quantitative comparisons can often be misleading because of differences in the definition of a hydrogen bond and the method of calculating N_{hb}. Dang and Chang, for example integrate $g_{\mathrm{OH}}(r)$ up to the first minimum in order to find N_{hb}. Wertheim theory, in contrast, allows direct calculation of N_{hb} from the self-consistent partial densities $\rho^{(j)}(\mathbf{1})$ —the $g(r)$ of our model most closely resembles the oxygen–oxygen radial distribution function $g_{\mathrm{OO}}(r)$ from such simulations.

The variation of these partial densities for the water model are shown in Fig. 5.8 as the average monomer mole fraction X_j, Eq. (5.28). The qualitative behavior is as expected, with a majority of monomers fully hydrogen bonded at the freezing point. As temperature increases X_4 accordingly drops while all other fractions X_j increase, particularly those doubly and triply bonded, X_2 and X_3 respectively. Above $T \simeq 82\,^{\circ}\mathrm{C}$ the majority of monomers are triply rather than of fully bonded. These theoretical results agree with the experimental fact that the relatively open, tetrahedral structure of ice largely remains intact in the liquid

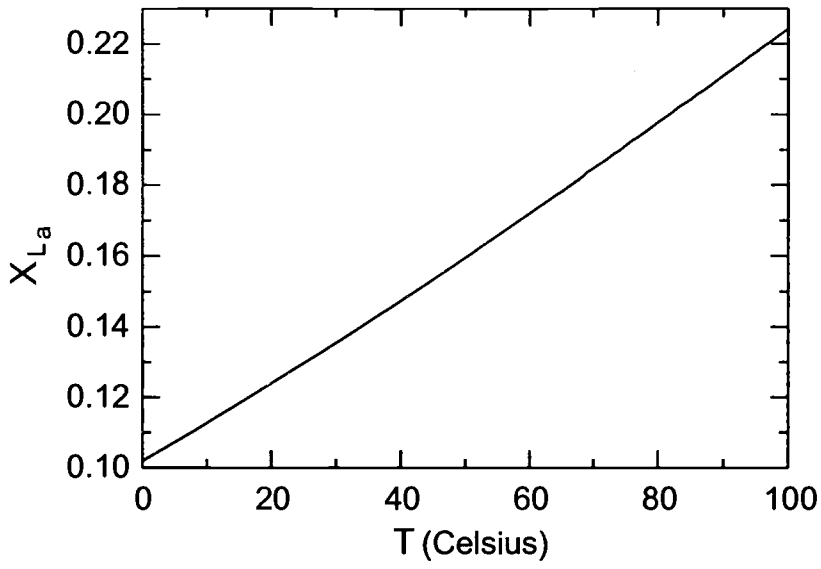

FIGURE 5.9. Average mole fraction of monomers with at least one *unbonded* attraction site as a function of temperature with the empirical $\rho(T)$ [197].

---

phase well above the freezing point, highlighting the import of hydrogen bonds in determining the properties of pure water and liquid mixtures.

The similarly related average mole fraction X_{L_a} of monomers with at least one *unbonded* attraction site, Eq. (5.29), is shown in Fig. 5.9. This fraction increases with temperature, but is relatively small around room temperature. As suggested by Section 5.2.2, X_{L_a} plays a more central role in determining the self-consistent partial densities than does X_j. It also plays a fundamental role in defining the mean cluster size of the system and the percolation threshold; this will be discussed in Section 5.5.6.

5.5.4. Energy Functions

The system internal energy follows from the TPT result (5.38) on page 149 and $\bar{f}$, Eq. (5.81),

$$\frac{E}{N} = 3k_BT - \frac{\frac{1}{2}\epsilon N_{hb}}{1-\exp(-\beta\epsilon)}, \tag{5.94}$$

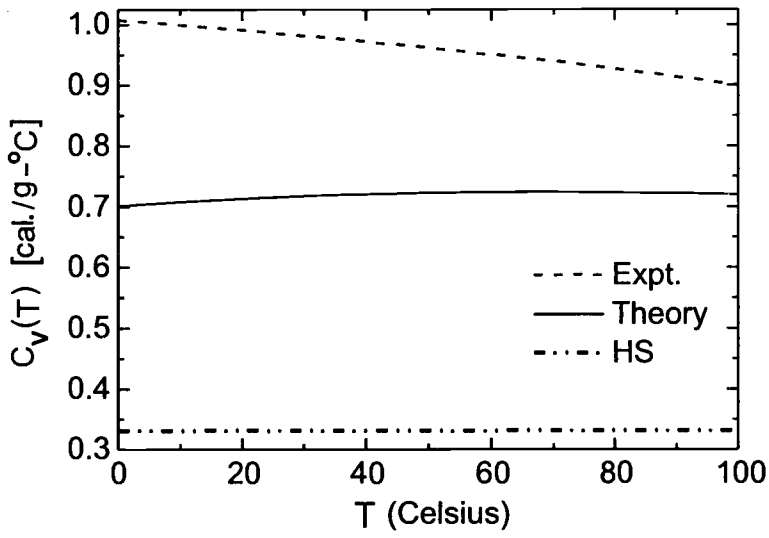

FIGURE 5.10. Temperature dependence of the constant volume heat capacity c_v. Experimental values were obtained from Eisenberg and Kauzmann for water at 1 atm [4]. Theoretical results are the TPT and the hard sphere (HS) curves.

---

and, as we have $N_{hb}(T)$ through Eq. (5.27) on page 146, the TPT heat capacity can be easily calculated as well,

$$c_v = \left(\frac{\partial E}{\partial T}\right)_V ,$$

$$\frac{c_v}{Nk_B} = 3 + \frac{1}{2}(\beta\varepsilon)^2 N_{hb} \frac{4\left[1-\exp(-\beta\varepsilon)\right] - N_{hb}\left[1+\exp(-\beta\varepsilon)\right]}{\left[1-\exp(-\beta\varepsilon)\right]^2 (4+N_{hb})} . \qquad (5.95)$$

Plotted in Fig. 5.10 is $c_v(T)$ for the TPT theory and a hard sphere fluid (which contains only ideal gas contributions to the energy), along with an experimental curve reported by Eisenberg and Kauzmann [4]. For water at 15°C, $c_p \equiv 1$ cal/g, and for historical reasons we present our c_v values in units of cal/g as well. TPT results yield c_v values roughly half way between those of hard spheres and experiment. Here again, we have evidence to the neglect of forces rather than technical details of the solutions of the matrix equations or thermodynamic self-consistency.

The latent heat of vaporization, $\Delta H = \Delta E + P\Delta V$, can be estimated without the need for numerical solution of liquid and gas coexistence densities, η_ℓ and η_g, by assuming that the vapor is ideal, *i.e.* consists primarily of free monomers. Moreover, since $V_g \gg V_\ell$, $P\Delta V$ can be approximated by its limit Nk_BT. With

the average number of hydrogen bonds in the liquid at boiling point, taken from Fig. 5.7, $N_{hb}(\ell) = 3.10$, and that for the gas approximated by $N_{hb}(g) \simeq 0$, we find that

$$\begin{aligned} \Delta H &\simeq N\left(\frac{1}{2}\varepsilon\left[N_{hb}(\ell) - N_{hb}(g)\right] + k_B T\right), \\ &\simeq 23.4\,\mathrm{kJ/mol}, \end{aligned} \tag{5.96}$$

compared to the experimental value of 40.7 kJ/mol [4]. Clearly, the errors and omissions in our treatment of attractive forces are apparent in this result. The existence of dimers in the gas (known to exist) would tend to lower γ, but nonetheless $N_{hb}(g) \ll 1$ and given the form of Eq. (5.96) the theory properly characterizes the reaction as endothermic, *i.e.* $\Delta H > 0$.

5.5.5. Surface Tension

The surface tension γ can be approximated by the same methods used in Chapter 4 [150],

$$\gamma \simeq \frac{3k_B T}{2}\frac{(\eta_L - \eta_G)^2 m^2(T)}{\xi R^3}, \tag{5.97}$$

which we do not write in dimensionless form here for ease of comparison with experiment. As before, $m^2(T)$ is an integral of the direct correlation function,

$$\frac{m^2(T)}{R^2} = \frac{1}{6v_0R^2}\int d\mathbf{r}\, r^2 c(r),$$

which becomes

$$\frac{m^2(T)}{R^2} = \frac{1}{20}\frac{(16 - 11\eta + 4\eta^2)}{(1-\eta)^4} + \frac{N_{hb}}{60}\frac{(\eta^2 - 2\eta + 10)}{\eta(1-\eta)^3} + \frac{N_{hb}^2}{320}\frac{(2\eta - 5)}{\eta(1-\eta)^2} \tag{5.98}$$

after inserting Eqs. (5.61a)–(5.61c) for $c(r)$.

The bulk correlation length ξ, again, is defined in our square gradient treatment through the hyperbolic tangent interface profile,

$$\rho(z) = \rho_\ell - \frac{(\rho_\ell - \rho_g)}{1 + \exp[z/\xi]}, \tag{5.99}$$

which gives

$$\xi = \frac{m(T)}{(\eta_L - \eta_G)(\omega/v_0)}. \tag{5.100}$$

TABLE 5.2. Bulk correlation length and surface tension values for water at 25°C and 1 atm from theory, simulation, and experiment.

WATER INTERFACE PROPERTIES		
$T = 298\,\mathrm{K}$	**Theory**[§]	**Expt**[†]
ξ (Å)	0.60	1.6
γ (mJ/m^2)	36.5	72

[§] $N_{hb} = 3.48$; $\omega/v_0 = 10$; $\eta_\ell \simeq 0.383$; $\eta_g = 0$
[†] ξ from MC simulations [150]
γ from capillary measurements [207]

Recall that ω is related to the third density derivative of the pressure,

$$\frac{\omega}{v_0} = \sqrt{\frac{1}{12\eta_c}\left(\frac{\partial^3 \beta p v_0}{\partial \eta^3}\right)_c} \,, \tag{5.101}$$

and is to be evaluated at the critical point. Using the derived parameters for water at 298K in Eqs. (5.97) and (5.100), we find, in Table 5.2, surface tension and bulk correlation length values roughly 50% less than experimental [150] and simulation [207] results, respectively. Given our omission of some attractive forces it is not surprising that our surface tension is below that of experiment. However, this is not consistent with our intrinsic interface width ξ, which predicts a much sharper profile than that found by Dang and Chang's simulation results [207]; a sharper interface should correspond to a higher γ value.

5.5.6. System Structure

Apart from the specific (monomeric) structural informational somewhat naturally contained within the Wertheim theory, *e.g.* X_j and N_{hb}, more general structural information is obtainable from solution of the AOZ integral equation. Aided by the simplifications of the PY and INA, solutions for the model distribution functions are possible, including an analytical form for the static structure factor $S(\kappa)$ —which no one else seems to have presented before for the four-site sticky spot model. From this $S(k)$ we are able to calculate the radial distribution function $g(r)$, as well as the system coordination number $n(r)$. Current results generally agree with similar theoretical and simulation work on the four-site model

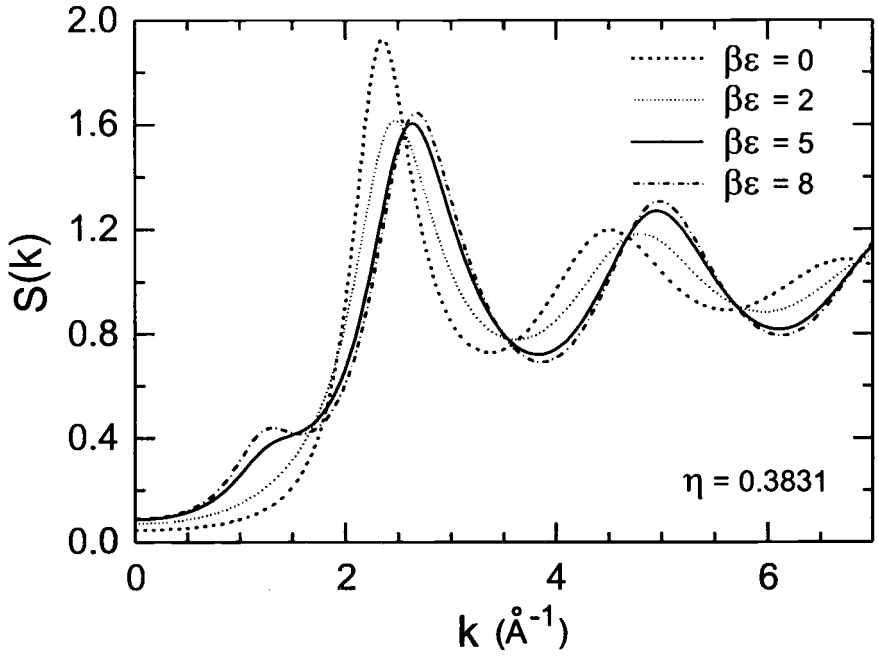

FIGURE 5.11. Variation of the structure factor $S(k)$ with association strength $\beta\varepsilon$ at fixed density. All association strength curves $\beta\varepsilon = 0$, 2, 5, and 8 are plotted using $\eta = 0.3831$.

[105, 190, 189, 47, 191], and the link between the liquid–gas transition and the (structural) percolation transition will be briefly discussed.

5.5.6.1. Structure Factor

The static structure factor $S(k)$ for our water-like model at 25 °C proceeds by evaluation of Eq. (5.78a) on page 162. The effects of association can be seen in Fig. 5.11 through the variation of $S(k)$ with association strength $\beta\varepsilon$ at fixed density, chosen as $\eta = 0.3831$, or the density of water at 25 °C. As $\beta\varepsilon$ increases from its hard sphere value of 0, we see changes at all k values. Initially there is a general outward shift of all $S(k)$ peaks, followed by an increase in magnitude of the second and higher-order peaks, marking the change in short range correlations resulting from the local ordering and the singularity in the F-bond. Any increase in $\beta\varepsilon$ beyond about 5 appears to mainly increase the oscillation amplitudes at high k values. The changes in $S(k)$ for $k \lesssim 3\,\text{Å}^{-1}$ however, are, more drastic. As association increases the magnitude of the first peak drops and shifts inward

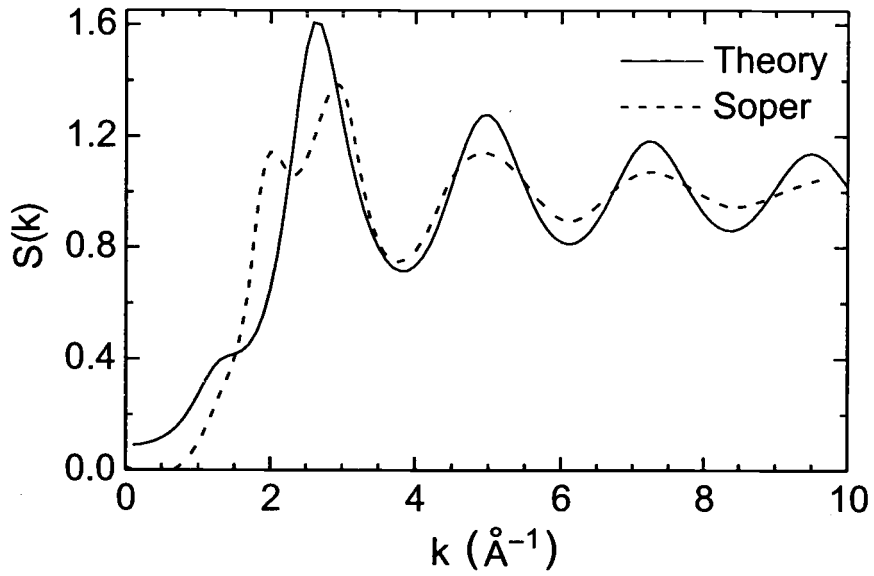

FIGURE 5.12. Structure factor $S(k)$ for water at 25 °C and 1 atm from the present (analytical) theory and the experimental results of Soper [210]. The theory curve uses the empirical $\rho(T)$.

---

quickly, while a "shoulder" or pre-peak forms in the range $1\,\text{Å}^{-1} \lesssim k \lesssim 2\,\text{Å}^{-1}$. The location of the pre-peak shifts to lower k values as $\beta\varepsilon$ increases, with a value around $k_p \simeq 1.35\,\text{Å}^{-1}$ at $\beta\varepsilon = 8$. These results are consistent with that found by Vakarin *et. al.* [105, 208, 209], and indicate the increase in intermediate-ranged correlations reflecting the size and connectivity of the molecular clusters present. Variations in density at fixed association strength, on the other hand, appear to affect $S(k)$ only at small k values, less than about 1.5 Å^{-1}. The pre-peak significantly increases in magnitude as η decreases towards gas phase values, and shifts to smaller k values, although the actual $S(k=0)$ limit follows the relation

$$S(k=0) \;=\; \frac{(3N_{hb}+8)\,(N_{hb}-8)\,(1-\eta)^4}{\left[3N_{hb}\,(\eta^2-3\eta+1)-16\eta-8\right]^2}\,, \tag{5.102}$$

where Eq. (5.26) has been used for N_{hb}. The thermodynamic stability condition implied by (5.102) above contains an intrinsic temperature dependence as expected, *i.e.* $N_{hb} \propto \bar{f} \propto \exp[\beta\varepsilon]$, unlike the analogous hard sphere relation Eq. (5.79). Yet our use of a temperature dependent density $\eta(T)$ introduces an external temperature dependence into the stability relation. From the plot of $S(k)$ above, however,

it would appear that the liquid phase is thermodynamically stable over the range of association values shown. Over the small range of values $\eta(T)$ assumes for liquid water as T varies from 0 °C to 100 °C, the changes in $S(k)$ are negligible, including the pre-peak.

Early experimental work demonstrated the existence of a split peak in the structure factor of water [211]; however, we compare our theoretical $S(k)$ results with the more recent X-ray data of Soper [210], both of which are plotted in Fig. 5.12 for water at 25 °C at 1 atm. The similarity between the theoretical pre-peak and the split peak of the experimental data is encouraging. The ratio of distances between the "first" and second peaks for both curves is approximately 1.6, although the pre-peak obviously occurs at lower k values and is diminished in magnitude compared to that of experiment. Using $R = 2.8\,\text{Å}$ as the molecular diameter, at 25 °C, the model pre-peak or "shoulder" is located around $k_p \simeq 1.4\,\text{Å}^{-1}$ as opposed to $k_p \simeq 2\,\text{Å}^{-1}$ for the water curve. The sharper and better developed first peak in the experimental data implies a comparatively more narrow equilibrium distribution of smaller cluster sizes in real water. The broad shape of the theoretical pre-peak at room temperature conditions may indicate a wide distribution of relatively large clusters (*e.g.* branched chains), but the pertinent physical mechanisms involved are not yet clear; certainly the intermediate-ranged correlations implied by Fig. 5.12 are not necessarily unique to any one possible liquid structure. Similar pre-peaks have been found in other network-forming fluids, but also in systems like polymer chain and ionic fluids, which are not expected to form network structures (see [105] and references therein). Other evidence has suggested that a four-fold coordinated network is one possible origin of these correlations [212, 213, 208, 209].

The formation of a pre-peak in $S(k)$ for the four site sticky spot model, nonetheless, stands in contrast to the theoretical and simulation results found for the (isotropic) adhesive hard sphere model [214], which exhibits no such feature — although it does indicate a divergence at $k = 0$ as the spinodal line is approached. This functional difference suggests that, even though our four attractive sites act independently and are orientationally averaged, at least some water-like steric effects are properly accounted for. It is also true that the PY approximation does not properly account for the positional correlations attributable to large rigid clusters [214], and the INA, apart from omitting ring structures, is only qualitatively

correct at low temperatures, *i.e.* when X_{L_a} is small. These factors may explain, at least in part, some of the disagreement between theory and experiment. The close agreement between the MD simulations of Dang and Chang [207] and the X-ray measurements of Thiessen and Narten [215] for $S(k)$, *i.e.* concerning the split first peak, further suggests that rigid orientational effects may play an important role in the structure of $S(k)$, as well as the fact that more complex interactions may need to be included in the model: the rigid, four site model of Dang and Chang includes many-body (polarization) effects and ring structures. Some evidence suggests that the pre-peak may involve a structural percolation transition [189, 188, 216–218, 190], and will be briefly discussed in Section 5.5.6.4.

5.5.6.2. Radial Distribution Function

Given the "atomic" nature of our primitive model for water, with conical attractive wells centrally located in hard spherical cores, our theoretical radial distribution function $g(r)$ most closely resembles the experimental atomic oxygen–oxygen radial distribution function $g_{OO}(r)$, and it is this function with which we compare our theoretical results. In the present model $g(r)$ is represented in a disjointed fashion, containing two parts, one arising from the singular "sticky-spot" contribution $g^{sing}(r)$ and the other from the more smooth background $g^{smth}(r)$,

$$g(r) \;=\; g^{sing}(r) \;+\; g^{smth}(r)\,. \tag{5.103}$$

The factorization solution to the AOZ relation provided only the contact value $g^{smth}(R)$ [Eq. (5.60)], but we can obtain $g(r)$ for $r > R$ by a numerically delicate inverse Fourier transform of $S(k)$ [Eq. (5.78a)],

$$g(r) \;=\; \frac{1}{(2\pi)^3\rho}\int d\mathbf{k}\,\exp[-i\mathbf{k}\cdot\mathbf{r}]\,(S(k)-1)\;.$$

By the application of Eq. (5.59) on page 156 we find that

$$g^{sing}(r) \;=\; \frac{N_{hb}\,\delta(r-R^{+})}{4\pi r^2\rho}\,, \tag{5.104}$$

which serves as a defining relation for the average number of hydrogen bonds

$$N_{hb} \;=\; \rho\int_{R^{-}}^{R+} d\mathbf{r}\; g^{sing}(r)\,. \tag{5.105}$$

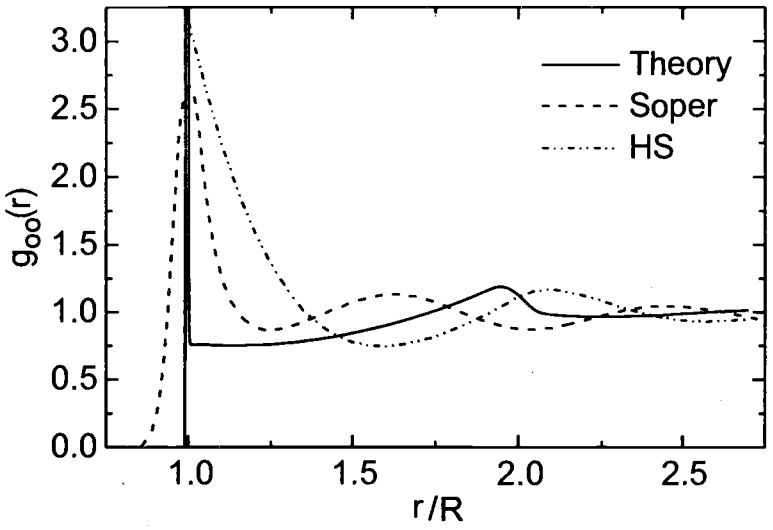

FIGURE 5.13. Comparison of radial distribution functions $g(r)$ for water at 25°C and 1 atm from PY-hard sphere theory, the present theory, and the neutron data of Soper [210]. The delta-function contribution to the theoretical $g(r)$ at $r/R = 1$ has been exaggerated for clarity.

The discontinuity in our $g(r)$, clearly evident in Fig. 5.13, reflects the pathological nature of the sticky spot model itself, where both attractive and repulsive forces are represented by delta-functions. Comparing our results with the experimental $g_{OO}(r)$ of Soper [210] obtained from neutron scattering data, along with the Percus-Yevick hard sphere curve, we see that our theoretical $g(r)$ displays some qualitative features resembling water —albeit in a decidedly crude manner. The first peak in $g(r)$ generally describes the number of nearest neighbors, which, for associating fluids includes the number of *bonded* neighbors; hence this peak is often referred to as the *intramolecular* peak. Our singular function $g^{sing}(r)$ uniquely describes the bonded contribution, *i.e.* the average number of hydrogen-bonded neighbors N_{hb} as the area under the delta-function contact peak (at $r/R = 1$), Eq. (5.105), with a precision dictated by $\bar{f}$ and therefore dependent upon the model parameters R, ε, and δV. The non-bonded contribution to the first peak and all higher-order peaks in $g(r)$ —which describe correlations at larger separations— is contained in our smooth contribution $g^{smth}(r)$; for an associating fluid these peaks are often referred to as *intermolecular* peaks.

Comparing, for the moment, the PY hard sphere and experimental radial distribution function curves in Fig. 5.13, we see that the formation of hydrogen bonds in water, which carry tetrahedral symmetry, corresponds to a structural re-ordering of the hard sphere fluid into a more open (tetrahedral) arrangement, wherein the number of (close-packed) nearest neighbors is reduced.[7] The depletion of non-bonded nearest neighbors with the concomitant increase in bonded neighbors (up to a maximum of four for water) correspondingly decreases and narrows the first peak in $g_{OO}(r)$ as compared to the hard sphere fluid. The exact height and shape of this peak is governed by the large wave vectors ($k \gtrsim 7.0\,\text{Å}^{-1}$) of $S(k)$. Accompanied by the formation of hydrogen bonds is a structural re-ordering which occurs in the more distant environment. The second coordination shell or intermolecular peak for water shifts inward from the hard sphere position to roughly $2R\sin(\frac{1}{2} \times 109° 28')$, or $r = \sqrt{8/3}\,R \simeq 1.63R$, and arises from "attaching" additional triply-bonded particles to a tetrahedral cluster. Less noticeable in Fig. 5.13 is that the oscillations in $g_{OO}(r)$ decay towards unity more rapidly than the hard sphere curve as the equilibrium liquid structure becomes uniform, indicating shorter-ranged correlations than in the hard sphere fluid.

The non-singular function $g^{smth}(r)$ displays, in Fig. 5.13, some of this local structural ordering that occurs in water. Having "lost" the delta-function bonding contribution, $g^{smth}(r)$ shows a contact value less than unity and a weak dependence on r, with a broad shallow minimum between the intra– and intermolecular peaks, in qualitative agreement with the Monte Carlo simulations[8] of Bratko *et. al.* [60]. This reflects the depletion of non-bonded nearest neighbors next to the central molecule, or an open structural order characteristic of hydrogen-bonded liquids. The full structural re-ordering consistent with real water, however, is clearly lacking in the present model. The location of the second peak or coordination

---

[7]The densest packing of equal spheres occurs when each has twelve nearest neighbors, in either a face-centered cubic (FCC) or close-packed hexagonal (CPH) lattice. For a simple liquid near its freezing point n is typically around 10 or 11, although there is no unique definition for the coordination number n in a liquid.

[8]The models used by Bratko *et. al.* consist of extensions of the SP1, SP2, and SP3 models: hard spheres with a point dipole and an embedded, narrow tetrahedral octupole potential formed by spherical harmonics.

shell, although shifted inward to lower r values, is still closer to $r \simeq 1.9R$ than $1.63R$, as true tetrahedral order would dictate. Duda *et. al.* [190] contend that this disagreement is the direct result of the absence of rigid tetrahedral symmetry in the four-site, sticky-spot model. Their conclusion is based upon MC simulations which purportedly include the rigid, tetrahedral orientation of the attraction sites, and is apparently in agreement with the water-like structure found by Kolafa and Nezbeda [191], even at low temperatures and densities.

Duda's simulation results for the four-site model have further indicated that the gap between the intra– and intermolecular peaks in $g(r)$ increases with increasing association strength or density, consistent with the increase in N_{hb} and mean cluster size S predicted theoretically [105, 219, 220]. This association and density-dependent shift of the intermolecular peak is not accurately represented by the current theory, and from such a comparison can be linked to the orientational averaging over attraction sites. The angle averaging also affects some other density-related behavior of $g(r)$. Duda's simulations suggest that as η is increased at fixed $\beta\varepsilon$, the oscillations in $g(r)$ are enhanced along with an increase in the contact peak; while our N_{hb} accounts for contact peak changes, angle averaging over dampens oscillations in $g^{smth}(r)$, especially outside the second peak, as is visible in Fig. 5.13. Beyond the intermolecular peak, $r \gtrsim 2$, the current model predicts a more uniform fluid than found experimentally. In contrast, as $\beta\varepsilon$ increases at fixed density η, simulations indicate an increase in the intramolecular peak (as N_{hb} does), but a decrease in the oscillatory behavior of $g(r)$. As such, the theory seems more able to account for changes in association strength than in density. It should also be noted that the singular nature of the model turns up as an asymmetry in the second peak of $g(r)$ —visible in Fig. 5.13. This asymmetry or discontinuity has been linked to the difference between the average number of bonded and non-bonded nearest neighbors [190] and becomes more discontinuous as $\beta\varepsilon$ increases.

Indeed, it appears that the connectivity constraints of the model, coupled with the water-like steric effects (SBC and SI-2W), begins to account for association-related changes in $g(r)$, *e.g.* the behavior the central peak or N_{hb}, the general exclusion of non-bonded neighbors, and the onset of a local structural reordering marked by the inward shift of the second peak. Yet it is a crude beginning, and fails to account for some density-related shifts which seem to be intricately tied to the tetrahedral orientation of attraction sites. Angle averaging effects clearly

limit the structural ordering of the model fluid, and hence limit the accuracy of $g(r)$. Although informative, use of this $g(r)$ to determine system properties is obviously not recommended.

5.5.6.3. Coordination Number

Some of the structural information available from the radial distribution function is the average number of particles, of type α for example, that surround a particle of type β at the origin out to some distance r,

$$n_{\alpha\beta}(r) \;=\; \rho_\beta \int_0^r d\mathbf{r}'\; g_{\alpha\beta}(r')\,, \tag{5.106}$$

known as the *partial* coordination number (α and β refer to particle types here, instead of attraction site labels). There is no unique value for r used to define the coordination number; often r is taken as the location of the first minimum in $g_{ij}(r')$, giving the number of nearest neighbors, but even then there is no unique method for evaluating the integral. For our unary model system the obvious simplification of (5.106) is

$$n(r) \;=\; \rho \int_0^r d\mathbf{r}'\; g(r')\,, \tag{5.107a}$$

into which we insert Eq. (5.103) to immediately obtain

$$n(r) \;=\; N_{hb} \;+\; \rho \int_0^r d\mathbf{r}'\; g^{smth}(r')\,; \tag{5.107b}$$

looking at Fig. 5.13 again, we note that for $r \lesssim 1.5R$, the wide, shallow minimum of $g_{smooth}(r)$ allows us to make the approximation $g_{smooth}(r) \approx g(R)$, which is given by Eq. (5.60) on page 157. Integrating (5.107b) then, we obtain the approximate coordination number for our sticky spot model

$$n(r) \simeq N_{hb} + 8\eta g(R)\left[(r/R)^3 - 1\right]\,, \qquad r \lesssim 1.5R\,. \tag{5.107c}$$

As expected, the hard sphere, singular nature of the model shows up here as well, with $n(r)$ abruptly increasing from zero to N_{hb} at $r = R$. This stands in contrast with soft core potential models.

Our present result for the running coordination number is plotted in Fig. 5.14, along with results from the $n_{OO}(r)$ obtained by Duh *et al.* [221] using the *hypernetted chain approximation* (HNC), from Pettitt and Rossky's [182]

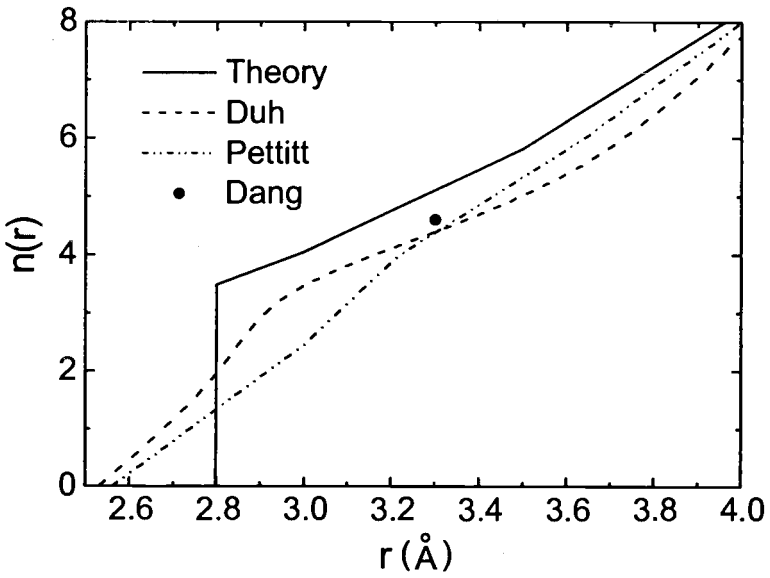

FIGURE 5.14. Running coordination number $n(r)$ for water at 25°C and 1 atm pressure. Also shown are the experimental value, 4.6, of Dang and Chang [207] and the simulation results of Duh [221] and Pettitt [182]. The model molecular diameter is $R = 2.8$Å.

---

simulations using the MCY potential, and a data point from Dang and Chang's [207] MD simulations. In comparing these curves the effective "molecular" diameter [or the location of the first minimum in $g(r)$], of course, should be considered. For example, Dang and Chang integrated their $g_{OO}(r)$ up to $r = 3.3$Å, with an effective molecular diameter of $R \simeq 3.23$Å; hence their *nearest neighbor* value of 4.6 is actually greater than our theoretical contact value of $n(R) = N_{hb} \simeq 3.5$. Apart from the singularity at hard core contact, therefore, the basic variation of the running coordination number $n(r)$ is sensibly portrayed by the present theory out to approximately $r \simeq 1.5R$, and is consistent with our underestimation of N_{hb}. A coordination number less than five (corresponding to integration over the first $g(r)$ peak) is indicative of the open, ice-like tetrahedral structuring of liquid water [222].

5.5.6.4. Percolation?

Our analysis of the four-site, sticky-spot model in the preceding sections has predicted a thermodynamically stable liquid phase that consists mainly of three– and four-coordinated monomers within a temperature range of 0 °C – 100 °C. Yet the question remains as to whether this liquid consists of some distribution of tree-like aggregate structures or a single, infinite cluster. This latter possibility corresponds, in some sense, to a gelation or "structural" percolation transition. It has been postulated that the formation of a pre-peak (low k values) in $S(k)$ may correspond to just such a structural transition [191, 189].

Within Wertheim theory proper, information about the distribution of s-mer structures is limited when three or more attraction sites are involved, *i.e.* when chain branch points are possible. The partial densities $\rho^{(m)}$ record the average *connectivity* of the monomers in the fluid, but do not contain enough information to uniquely define any particular distribution of aggregate sizes; there are many different s-mer configurations for any given set of X_j values. When only linear chain structures are possible, a purely statistical analysis can provide a definition of mean aggregate size, and this approach is, in fact, that taken by Ghonasgi and Chapman [47]. Defining a mean cluster size S by which to judge the size distribution of branched chains, and its divergence at percolation, requires an extension of the standard formalism.

Coniglio *et. al.* [223] were one of the first to develop a PY-like analytical calculation of mean cluster sizes and percolation behavior of fluids. Connectivity in systems with central attractive potentials have been widely studied (see [189]and references therein), including the adhesive hard sphere model [224]. For chain-like fluids RISM [225, 226] as well as Wertheim methods [19–22, 156, 227] have been used to study monomer connectivity properties, while evidence of a percolation transition in a network-forming system was found through MD studies on the ST2 model of water [216–218]. Kolafa and Nezbeda [191] as well as Vakarin *et. al.* [189] have specifically addressed this relation between percolation and the liquid–gas phase transitions for the four-site, sticky-spot model.

Kolafa and Nezbeda, using Wertheim-based TPT, looked at the existence of a percolation threshold for primitive models of water, ammonia, and methanol[9] under the Cayley tree approximation. Their numerical results show that systems with only one interaction site of either kind (*e.g.* ammonia has only one electron lone pair site and methanol only one hydrogen site) do no posses any percolation threshold; such fluids can be treated as mixtures of finite-sized hydrogen bonded clusters interacting through hard core repulsion in a single fluid phase (no condensation). Hydrogen bonding in these systems, they contend, may be accurately treated as a perturbation. Water, in contrast, with two sites of each kind, displayed a percolation transition and therefore a liquid–gas critical point.

Vakarin *et. al.* [189] simply extended the Wertheim graphical formalism in their definition of mean cluster size. They analyzed percolation in the four-site model through integral equation rather than TPT methods by reformulating the Wertheim AOZ relation in terms of "cluster connectivity". Cluster size in their approach is obtained by extracting from each partial correlation function the subset of graphs which contain *at least* one unbroken F-bond path between the root points; this corresponds to a regrouping of the correlation function graph sums. These graphs define *pair connectedness* functions, denoted by a superscript dagger †, that they then use to analytically calculate a mean cluster size S,

$$\begin{aligned} S &= 1 + \rho \int d\mathbf{r}\; g^{\dagger}(r)\,, \\ &= 1 + \rho \lim_{k \to 0} \tilde{g}^{\dagger}(k)\,, \end{aligned} \tag{5.108}$$

which, in k-space, can be expressed through the auxiliary functions defined by the AOZ factorization solution,

$$\begin{aligned} S &= 1 + 8\rho X_{L_a}^2 \\ &\quad \times \lim_{k \to 0} \left\{ \left(\left[\boldsymbol{q}(k) \boldsymbol{\sigma} \boldsymbol{q}^T(-k) \right]^{-1} - \boldsymbol{\sigma} \right)^{00} + \left(\left[\boldsymbol{q}(k) \boldsymbol{\sigma} \boldsymbol{q}^T(-k) \right]^{-1} - \boldsymbol{\sigma} \right)^{10} \right\} . \end{aligned} \tag{5.109}$$

Comparing this result to our $S(k)$, Eq. (5.74), it is apparent that extra graph terms have been included in this pair connectedness analysis. After insertion of

---

[9]Methanol, CH_3OH, is a non-spherical molecule, and was modelled as a fused, homonuclear hard sphere dumbbell.

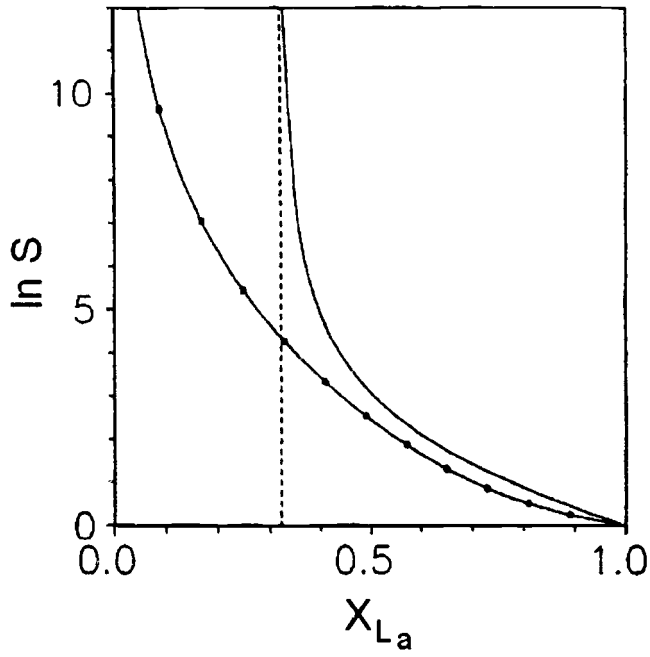

FIGURE 5.15. Mean cluster size $\ln S$ as a function of X_{L_a}. The solid line is S as derived by Vakarin *et. al.* [189] while the dotted solid line is that of Ghonasgi and Chapman [47]. The vertical dashed line marks the percolation threshold $X_{L_a} = 1/3$ given by Vakarin *et. al.* .

---

the auxiliary functions and simplifying, Vakarin and co-workers find their mean cluster size to be

$$S = \frac{4\left(4 + X_{L_a} - 2X_{L_a}^2\right)}{3\left(1 - 6X_{L_a} + 9X_{L_a}^2\right)}, \qquad \text{Vakarin } \textit{et. al.} \quad [189] \qquad (5.110a)$$

as compared to the TPT results of Ghonasgi and Chapman:

$$S = \frac{3X_{L_a}^3 - 3X_{L_a}^2 + 1}{X_{L_a}^4\left(1 - X_{L_a}^2 + X_{L_a}^3\right)}, \qquad \text{Ghonasgi \& Chapman} \quad [47]. \qquad (5.110b)$$

Again, the latter is based upon a straight statistical analysis of monomer connectivity and ignores branched chains. Given the values of X_3 and X_4 at room temperatures (see Fig. 5.8 on page 176), Eq. (5.110b) would seem to be quite a crude estimate for S. Nevertheless, at high temperatures (X_{L_a} values), where TPT is more accurate, this definition gives results which agree well with the MC simulation data of Ghonasgi and Chapman. Meanwhile, the S values predicted by Eq. (5.110a) tend to overestimate the MC simulation data at intermediate X_{L_a}

values, but agreement improves as $X_{L_a} \rightarrow 1$. This has been attributed to the use of the PY approximation in deriving Eq. (5.110a).

The percolation transition is now defined by the divergence of S. The logarithmic behavior of Eqs. (5.110a) and (5.110b) for S is shown in Fig. 5.15 as a function of X_{L_a}. The cluster definition used by Ghonasgi and Chapman predicts $S \rightarrow \infty$ when $X_{L_a} \rightarrow 0$ (at zero temperature), whereas Eq. (5.110a) predicts the percolation transition to occur at a finite temperature: $S \rightarrow \infty$ at $X_{L_a} = 1/3$. This percolation threshold corresponds to $N_{hb} \simeq 2.65$, and is apparently consistent with that found for the ST2 model of water [218]. Based upon spinodal curve calculations, Vakarin *et. al.* [189] find that $N_{hb} \simeq 3.05$ at the critical point, from which they conclude that the liquid phase for the four-site, sticky-spot model lies inside the percolation region. It is interesting to note that at the percolation threshold the network is not maximally connected, *viz.* $N_{hb} \simeq 2.65$.

These conclusions are not inconsistent with our findings: the divergence of our structure factor $S(k = 0)$, Eq. (5.102), implies that $N_{hb} \simeq 2.67$, while at our critical point $N_{hb} \simeq 3.10$. Our mean-field treatment of dispersion forces, however, clearly limits any extensive quantitative comparison. In addition, the transition point found by Vakarin *et. al.* is shifted relative to that for spherically symmetric association models like the adhesive hard sphere, indicating that anisotropy may play a large role in the transition. A proper account of the true tetrahedral coordination in water may have a big impact upon the cluster size S. Verifying any structural information, *i.e.* the functional form of S, at low temperatures where X_{L_a} is small is difficult using current simulation methods and will require further work. It is also not clear what significance, if any, such structural information contains. The F-bonds responsible for the formation of s-mers or molecular aggregates are relatively short-lived, and so the exact consequences of a structural percolation transition are not clear.

Whatever the structural state of the liquid, whether a distribution of tree-like aggregates or an infinite cluster, the liquid phase for this simple model satisfies all of the criteria for stability, evident from the Helmholtz free energy as X_{L_a} varies over it's full range of 0 to 1. This stands in contrast, for example, to Baxter's symmetric adhesive hard sphere model, which does display thermodynamic instability. It appears, at present, that the theory is both incapable of confirming the reality

of such derived liquid structure as well as identifying any physical (*e.g.* thermodynamic) significance that such structure might have.

5.6. WATER MODEL CONCLUSIONS

Our primitive model of water as a hard sphere with two electron lone pair and two hydrogen attraction sites followed the lead of Vakarin [105], Duda [121], and Ghonasgi and Chapman [47]. Based upon the equal site–site energetics of water, we were able to simplify the self-consistent solution of the partial densities as well as the AOZ equation by sequestering the site-specific details in favor of generic terms. This greatly reduced the notational complexities inherent in multiple attraction site models. Our work faithfully reproduces the TPT results of Ghonasgi and Chapman as well as the integral equation results of Duda. These and related works, however, have largely focused upon the calculation of an equation of state and the radial distribution function —presumably because of its widespread use in computing thermodynamic quantities. We decided to take advantage of the general applicability of the Wertheim formalism by extending these previous efforts through the calculation of every structural and thermodynamic quantity possible within the theory. We calculated the model pressure using four different thermodynamic routes, allowing for self-consistency checks. Moreover, we calculated the direct correlation functions and a simplified, analytical form of the structure factor. By determining numerous thermodynamic and structural quantities, we were better able to comprehensively test the ability of the four-site, sticky-spot model to mimic water.

This simple model has several strengths. It predicts a critical point for water without long-range dispersion forces, with reasonable critical point values predicted by the TPT-based results. The TPT results also predict the temperature variation of the average number of hydrogen bonds per particle N_{hb}, which is directly incorporated into both the thermodynamic and structural functions. Overall, our results underscore the utility of the TPT representation, at least concerning pressures and critical points [47]. Finally, this model has an exactly PY equation, not surprising because of its linkage to Baxter's adhesive hard sphere model and its firm diagrammatic basis.

The current model has several weaknesses as well. Thermodynamic properties like $c_v, \Delta H, \kappa_T$, *etc.* have contributions from intermolecular forces in the

present theory, but clearly the agreement with experiment is lacking. The structure factor $S(k)$ displays a pre-peak but is displaced and not as pronounced as that from experiment. This may be an indication that the liquid, as soon as it forms, becomes an infinite network or cluster. If this is true, then the sticky-spot model may be manifestly limited in its ability to describe the unique thermodynamic properties of water. While the theory is seemingly capable of describing the average number of hydrogen bonds per monomer, this information may not represent a useful descriptor of the overall properties of the liquid, *viz.* a key parameter in the language of associating fluids. Nonetheless, N_{hb} is inescapably linked to all the derived properties in the present model. The theory accounts for the proper type and number of hydrogen bonds per monomer, but lacks any straightforward method of incorporating the rigid tetrahedral orientation of the attraction sites and the concomitant SI-3 effects. This omission limits the accuracy with which the correlations can be calculated, and therefore all quantities derived from them, such as the virial and compressibility pressures. A proper account of the tetrahedral orientation of attraction sites might eliminate the percolation dilemma, it could at the same time lead to a much larger disagreement in N_{hb} values. Also, while the model affords analytical solutions of many quantities (*e.g.* the structure factor), its singular nature dictates a piecemeal treatment of $g(r)$ that limits the predictive power of the theory.

Clearly this work suggests that the TPT route to system thermodynamics is preferable to all others. The singular nature of the model itself seems to manifestly dictate that the virial-based results are the least accurate. Yet the importance of understanding water demands that we continue to address the steric aspects of hydrogen-bonded fluids. It can be anticipated that the thermodynamic properties will probably be insensitive to the orientational constraints of hydrogen bonding; their misrepresentation by the present theory points to the omission of multipolar potentials. A proper account of the steric effects in the model will better represent the network character of water and that, even in the context of adhesive hard spheres, would be a large step forward in the theory of associating fluids.

6. FINAL REMARKS

> Gardener and garden– *Out of damp and gloomy days, out of solitude, out of loveless words directed at us, conclusions grow up in us like fungus: one morning they are there, we know not how, and they gaze upon us, morose and gray. Woe to the thinker who is not the gardener but only the soil of the plants that grow in him!*
>
> —Friedrich Nietzsche
> *Daybreak*

In the previous chapters we have briefly introduced statistical mehcanics-based theories of associating liquids, reviewed the intricacies of modeling hydrogen bonds, and discussed in detail the use of graph theory in solving for system thermodynamics and structure, culminating with the unique, multi-density graph formalism of Wertheim [19–22]. Incorporating the the theoretical insights of Andersen [23] and Lockett [24], Wertheim presented an elegant theory written in terms of partial densities which reflect the bonding constraints of the particles. These partial densities, being based upon expansions in fugacity, allow the theory to be easily transferred to the standard methods of statistical mechanics of simple fluids. Couched in terms of the direct correlation function hierarchy, wherein approximations or closure conditions are more easily implemented [as compared to $g(r)$ or $h(r)$], Wertheim theory seemed an ideal formalism through which the thermodynamic and structural effects of interaction anisotropy (hydrogen bonding) could be directly explored. our intent was two-fold, (i) to test a primitive interaction model as a paradigm of association, and (ii) to test the capabilities and limitations of the theory itself in addressing hydrogen-bonded fluids [25, 26].

We began in Chapter 4, where we explored, in the simplest of possible terms, the effects of dimerization on a planar liquid–vapor interface using the highly anisotropic sticky-spot model of hydrogen bonding. While the suppression of the gas–liquid transition for the single-site case had been noted before, the direct role of anisotropic attraction (hydrogen bonding) upon the structure and thermodynamic properties of a simple interface have been much less discussed, at least in terms of Wertheim theory [165]. Our approach represented a first step in the extension of well-established theories in order to describe the dimerization effects on an already formed interface. The predictions of the theory were surprising in many respects. The system thermodynamics, *e.g.* critical points, coexistence densities, and surface

tension, proved to be more sensitive to dimerization in the sticky-spot limit than did the interface density profile. While the overall effects were small, they proved to be nontrivial. The inclusion of tetrahedral coordination and more complex forces (beyond mean field) represent the next steps in the analysis of interface properties, such that the full impact of interaction anisotropy might be judged.

In Chapter 5 we expanded the application of Wertheim theory to a four-site, hard-sphere model, again evaluated in the stick-spot limit, in order to test the model as a paradigm for water. The unique, graphical treatment of steric incompatibility effects —crucial in the description of water— and general applicability of Wertheim theory to the standard methods of statistical mechanics presented an efficient formalism in which to test the utility of the model and the capabilities of the theory to treat water. We calculated all possible thermodynamic and structural properties for this model, and discovered some limitations of the theory to treat multi-site attraction models of hydrogen-bonded fluids. The theory properly accounted for the water-like connectivity constraints, and elegantly incorporated the average number of hydrogen bonds per particle into its thermodynamic and structural results, and with four attraction sites (even with infinitesimal range) the theory predicts a critical point. Yet it's apparent inability to incorporate the proper tetrahedral coordination in water greatly limits the prospects of accurately modeling the full SI effects characteristic of water.

As for future research, the need for a simple yet comprehensive model or paradigm of hydrogen bonding that can act in a capacity analogous to that of the hard sphere model remains obvious. It is clear from the present work that any fundamental understanding will require the proper implementation of the steric constraints unique to associating fluids. The current model has gone a long way towards treating the connectivity requirements inherent in associating fluids through the introduction of the partial densities. Yet the typical SI conditions consistent with associating fluids like water lead to underlying complications in the topological reduction process when multiple attraction sites are involved. These (SI-3) complications involve the implementation of rigid bond angles between attraction sites, and greatly limit the otherwise efficient s-mer graph cancellation strategy fundamental to the Wertheim theory. Presently, the means by which this obstacle in the theory can be overcome appear to be absent. While an elegant formalism in

many respects, Wertheim theory as it stands does not seem to be optimally suited to the pursuit of a simple paradigm for water.

BIBLIOGRAPHY

[1] R. Kirschstein, *Opening Statement on the FY 2003 President's Budget Request*, Technical report, National Institutes of Health, February, 2002, [http://www.nih.gov/about/director/budgetrequest/FY2003budreq.htm].

[2] G. Robinson, S. Zhu, S. Singh, and M. W. Evans, *Water in Biology, Chemistry, and Physics: Overview and Computational Methodologies*, (World Scientific, Singapore, 1996).

[3] Editor F. Franks, *Water, A Comprehensive Treatise*, volume 1–7, (Plenum Press, New York, 1972-82).

[4] D. Eisenberg and W. Kauzmann, *The Structure and Properties of Water*, (Oxford University Press, New York, 1969).

[5] P. J. F. de Rege, S. A. Williams, and M. J. Thieren, *Science* **269**, 1409 (1995).

[6] M. C. Etter, *J. Phys. Chem.* **95**, 4601 (1991).

[7] S. C. Zimmerman, F. Zeng, D. E. C. Reichert, and S. V. Kolotuchin, *Science* **271**, 1095 (1996).

[8] J. D. Hartgerink, J. R. Granja, R. A. Milligan, and M. R. Ghadiri, *J. Am. Chem. Soc.* **118**, 43 (1996).

[9] C. M. Henry, *Chem. & Chem. Eng. News*, August 2002, p. 39.

[10] A. Kreglewski, *Equilbrium Properties of Fluids and Fluid Mixtures*, Texas Engineering Experiment Station Monograph Series, (Texas A&M University Press, College Station, TX, 1984).

[11] J. P. K. Doye, *The Structure, Thermodynamics, and Dynamics of Atomic Clusters*, Doctoral dissertation, Cambridge, 1996.

[12] J. C. Gimel, T. Nicolai, and D. Durand, *Phys. Rev. E* **66**, 061405 (2002).

[13] J. Israelachvili, *Intermolecular and Surface Forces*, (Academic Press, San Diego, Second Edition, 1992).

[14] A. Ben-Naim, *Water and Aqueous Solutions*, (Plenum Press, New York, 1974).

[15] W. R. Smith and I. Nezbeda, *J. Chem. Phys.* **81**, 3694 (1984).

[16] J. Janzen and L. S. Bartell, *J. Chem. Phys.* **50**, 3611 (1969).

[17] J. W. Ring and P. A. Egelstaff, *J. Chem. Phys.* **51**, 762 (1969).

[18] T. R. Dyke, B. J. Howard, and W. Klemperer, *J. Chem. Phys.* **56**, 2442 (1972).

[19] M. S. Wertheim, *J. Stat. Phys.* **35**, 19 (1984).

[20] M. S. Wertheim, *J. Stat. Phys.* **35**, 35 (1984).

[21] M. S. Wertheim, *J. Stat. Phys.* **42**, 459 (1986).

[22] M. S. Wertheim, *J. Stat. Phys.* **42**, 477 (1986).

[23] H. C. Andersen, *J. Chem. Phys.* **59**, 4717 (1973).

[24] I. A. M. Lockett, *J. Chem. Phys.* **72**, 4822 (1980).

[25] T. Peery and G. T. Evans, *J. Chem. Phys.* **114**, 2387 (2001).

[26] T. Peery and G. T. Evans, *J. Chem. Phys.* **118**, 2286 (2003).

[27] T. Andrews, *Phil. Trans. Roy. Soc.* **159**, 575 (1869).

[28] J. D. van der Waals, Doctoral dissertation, Leiden, 1873.

[29] B. J. Alder, H. G. Hoover, and D. A. Young, *J. Chem. Phys.* **49**, 3688 (1968).

[30] P. C. Hemmer and J. L. Lebowitz, *Critical Phenomena and Phase Transitions 5b*, (Academic Press, New York, 1976).

[31] J. L. Lebowitz, G. Stell, and S. Baer, *J. Math. Phys.* **6**, 1282 (1965).

[32] J. L. Lebowitz and O. Penrose, *J. Math. Phys.* **7**, 98 (1966).

[33] P. A. Egelstaff, *An Introduction to the Liquid State*, (Clarendon Press, Oxford, Second Edition, 1992).

[34] J. A. Barker and D. Henderson, *Rev. of Mod. Phys.* **48**, 587 (1976).

[35] A. R. Leach, *Molecular Modelling: Principles and Applications*, (Longman, Singapore, 1996).

[36] T. S. Moore and T. F. Winmill, *J. Chem. Soc.* **101**, 1635 (1912).

[37] M. L. Huggins, *J. Org. Chem.* **1**, 407 (1936).

[38] L. Pauling, *The Nature of the Chemical Bond*, (Cornell University Press, New York, 1939).

[39] M. L. Huggins, *Angew. Chem., Int. Ed. Engl.* **10**, 147 (1971).

[40] S. Scheiner, *Hydrogen Bonding: A Theoretical Perspective*, (Oxford University Press, New York, 1997).

[41] F. Dolezalek, *Z. Phys. Chem.* **64**, 727 (1908).

[42] G. Jackson, W. G. Chapman, and K. E. Gubbins, *Mol. Phys.* **65**, 1 (1988).

[43] G. M. Wilson, *J. Amer. Chem. Soc.* **86**, 127 (1964).

[44] D. Abrams and J. M. Prausnitz, *A.I.Ch.E. J.* **21**, 116 (1975).

[45] I. G. Economou and M. D. Donohue, *A.I.Ch.E. J.* **37**, 1875 (1991).

[46] A. G. Zilman and S. A. Safran, *Phys. Rev. E* **bf 66**, 051107 (2002).

[47] D. Ghonasgi and W. Chapman, *Mol. Phys.* **79**, 291 (1993).

[48] W. G. Chapman, K. E. Gubbins, C. G. Joslin, and C. G. Gray, *Pure Appl. Chem.* **59**, 53 (1987).

[49] P. T. Cummings and G. Stell, *Mol. Phys.* **51**, 253 (1984).

[50] P. T. Cummings and L. Blum, *J. Chem. Phys.* **84**, 1833 (1986).

[51] H. C. Anderson, *J. Chem. Phys.* **61**, 4985 (1974).

[52] Y. Zhou and G. Stell, *J. Chem. Phys.* **96**, 1504 (1992).

[53] L. W. Dahl and H. C. Andersen, *J. Chem. Phys.* **78**, 1980 (1983).

[54] J. S. Høye and K. Olaussen, *Physica* **104A**, 435 (1980).

[55] J. P. Hansen and I. R. McDonald, *Theory of Simple Liquids*, (Academic Press, San Diego, Second Edition, 1986).

[56] J. N. Murrell and A. D. Jenkins, *Properties of Liquids and solutions*, (Wiley & Sons, New York, Second Edition, 1994).

[57] B. M. Axilrod and E. Teller, *J. Chem. Phys.* **11**, 299 (1943).

[58] Y. Rosenfeld, *Mol. Phys.* **94** , 929 (1998).

[59] C. Cacomo, *Phys. Reports* **274** , 1 (1996).

[60] D. Bratko, L. Blum, and A. Luzar, *J. Chem. Phys.* **83**, 6367 (1985).

[61] J. L. Lebowitz and J. K. Percus, *Phys. Rev.* **144**, 251 (1966).

[62] W. R. Smith, D. Henderson, and Y. Tago, *J. Chem. Phys.* **67**, 5308 (1977).

[63] T. Boublík, I. Nezbeda, and K. Hlavatý, *Statistical Thermodynamics of Simple Liquids and their Mixtures*, Studies in Physical and Theoretical Chemistry 2, (Elsevier Scientific, New York, 1980).

[64] J. D. Weeks, D. Chandler, and H. C. Anderson, *J. Chem. Phys.* **54**, 5237, 5422 (1971).

[65] J. A. Barker and D. Henderson, *J. Chem. Phys.* **47**, 4714 (1967).

[66] C. Tutschka and G. Kahl, *Phys. Rev. E* **62**, 3640 (2000).

[67] N. D. Mermin, *Phys. Rev. A* **137**, 1441 (1965).

[68] R. Evans, *Adv. Phys.* **28**, 2, 143 (1979).

[69] J. T. Chayes, L. Chayes, and E. H. Lieb, *Commun. Math. Phys. 93*, 57 (1984).

[70] J. T. Chayes and L. Chayes, *J. Stat. Phys.* **36**, 471 (1984).

[71] W. F. Saam and C. Ebner, *Phys. Rev. A* **15**, 2566 (1977).

[72] J. S. Rowlinson and B. Widom, *Molecular Theory of Capillarity*, (Oxford Science Publications, Cambridge, 1989).

[73] D. Chandler and L. R. Pratt, *J. Chem. Phys.* **65**, 2925 (1976).

[74] L. R. Pratt and D. Chandler, *J. Chem. Phys.* **66**, 147 (1977).

[75] K. Olaussen and G. Stell, *J. Stat. Phys.* **62**, 221 (1991).

[76] D. Chandler and H. C. Anderson, *J. Chem. Phys.* **57**, 1930 (1972).

[77] G. Stell and Y. Zhou, *Fluid Phase Equilibria* **79**, 1 (1992).

[78] J. E. Mayer and E. Montroll, *J. Chem. Phys.* **9**, 2 (1941).

[79] J. E. Mayer, *J. Chem. Phys.* **10**, 629 (1942).

[80] N. N. Bogoliubov, *Vest. Mosk. Gos. Univ.* **10**, 115 (1955).

[81] T. Morita and M. Hiroike, *Prog. Theor. Phys.* **25**, 537 (1961).

[82] C. de Dominicis, *J. Math. Phys.* **3**, 983 (1962).

[83] G. Stell, *The Equilibrium Theory of Classical Fluids*, (Benjamin, New York, 1964).

[84] J. E. Mayer, *J. Chem. Phys.* **5**, ; J. E. Mayer and P. F. Ackermann, *ibid.*, **5**, 74 (1937).

[85] J. E. Mayer and M. G. Mayer, *Statistical Mechanics*, (Wiley & Sons, New York, 1940).

[86] B. M. Landanyi and D. Chandler, *J. Chem. Phys.* **62**, 4 (1975).

[87] J. K. Percus, *Phys. Rev. Lett.* 8, 462 (1962).

[88] J. K. Percus, *Trans. N. Y. Acad. Sci.* **26**, 1062 (1964).

[89] J. K. Percus, *Recent Developments and Applications of Modern Density Functional Theory*, (Elsevier Scientific, Amsterdam, 1996).

[90] A. Bijl, Doctoral dissertation, Leiden, 1938.

[91] W. Band, *J. Chem. Phys.* **7**, 324, 927 (1939).

[92] J. Frenkel, *J. Chem. Phys.* **7**, 538 (1939).

[93] T. L. Hill, *Statistical Mechanics*, Chap. 5, pp. 152–164 (McGraw–Hill, New York, 1956).

[94] F. H. Stillinger, *J. Chem. Phys.* **47**, 2513 (1967).

[95] H. P. Gillis, D. C. Marvin, and H. Reiss, *J. Chem. Phys.* **66**, 214, 223 (1977).

[96] W. G. Courtney, *J. Chem. Phys.* **35**, 2249 (1951).

[97] J. K. Percus, *The Equilibrium Theory of Classical Fluids*, (Benjamin, New York, 1964).

[98] Y. V. Kalyuzhnyi, I. A. Protsykevytch, and M. F. Holovko, *Chem. Phys. Lett.* **215**, 1 (1993).

[99] G. Stell, *J. Stat. Phys.* **63**, 1203 (1991).

[100] G. Stell and Y. Zhou, *J. Chem. Phys.* **91**, 3618 (1989).

[101] Y. Zhou and G. Stell, *J. Chem. Phys.* **98**, 5777 (1993).

[102] Y. V. Kalyuzhnyi, G. Stell, M. L. Llano-Restrepo, W. G. Chapman, and M. F. Holovko, *J. Chem. Phys.* **101**, 7939 (1994).

[103] Y. V. Kalyuzhnyi, C. T. Lin, and G. Stell, *J. Chem. Phys.* **106**, 1940 (1997).

[104] A. . G. T. Evans, Personal communication, March 2003.

[105] E. Vakarin, Y. U. Duda, and M. F. Holovko, *Mol. Phys.* **90**, 611 (1997).

[106] R. J. Baxter, *J. Chem. Phys.* **49**, 4559 (1968).

[107] Editor D. Henderson, *Fundamentals of Inhomogeneous Fluids*, (Marcel Dekker, New York, 1992).

[108] A. W. Adamson, *Physical Chemistry of Surfaces*, (Wiley Interscience, Sixth Edition, New York, 1991).

[109] B. Widom, *Science* **157**, 375 (1967).

[110] Editor C. A. Croxton, *Fluid Interfacial Phenomena*, (Wiley & Sons, Cinchester, 1986).

[111] *Les Houches Summer School Lectures*, Session XLVIII, (Elsevier Scientific, Amsterdam, 1990).

[112] G. Pétré and A. Sanfeld, *Capillarity Today*, Springer, Berlin, 1991.

[113] G. Gomper and M. Schick, in *Phase Transitions and Critical Phenomena.*

[114] W. T. Góźdź and R. Holyst, *Phys. Rev. E* **54**, 5012 (1996).

[115] S. A. Safran, *Statistical Thermodynamics of Surfaces, Interfaces, and Membranes*, Frontiers in Physics, (Addison-Wesley, New York, 1994).

[116] M. S. Wertheim, *J. Chem. Phys.* **78**, 4619 (1983).

[117] M. S. Wertheim, *J. Chem. Phys.* **78**, 4625 (1983).

[118] D. Ghonasgi and W. G. Chapman, *J. Chem. Phys.* **102**, 2585 (1995).

[119] Y. V. Kalyuzhnyi and P. T. Cummings, *J. Chem. Phys.* **104**, 3325 (1996).

[120] Y. V. Kalyuzhnyi and P. T. Cummings, *J. Chem. Phys.* **105**, 2011 (1996).

[121] Y. Duda, *J. Chem. Phys.* **109**, 9015 (1998).

[122] E. A. Muller, L. F. Vega, and K. E. Gubbins, *Int. J. Thermophys.* **16**, 705 (1995).

[123] E. A. Muller and K. E. Gubbins, *Equations of State for Fluids and Mixtures*, Editors J. V. Sengers, M. B. Ewing, R. F. Kayser, and C. J. Peters, (Blackwell Scientific, Oxford, 1995).

[124] M. F. Holovko and Y. V. Kalyuzhnyi, *Mol. Phys.* **73**, 1145 (1991).

[125] R. P. Sear and G. Jackson, *Phys. Rev. E* **50**, 386 (1994).

[126] Y. V. Kalyuzhnyi and I. Nezbeda, *Mol. Phys.* **73**, 703 (1991).

[127] F. W. Tavares, J. Chang, and S. I. Sandler, *Mol. Phys.* **86**, 1451 (1995).

[128] G. Stell, *Physcia A* **231**, 1 (1996).

[129] C. J. Segura, W. G. Chapman, and K. P. Shukla, *J. Chem. Phys.* **109**, 9015 (1998).

[130] A. D. Trokhymchuk, D. Henderson, and S. Sokolowski, *Phys. Lett. A* **209**, 317 (1995).

[131] R. Evans, Fundamentals of Inhomogeneous Fluids, in *Density Functionals in the Theory of Nonuniform Fluids*, Editor D. Henderson, Chapter 3 (Marcel Dekker, New York, 1992).

[132] R. P. Sear and W. M. Gelbart, *J. Chem. Phys.* **110**, 4582 (1999).

[133] G. Malescio and G. Pellicane, *Phys. Rev. E* **63**, 020501(R) (2001).

[134] Y. Levin, *Phys. Rev. Lett.* **83**, 1159 (1999).

[135] P. J. Camp, J. C. Shelley, and G. N. Patey, *Phys. Rev. Lett.* **84**, 115 (2000).

[136] H. L. Friedman, *A Course in Statistical Mechanics*, (Prentice Hall, New Jersey, 1985).

[137] H. Huang and M. Radosz, *Ind. Eng. Chem. Res.* **29**, 2284 (1990).

[138] E. Kierlik and M. L. Rosinberg, *J. Chem. Phys. 97*, 9222 (1992).

[139] J. Chang and S. I. Sandler, *J. Chem. Phys.* **102**, 437 (1995).

[140] G. Stell and C.-T. Lin, *J. Chem. Phys.* **110**, 5444 (1999).

[141] C. Vega and L. G. MacDowell, *Mol. Phys.* **98**, 1295 (2000).

[142] D. A. McQuarrie, *Statistical Mechanics*, (University Science Books, Sausalito, 2000).

[143] E. Velasco, L. Mederos, G. Navascués, P. C. Hemmer, and G. Stell, *Phys. Rev. Lett.* **85**, 122 (2000).

[144] L. D. Landau and E. M. Lifshitz, *Statistical Physics*, (Pergamon, New York, Third Edition, 1989).

[145] J. K. Percus, *The Liquid State of Matter: Fluids, Simple and Complex*, (North Holland, Amsterdam, 1982).

[146] R. Evans, P. Tarazona, and U. M. B. Marconi, *Mol. Phys.* **50**, 993 (1983).

[147] R. Evans and U. M. B. Marconi, *Phys. Rev. A* **34**, 3504 (1986).

[148] N. F. Carnahan and K. F. Starling, *J. Chem. Phys.* **51**, 635 (1969).

[149] L. Verlet and J. Weis, *Phys. Rev.* **5A**, 939 (1972).

[150] J. S. Rowlinson, Development of theories of inhomogeneous fluids, in *Density Functionals in the Theory of Nonuniform Fluids*, Editor D. Henderson, Chapter 1 (Marcel Dekker, New York, 1992).

[151] F. P. Buff, R. A. Lovett, and F. H. Stillinger, *Phys. Rev. Lett.* **15**, 621 (1965).

[152] J. V. Sengers and J. M. J. van Leeuwen, *Phys. Rev. A* **39**, 6346 (1989).

[153] D. E. Sullivan, *Phys. Rev. A* **25**, 1669 (1982).

[154] N. G. van Kampen, *Phys. Rev.* **135**, A362 (1964).

[155] S. Iatsevitch and F. Forstmann, *Mol. Phys.* **98**, 1309 (2000).

[156] M. S. Wertheim, *J. Chem. Phys.* **85**, 2929 (1986).

[157] M. S. Wertheim, *J. Math. Phys.* **5**, 643 (1964).

[158] R. J. Baxter, *J. Chem. Phys.* **49**, 2770 (1968).

[159] J. K. Percus and J. G. Yevick, *Phys. Rev.* **110**, 1 (1958).

[160] J. L. Lebowitz, *Phys. Rev. A* **133**, 895 (1964).

[161] M. P. Allen, G. T. Evans, D. Frenkel, and B. M. Mulder, *Adv. in Chem. Phys.* **LXXXVI**, Editors I. Prigogine and S. A. Rice, Chapter 5, (Wiley & Sons, New York, 1993); see, for example, Eq. (5.9).

[162] B. Widom, *Liquids, Freezing, and the Glass Transition*, in Les Houches 1989 Part II, Editors J. P. Hansen and D. Levesque and J. Zinn-Justin, (North-Holland, Amsterdam, 1989).

[163] R. J. Baxter, *Aus. J. Phys.* **21**, 563 (1968).

[164] R. J. Baxter, *Phys. Rev.* **154**, 170 (1967).

[165] W. G. Chapman, *J. Chem. Phys.* **93** , 4299 (1990).

[166] E. A. Müller, K. E. Gubbins, D. M. Tsangaris, and J. J. de Pablo, *J. Chem. Phys.* **103**, 3868 (1995).

[167] M. Mecke and J. Winkelmann, *J. Chem. Phys.* **107**, 9264 (1997).

[168] B. Q. Lu, R. Evans, and M. M. T. da Gamma, *Mol. Phys.* **55**, 1319 (1985).

[169] W. L. Jorgensen, J. Chandrasekhar, J. D. Madura, R. W. Impey, and M. L. Klein, *J. Chem. Phys.* **79**, 926 (1983).

[170] L. Blum, F. Vericat, and L. Degrève, *Physica A* **265**, 369 (1999).

[171] S. Zhu, S. Singh, and G. W. Robinson, *Adv. Chem. Phys.* **LXXXV**, 627 (1994).

[172] S. S. Xantheas and J. T. H. Dunning, *J. Chem. Phys.* **99** , 8774 (1993).

[173] J. van Duijneveldt-van de Rijdt and F. B. van Duijneveldt, *Chem. Phys.* **175**, 271 (1993).

[174] O. Matsuoka, E. Clementi, and Y. Yoshimine, *J. Chem. Phys.* **64**, 1351 (1976).

[175] G. C. Lie, E. Clementi, and M. Yoshimine, *J. Chem. Phys.* **64**, 2314 (1976).

[176] G. C. Lie and E. Clementi, *J. Chem. Phys.* **62**, 2195 (1976).

[177] N. Bjerrum, *Science* **115**, 385 (1952).

[178] H. J. C. Berendsen, J. P. M. Postma, W. F. von Gunsteren, and J. Hermans, *Intermolecular Forces*, Editor B. Pullman (Reidel, Dordrecht, 1981); see p. 331.

[179] H. J. C. Berendsen, J. R. Grigera, and T. P. Straatsma, *J. Phys. Chem.* **91**, 6269 (1987).

[180] F. H. Stillinger and A. Rahman, *J. Phys. Chem.* **60**, 1545 (1974).

[181] W. L. Jorgensen and J. D. Madura, *Mol. Phys.* **56**, 1381 (1985).

[182] M. B. Pettitt and P. J. Rossky, *J. Chem. Phys.* **77**, 1451 (1982).

[183] W. G. Chapman, Doctoral dissertation, Cornell University, 1988.

[184] W. Bol, *Molec. Phys.* **45**, 605 (1982).

[185] L. Blum and F. Vericat, *J. Phys. Chem.* **100**, 1197 (1997).

[186] J. Kolafa and I. Nezbeda, *Mol. Phys.* **61**, 161 (1987).

[187] I. Nezbeda, J. Kolafa, and Y. V. Kalyuzhnyi, *Mol. Phys.* **68**, 143 (1989).

[188] I. Nezbeda and G. A. Iglesias-Silva, *Mol. Phys.* **69**, 767 (1990).

[189] E. Vakarin, Y. Duda, and M. F. Holovko, *J. Stat. Phys.* **88**, 1333 (1997).

[190] Y. Duda, C. J. Segura, E. Vakarin, M. F. Holovko, and W. G. Chapman, *J. Chem. Phys.* **108**, 9168 (1998).

[191] J. Kolafa and I. Nezbeda, *Mol. Phys.* **72**, 777 (1991).

[192] M. Masella and J. P. Flament, *J. Chem. Phys.* **107**, 9105 (1997).

[193] J. E. D. Bene, *J. Chem. Phys.* **57**, 1899 (1972).

[194] G. T. Evans and V. Vaida, *J. Chem. Phys.* **113**, 6652 (2000).

[195] A. K. Soper and M. G. Phillips, *Chem. Phys.* **107**, 47 (1986).

[196] L. A. Curtiss, D. J. Frurip, and M. Blander, *J. Chem. Phys.* **71** , 2703 (1979).

[197] G. S. Kell, *J. Chem. Engng. Data* **12**, 66 (1967).

[198] R. O. Watts and I. J. McGee, *Liquid State Chemical Physics*, (Wiley & Sons, New York, 1976).

[199] D. Henderson and R. D. Murphy, *Phys. Rev.* **A 6**, 1224 (1972).

[200] M. I. Guerrero, G. Saville, and J. S. Rowlinson, *Mol. Phys.* **29**, 1941 (1975).

[201] R. O. Watts, *J. Chem. Phys.* **50**, 1358 (1969).

[202] J. Kolafa and I. Nezbeda, *Mol. Phys.* **61**, 161 (1987).

[203] J. M. Velarde, P. P. nero, L. F. Rull, and J. J. Morales, *Mol. Phys.* **65**, 287 (1988).

[204] L. L. Lebowitz and J. K. Percus, *J. Math. Phys.* **4**, 248 (1963).

[205] J. J. Brey and A. Santos, *J. Chem. Phys.* **82**, 4312 (1985).

[206] H. E. Stanley, *Introduction to Phase Transitions and Critical Phenomena*, (Oxford University Press, New York, 1971).

[207] L. X. Dang and T. M. Chang, *J. Chem. Phys.* **106**, 8149 (1997).

[208] A. D. Trokhymchuk, M. F. Holovko, and K. Heinzinger, *Naturforsch* **50**, 18 (1995).

[209] A. D. Trokhymchuk, M. F. Holovko, and K. Heinzinger, *Mol. Phys.* **86**, 797 (1995).

[210] A. K. Soper, *Chem. Phys.* **258**, 121 (2000).

[211] A. H. Narten and H. A. Levy, *J. Chem. Phys.* **55**, 2263 (1971).

[212] M. P. Tosi, *J. Condens. Matter* **6**, A13 (1994).

[213] M. Wilson and P. A. Madden, *Phys. Rev. Lett.* **72**, 3033 (1994).

[214] W. G. T. Kranendonk and D. Frenkel, *Mol. Phys.* **64**, 403 (1988).

[215] W. E. Thiessen and A. H. Narten, *J. Chem. Phys.* **77**, 2656 (1971).

[216] H. E. Stanley and J. Teixeira, *J. Chem. Phys.* **73**, 3404 (1980).

[217] H. E. Stanley, J. Teixeira, A. Geiger, and R. L. Blumberg, *Physica* **106 A**, 260 (1981).

[218] R. L. Blumberg, H. E. Stanley, A. Geiger, and P. Mausbach, *J. Chem. Phys.* **80**, 5230 (1984).

[219] E. Vakarin, M. F. Holovko, and Y. Duda, *Mol. Phys.* **91**, 203 (1997).

[220] E. Vakarin, Y. Duda, and M. F. Holovko, *J. Chem. Phys.* **107**, 5569 (1997).

[221] D.-M. Duh, D. N. Perera, and A. D. J. Haymet, *J. Chem. Phys.* **102**, 3736 (1995).

[222] T. Head-Gordon and G. Hura, *Water structure from scattering experiments and simulation*, Dept. of Bioengineering, UC Berkeley, pre-publication notes.

[223] A. Coniglio, U. D. Angelis, A. Forlani, and G. Lauro, *J. Phys. A* **10**, 219 (1977).

[224] Y. C. Chiew and E. D. Glandt, *J. Phys. A* **16**, 2599 (1983).

[225] D. Laria and F. Vericat, *Phys. Rev. B* **40**, 353 (1989).

[226] K. Leung and D. Chandler, *J. Stat. Phys.* **63**, 837 (1991).

[227] M. S. Wertheim, *J. Chem. Phys.* **87**, 73 (1987).

APPENDICES

APPENDIX A. GLOSSARY OF NOTATION

AOZ	Associated Ornstein–Zernicke
AP	Articulation Point
APY	Associative Percus–Yevick
BH	Barker Henderson perturbation theory
c-AP	Constraint Articulation Point
HNC	Hypernetted Chain Approximation
IET	Integral Equation Theory
INA	Ideal Network Approximation
MC	Monte Carlo
MD	Molecular Dynamics
MSA	Mean Spherical Approximation
OZ	Ornstein–Zernicke
PY	Percus–Yevick
RAM	Reference Average Mayer (function)
RDF	Radial Distribution Function
RISM	Reference Interaction Site Model
SAFT	Statistical Associating Fluid Theory
SBC	Single Bonding Condition
SGT	Square Gradient Theory
SI	Steric Incompatibility
TPT	Thermodynamic Perturbation Theory
vdW	van der Waals
WDA	Weighted-density Approximation

$\mathbf{1}$	Spatial coordinate $\boldsymbol{r}_1$
e	Boltzmann factor or "e-bond"
e_R, e^R	Repulsive e-bond
f	Mayer f-bond
f_A	Modified Mayer f-bond of Lockett
f^R	Repulsive Mayer f-bond
F	Modified Mayer f-bond operator of Wertheim
f_{ij}^A	Site-specific Wertheim attractive bond

$\rho(\mathbf{1})$	One-body density distribution function
$\rho^{(m)}(\mathbf{1})$	One-body partial density distribution function
$\rho(\mathbf{1},\mathbf{2})$	Two-body density distribution function
$\hat{\rho}(\mathbf{1},\mathbf{2})$	Truncated two-body density distribution function
ψ	Helmholtz free energy density
$W[\rho]$	Excess grand potential energy density
$\sigma^{(m)}(\mathbf{1})$	Complementary density parameter with m available attraction sites
$u_{ij}^{A}(\mathbf{1},\mathbf{2})$	Attractive potential between attraction site i on hyperpoint 1 and site j on 2
$u^{R}(\mathbf{1},\mathbf{2})$	Repulsive potential between hyperpoints 1 and 2
$c(\mathbf{1},\mathbf{2})$	Direct correlation function
$c^{m}(\mathbf{1})$	One-body partial correlation function with m incident F-bonds at labeled point 1
$c^{mn}(\mathbf{1},\mathbf{2})$	Partial direct correlation function with $m\,(n)$ incident F-bonds and labeled point 1 (2)
$h(\mathbf{1},\mathbf{2})$	Total correlation function
$h^{mn}(\mathbf{1},\mathbf{2})$	Partial total correlation function with $m\,(n)$ incident F-bonds at labeled point 1 (2)
$g(\mathbf{1},\mathbf{2})$	Radial distribution function
$g^{mn}(\mathbf{1},\mathbf{2})$	Partial radial distribution function with $m\,(n)$ incident F-bonds at labeled point 1 (2)
$y(\mathbf{1},\mathbf{2})$	Background distribution function
$y^{mn}(\mathbf{1},\mathbf{2})$	Partial background distribution function with $m\,(n)$ incident F-bonds at labeled point 1 (2)

APPENDIX B. GRAPH THEORY DEFINITIONS

Wertheim theory is a graphical formalism, where diagram manipulations require strict adherence to a particular rules. Below are some basic *definitions* which aid in the classification of these graphs and their subsequent manipulation, but is by no means extensive. The formal set of rules by which graphs are actually manipulated are contained in a set of of five lemmas derived by Morita and Hiroike [81] and Stell [83]. For a detailed overview of these lemmas, see Section 4.4 of Hansen and McDonald's text [55].

[DIAGRAM] A graphical representation of a statistical mechanical functional (including the unit function) which consists of a multi-coordinate integral of one or more functions, and is represented by vertices or "circles", various pairs of which are connected by lines and represent particle interactions: *e.g.*

$$\overset{1}{\bullet} \equiv \int d\mathbf{1}\, z(\mathbf{1})\,,$$

$$\equiv \int d\mathbf{1}d\mathbf{2}d\mathbf{3}d\mathbf{4} \prod_{i=1}^{4} z(i) f(\mathbf{1},\mathbf{2}) f(\mathbf{2},\mathbf{4})\,.$$

Note that the spatial labels 1, 2, *etc.* are dummy variables of integration, and so are usually omitted (see *labeled* versus *unlabeled* diagrams below).

[GRAPH VERTEX] A diagram element drawn as an open or closed "circle", ○ or ● , that represents some function of one coordinate variable: a 1-circle represents the unit function 1, a z-circle represents the fugacity at some coordinate i, $z(i)$, a ρ-circle represents the density $\rho(i)$, *etc.* These functions may not always be explicitly shown, especially if the vertex coordinate i is not labeled.

[FIELD POINT] Diagram element ● , often called a black circle, that represents a vertex coordinate that is an integration variable. A distinction between labeled and unlabeled black circles is essential in graph manipulations.

[ROOT POINT] Diagram element ○ , or white circle, that represents vertex coordinates which are *not* integration variables. Root points ○ are obtained from ● points via functional differentiation, wherein integration over that coordinate is eliminated, ● → ○ , transforming the vertex function (whatever it is) into the unit function, *i.e.* a 1-circle. Topological reduction may further transform such 1-circles into, for example, ρ-circles.

[GRAPH BOND] A diagram element indicated by a line, *e.g.* — or ⊣⊢ , between vertices, representing interactions between the particles located at the vertex coordinates.

[CONNECTED DIAGRAM] A diagram in which any two vertices are connected by a path of lines or "bonds" either directly or through other vertices.

[SIMPLE DIAGRAM] A diagram in which any pair of vertices are connected by no more than one bond.

[S-MER GRAPH] Any diagram or subdiagram containing s circles that are directly connected via attractive F-bonds $\dashv\vdash$.

[LABELED DIAGRAM] A diagram consisting of circles, certain pairs of which are linked by bonds, and carries coordinate labels for *each* graph vertex. The *value* I of a labeled diagram is the value of the integral that the diagram represents, *e.g.*

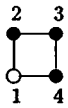

$$\equiv I = \iiint \prod_{i=1}^{4} z(i)\, f(1,2) f(2,3) f(3,4) f(1,4)\, d2\, d3\, d4\,.$$

I is a function of the coordinates attached to the white circles and a functional of the coordinates attached to field points.

[UNLABELED DIAGRAM] A labeled diagram from which all field point labels have been removed. It's *value* includes a combinatorial factor related to the topological structure of the diagram. An unlabeled diagram is related to labeled diagrams by enumerating all possible permutations of field point labels which give rise to distinct connectivity, *e.g.*

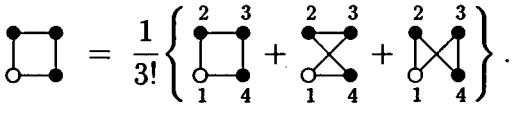

The value of an ***unlabeled*** diagram Γ containing n white circles labeled 1 to n and m unlabeled field points is

$$\Gamma = \frac{1}{S}\left\{\begin{array}{l}\text{Sum of all topologically inequivalent diagrams ob-}\\ \text{tained by attaching labels } n+1,\ldots,n+m \text{ to the}\\ \text{field points.}\end{array}\right\}$$

The number of labeled diagrams appearing on the right-hand side above equals $m!/S$.

[TOPOLOGICAL EQUIVALENCE] Two labeled diagrams are topologically equivalent if they are characterized by the same set of (bond) connections. Topological equivalence means that the integrand is unaltered by the relabelling. The subgroup of field point label permutations that leave the connections the same is the *graph group*. Two ***unlabeled*** diagrams are topologically ***distinct*** if it is impossible to find a permutation that leaves converts a labeled version of one diagram into the other.

[SYMMETRY NUMBER] To determine the symmetry number S of a diagram, first label its field points in an arbitrary fashion. For the case that all field points are associated with the same function, the symmetry number of a simple diagram is the order of the graph group, or the number of unique permutations of field point labels which leaves the connectivity unchanged. For example,

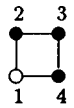

$\Rightarrow S = 2\,.$

[CONNECTING CIRCLE] Any circle which, upon removal from the diagram, causes the diagram to become disconnected. Note that when a circle is removed, all bonds connected to it are eliminated as well.

[ARTICULATION CIRCLE] Any circle which, upon removal, causes the diagram to separate into two or more components, of which at least one contains *no* white circles.

[NODAL CIRCLE] Any circle through which *all* paths between two particular white circles must pass.

[BRIDGE CIRCLE] Any circle which, upon removal from the diagram, causes the diagram to separate into two or more pieces, at least two of which contain a white circle.

[IRREDUCIBLE GRAPH] Any diagram that is free of articulation circles.

[STAR PRODUCT] The star product $\Gamma_3 = \Gamma_1 * \Gamma_2$ of two graphs, Γ_1 and Γ_2, is the diagram obtained by linking together Γ_1 and Γ_2 such that the white 1-circles carrying the same root labels coincide. An example of a star product is shown below:

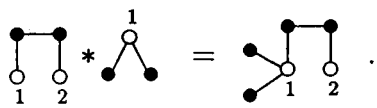

If the root points of Γ_1 and Γ_2 have no label in common, or if one diagram contains no root points ○ , the star product $\Gamma_1 * \Gamma_2$ is a disconnected diagram with Γ_1 and Γ_2 as components.

[SUBDIAGRAM] Any diagram that can be obtained from a connected diagram by removal of circles or elimination of bonds, or by any combination of these procedures.

[MAXIMAL SUBDIAGRAM] A subdiagram is *maximal* with respect to a given property if it is not embedded in any other subdiagram with the same property. Maximal subdiagrams are not necessarily unqiue, and "maximal" should not be interpreted in the sense of "largest".

[TOPOLOGICAL REDUCTION] The resummation of a graph series into another series with fewer terms, even though both may be infinite.

[HYPERPOINTS] Vertices or graph circles with multiple attraction sites. Hyperpoints represent the monomeric species of the theory with some specified set of attraction sites.

[BOND–CONNECTED] Any two attraction sites are *bond–connected* if and only if there is an uninterrupted path between them consisting of attraction bonds f_{ij}^{A} and other attraction sites.

[CONSTRAINT–CONNECTED] Two attraction sites are *constraint–connected* if and only if they are located on the same hyperpoint.

[BARE S-MER GRAPH] An s-mer diagram with no f^{R} bonds between hyperpoints *not* directly bond-connected; e^{R} bonds between bond-connected hyperpoints are never broken up into a 1-bond and a f^{R}-bond.

APPENDIX C. GRAPH-BASED HNC & PY APPROXIMATIONS

Both the hypernetted chain (HNC) and the closely related Percus–Yevick (PY) approximations involve the neglect of certain terms in three-body distribution functions which make the summation of the expansion difficult. The components that are retained can be written conveniently in terms of the cluster expansion for $c(\mathbf{1},\mathbf{2})$. A careful graphical analysis suggests that, for pair potentials that decrease rapidly to zero with increasing distance, the f-bond is effectively equal to zero beyond a certain limit $r = r_c$ (*i.e.* $u(r) \approx 0$ for $r > r_c$). Hence, the value of a graph (integral) is smaller the more highly connected it is, the more "crossed" f-bonds it contains [63]. This behavior is used as justification for neglecting the more highly connected graphs at all orders in the density expansion of $c(\mathbf{1},\mathbf{2})$. There are successive versions of these approximations, based upon how the higher order terms are treated. The simplest version enables the series to be summed and corresponds to the relations given in Section 2.3.2, characterized specifically by the second-order graphs kept (square brackets below) in the approximation, namely

$c(\mathbf{1},\mathbf{2}) =$ 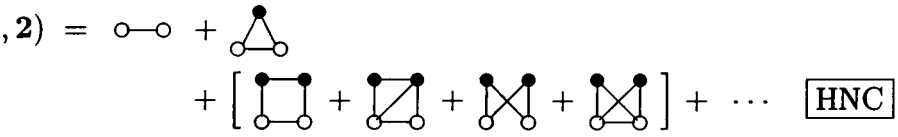 HNC (C1)

$c(\mathbf{1},\mathbf{2}) =$ 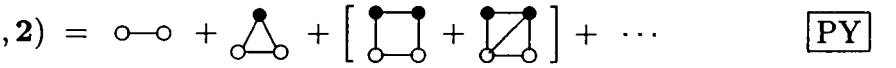 PY (C2)

Both approximations are accurate at low densities because only the more highly connected terms in the higher-order cluster expansions are affected by the approximation. Yet, since the expansions are summed to all orders in the density, they can be used to obtain qualitative (if not quantitative) results [33]. Comparison of Eqs. (C1) and (C2) shows that the PY approximation neglects four, as opposed to just two, of the second-order graphs in the full cluster expansion of $c(\mathbf{1},\mathbf{2})$. Despite this fact, the PY approximation is found to superior when repulsive forces dominate, allegedly because the diagrams neglected tend to cancel each other in such an environment. For a hard sphere fluid the PY approximation neglects the direct correlation function for $r > R$, while $c(r)$ has a "tail" for $r > R$ using the HNC approximation. Such a tail can be important for inhomogeneous or confined fluids. Many attempts have been made to combine the HNC and PY approximations in IET schemes such that thermodynamic self-consistency can be guaranteed.